TECHNISCHE
UNIVERSITÄT
DARMSTADT

COVARIANT REGULARIZATION FOR HOT AND DENSE QCD

Vom Fachbereich Physik
der Technischen Universität Darmstadt

zur Erlangung des Grades
Doctor rerum naturalium
(Dr. rer. nat.)

genehmigte Dissertation von

M.SC. SEBASTIAN TÖPFEL

Erstreferent: Prof. Dr. Jens Braun
Korreferent: Prof. Dr. Hans-Werner Hammer

Darmstadt 2025

Covariant regularization for hot and dense QCD
Kovariante Regularisierung für heiße und dichte QCD

Dissertation von M.Sc. Sebastian Töpfel

Tag der mündlichen Prüfung: 10.02.2025
Jahr der Veröffentlichung: 2025

Darmstadt, Technische Universität Darmstadt

Abstract

We employ the functional renormalization group to study the chiral phase transition in the phase diagram of hot and dense QCD. In our phenomenological investigation of strongly interacting matter, we consider a low-energy effective model of two massless quark flavors that interact through a Yukawa term. Specifically, we work with a simple quark-meson model that includes quarks, the scalar sigma meson, and the pseudoscalar pions as its relevant field degrees of freedom. We compute meson curvature masses, which we use to determine the phase boundary associated with the chiral phase transition. Additionally, we calculate meson spectral functions, which provide information about, e.g., particle resonances and decay processes, thereby establishing a direct link between theory and experiment. Based on our calculations of chiral observables in different regularization schemes, we examine the scheme dependence of curvature masses and spectral functions. In particular, we focus on investigating the effects of regulator-induced symmetry breaking. To this end, we begin by employing canonical polynomial regulator functions, with and without explicit Lorentz symmetry breaking. Both the spatial and the covariant regulators respect chiral symmetry and the Silver-Blaze symmetry. We discuss the challenges associated with momentum-dependent covariant regulators at finite external parameters and demonstrate a procedure for their implementation. A comprehensive comparison of results obtained within the spatial and covariant schemes then allows us to assess the relevance of artificial Lorentz symmetry breaking at finite temperature and chemical potential. Furthermore, we make use of the Callan-Symanzik regulator, which is momentum-independent and thus inherently covariant. This regulator also respects the Silver-Blaze symmetry but breaks chiral symmetry. To allow for a meaningful implementation of this covariant regulator, we construct a symmetrization procedure based on Ward-Takahashi identities, which systematically eliminates the regulator-induced chiral symmetry breaking from the theory. Subsequently, we demonstrate the applicability of our symmetry-constrained Callan-Symanzik scheme through computations of curvature masses, spectral functions, and the phase diagram. In particular, we highlight the impact of artificial chiral symmetry breaking on chiral observables when our symmetrization procedure is not employed.

In addition to our investigation of regulator artifacts associated with explicit symmetry breaking, we collect and analyze various mathematical subtleties that arise in calculations of loop diagrams at finite temperature and/or chemical potential. In general, the calculation of correlation functions involves integration, differentiation, and the computation of limit processes. A priori, these mathematical operations do not commute. We present several scenarios in which the order of applying these operations is essential for obtaining consistent and unambiguous results. An understanding of these subtleties is of principal importance for quantum field theories and, in particular, underlies our calculations of chiral observables from the quark-meson model.

Zusammenfassung

Wir verwenden die Funktionale Renormierungsgruppe, um den chiralen Phasenübergang im Phasendiagramm von heißer und dichter QCD zu untersuchen. In unserer phänomenologischen Untersuchung stark wechselwirkender Materie betrachten wir ein effektives Niederenergie-Modell mit zwei masselosen Quarkflavors, die über einen Yukawa-Term miteinander wechselwirken. Konkret arbeiten wir mit einem einfachen Quark-Meson-Modell, das Quarks, das skalare Sigma-Meson und die pseudoskalaren Pionen als relevante Feldfreiheitsgrade berücksichtigt. Wir berechnen Krümmungsmassen der Mesonen, die wir zur Bestimmung der Phasengrenze des chiralen Phasenübergangs heranziehen. Darüber hinaus berechnen wir mesonische Spektralfunktionen, die Informationen über beispielsweise Teilchenresonanzen und Zerfallsprozesse liefern und somit eine direkte Verbindung zwischen Theorie und Experiment herstellen. Basierend auf unseren Berechnungen chiraler Observablen in verschiedenen Regularisierungsschemen untersuchen wir die Schemenabhängigkeit von Krümmungsmassen und Spektralfunktionen. Insbesondere konzentrieren wir uns auf die Untersuchung der Auswirkungen von durch Regulatoren induzierten Symmetriebrechungen. Zu diesem Zweck verwenden wir zunächst kanonische polynomiale Regulatorfunktionen, sowohl mit als auch ohne explizite Brechung der Lorentz-Symmetrie. Sowohl der räumliche als auch der kovariante Regulator respektieren die chirale Symmetrie und die Silver-Blaze-Symmetrie. Wir diskutieren die Herausforderungen, die mit impulsabhängigen kovarianten Regulatoren bei endlichen externen Parametern verbunden sind, und zeigen ein Verfahren zu ihrer Implementierung. Ein umfassender Vergleich der Ergebnisse, die in dem räumlichen und dem kovarianten Schema erzielt wurden, ermöglicht es uns anschließend, die Relevanz der künstlichen Lorentz-Symmetrie-Brechung bei endlicher Temperatur und chemischem Potential zu bewerten. Darüber hinaus nutzen wir den Callan-Symanzik-Regulator, der impulsunabhängig und daher inhärent kovariant ist. Dieser Regulator respektiert ebenfalls die Silver-Blaze-Symmetrie, bricht jedoch die chirale Symmetrie. Um eine sinnvolle Implementierung dieses kovarianten Regulators zu ermöglichen, entwickeln wir ein Symmetrisierungsverfahren basierend auf Ward-Takahashi-Identitäten, das die durch den Regulator induzierte Brechung der chiralen Symmetrie systematisch aus der Theorie entfernt. Anschließend demonstrieren wir die Anwendbarkeit unseres symmetrieerhaltenden Callan-Symanzik-Schemas durch Berechnungen von Krümmungsmassen, Spektralfunktionen und des Phasendiagramms. Insbesondere zeigen wir die Auswirkungen der künstlichen chiralen Symmetriebrechung auf chirale Observablen, wenn unser Symmetrisierungsverfahren nicht angewendet wird.

Zusätzlich zu unserer Untersuchung von Regulatorartefakten, die mit expliziter Symmetriebrechung verbunden sind, sammeln und analysieren wir verschiedene mathematische Feinheiten, die bei Berechnungen von Loop-Diagrammen bei endlicher Temperatur und/oder chemischem Potential auftreten. Im Allgemeinen umfasst die Berechnung von Korrelationsfunktionen Integration, Differentiation und die Durchführung von Grenzwert-Prozessen. A priori vertauschen diese mathematischen Operationen nicht. Wir präsentieren mehrere Szenarien, in denen die Reihenfolge dieser Operationen entscheidend ist, um konsistente und eindeutige Ergebnisse zu erhalten. Das Verständnis dieser Feinheiten ist von grundlegender Bedeutung für Quantenfeldtheorien und bildet insbesondere die Grundlage für unsere Berechnungen chiraler Observablen im Quark-Meson-Modell.

Danksagung

Die vorliegende Arbeit ist im Rahmen meiner Tätigkeit als wissenschaftlicher Mitarbeiter am Institut für Kernphysik (Theoriezentrum) an der Technischen Universität Darmstadt entstanden. Während meiner Zeit an der TU hatte ich das Privileg, einer Vielzahl von Menschen zu begegnen, deren Eindrücke mich auch in Zukunft begleiten werden. Jeder Austausch bot mir die Möglichkeit, mich sowohl fachlich als auch persönlich weiterzuentwickeln, und für die zahlreichen Erfahrungen bin ich außerordentlich dankbar. Einige Personen möchte ich an dieser Stelle ausdrücklich hervorheben.

Mein besonderer Dank gebührt meinem Doktorvater Jens Braun für die Betreuung meines Forschungsvorhabens. Ohne Dich und Deine Unterstützung wäre diese Dissertation in ihrer heutigen Form nicht möglich gewesen. Mit Deinem umfangreichen Wissen sowie Deinen stets konstruktiven Anmerkungen hast Du mir während meiner gesamten Zeit in Deiner Arbeitsgruppe immer wieder wertvolle Impulse in die richtige Richtung gegeben. Ich schätze es sehr, dass Du mir den nötigen Freiraum gegeben hast, um kreative Ideen zu entwickeln und neue Lösungsansätze auszuarbeiten. Außerdem möchte ich betonen, dass die Gespräche mit Dir – über Physik und auch darüber hinaus – mir immer eine Menge Spaß gemacht haben. Nicht selten waren die Treffen mit Dir eine Quelle der Inspiration für mich. Vielen herzlichen Dank, dass ich von Dir lernen durfte!

Des Weiteren möchte ich Hans-Werner Hammer meinen Dank für die Übernahme des Zweitgutachtens aussprechen.

Eine nicht zu unterschätzende Tatsache ist, dass eine gute Arbeitsatmosphäre eine wichtige Voraussetzung für produktives Arbeiten darstellt. Ich möchte mich daher ganz besonders bei Florian Ehmann bedanken, der mein Arbeitserlebnis so positiv geprägt und meine Zeit am Institut maßgeblich aufgewertet hat. Vielen Dank für die wunderbare Zusammenarbeit.

Ein weiterer großer Dank gilt Andreas Geißel. Das gemeinsame Forschungsprojekt mit Dir hat mir ungemein viel Freude bereitet und unser wissenschaftlicher Austausch hat mich fortwährend dazu angeregt, mein Wissen weiter zu vertiefen. Vielen Dank für die Motivation, die Du mir mit Deiner Begeisterung und Deinem Interesse an meiner Arbeit so oft geschenkt hast.

Das Fertigen dieser Dissertation hat über eine lange Zeit hinweg alle Bereiche meines Lebens bestimmt. Ich möchte mich daher besonders bei Robin Köster für die moralische Unterstützung bedanken, die für mich von unschätzbarem Wert war. Vielen lieben Dank für Deinen stetigen Rückhalt, der mich durch diese anspruchvolle Zeit begleitet hat.

CONTENTS

1

INTRODUCTION

Almost all matter around us is composed of several dozen chemical elements and their isotopes. Each atom has a compact nucleus, made of interacting protons and neutrons, and a cloud of electrons surrounding the nucleus. This is, however, an effective description of nature, suitable only at certain length or energy scales. In particular, results from deep inelastic scattering experiments as well as the discovery of excited states inside Baryons have pointed towards the fact that nucleons are not fundamental point-like particles but have a deeper substructure [1, 2]. Therefore, the theory of interacting nucleons fails to correctly describe our world at sufficiently high energies as more fundamental degrees of freedom become relevant. Nowadays, the widely accepted theory for describing the substructure of nucleons is quantum chromodynamics (QCD). It is known as the theory of the strong interaction, one of the four fundamental forces in nature, and is an important cornerstone of the Standard Model of particle physics. More specifically, QCD is the theory of fermionic fields, so-called quarks, and non-Abelian gauge fields, so-called gluons, whose mutual interactions are based on the $SU(N_c)$ symmetry group, where $N_c = 3$ is the number of color charges. QCD is a mathematically rich and conceptually intriguing theory, see, e.g., Refs. [3–5] for an introduction. For example, it gives rise to the non-perturbative phenomenon of confinement at low energies, whereby physical observables appear only as color-singlet states. Phenomenologically speaking, as the strong interaction becomes stronger at larger distances, quarks and gluons are never observed in isolation but are always confined into bound states such as the nucleons. Conversely, at high energies or short distances, the interaction weakens, allowing quarks to behave almost like free particles. This phenomenon, known as asymptotic freedom, is a distinct property of non-Abelian gauge theories [6].

The phase structure of strongly coupled systems is a subject of intense investigation across various fields of physics, ranging from cosmology and high-energy physics to condensed-matter physics. In the plane of temperature and chemical potential, QCD gives rise to a plethora of different equilibrium phases whose detailed analysis is crucial for our understanding of the formation of matter, see, e.g., Refs. [7–19]. In particular, at low temperatures and densities, QCD gives rise to the hadronic phase, which is governed by confinement and the dynamical generation of quark masses. The investigation of this phase is important for understanding the properties of strongly interacting matter under normal conditions. It provides a microscopic understanding of the interactions that govern the behavior of nucleons and nuclei. Under more extreme conditions, the strong force can give rise to different phases in which hadronization processes do not dominate.

For example, with increasing temperatures, the thermal excitation of hadronic matter becomes strong enough to overcome the confinement force and triggers a transition into a plasma of quarks and gluons. Studying QCD at high temperatures is essential for our understanding of the early universe, in particular, how it transitioned from a plasma state into the cooled state we observe today. For further information, we refer to, e.g., Refs. [20–24]. At low temperatures and high densities, quarks form Cooper pairs near the Fermi surface, leading to the phenomenon of color superconductivity, see, e.g., Refs. [25–30]. The investigation of quark matter in this regime of high densities provides direct insights into the interior structure of neutron stars, where densities can exceed several times nuclear saturation density. In particular, the equation of state of dense matter plays a vital role in this context as it is a basic ingredient for modeling various astrophysical phenomena related to neutron stars, such as core-collapse supernovae and binary neutron star mergers [31]. At the moment, it is not possible to access the high-density regime of strong-interaction matter by experiment. However, recreating the conditions necessary for a systematic study of the QCD phase diagram up to intermediate densities can be achieved by collisions of heavy ions at ultrarelativistic energies [32–37]. In particular, one of the main goals of the heavy-ion collision program is to shed light on the possible existence and location of the chiral critical endpoint [38–41]. This is a hypothetical point in the QCD phase diagram, at which the nature of the chiral phase transition is expected to change from a first-order transition to a smooth crossover as temperature increases. The quest for the critical endpoint is also increasingly supported by efforts of theoretical physics, see, e.g., Refs. [18, 42–47].

The region of low temperatures and low densities in the QCD phase diagram is well-understood by means of chiral perturbation theory [48–50] and nuclear many-body theory [51–53]. Observables in this region can often be directly compared with experimental data from nuclear physics. The dynamics of quarks and gluons under extreme conditions, particularly at high temperatures and densities, can be explored using weak-coupling approaches. More specifically, by performing systematic expansions in the coupling constant, perturbation theory can provide valuable insights into the thermodynamic properties of hot and dense quark matter, such as pressure, energy density, and transport coefficients [54–57]. Furthermore, perturbative results serve as benchmarks for non-perturbative approaches, which helps to identify regions where these methods converge or deviate. Investigating QCD at intermediate scales, however, poses severe challenges due to the emergence of inherently non-perturbative phenomena such as critical behavior and phase transitions. As a result, the exploration and understanding of the QCD phase diagram at intermediate temperatures and densities remains an active field of research up to this day [58–60].
There are conceptually different approaches to meet the challenges of exploring the QCD phase diagram. Computational approaches such as lattice calculations and statistical Monte-Carlo methods have become quite successful over the last years [61–65]. Nevertheless, lattice approaches severely suffer from the sign problem [66–68], which limits their applicability to small chemical potentials. Furthermore, the AdS/CFT correspondence [69–71] can be employed to perform calculations for strongly interacting systems. This method is based on the holographic principle and maps a strongly coupled field theory to a string theory in its weak-coupling limit. In addition, functional approaches to QCD in terms of Dyson-Schwinger equations [72, 73] can be used. These form a set of self-consistent equations for correlation functions, which encode the interactions between particles in a system.
These non-perturbative methods are invaluable tools for studying strongly interacting systems, especially in regimes where perturbative methods break down. Nevertheless, their applicability to pure QCD often faces practical limitations due to the inherent complexity of the non-Abelian gauge theory. Therefore, the exploration of the phase diagram at intermediate scales mainly relies on effective low-energy models. Effective models aim at a simplified description of the full theory by

encoding only those low-energy degrees of freedom that are relevant for the phenomenon of interest. In other words, effective models are strategically designed approximations that capture the essential physics in a certain region of parameter space. The most prominently used models for QCD are Nambu–Jona-Lasinio (NJL) models [74, 75] and their relatives, see, e.g., Refs. [28, 76, 77] for reviews. NJL-type models essentially rephrase the quark-gluon dynamics at high energies as four-quark interactions at lower energies, which provides more direct access to the mechanisms that underlie the phase structure of QCD at intermediate scales. In particular, NJL-type models have been found extremely useful in the description of the chiral phase transition and keep performing successfully within their domain of reliability. It is worth mentioning that the determination of the relevant low-energy degrees of freedom generally requires a great amount of physical as well as mathematical insight. Therefore, the phenomenological analysis of results obtained from effective models can suffer from generic features and underlying approximations.

In this thesis, we shall employ the functional renormalization group (fRG) for the analysis of hot and dense QCD. The fRG is a powerful and versatile non-perturbative approach to studying quantum field theories. It is based on the concept of progressively incorporating quantum or thermal fluctuations from high to low energy scales. In particular, the systematic examination of high-energy degrees of freedom allows for capturing the emergence and evolution of effective degrees of freedom. Thereby, the fRG is capable of describing the physics of a given system over a wide range of scales. This makes it particularly well-suited to study phase transitions and critical phenomena. Specifically, for an overview of recent progress in studies of QCD at finite temperature and density using the functional renormalization group approach, see, e.g., Refs. [42, 78–80]. The fRG relies on the introduction of an auxiliary function, the regulator, enabling us to control the amount of quantum or thermal fluctuations contributing to the theory. By varying this amount, we can effectively interpolate between the microscopic and macroscopic descriptions of the system. Once all fluctuations are taken into account, the formalism provides us with the action functional of the full quantum theory. It is worth noting already at this point that the regulator serves primarily as a tool in the renormalization group approach to quantum field theory. As such, it is in general not a physically meaningful object and should not spoil the predictions for physical observables. This means that the behavior of the regulator should in particular be constrained by the symmetry properties of the underlying theory. Nevertheless, imposing too many restrictions on the regulator function often renders concrete calculations extremely expensive and thus hinders its practical use. As a consequence, it has become common practice for phenomenological studies to implement regulator functions that induce an explicit symmetry breaking. This symmetry breaking is artificial such that results for observables in principle suffer from regulator artifacts. Concretely, in the presence of finite external parameters, fRG studies usually consider spatial regulators that explicitly break Lorentz symmetry in the vacuum limit. In order to properly assess the impact of regulator artifacts on predictions for physical observables, an extensive analysis of results is required.

1.1 Focus and outline of this thesis

The aim of this thesis is twofold. We conduct a comprehensive study of observables relevant to the chiral phase transition in hot and dense QCD while also analyzing their scheme dependences arising from regulator-induced symmetry breaking in the fRG framework. In particular, we focus on covariant regularization schemes in our study of the chiral phase boundary and discuss their individual challenges, correct implementation, and significance in this context.

Let us further elaborate on these points in the following. For our investigation of the QCD phase diagram, we consider a low-energy effective model of two massless quark flavors that interact

through a Yukawa term. To be specific, we work with a simple quark-meson model, a special form of NJL-type model. This model considers quarks and (pseudo-)scalar mesons as its relevant field degrees of freedom, which makes it well-suited to describe the physics of the chiral phase transition. In order to access chiral observables, we take a renormalization group approach to quantum field theory. More specifically, we employ the fRG, taking into account only purely fermionic loops for simplicity. In addition, we make use of the one-loop approximation since leading-order effects are expected to dominate the behavior of the system near critical points. For our study of the quark-meson model, we focus on the computation of meson curvature masses and meson spectral functions. In particular, the behavior of curvature masses as functions of external parameters such as temperature and chemical determines the phase boundary associated with the chiral phase transition. Spectral functions, on the other hand, provide access to, e.g., particle resonances and transport coefficients, thereby establishing a direct connection between theory and experiment, such as heavy-ion collision experiments.
In our endeavor to analyze the scheme dependences of curvature masses and spectral functions, we first consider polynomial regulator functions with and without Lorentz symmetry breaking. Both the spatial and covariant polynomial regulators that we consider respect chiral symmetry as well as the Silver-Blaze symmetry. We stress that momentum-dependent covariant regulators render the computation of correlation functions at finite external parameters extremely difficult. Therefore, we discuss and demonstrate a systematic procedure for their implementation. A comprehensive comparison of results as obtained within the spatial and covariant schemes then lets us assess the relevance of the artificial Lorentz symmetry breaking at finite external parameters. Furthermore, we consider a Callan-Symanzik (CS) regulator, which is momentum-independent and thus inherently covariant. This regulator also respects the Silver-Blaze symmetry but breaks chiral symmetry. Chiral symmetry is the key symmetry principle of massless QCD in the context of the chiral phase transition. As a result, the CS regulator has not yet received much attention in the study of chiral fermion-boson models. To allow for a meaningful implementation of this covariant regulator, we construct a symmetrization procedure based on Ward-Takahashi identities, which systematically eliminates the regulator-induced chiral symmetry breaking from the theory. Afterwards, we demonstrate the applicability of our symmetry-constrained CS scheme. In particular, we address the impact of artificial chiral symmetry breaking on chiral observables when our symmetrization procedure is not employed. In the end, we take effects of renormalization into account and compute the phase diagram in our symmetrized CS framework.

In addition to our phenomenological study of QCD and the investigation of regulator artifacts associated with explicit symmetry breaking, we present and analyze various subtleties that can be encountered in calculations of correlation functions at finite temperature and/or chemical potential. In general, the calculation of correlation functions involves integration, differentiation, and the computation of limit processes. A priori, these mathematical operations do not commute. Nevertheless, expansion schemes and the application of projection prescriptions often rely on the assumption that the involved operations are commutative. We demonstrate explicitly that this assumption can easily fail in studies of dense systems. More specifically, we present several scenarios in which the order of applying these operations is essential for obtaining consistent and unambiguous results. An understanding of subtleties appearing in finite-density studies is of great relevance with respect to both perturbative and non-perturbative computations of the equation of state of quantum field theories as well as their phase structure. In particular, a careful treatment of complications arising from the non-commutative nature of mathematical operations underlies our calculations of chiral observables from the quark-meson model.

The present work is organized as follows: Chapter 2 is devoted to all aspects of quantum field theory which are crucial for our investigation of the QCD phase diagram and an analysis of scheme dependences. In particular, after a recapitulation of fundamental aspects of quantum field theory in Section 2.1, we introduce the functional renormalization group method in Section 2.2. Here, we not only derive the characteristic RG flow equation for the fRG but also discuss general properties of regulators and the importance of RG consistency. The general incorporation of temperature and chemical potential into the framework of quantum field theory is addressed in Section 2.3. In this section, we explain the imaginary-time formalism and discuss the Silver-Blaze property, which is an important feature for theories of fermions that couple to a chemical potential. A detailed discussion of mathematical subtleties that arise in the calculation of loop integrals at finite external parameters can be found in the subsequent Section 2.4. Our comprehensive study of chiral observables and their dependence on regulator artifacts is fully contained in Chapter 3. Here, we start with an introduction of the quark-meson model in Section 3.1 and also address details of our particular fRG framework. After the presentation of our methodology, we continue with our first phenomenological study. Concretely, we discuss the implementation of polynomial regulator functions in the context of the chiral phase transition in Section 3.2. Our fRG study of the QCD phase diagram using the Callan-Symanzik regulator is detailed in Section 3.3. Finally, we summarize our results in Chapter 4 and briefly discuss potential future research objectives.

1.2 List of publications

The compilation of this dissertation was done solely by the author. The results were obtained with my collaborators and are largely published or available as a preprint, see the following listing:

[81] Title: “Renormalization Group Studies of Dense Relativistic Systems”
Authors: Jens Braun, Timon Dörnfeld, Benedikt Schallmo, and Sebastian Töpfel
Published in: Phys. Rev. D **104**, 096002 (2021)
E-print: arXiv:2008.05978 [hep-ph]

[82] Title: “Renormalised spectral flows”
Authors: Jens Braun *et al.*
Published in: SciPost Phys. Core **6**, 061 (2023)
E-print: arXiv:2206.10232 [hep-th]

[83] Title: “Subtleties in the calculation of correlation functions for hot and dense systems”
Authors: Sebastian Töpfel, Andreas Geißel, and Jens Braun
Published in: Phys. Rev. D. **111**, 016023 (2025)
E-print: arXiv:2410.06674 [nucl-th]

[84] Title: “Phase structure of quark matter and in-medium properties of mesons from Callan-Symanzik flows”
Authors: Sebastian Töpfel, Jan M. Pawlowski, and Jens Braun
E-print: arXiv:2412.16059 [hep-ph]

Texts and figures in this thesis that are taken from or based on these references are not marked explicitly. However, the references are incorporated as follows: Section 2.4 and parts of Appendix C are based on Ref. [83], whereas Section 3.3 and parts of Appendix D are based on Ref. [84].

2

QUANTUM FIELD THEORY

In this chapter, we recapitulate the basic principles of the path integral approach to quantum field theory and establish generating functionals as needed in order to systematically access correlation functions. Based on the Wilsonian viewpoint [85, 86], we then introduce the renormalization group method, which will serve as a key concept for our investigation of strong-interaction matter in Chapter 3. In particular, we derive the Wetterich equation [87], which represents the characteristic flow equation for the functional renormalization group, and present the concept of renormalization group consistency [88]. Lastly, we demonstrate how the vacuum formalism can be extended to finite external parameters, i.e., temperature and chemical potential. The physical implications as well as the mathematical subtleties that come along with the introduction of finite external parameters will be discussed in detail.

2.1 Fundamentals

Having evolved as a species that experiences the world at specific length and time scales, it is only natural that everyone has ingrained quite an intuitive understanding of the character of the physical laws relevant at such scales. These laws have been historically the first to be formally derived and studied and they can be collected into what is commonly known as classical, non-relativistic mechanics. The predictions from this branch of physics, however, get less and less accurate the further away from macroscopic scales we operate. In other words, the classical, non-relativistic picture of the world has only a certain range of reliability and has to be considered some kind of limit of a more general description. From a phenomenological standpoint, this thesis does not deal with questions of cosmology, which is the physics at very large length scales, but rather with topics related to the behavior of elementary particles, i.e., the physics at sub-atomic length scales. In order to reliably describe the physics at these scales, we need a quantum description of the world. A quantum theory is constructed from a classical theory by a so-called quantization procedure.

There are various ways of constructing a quantum theory from a classical one, e.g., canonical quantization, deformation quantization [89, 90], or geometric quantization [91, 92]. Our approach to quantum field theory is based on the path integral formalism, whose origin can be traced back to Dirac [93] but which was worked out by Feynman [94, 95]. The foundation for the functional integral viewpoint is the quantum-mechanical completeness relation, which gives

rise to a representation of the evolution kernel in terms of an integral formula. For a quantum-mechanical system, whose Hamiltonian H as a function of the momentum is a non-degenerate quadratic form with constant coefficients, the matrix elements of the time evolution operator in the basis of localized states are given by

$$\langle \vec{x}_b | \exp\left(-\int_{t_a}^{t_b} \mathrm{d}t \; H(\hat{\vec{p}}, \hat{\vec{x}}, t) \right) | \vec{x}_a \rangle = \mathscr{C} \int_{\vec{x}(t_a)=\vec{x}_a}^{\vec{x}(t_b)=\vec{x}_b} \mathcal{D}\vec{x} \; \exp\left(-\int_{t_a}^{t_b} \mathrm{d}t \; L(\vec{x}, \dot{\vec{x}}, t) \right) , \tag{2.1}$$

where $\mathcal{D}\vec{x}$ is a symbolic notation for a translation-invariant measure on the infinite-dimensional vector space of paths from $\vec{x}_a$ to $\vec{x}_b$.[1] Also symbolically, $\mathscr{C}$ denotes some constant that ensures the correct physical dimensions for the path integral expression. The path integral formula (2.1) overall leads to the notion that quantum-mechanical evolution simultaneously considers all possible paths. Intuitively, the need for integration might not be that unexpected. The position operator does not commute with the Hamiltonian and, as a consequence, time evolution changes the position eigenstate into one in which position is not determined. The quantum system has no definite trajectory and it is necessary to take the sum over all possible ones, according to the superposition principle. Notice that we follow Feynman's construction of the path integral in which the dynamics of the system is not dictated by a Hamiltonian but by a corresponding Lagrangian L, which, when integrated over with respect to time, leads us to the classical action

$$S[\vec{x}] = \int_{t_a}^{t_b} \mathrm{d}t \; L(\vec{x}, \dot{\vec{x}}, t) \, . \tag{2.2}$$

This formulation allows for a relatively simple understanding of the classical limit since we can see classical mechanics emerge from the saddle point approximation to quantum mechanics. More concretely, if the action functional gets sufficiently large, $S[\vec{x}] \gg 1$,[2] the path integral is dominated by trajectories close to the classical one, $\vec{x}_\mathrm{c}$, which minimizes the action and hence satisfies $\delta S[\vec{x}_\mathrm{c}] = 0$.[3] This demonstrates that, where the global minimum of the classical action is sufficient to determine the evolution in (Euclidean) classical mechanics, quantum-mechanical evolution is sensitive to the entire action.

2.1.1 Generating functionals

Aiming for a description of systems including elementary particles, we now promote the concept of path integral quantization to quantum field theory. Functional integral methods greatly simplify the construction of interacting quantum field theories compared to, e.g., canonical quantization and allow for the investigation of non-perturbative phenomena. In addition, the path integral formulation lets us easily incorporate effects of equilibrium thermodynamics into the vacuum quantum theory, see Section 2.3. Practically speaking, the most important objects to compute in any quantum field theory are expectation values called correlation functions. These n-point correlators with $n \in \mathbb{N}$ are associated with n-particle interactions and can be directly related to quantities accessible through experiment, i.e., scattering cross sections and decay rates. The path integral

[1] In fact, there is no non-trivial Lebesgue measure on an infinite-dimensional vector space. The continuum functional integral is not very well defined from a mathematical perspective, yet in physical applications, its definition as a limit of the discrete functional integral is quite well-behaved. Therefore, the quantum-mechanical path integral can be made rigorous by rewriting the r.h.s. of Eq. (2.1) as an integral with respect to the so-called Wiener measure [96–99]. For simplicity, however, we will stick with the physicist notation. For more technical details on the path integral, see, e.g., Refs. [100–105].

[2] When working in SI units, the exponential in the path integral has the structure $\exp(-S[\vec{x}]/\hbar)$. Treating Planck's constant as a formal parameter and considering $\hbar \ll 1$ then justifies the use of the saddle point approximation. In natural units, however, there is no explicit dependence on $\hbar$ so the classical limit is realized by letting the action take large values.

[3] While Hamilton's principle is a stationary-action principle in real time, it is indeed a least-action principle in Euclidean time.

formalism conveniently allows to obtain every correlation function from a single generating functional such that the construction of suitable generating functionals will play an essential role in the following.

We consider a general (vacuum) quantum field theory, which is governed by the action functional $S[\Phi]$.[4] All field degrees of freedom of the theory are contained within the purely generic variable Φ, sometimes also called superfield, which we define as

$$\Phi(x) = \begin{pmatrix} \varphi(x) \\ \psi(x) \\ \overline{\psi}^{\intercal}(x) \end{pmatrix} = \int_p \mathrm{e}^{\mathrm{i}p^{\intercal}x} \begin{pmatrix} \varphi(p) \\ \psi(p) \\ \overline{\psi}^{\intercal}(-p) \end{pmatrix} = \int_p \mathrm{e}^{\mathrm{i}p^{\intercal}x}\, \Phi(p)\,. \tag{2.3}$$

Here, φ represents a real-valued ordinary function and corresponds to a scalar field, whereas ψ and $\overline{\psi}$ represent Grassmann-valued Dirac spinors denoting fermion and antifermion fields,[5] respectively. In terms of what types of fields are incorporated, this is the most basic setup but a generalization is straightforward since tensor bosons behave like φ with additional indices and complex scalar fields, such as diquarks or Faddeev-Popov ghosts [112], come in pairs and can therefore enter the superfield just like the fermions. We remark that, from a phenomenological standpoint, our superfield Φ may be considered bosonic as there is an even number of fermions involved. This simplifies the following presentation of generating functionals in quantum field theory.

An important functional which underpins all further discussions is defined by

$$\mathcal{Z}[J] = \mathcal{N} \int \mathcal{D}\Phi\, \mathrm{e}^{-S[\Phi]+J^{\intercal}\cdot\Phi}\,, \tag{2.4}$$

where $\mathcal{N}$ denotes a normalization constant rendering $\mathcal{Z}$ dimensionless. This functional is reminiscent of the partition function of statistical mechanics and, for that reason, we will refer to $\mathcal{Z}$ as the partition functional in the context of quantum field theory. In the calculation of the path integral above, in principle boundary conditions have to be imposed,

$$\lim_{x_a^0\to-\infty} \Phi(x_a^0,\vec{x}) = \Phi_a(\vec{x})\,, \qquad \lim_{x_b^0\to\infty} \Phi(x_b^0,\vec{x}) = \Phi_b(\vec{x})\,, \tag{2.5}$$

but in the limit as the time coordinate goes to positive or minus infinity, the normalized functional integral does not actually depend on the choice of the spatial configurations Φ_a and Φ_b [113]. The

[4] Guided by the Hilbert space description of quantum mechanics, one could argue that a Hamiltonian formulation of the path integral would be more fundamental than a Lagrangian one. In fact, if we consider a general field theory, which is only constrained by a set of symmetry transformations, and start with a Hamiltonian form of the path integral, then the existence of a Lagrangian version of the functional integral is not guaranteed. However, we do not follow that line of argumentation and simply define our quantum field theory by a Lagrangian. It is also worth noting that there are quantum field theories that do not admit a Lagrangian description [106, 107], even though we will not consider such cases here.

[5] In order to allow for a path integral description for fields obeying the Fermi-Dirac statistics, we need complex-valued Grassmann variables. The Dirac spinors are then based on a Grassmann algebra that is constructed from two independent sets of Grassmann variables. This means that, compared to Minkowski quantum field theory, our Dirac spinors $\overline{\psi}$ and ψ are independent and not related by any notion of complex conjugation [108]. For more details on the Grassmann calculus, see, e.g., Refs. [109–111].

partition functional $\mathcal{Z}$ is a functional of the supersource

$$J(x) = \begin{pmatrix} j(x) \\ \bar{\eta}^{\intercal}(x) \\ -\eta(x) \end{pmatrix} = \int_p \mathrm{e}^{\mathrm{i}p^{\intercal}x} \begin{pmatrix} j(p) \\ \bar{\eta}^{\intercal}(-p) \\ -\eta(p) \end{pmatrix} = \int_p \mathrm{e}^{\mathrm{i}p^{\intercal}x}\, J(p)\,, \tag{2.6}$$

which is the generic source field corresponding to the superfield (2.3). It consists of the real-valued function j as well as the Grassmann-valued spinors $\bar{\eta}$ and η. The source field can be considered as an externally applied perturbation, whose insertion is common practice to learn about the dynamical properties of a quantum system. Furthermore, we have declared the scalar product[6]

$$J^{\intercal} \cdot \Phi = \int_x (J^{\intercal})_\alpha(x)\, \Phi^\alpha(x) = \int_x \Big(j(x)\, \varphi(x) + \bar{\eta}(x)\, \psi(x) + \bar{\psi}(x)\, \eta(x) \Big)\,, \tag{2.7}$$

where the summation index α runs over the field degrees of freedom.

With the partition functional at hand, we are now ready to engineer suitable generating functionals. The overall idea behind the construction of generating functionals is to obtain correlation functions by a projection procedure involving functional differentiation. In particular, the generating functional for n-point correlation functions, also called vacuum persistence amplitude, is given by

$$\mathcal{A}[J] = \langle \Omega | \hat{T}\ \mathrm{e}^{J^{\intercal}\cdot\hat{\Phi}} | \Omega \rangle = \frac{\mathcal{Z}[J]}{\mathcal{Z}[0]}\,, \tag{2.8}$$

where $|\Omega\rangle$ represents the ket state of the interacting vacuum and $\hat{T}$ is the time-ordering operator for the Heisenberg field operators. Notice that, by construction, the vacuum persistence amplitude is normalized to unity, $\mathcal{A}[0] = 1$. In general, the n-point function is then given by

$$\langle \mathcal{O}_1 \dots \mathcal{O}_n \rangle := \frac{\int \mathcal{D}\Phi\ \mathcal{O}_1 \dots \mathcal{O}_n\ \mathrm{e}^{-S[\Phi]}}{\int \mathcal{D}\Phi\ \mathrm{e}^{-S[\Phi]}} = \left(\frac{\vec{\delta}}{\delta \mathcal{J}_1} \dots \frac{\vec{\delta}}{\delta \mathcal{J}_n} \mathcal{A}[J] \right) \Bigg|_{J=0}\,, \tag{2.9}$$

where $\mathcal{J}_i$ denotes the appropriate source corresponding to the field-dependent quantity $\mathcal{O}_i$ for $i \in \{1, \dots, n\}$. Note that the anticommutativity property of the Grassmann-valued field variables directly translates to the corresponding differential operators. Consequently, it does make a difference whether functional derivatives act on a field-dependent object from the left or from the right if that object contains even-numbered multiples of Grassmann variables.[7] We hence use an arrow

[6] To be more precise, only the spacetime integral over the bosonic fields yields an ordinary scalar. Performing the spacetime integral of a spinor bilinear results in an even supernumber since ordinary integration does not affect any properties inherited from the Grassmann algebra. Those properties, however, do not survive the functional Grassmann integration such that $\mathcal{Z}[0]$ is indeed an ordinary scalar. For more information about supernumbers, see, e.g., Refs. [102, 114, 115].

[7] In the fermionic subspace, differentiation from the right-hand side is defined as differentiation from the left-hand side with an additional factor compensating for the difference in the number of anticommutations. Specifically, for an n-dimensional Grassmann algebra with generators θ_i we have

$$\theta_1 \dots \theta_i \dots \theta_n\, \frac{\overleftarrow{\partial}}{\partial \theta_i} = (-1)^{n+1} \frac{\vec{\partial}}{\partial \theta_i}\, \theta_1 \dots \theta_i \dots \theta_n\,,$$

where the index i can take integer values from 1 to $n \in \mathbb{N}$.

notation to indicate the direction of functional differentiation. More concretely, we consider the example of the (matrix-valued) two-point function, which reads

$$\langle \Phi(x)\, \Phi^{\intercal}(y)\rangle = \left(\frac{\overrightarrow{\delta}}{\delta J^{\intercal}(x)} \frac{\overrightarrow{\delta}}{\delta J(y)} \mathcal{A}[J] \right)\Bigg|_{J=0} . \tag{2.10}$$

We emphasize that the classical action serves as a crucial ingredient for the definition of a Borel probability measure for the bosonic path integral [101, 116], which automatically leads to the understanding of correlation functions as expectation values. In the case of fermions, there is no underlying measure space for the path integral but the functional integral formulation of fermions follows closely that of bosons since this strategy has proven to be very successful for the construction of generating functionals and correlation functions with the correct fermionic properties. It is also important to realize that, while the action S fully determines our theory at the classical level, the generation of quantum effects and their incorporation into observables happens only through the process of functional integration. According to the reconstruction theorem [101, 117], a quantum field theory is uniquely determined by its correlation functions. Since any correlation function can be obtained from the generating functional, $\mathcal{A}$ contains all information of the underlying physical system and the theory would be completely solved once the generating functional is exactly known. Unfortunately, the functional integral can be carried out exactly only in rare cases.

An asymptotic expansion of correlation functions (2.9) in terms of couplings exhibits that the generating functional $\mathcal{A}$ encodes the information of the underlying physical system rather inefficiently. As a matter of fact, we often observe multiplicative expressions appearing repetitively throughout the expansion. In a more pictographic language, this means that the Feynman diagrams contributing to the n-point correlators contain disconnected pieces [118–120]. Contributions to correlation functions of higher order get quite redundant since there is always the possibility of particles passing each other without interacting. Because Feynman diagrams of disconnected pieces do not contribute to scattering amplitudes (T-matrix elements), it is more convenient to work with the generating functional

$$W[J] = \ln\big(\mathcal{Z}[J]\big) \tag{2.11}$$

of connected n-point correlation functions, also called Schwinger functional. It is simply a more efficient way to capture the information of the physical system as W only contains connected diagrams. As before, correlation functions are constructed from the corresponding functional by means of functional differentiation:

$$\langle \mathcal{O}_1 \dots \mathcal{O}_n\rangle^{\text{conn}} := \left(\frac{\overrightarrow{\delta}}{\delta \mathcal{J}_1} \dots \frac{\overrightarrow{\delta}}{\delta \mathcal{J}_n} W[J] \right)\Bigg|_{J=0} . \tag{2.12}$$

The general strategy for the generation of connected correlators is to take the full correlation function and then subtract all disconnected contributions. Due to the presence of the logarithm in Eq. (2.11), this method is implemented automatically when calculating correlation functions from the Schwinger functional. This will be illustrated in the following by the example of the connected

two-point function.

$$\begin{aligned}
\langle \Phi(x)\, \Phi^\intercal(y)\rangle^{\text{conn}} &= \left(\frac{\overrightarrow{\delta}}{\delta J^\intercal(x)}\frac{\overrightarrow{\delta}}{\delta J(y)} W[J]\right)\Big|_{J=0} = \left(\frac{\overrightarrow{\delta}}{\delta J^\intercal(x)}\left(\frac{1}{\mathcal{Z}[J]}\frac{\overrightarrow{\delta}}{\delta J(y)}\mathcal{Z}[J]\right)\right)\Big|_{J=0} \\
&= \left(\frac{1}{\mathcal{Z}[J]}\frac{\overrightarrow{\delta}}{\delta J^\intercal(x)}\frac{\overrightarrow{\delta}}{\delta J(y)}\mathcal{Z}[J]\right)\Big|_{J=0} - \left(\frac{1}{\mathcal{Z}[J]^2}\left(\frac{\overrightarrow{\delta}}{\delta J^\intercal(x)}\mathcal{Z}[J]\right)\left(\frac{\overrightarrow{\delta}}{\delta J(y)}\mathcal{Z}[J]\right)\right)\Big|_{J=0} \\
&= \left(\frac{\overrightarrow{\delta}}{\delta J^\intercal(x)}\frac{\overrightarrow{\delta}}{\delta J(y)}\mathcal{A}[J]\right)\Big|_{J=0} - \left(\frac{\overrightarrow{\delta}}{\delta J^\intercal(x)}\mathcal{A}[J]\right)\Big|_{J=0}\left(\frac{\overrightarrow{\delta}}{\delta J(y)}\mathcal{A}[J]\right)\Big|_{J=0} \\
&= \langle \Phi(x)\, \Phi^\intercal(y)\rangle - \langle \Phi(x)\rangle\, \langle \Phi^\intercal(y)\rangle \ . \qquad (2.13)
\end{aligned}$$

That any further moments of the Schwinger functional are connected correlation functions according to the principle demonstrated above, can be shown inductively [120], see also Refs. [121, 122]. The connected and the full one-point function are identical but notice that this equality breaks down as soon as we allow for finite sources.

For everything that follows it is beneficial to introduce the generalized n-point correlator

$$\langle\!\langle \mathcal{O}_1 \dots \mathcal{O}_n \rangle\!\rangle_J := \frac{1}{\mathcal{Z}[J]}\,\mathcal{N}\int \mathcal{D}\Phi\; \mathcal{O}_1 \dots \mathcal{O}_n\; \mathrm{e}^{-S[\Phi]+J^\intercal\cdot\Phi}\ , \qquad (2.14)$$

which reduces to the ordinary full n-point function (2.9) in the case of $J = 0$. We are now prepared to define the source-dependent connected two-point Green's function[8],

$$\begin{aligned}
G^{(2)}[J](x,y) \equiv \langle \Phi(x)\, \Phi^\intercal(y)\rangle_J^{\text{conn}} &:= \frac{\overrightarrow{\delta}}{\delta J^\intercal(x)}\frac{\overrightarrow{\delta}}{\delta J(y)} W[J] \\
&= \langle\!\langle \Phi(x)\, \Phi^\intercal(y)\rangle\!\rangle_J - \langle\!\langle \Phi(x)\rangle\!\rangle_J\, \langle\!\langle \Phi^\intercal(y)\rangle\!\rangle_J \\
&= \langle\!\langle \big(\Phi(x) - \langle\!\langle \Phi(x)\rangle\!\rangle_J\big)\big(\Phi(y) - \langle\!\langle \Phi(y)\rangle\!\rangle_J\big)^\intercal \rangle\!\rangle_J \ , \qquad (2.15)
\end{aligned}$$

which is a functional of the supersource J as well as a function of the spacetime variables x and y. Evaluating the source-dependent connected two-point correlator at $J = 0$ yields the result (2.13) again. We note that this Green's function is also the Hessian of the Schwinger functional. In particular, for general fields Ξ from the space of supersources, we find

$$\begin{aligned}
\mathrm{Tr}\left\{\Xi\, \Xi^\intercal \cdot G^{(2)}[J]\right\} = (-1)_\Psi\, \Xi^\intercal \cdot G^{(2)}[J] \cdot \Xi &= (-1)_\Psi \int_x \int_y \Xi^\intercal(x)\, G^{(2)}[J](x,y)\, \Xi(y) \\
&= \langle\!\langle \big(\Xi^\intercal \cdot (\Phi - \langle\!\langle \Phi\rangle\!\rangle_J)\big)^2 \rangle\!\rangle_J \geq 0 \ , \qquad (2.16)
\end{aligned}$$

where the object $(-1)_\Psi$ is used to indicate that there is an additional minus sign in the subspace that involves fermions. The result (2.16) displays that the functional Hessian is positive semi-definite and, consequently, that the Schwinger functional W is convex. As we will see in the following, convexity is an important property as it allows us to perform the Legendre transformation [123] of the Schwinger functional.

[8] Correlation functions are referred to as Green's functions in the literature most commonly. This roots back to the fact that, in free scalar field theory, the two-point function is indeed a Green's function to the Klein-Gordon operator in the mathematical sense. Analogously, the two-point function for free fermions is a Green's function to the Dirac operator.

Although the connected correlation functions do not contain contributions that arise from the multiplication of lower-order n-point functions, we can still further subdivide the connected diagrams into simpler units, which leads us to a minimal basis of Feynman diagrams for a given theory. To be more precise, the class of connected diagrams is reducible to a set of Feynman diagrams that remains connected when any internal line is cut. These diagrams, which cannot be decomposed into two disjoint graphs by cutting one internal line, are called one-particle-irreducible (1PI). Topologically, this criterion indicates that the diagram is held together by loops. The irreducible diagrams are of great importance in perturbation theory since every higher-order diagram can be obtained in a unique way by taking 1PI diagrams and free propagators as building blocks. The generating functional of 1PI correlation functions is found to be the Legendre transformation of the Schwinger functional [124, 125]:

$$\Gamma[\Phi_{\mathrm{cl}}] = \sup_J \left(J^\intercal \cdot \Phi_{\mathrm{cl}} - W[J] \right) . \tag{2.17}$$

The functional Γ is called the quantum effective action and is convex by construction. Technically, this means that for all $\alpha \in [0,1]$ it holds that

$$\begin{aligned} \Gamma[\alpha\chi_1 + (1-\alpha)\chi_2] &= \sup_J \left(\alpha\, J^\intercal \cdot \chi_1 + (1-\alpha)\, J^\intercal \cdot \chi_2 - (\alpha + 1 - \alpha)\, W[J] \right) \\ &\leq \alpha \sup_J \left(J^\intercal \cdot \chi_1 - W[J] \right) + (1-\alpha) \sup_J \left(J^\intercal \cdot \chi_2 - W[J] \right) \\ &= \alpha\, \Gamma[\chi_1] + (1-\alpha)\, \Gamma[\chi_2] . \end{aligned} \tag{2.18}$$

Notice that the convexity of the Schwinger functional is necessary in order to ensure that the quantum effective action is differentiable everywhere. The newly introduced field variable Φ_{cl} is usually referred to as the classical field since it corresponds to the expectation value of the quantum field Φ in the presence of the external source. This is implied through the supremum condition:

$$\forall x \in \mathbb{R} : \quad \left(\frac{\vec{\delta}}{\delta J^\intercal(x)} \left(J^\intercal \cdot \Phi_{\mathrm{cl}} - W[J] \right) \right) \Bigg|_{J=J_{\mathrm{sup}}} \stackrel{!}{=} 0 \tag{2.19}$$

$$\Rightarrow \Phi_{\mathrm{cl}}(x) = \left(\frac{\vec{\delta}}{\delta J^\intercal(x)} W[J] \right) \Bigg|_{J=J_{\mathrm{sup}}} = \langle\!\langle \Phi(x) \rangle\!\rangle_{J_{\mathrm{sup}}} . \tag{2.20}$$

Recall that the supersource is not part of the underlying physical system but serves as an auxiliary field enabling us to obtain correlation functions by a simple projection procedure, see Eq. (2.9). Thus, the field expectation value (2.20) in the presence of a finite source does not relate to any measurable quantity. The source term (2.7) in particular spoils the invariance of the path integral (2.4) with respect to unitary transformations of the fermion fields, which include Lorentz transformations, gauge transformations, negation, etc. As a consequence, the fermionic components of the classical field do not vanish,[9] which is an unphysical result. Manually setting the supersource to zero, however, lets us obtain the physical field expectation value:

$$\Phi_{\mathrm{cl},0}(x) = \Phi_{\mathrm{cl}}(x) \Big|_{J_{\mathrm{sup}}=0} = \langle\!\langle \Phi(x) \rangle\!\rangle_0 = \langle \Phi(x) \rangle^{\mathrm{conn}} = \langle \Phi(x) \rangle \ . \tag{2.21}$$

[9] The explicit breaking of symmetry with respect to the negation of fermion fields, i.e., the simultaneous transformations $\psi \to -\psi$ and $\overline{\psi} \to -\overline{\psi}$, is in fact the most general reason for the appearance of a finite fermion expectation value since it also applies to theories of non-relativistic fermions or generic constructions without any direct connection to quantum field theory. The reason for the appearance of negation symmetry in the unperturbed system is that fermionic theories are built from spinor bilinears. Since fermion fields are complex-valued objects defined on a Grassmann algebra, the restriction to bilinear structures ensures a consistent path integral quantization for fermions.

Here, the fermionic contributions indeed vanish identically as would be expected from a physical theory. For a given function Φ_{cl}, the relation (2.20) implies that the specific source obeying the supremum condition is actually a functional of the classical field, i.e., $J_{\mathrm{sup}} \equiv J_{\mathrm{sup}}[\Phi_{\mathrm{cl}}]$.

It is now possible to rewrite the quantum effective action,

$$\Gamma[\Phi_{\mathrm{cl}}] = J^{\intercal}_{\mathrm{sup}}[\Phi_{\mathrm{cl}}] \cdot \Phi_{\mathrm{cl}} - W[J_{\mathrm{sup}}] \,, \tag{2.22}$$

and also calculate the first derivative,[10]

$$\begin{aligned}
\Gamma[\Phi_{\mathrm{cl}}] \frac{\overleftarrow{\delta}}{\delta \Phi_{\mathrm{cl}}(x)} &= J^{\intercal}_{\mathrm{sup}}[\Phi_{\mathrm{cl}}](x) + (-1)_{\Psi} \left(J^{\intercal}_{\mathrm{sup}}[\Phi_{\mathrm{cl}}] \frac{\overleftarrow{\delta}}{\delta \Phi_{\mathrm{cl}}(x)} \right) \cdot \Phi_{\mathrm{cl}} \\
&\quad - \left(W[J_{\mathrm{sup}}] \frac{\overleftarrow{\delta}}{\delta J_{\mathrm{sup}}[\Phi_{\mathrm{cl}}]} \right) \cdot \left(J_{\mathrm{sup}}[\Phi_{\mathrm{cl}}] \frac{\overleftarrow{\delta}}{\delta \Phi_{\mathrm{cl}}(x)} \right) \\
&= J^{\intercal}_{\mathrm{sup}}[\Phi_{\mathrm{cl}}](x) \,.
\end{aligned} \tag{2.23}$$

This equation is known as the quantum equation of motion by which the quantum effective action governs the dynamics of the field expectation value, taking the effects of all quantum fluctuations into account [126]. According to Eq. (2.21), evaluating the left-hand side of the quantum equation of motion at fields $\Phi_{\mathrm{cl},0}$ implies evaluating the right-hand side at vanishing source:

$$\forall x \in \mathbb{R} : \qquad \left(\Gamma[\Phi_{\mathrm{cl}}] \frac{\overleftarrow{\delta}}{\delta \Phi_{\mathrm{cl}}(x)} \right) \Bigg|_{\Phi_{\mathrm{cl}} = \Phi_{\mathrm{cl},0}} = 0 \,. \tag{2.24}$$

In other words, the physical field expectation value defines an extremal point of the quantum effective action. Since Γ is convex, $\Phi_{\mathrm{cl},0}$ must be its minimum. The physical field expectation value therefore represents the ground state of the system as defined by the quantum effective action. Thus, Eq. (2.24) is the quantum analog of the action principle of classical mechanics. In fact, it rather generalizes the classical action principle since the quantum effective action is identical to the classical action at leading order in the loop expansion. In order to see this, we will consider the path integral representation of the quantum effective action. Putting everything together, we obtain

$$\begin{aligned}
\mathrm{e}^{-\Gamma[\Phi_{\mathrm{cl}}]} &= \mathrm{e}^{W[J_{\mathrm{sup}}] - J^{\intercal}_{\mathrm{sup}}[\Phi_{\mathrm{cl}}] \cdot \Phi_{\mathrm{cl}}} = \mathcal{N} \int \mathcal{D}\Phi \; \mathrm{e}^{-S[\Phi] + J^{\intercal}_{\mathrm{sup}}[\Phi_{\mathrm{cl}}] \cdot (\Phi - \Phi_{\mathrm{cl}})} \\
&= \mathcal{N} \int \mathcal{D}\Phi \; \mathrm{e}^{-S[\Phi + \Phi_{\mathrm{cl}}] + J^{\intercal}_{\mathrm{sup}}[\Phi_{\mathrm{cl}}] \cdot \Phi} \\
&= \mathcal{N} \int \mathcal{D}\Phi \; \exp\left(-S[\Phi + \Phi_{\mathrm{cl}}] + \left(\Gamma[\Phi_{\mathrm{cl}}] \frac{\overleftarrow{\delta}}{\delta \Phi_{\mathrm{cl}}} \right) \cdot \Phi \right) \,,
\end{aligned} \tag{2.25}$$

where, from the first to the second line, we have performed a shift in the fields according to $\Phi \to \Phi + \Phi_{\mathrm{cl}}$, under which the differential remains unchanged. We have now arrived at a nonlinear first-order functional differential equation for the generating functional Γ. An exact solution to this differential equation has so far been found only for rare, special cases. Expanding the classical

[10] Understanding the first derivative of the quantum effective action as a right-derivative is motivated by the definition (2.17) or, equivalently, Eq. (2.22), in which the classical field is placed right to the source field. Our convention for the first derivative is convenient as it reproduces the same sign structure for the sources as defined in Eq. (2.6).

action around the field configuration at which the exponent on the right-hand side is stationary results in the loop expansion of the quantum effective action [121, 127–129]. The expansion up to one-loop order yields

$$\Gamma[\Phi_{\mathrm{cl}}] + W[0] = S[\Phi_{\mathrm{cl}}] + (-1)_{\Psi}\,\frac{1}{2}\,\mathrm{Tr}\left\{\mathrm{Ln}\left(\frac{S^{(1,1)}[\Phi_{\mathrm{cl}}]}{S^{(1,1)}[0]}\right)\right\} + \dots\,, \tag{2.26}$$

where we have used the notation

$$S^{(1,1)}[\Phi_{\mathrm{cl}}](x,y) = \frac{\overrightarrow{\delta}}{\delta\Phi^{\intercal}_{\mathrm{cl}}(x)} S[\Phi_{\mathrm{cl}}] \frac{\overleftarrow{\delta}}{\delta\Phi_{\mathrm{cl}}(y)}\,. \tag{2.27}$$

Through the perturbative treatment, we thus see that the functional Γ is composed of the classical action and a series of quantum corrections up to arbitrarily high loop orders. The classical limit would let the correction terms diminish until we are left with the classical action in the expansion above. Further notice that the classical and quantum effective action coincide up to some constant in case of a non-interacting theory.[11]

Having a look at the definition of the full and connected correlation functions, we identify Eq. (2.24) as the 1PI one-point correlation function, which always vanishes per construction. In the same spirit, we can also calculate all higher-order correlation functions from the quantum effective action. The 1PI Green's functions, also called proper vertex functions, are given by

$$\Gamma^{(n,m)}(x_1,\dots,y_m) = \left(\frac{\overrightarrow{\delta}}{\delta\Phi^{\intercal}_{\mathrm{cl}}(x_n)}\cdots\frac{\overrightarrow{\delta}}{\delta\Phi^{\intercal}_{\mathrm{cl}}(x_1)}\Gamma[\Phi_{\mathrm{cl}}]\frac{\overleftarrow{\delta}}{\delta\Phi_{\mathrm{cl}}(y_1)}\cdots\frac{\overleftarrow{\delta}}{\delta\Phi_{\mathrm{cl}}(y_m)}\right)\Bigg|_{\Phi_{\mathrm{cl}}=\Phi_{\mathrm{cl},0}}\,. \tag{2.28}$$

2.1.2 Controlling the infinities

Let us take a few steps back and review the path integral formulation of quantum field theory more closely. One of the fundamental differences between mechanics and field theory is the fact that the former deals with systems with a finite number of degrees of freedom while the latter describes systems with an infinite number of degrees of freedom, provided that space is assumed to be continuous. As a consequence, not all methods that have proven successful in mechanics can be easily carried over to field theory. In particular, a direct translation of the path integral from quantum mechanics into quantum field theory does not exist.[12] This also shows through UV divergences, that correlation functions in quantum field theory are notoriously plagued by.[13] These issues are particularly apparent in perturbation theory beyond tree level, even for processes including only small external momenta, since momentum conservation at each vertex of a Feynman diagram allows for arbitrarily high internal momenta to circulate around the loop. This leads to the realization that the partition functional (2.4) as well as all related objects are actually ill-defined and have so far only conceptual value. If a theory is supposed to yield physical predictions, the divergences need

[11] We could redefine the Schwinger functional to $W[J] = \ln(\mathcal{A}[J])$ to make the constant vanish, $W[0] = 0$. However, with foresight regarding the functional renormalization group, we decide to stick with the Schwinger functional as defined in Eq. (2.11). Also notice that field-independent terms added to the action do not alter the physics since they have no effect on the equations of motion or the correlation functions.

[12] There exists a Gaussian measure on the space of fields on $\mathbb{R}^d$ for all $d \geq 1$, but for $d \geq 2$ this measure is not supported on the space of ordinary functions [103].

[13] Notice that low-dimensional quantum field theories indeed can generate convergent correlation functions. There are also some four-dimensional supersymmetric theories that are actually free of divergences [130]. Moreover, non-relativistic Hamiltonian field theories with a so-called interior-boundary condition [131] also lead to well-defined results.

to be brought under control in some systematic manner.[14] More technically, this means that the divergent integrals must be subjected to a deformation procedure, the so-called regularization.

For the sake of simplicity, we perform the regularization process in momentum space and define the UV-regularized partition functional analogously to Eq. (2.4) but with a functional integral over the space of fields with energy at most $\Lambda \in \mathbb{R}^+$. More precisely, we modify all ordinary momentum-space integrals by restricting the integration domain to momenta satisfying the condition $|p| \lesssim \Lambda$.[15] As a consequence, the newly introduced momentum scale Λ is often referred to as the UV cutoff. We write the Λ-dependent functional as

$$\mathcal{Z}^\Lambda[J] = \mathcal{N} \int \mathcal{D}\Phi \; \mathrm{e}^{-S^\Lambda[\Phi]+J^\intercal\cdot\Phi} \,, \tag{2.29}$$

where the actual regularization process for the path integral is controlled by the Λ-dependence of the Gaussian measure. The normalization constant $\mathcal{N}$ can also carry a dependence on the cutoff but we will keep this dependence implicit for simplicity. Assuming Λ to be finite, we now have UV-regularized the theory by declaring that only momentum modes up the cutoff are allowed. In fact, there can be no UV divergence in any loop integral following from Eq. (2.29) since the UV region is simply absent. Moreover, the regularization procedure comes along with the benefit of giving the UV divergences a precise quantitative character, i.e., we are able to determine the degree of divergence from the behavior of the loop integral with respect to the cutoff as the cutoff tends to infinity.[16] Analogous to Eq. (2.9), the n-point functions are to be projected out of the generating functional and can be represented as a functional integral over fields, whose momentum modes are now constrained by the presence of a finite UV cutoff. The regularized functional (2.29) then serves as the formal basis for any investigation of quantum field theories. Phenomenologically speaking, the introduction of the cutoff, however, seems somewhat artificial because it is a priori unclear what a reasonable choice for the value of Λ would be. In order to make more sense of Eq. (2.29), we will discuss the Wilsonian viewpoint on quantum field theory, which also provides a comprehensive and illustrative approach to the renormalization group (RG) method.

The aforementioned infinities only occur if we consider phenomena at arbitrarily short distances or, equivalently, arbitrarily high energies. Put differently, the framework of quantum field theory as defined by Eq. (2.4) breaks down if we assume the theory to be valid at all momentum scales, no matter how high. It would, however, be naive to believe that a given theory would hold to arbitrarily high energies. We would instead expect that, with increasing energy, other particles would become more relevant until that theory under consideration would become merely part of a larger and richer theory. Our ability to experience the world of high-energy physics is limited, either by the resolution of a detector or by the power of the particle accelerator, and in principle we cannot know what new physics may lay just out of reach of our best measuring apparatus. We should therefore follow the philosophy from the very beginning of this section and assume

[14] On a non-compact spacetime manifold, quantum field theories with massless particles also suffer from IR divergences. This is, however, a separate issue and unrelated to the origin of UV divergences.

[15] Many textbooks use the historically motivated prescription $|p| \leq \Lambda$, which indicates the implementation of a so-called sharp UV regularization, $(2\pi)^{-4} \int_{|p|\leq\Lambda} \mathrm{d}^4p \, f(p) = \int_p \theta(\Lambda^2 - p^2) \, f(p)$ with θ being the Heaviside step function. However, a sharp cutoff leads to non-local interactions and spoils the derivative expansion [132, 133]. Our notation therefore indicates that the suppression of high-momentum modes can also be implemented more smoothly.

[16] In very simple scenarios, the chosen regularization prescription may already be enough to eliminate the divergence and can assign a definite value to the regularized integral even in the limit $\Lambda \to \infty$. For example, applying a symmetric UV regularization to the one-dimensional integral over an odd function and then considering the limit $\Lambda \to \infty$ corresponds to taking the Cauchy principal value, which yields zero, regardless of the function's behavior at large values of the cutoff. The majority of divergences in quantum field theory, however, survive the regularization process and can be categorized as logarithmic divergences, $\lim_{\Lambda\to\infty} \ln(\Lambda)$, or divergences of order $n \in \mathbb{N}$, $\lim_{\Lambda\to\infty} \Lambda^n$.

that every theory comes with an inherent restriction for its domain of reliability. In fact, models for statistical systems usually come with a microscopic scale $a > 0$, which corresponds to, e.g., a lattice spacing, an intermolecular distance, the Planck length, etc. That scale then represents a lower bound of resolution in position space and may as well be translated into an upper bound of energy in momentum space, $\Lambda \sim a^{-1} < \infty$. This line of argumentation has been formalized by Wilson [85, 86, 132, 134, 135] such that the cutoff Λ does not primarily represent a technical tool to allow for a well-defined framework but instead parameterizes the domain of validity for our theory. Then the cutoff has physical significance and should be regarded as being part of the definition of the theory at hand. Notice that, generally speaking, mathematical and physical validity are completely separate issues. In fact, a theoretical description of a physical system can be mathematically well-defined yet physically unreasonable and even be mathematically ill-defined while allowing us to extract meaningful results [136, 137]. The interesting observation, however, is that these two concepts can be conveniently connected in the Wilsonian approach to quantum field theory.

In the context of condensed-matter theory, the short-distance physics, i.e., the interactions between electrons and ions at atomic length scales, is well understood. Once all parameters in the classical action are set to their physical values, macroscopic observables can be computed by evaluating the path integral. In the spirit of Wilson, we understand a theory as defined by S^Λ as an effective field theory, which embodies the part of physics that is experimentally accessible at the energy scale Λ. Phenomenologically speaking, the cutoff then represents a threshold beyond which physics relevant for shorter distances is not included. This has laid the philosophical foundation for modern quantum field theory in the sense that most theories are nowadays considered effective descriptions of the world. For all practical purposes, the effective theory should only include degrees of freedom, which are relevant for the observable of interest, even if we know what the more general theory would be. The idea behind constructing an effective theory is that it allows us to do physics at energy scales lower than Λ while consistently ignoring phenomena occurring at energy scales above Λ. That this is indeed possible should become clear from the fact that, for example, we are able to reliably do chemistry without needing to know anything about quarks and gluons. Likewise, we do not need quantum gravity in order to understand the hydrogen atom. So there is a hierarchy of scales in nature that enables us to consistently leave out high-energy degrees of freedom in the description of low-energy phenomena. Some theories defined at Λ may have zero or even multiple UV extensions, which give rise to the same infrared physics. The existence of such an extension to higher energy scales is, however, of no relevance if we are interested in observables as obtained from experiments run at energies much lower than Λ. Effective field theories are therefore strategically crafted approximations by definition and form the counterpart to the "theory of everything", which is supposed to hold up to arbitrarily high energies. Overall, effective field theories have proven to be extremely successful not only because they help establish the correct effective degrees of freedom for a given low-energy phenomenon but also because they can be used to narrow down the energy scale at which new physics is supposed to come in. For more information on effective field theories and their applications see, e.g., Refs. [138–141].

By construction, the UV-regularized generating functional (2.29) ensures that we restrict our investigation of phenomena to those occurring at energies less than Λ rather than infinitely high energies. According to the statistical analogy, the cutoff value would ideally be chosen based on physics to match the energy scale at which our effective field degrees of freedom are an appropriate description of the world. However, in the realm of high-energy physics, the multitude of possible effective interactions is more difficult to control experimentally we cannot directly infer the cutoff value associated with some given action from experiment. Composite particles can be stable

over ranges of energy, elementary particles may principally not be detectable in isolation, some suggested particles might not even exist, and lastly, for reasons of time and budget, we certainly cannot turn to the nearest particle accelerator every time someone comes up with new ideas on how to construct the classical action. In addition, the world is continuous on measurable scales of space and time, i.e., the behavior of particles in high-energy physics is best understood in terms of continuum field theories which have no explicit dependence on a fundamental microscopic scale. Therefore, the cutoff of a continuum quantum field theory does a priori not refer to a physical scale of the system. But if the cutoff value is unknown and the calculations are sensitive to its choice, then Λ acts as a free parameter, reducing the predictive power of our theory. Generally speaking, the solution to this problem involves a tuning of the couplings of the effective field theory S^Λ so that the low-energy predictions are independent of the high-energy cutoff. In modern quantum field theory, the couplings contained in the classical action are not measurable quantities but rather mathematical parameters that must be defined such that reasonable results for observables can be obtained. In principle, one can require the couplings of the theory to depend on the cutoff in a way that ensures the low-energy physics to be Λ-independent although, in practice, this tuning is most commonly based on the introduction of counterterms [118, 142]. Coupling parameters, which have been tuned in this way, will be referred to as fixed couplings in the following and together constitute a fixed theory. Once the parameters at the cutoff scale have been fixed, we have

$$\frac{\mathrm{d}}{\mathrm{d}\Lambda}\langle \mathcal{O}_1 \dots \mathcal{O}_n \rangle^\Lambda = 0 \,, \tag{2.30}$$

where the momentum transfer associated with the observable is assumed to be small compared to Λ. It is important to mention that Eq. (2.30) does not automatically imply that we can perform a meaningful continuum limit, i.e., set $\Lambda \to \infty$, and thereby completely remove the cutoff from the framework. Nevertheless, Λ should always be much greater than any dimensionful quantity of interest to make sure their influence on the dynamics of the system does not get spoiled by the presence of a momentum cutoff. Therefore, the phenomenological meaning of the cutoff in quantum field theory is only loosely connected to the inherent validity bound of the theory in the sense that the value of Λ is constrained from below by all internal scales of the system. For a related discussion with emphasis on the effective average action and the influence of external parameters such as temperature or chemical potential, see Section 2.2.4. Furthermore, we would like to highlight that the independence of all physical observables from the scale Λ at which we fix the theory is only ensured if we can perform the path integral exactly. In other words, the implementation of approximations generally leads to a residual dependence on Λ. As a result, the ability to make a choice for Λ, which renders our results reliable to the extent of the approximation in use, requires a lot of physical as well as mathematical insight.

The path integral approach to quantum field theory is now well-defined through the imposition of a high-momentum cutoff. Based on the work of Kadanoff [143], Wilson proceeded by laying out the momenta contributing to the path integral in an orderly set of regions such that they could be analyzed one by one. Fluctuations at high energies can be progressively integrated out to obtain an effective description of the same theory at lower energies. Let us follow Wilson's approach and consider having a theory fixed at some UV scale Λ. For any lower energy scale $b\Lambda < \Lambda$ with

$b \in (0,1)$, we can decouple the high-momentum modes of the fields according to

$$\begin{aligned}\Phi(x) &= \int_{|p|\lesssim\Lambda} \frac{\mathrm{d}^4p}{(2\pi)^4}\, \mathrm{e}^{\mathrm{i}p^\intercal x}\, \Phi(p) \\ &= \int_{|p|\lesssim b\Lambda} \frac{\mathrm{d}^4p}{(2\pi)^4}\, \mathrm{e}^{\mathrm{i}p^\intercal x}\, \Phi(p) + \int_{b\Lambda<|p|\lesssim\Lambda} \frac{\mathrm{d}^4p}{(2\pi)^4}\, \mathrm{e}^{\mathrm{i}p^\intercal x}\, \Phi(p) \\ &\coloneqq \Phi_-(x) + \Phi_+(x)\end{aligned} \tag{2.31}$$

and study their effects on the system.[17] Notice that the relation above captures the process of decoupling purely qualitatively. The actual separation of momentum modes depends on how the UV regularization is implemented, i.e., precisely how fluctuations with energy beyond a certain scale are suppressed within the path integral. In fact, there are infinitely many ways of performing the separation of high-momentum modes and choosing one way may be referred to as choosing a regularization scheme. Once all fluctuations are integrated out exactly, physical quantities are independent of our choice so it is not necessary to specify a particular scheme at this stage.[18] For the sake of clarity, we will portray the classical action in the following not only as a functional of the quantum field but also as a function of couplings g_i. In this context, we will count the mass parameter as a coupling. In accordance with our definition of the superfield, we use the notation

$$-D^2 = \begin{pmatrix} -\partial^2 & 0 & 0 \\ 0 & 0 & \mathrm{i}\not{\partial}^\intercal \\ 0 & \mathrm{i}\not{\partial} & 0 \end{pmatrix}, \qquad M^2 = \begin{pmatrix} m_\varphi^2 & 0 & 0 \\ 0 & 0 & -\mathrm{i}m_\psi^\intercal \\ 0 & \mathrm{i}m_\psi & 0 \end{pmatrix} \tag{2.32}$$

and write the action as

$$\begin{aligned}S^\Lambda[\Phi](g_{i,0}) &= \int_x \mathcal{L}(\Phi(x), \partial_\mu\Phi(x), g_{i,0}) \\ &= \int_x \left(\frac{1}{2}\Phi^\intercal(x) \left[-D^2\right] \Phi(x) + \Phi^\intercal(x)\, \frac{M_0^2}{2}\, \Phi(x) + \dots \right),\end{aligned} \tag{2.33}$$

where $\mathcal{L}$ denotes the corresponding Lagrangian density. However, for consistency with common terminology in field theory, we will omit the word *density* in the following and just refer to $\mathcal{L}$ as the Lagrangian. The differential of the path integral factorizes according to Eq. (2.31) such that we can integrate out the high-momentum degrees of freedom Φ^+ in the path integral. Performing the functional integral at vanishing sources yields[19]

$$\mathcal{Z}^\Lambda = \mathcal{N} \int \mathcal{D}\Phi\, \mathrm{e}^{-S^\Lambda[\Phi](g_{i,0})} = \mathcal{N}' \int \mathcal{D}\Phi_-\, \mathrm{e}^{-S^{b\Lambda}[\Phi_-](g'_{i,b})}, \tag{2.34}$$

[17] Such a decoupling of high-momentum modes is not possible for quantum field theories on a non-commutative spacetime [144]. We will, however, only consider the more conventional case in which the decoupling is indeed allowed.

[18] One may be worried about the impact of the regularization scheme on observables due to the clearly scheme-dependent contribution from fluctuations at scales close to Λ. Notice, however, that this is accounted for by the fixed couplings whose values also depend on the scheme. Two generating functionals defined with a different scheme but the same cutoff Λ are supposed to give the same n-point functions, if Λ is much bigger than any physical scale of interest and specifically if the parameters of the theory at the cutoff scale in each case are fixed based on the same IR physics. For a more in-depth discussion of scheme (in)dependence, we refer to, e.g., Refs. [145–147].

[19] A presentation of integrating out field degrees of freedom while taking into account finite sources is possible, see, e.g., Ref. [148]. For practical reasons, however, the source fields are defined on the support of the corresponding quantum fields and construct the generating functional once an effective field theory at some cutoff scale has been chosen. Therefore, our choice to set $J = 0$ does not interfere with Wilson's line of argumentation.

where we have used that

$$S^{b\Lambda}[\Phi_-](g'_{i,b}) = -\ln\left(\frac{\mathcal{N}}{\mathcal{N}'}\int \mathcal{D}\Phi_+ \, \mathrm{e}^{-S^{\Lambda}[\Phi_-+\Phi_+](g_{i,0})}\right) . \tag{2.35}$$

By integrating out the high-momentum degrees of freedom we have obtained a new low-energy effective action at the scale $b\Lambda$, which has all the short-range physics encoded that is associated with the dynamics of the underlying system within the spherical momentum shell of $b\Lambda < |p| \lesssim \Lambda$. In other words, through the process of functional integration, we can in principle determine the effects of a given field theory, which is defined at some energy scale Λ, on the physics at lower scales $b\Lambda < \Lambda$. Moreover, it directly follows from Eq. (2.34) that any observable with momenta of at most $b\Lambda$ as obtained from a theory defined at Λ is in particular an observable of a theory defined at $b\Lambda$ if the corresponding action functionals are related via Eq. (2.35). Strictly speaking, we aim at having a description of the system at mesoscopic length scales, i.e., lengths of order $\sim 1\,\mathrm{m}$ as encountered in our everyday life. These length scales translate to energies of $\sim 10^{-13}\,\mathrm{MeV}$, see Appendix A.2, which can in practice be safely set to zero for most numerical purposes. At the path integral level, such a procedure corresponds to integrating out all momenta or, equivalently, considering $b \to 0$, which ensures scheme independence. Following the line argumentation from above, lowering the parameter b down to zero would provide us with an action functional at infinitely large length scales. In practice, however, we do not end up with an action suitable for describing cosmic systems unless we incorporate the necessary degrees of freedom already at the cutoff scale.

The structure of the new Lagrangian generally follows the structure of the original Lagrangian $\mathcal{L}$ but shows additional correction terms, which compensate for the removal of high-momentum degrees of freedom from the path integral [118]. The newly generated terms are to arbitrary orders in the fields and are only constrained by the symmetries of the initial action. There is in particular the possibility for the generation of new local operators. These corrections carry all the information about the integration step and, after a reorganization of terms, change the original values of the couplings to $g'_{i,b}$. This leads us to

$$\begin{aligned} S^{b\Lambda}[\Phi_-](g'_{i,b}) &= \int_x \Bigg(\mathcal{L}(\Phi_-(x), \partial_\mu \Phi_-(x), g_{i,0}) \\ &\qquad + \frac{1}{2}\, \Phi_-^{\intercal}(x)\, X_b\left[-D^2\right]\, \Phi_-(x) + \Phi_-^{\intercal}(x)\, \frac{\Delta M_b^2}{2}\, \Phi_-(x) + \dots \Bigg) \\ &:= \int_x \left(\frac{1}{2}\, \Phi_-^{\intercal}(x)\, Z_b\left[-D^2\right]\, \Phi_-(x) + \Phi_-^{\intercal}(x)\, \frac{M_b'^2}{2}\, \Phi_-(x) + \dots \right) , \end{aligned} \tag{2.36}$$

where the dimensionless factor $Z_b = X_b + 1$ denotes the so-called wavefunction renormalization. In an ordering of the new Lagrangian in powers of derivative operators, the term of order D^2 is generally not only quadratic in the fields but rather incorporates a sum of all field combinations allowed by the symmetries of the theory. This means that the organization of terms into the form (2.36) leads to a general factor $Z_{\mathrm{gen},b}(\Phi)$ that carries a dependence on field degrees of freedom. For convenience, however, we will consider only its field-independent part here, i.e., we have $Z_b \equiv Z_{\mathrm{gen},b}(0)$. Furthermore, the wavefunction renormalization is generally different for bosons and fermions:

$$Z \equiv \begin{pmatrix} Z_\varphi & 0 & 0 \\ 0 & Z_\psi & 0 \\ 0 & 0 & Z_\psi \end{pmatrix} . \tag{2.37}$$

Notice that our choice for the shell parameter b was arbitrary. The implication is that, by integrating out momentum modes, the couplings and the wavefunction renormalization in the Lagrangian vary to account for the change in the degrees of freedom over which we take the path integral. This ensures that the value (2.34) is in fact independent of the scale at which we define our theory, provided this scale is not higher than our initial cutoff Λ.

After having integrated out short-distance degrees of freedom, the two actions S^{Λ} and $S^{b\Lambda}$ are not directly comparable since their theory content explicitly refers to different energy scales. In order to allow for a comparison, a rescaling of integration variables is necessary. We rescale the spacetime variables such that the quantum fluctuations are again limited from above by the initial cutoff and we further rescale the quantum fields in order to recover the canonically normalized kinetic term. Concretely, the rescaling is performed according to

$$x' = bx\,, \qquad p' = \frac{p}{b}\,, \qquad \Phi' = \begin{pmatrix} b^{-\varepsilon_\varphi} & 0 & 0 \\ 0 & b^{-\varepsilon_\psi} & 0 \\ 0 & 0 & b^{-\varepsilon_\psi} \end{pmatrix} \sqrt{Z_b}\,\Phi_-\,, \tag{2.38}$$

where ε_φ and ε_ψ denote the energy dimensions of the boson and fermion fields, respectively, see Appendix A.2 for details. The energy dimensions of the fermion and antifermion fields are the same. Although it has not been made explicit, the rescaled superfield is to be understood as a function of the rescaled representation-space variable. The relations above then lead us to

$$\begin{aligned} S^{b\Lambda}[\Phi_-](g'_{i,b}) &= S^{\Lambda}[\Phi'](g_i(b)) \\ &= \int_{x'} \left(\frac{1}{2}\,\Phi'^{\intercal}(x')\,\left[-D'^2\right]\Phi'(x') + \Phi'^{\intercal}(x')\,\frac{M^2(b)}{2}\,\Phi'(x') + \dots \right). \end{aligned} \tag{2.39}$$

The rescaled superfield Φ' again contains modes of momenta $|p'| \lesssim \Lambda$, which are, however, qualitatively different from the original ones since primed and unprimed variables refer to different physical scales. Still, the rescaling procedure is eminently beneficial because it lets us rewrite the operation of integrating out high-momentum degrees of freedom as a transformation of the Lagrangian. In particular, a term-by-term comparison of the Lagrangians corresponding to the classical actions (2.33) and (2.39) shows that a change in scale can be rephrased as a change in couplings. This leads to the realization that the couplings of the quantum fields are not constant but rather depend on the scale we choose to probe them.

A transformation describing the change of a quantity of interest under a change of scale through the process of eliminating and rescaling degrees of freedom is called a renormalization group transformation [149]. In general, RG transformations are complicated, non-linear transformations and depend on the chosen regularization scheme. All these transformations together form a set called the renormalization group, which is a group in the sense that it maps the set of all possible couplings onto itself. The RG, however, is only a semi-group in the mathematical sense since RG transformations are in general not invertible. Once we have integrated out field degrees of freedom in the path integral, we cannot integrate them back in. From a more phenomenological standpoint, renormalization group transformations typically involve a loss of information about the microscopic details of the system and, once information is lost, it cannot be recovered without ambiguities. Continuing the overall procedure by integrating over another momentum shell combined with another rescaling further transforms the Lagrangian. If we take the parameter b close to 1, the momentum shells eventually become infinitesimally thin such that the RG transformation

of the Lagrangian becomes a continuous one. In particular, notice that the value (2.34) or, more generally, the associated functional is an RG invariant,

$$\frac{\mathrm{d}}{\mathrm{d}b}\mathcal{Z}^{\Lambda}[J]=0\,, \tag{2.40}$$

such that this can be used to infer differential equations describing the change of a quantity of interest with respect to a change in b. Specifically, differential equations describing the change of a quantity under a continuous RG transformation are called RG flow equations. The rough idea here is that the solution to the RG flow equation describes a trajectory from high to low momentum scales in some mathematical space. This trajectory, the RG flow, is parameterized by the shell parameter b and the evolution of a quantity along this trajectory is driven by the process of integrating out quantum fluctuations associated with the scale $b\Lambda$.[20] Accordingly, successive integration steps in the path integral are often associated with a flow of the effective Lagrangian in so-called theory space, i.e., an abstract space in which each point corresponds to a specific set of coupling values. Once the RG transformation for an incremental change in scale has been established, finding the solution to the corresponding flow equation is equivalent to performing a non-perturbative calculation of the path integral.

The RG concept is surely appealing from a phenomenological point of view since it allows us to get a better understanding of the manifestations of a system at different scales. Moreover, the RG method as presented so far is exact, meaning that the strategy of gradually integrating out fluctuations must lead to the same result as the incorporation of all fluctuations at once. In particular, both options to compute a generating functional involve the need for functional integration. It is therefore important to point out that, if we could perform the integration step in Eq. (2.34) for some arbitrary value of b exactly, we might as well calculate the entire UV-regularized path integral and needed not to worry about any RG steps. In practice, however, exactly performing the path integral for some general interacting quantum field theory is not possible. One could in principle attempt to apply perturbation theory in order to turn one difficult integral into a series of simpler ones but this is not a universal solution. On the one hand, many interesting phenomena are inherently non-perturbative and, on the other hand, cases in which perturbative treatments are legitimate have often already been studied to a sufficient degree. Now, the usefulness of the RG method stems from the fact that it is considerably easier and overall more consistent to approximate the RG transformation than the generating functional itself. Provided that the momentum shell is sufficiently thin, the integration over this shell should result in an analytic RG transformation [149]. This does not contradict any properties of the generating functional, since non-analytic behavior can still arise in the end due to an infinite number of momentum shells that are to be integrated over. Nevertheless, as a consequence of the RG transformation being analytic, it is reasonable to introduce approximations into the calculation of the corresponding integral. In the RG approach, all momentum shells are treated uniformly and so the implemented approximations are uniformly good for all shells. If approximations are employed independently of a separation of degrees of freedom for different momentum shells, it is likely that those approximations will favor some momentum shells over others, which results in a qualitatively very different transition from the microscopic theory to the macroscopic description. It should, however, also be mentioned that truncations, which are employed during the RG process, generally lead to an artificial regularization scheme dependence for observables. Such a scheme dependence is unphysical but can be

[20] More generally, the RG flow is parameterized by the so-called RG scale, which is used to relate the lowered cutoff $\Lambda'=b\Lambda$ to the original one. We could call this RG scale t and generally write $\Lambda'\equiv\Lambda'_t=f(t)\,\Lambda$, where the function f determines the size of the momentum shell for some value of t. In the most simple case, the RG scale may be the shell parameter itself, i.e., $t=b$. A popular choice, however, is $f(t)=\mathrm{e}^{-t}$ such that RG scale $t=-\ln(\Lambda'/\Lambda)$ is logarithmic.

brought under control to some extent [150]. Nonetheless, genuine scheme independence can only be achieved for untruncated calculations.

There are many formulations of the RG method, which ultimately rely on the scaling ideas of Kadanoff and Wilson but nevertheless substantially differ in the way they are implemented,[21] see, e.g., Wegner [157, 158], Polchinski [159], Wetterich [87, 160, 161], or Refs. [162–164] for RG techniques specifically for quantum many-body systems. Therefore, the term RG is in practice more generically used to refer to the overall framework of characterizing the change in the description of a physical system when going from a microscopic to a macroscopic perspective. For introductory literature on the Wilson RG and its applications, see, e.g., Refs. [149, 165–169]. For general review articles on the RG, we refer to Refs. [170–174].

2.2 The functional renormalization group

We will now present a specific formulation of the renormalization group method, which is designed to study a generalized version of the quantum effective action. The so-called functional renormalization group (fRG) goes back to Wetterich [87] and combines the functional approach to quantum field theory with the concept of the Wilsonian RG. The fRG represents a powerful tool for investigating perturbative as well as non-perturbative effects in quantum field theory and statistical physics, for reviews see, e.g., Refs. [126, 175–180]. Therefore, the functional renormalization group constitutes the key method in our analysis of low-energy models of quantum chromodynamics in the subsequent chapter. At the heart of this method lies a characteristic RG flow equation, which we are going to carefully derive in the following. After that, we will discuss different aspects of regularization in the context of the fRG, in particular RG consistency.

2.2.1 Derivation of the characteristic RG flow equation

The starting point for our derivation is a properly regularized partition functional. As before, we assume the implementation of UV regularization as indicated by a superscript Λ. In addition, we introduce an auxiliary term $\Delta S_{k,\Lambda}$ in order to regularize the infrared modes in the path integral. The new scale $k \in [0, \Lambda]$ can be thought of as an IR cutoff such that modes with momenta $|p| \lesssim k$ are being suppressed. The goal of this approach is to build a one-parameter family of generating functionals, indexed by the RG scale k, that is able to interpolate between the initial state at $k = \Lambda$ in which nothing is integrated out and the final state at $k = 0$ in which all momenta are integrated out. In other words, quantum fluctuations contributing to the generating functional are taken into account smoothly by continuously lowering the RG scale. Concretely, the UV- as well as

[21] The name *renormalization group* has made its first appearance in a paper by Bogoljubov and Širkov [151], who picked up on the almost unnoticed work of Stückelberg and Petermann [152, 153] as well as independently developed ideas by Gell-Mann and Low [154]. The Stückelberg-Petermann RG is the group of finite renormalizations of the S-matrix in the framework of causal perturbation theory and predates the development of the RG in the context of condensed-matter field theory as done by Kadanoff and Wilson. However, the Stückelberg-Petermann RG did not find a way into mainstream physics and it was not until Wilson that conceptual problems with renormalization techniques could be resolved. Therefore, also forms of RG with a non-Wilsonian origin exist, which, of course, does not mean they cannot be linked [155, 156].

IR-regularized generating functional for full n-point correlation functions reads

$$\begin{aligned}\mathcal{Z}_k^\Lambda[J] &= \exp\left(-\Delta S_{k,\Lambda}\left[\frac{\vec{\delta}}{\delta J}\right]\right)\mathcal{Z}^\Lambda[J] \\ &= \mathcal{N}\int \mathcal{D}\Phi\ \exp\left(-S^\Lambda[\Phi]-\Delta S_{k,\Lambda}[\Phi]+J^\intercal\cdot\Phi\right) \\ &= \exp\left(W_k^\Lambda[J]\right)\,, \end{aligned} \tag{2.41}$$

where the new term $\Delta S_{k,\Lambda}$ is supposed to satisfy

$$\lim_{k\to 0}\Delta S_{k,\Lambda}[\Phi]=0\,,\qquad \lim_{k\to\Lambda}\left(\Delta S_{k,\Lambda}^{(1,1)}\right)^{-1}[0]=0\,. \tag{2.42}$$

The first condition guarantees that we recover the full partition functional in the infrared limit $k\to 0$, that is

$$\lim_{k\to 0}\mathcal{Z}_k^\Lambda[J]=\mathcal{Z}^\Lambda[J]\,. \tag{2.43}$$

The second condition in (2.42) states that $\Delta S_{k,\Lambda}$ carries a divergence in the UV limit such that the regularized propagator of the free theory suppresses any interactions at high scales. As a consequence, the vacuum persistence amplitude reduces to a constant in that limit,

$$\lim_{k\to\Lambda}\mathcal{A}_k^\Lambda[J]=1\,. \tag{2.44}$$

For a purely bosonic theory, the second condition can be expressed as $\lim_{k\to\Lambda}\Delta S_{k,\Lambda}[\varphi]\to\infty$ which then implies $\lim_{k\to\Lambda}\mathcal{Z}_k^\Lambda[j]=0$ and formalizes the idea that no quantum fluctuations are integrated out at $k=\Lambda$. In the case of having only fermions, the divergence in $\Delta S_{k,\Lambda}[\bar{\psi},\psi]$ now causes the partition functional to diverge at the UV cutoff as well, $\lim_{k\to\Lambda}\mathcal{Z}_k^\Lambda[\bar{\eta},\eta]\to\infty$. This antagonistic behavior will not prevent us from working with general scale-dependent generating functionals but rather shows that the reasoning behind the bosonic construction can rarely be carried over to the fermionic path integral and vice versa.

Through Eq. (2.41) we have already promoted the definition of the Schwinger functional to the scale-dependent case. In particular, the operator $\exp(-\Delta S_{k,\Lambda})$ should be positive on $\exp(W^\Lambda)$ [177], leading to a strictly convex Schwinger functional. In the framework of the renormalization group as introduced at the end of Section 2.1, Wilson introduced the shell parameter $b<1$ in order to characterize how momenta in the path integral description of generating functionals are getting integrated out. Specifically, this parameter was used to indicate that quantum fluctuations with momenta $b\Lambda<|p|\leq\Lambda$ have been integrated out. The integration process could then be described by successively lowering the effective UV cutoff by using smaller and smaller values of b. Notice that our description of the integration process is qualitatively different as we keep the UV cutoff fixed and instead lower the IR scale k. Moreover, the continuous scale k has been introduced independently of the scale Λ at which the theory is defined.

In principle, the structure of $\Delta S_{k,\Lambda}$ could be chosen arbitrarily as long as it regularizes the IR modes and fulfills the boundary conditions (2.42). In practice, however, the auxiliary term is chosen to be at most quadratic in the fields to guarantee the k-flow of the generating functional to have a one-loop structure [181]. It appears that the most suitable construction is an expression, which is exactly quadratic in the fields and which inherits all scale dependences from the regulator function $R_{k,\Lambda}$. Hence, the addition of $\Delta S_{k,\Lambda}$ to the classical action reflects the idea of introducing a

scale-dependent mass term, which suppresses the propagation of slow modes in the path integral [176, 179]. More specifically, the auxiliary term reads

$$\begin{aligned}\Delta S_{k,\Lambda}[\Phi] &= \frac{1}{2}\,\Phi^{\intercal}\cdot R_{k,\Lambda}\cdot\Phi = \frac{1}{2}\int_x\int_y \Phi^{\intercal}(x)\,R_{k,\Lambda}(x,y)\,\Phi(y) \\ &= \frac{1}{2}\int_x\int_y \varphi(x)\,R^{\varphi}_{k,\Lambda}(x,y)\,\varphi(y) + \int_x\int_y \bar{\psi}(x)\,R^{\psi}_{k,\Lambda}(x,y)\,\psi(y)\,, \end{aligned} \tag{2.45}$$

where the regulator function, or just regulator for short, has the following structure in field space,

$$R(x,y) = \begin{pmatrix} R^{\varphi}(x,y) & 0 & 0 \\ 0 & 0 & -\big(R^{\psi}\big)^{\intercal}(y,x) \\ 0 & R^{\psi}(x,y) & 0 \end{pmatrix} = R^{\intercal}(y,x)\,(-1)_{\Psi}\,. \tag{2.46}$$

Since fermionic and bosonic propagators are mathematically different, the regulator for fermions is also distinct from that for bosons. In principle, we do not want our regulator insertion to lead to artificial effects when calculating observables. This means that the regulator needs to respect certain physically motivated conditions. For example, the regulator is generally supposed to respect the symmetries of the unregularized theory. Likewise, UV regularization should not spoil any symmetries either but we simply assume here that the UV cutoff is properly implemented in order to focus on the behavior of the system with respect to k. The IR scale k does not necessarily refer to a physical scale since its meaning and the corresponding RG flow highly depend on the regularization scheme,[22] i.e., how exactly the regulator couples to the momentum modes in the path integral. As in the Wilsonian case, scheme dependences of observables are completely removed once all momenta are integrated out exactly.

We are now able to define the scale-dependent generalization of the full quantum effective action. The generating functional of one-particle irreducible correlation functions in the presence of an infrared cutoff scale k is usually called effective average action [182–184], but can also be referred to as the coarse-grained effective action because quantum fluctuations on length scales smaller than $1/k$ have been integrated out [185].

$$\Gamma^{\Lambda}_k[\Phi_{\mathrm{cl}}] = \sup_J\big(J^{\intercal}\cdot\Phi_{\mathrm{cl}} - W^{\Lambda}_k[J]\big) - \Delta S_{k,\Lambda}[\Phi_{\mathrm{cl}}]\,. \tag{2.47}$$

Compared to Eq. (2.17), this definition makes use of a modified Legendre transformation. As a consequence, the effective average action does not need to be convex for $k > 0$, whereas a pure Legendre transformation is always convex by definition [123]. Nevertheless, the additional term $\Delta S_{k,\Lambda}$ is necessary in order to ensure that the effective average action can be associated with the classical action in the limit $k \to \Lambda$. This UV boundary condition for the effective average action is reasonable as it is consistent with the loop expansion (2.26) in the sense that only the leading-order contribution survives when no quantum fluctuations are integrated out. As before, we use the supremum condition to work out the relation between the classical field and the source field in the definition of the effective average action.

$$\Phi_{\mathrm{cl}}(x) = \left(\frac{\vec{\delta}}{\delta J^{\intercal}(x)}W^{\Lambda}_k[J]\right)\bigg|_{J=J^{\Lambda}_{\mathrm{sup},k}} = \langle\!\langle\Phi(x)\rangle\!\rangle^{\Lambda}_{J^{\Lambda}_{\mathrm{sup},k},k} = \langle\!\langle\Phi(x)\rangle\!\rangle_{J_{\mathrm{sup}}}\,. \tag{2.48}$$

[22] In principle, the same argument applies to the Wilsonian shell parameter b, albeit in a much milder version. The concrete meaning of an RG scale and the corresponding flow always depends on the chosen implementation of regularization. In the Wilsonian case, however, the parameter b directly receives its meaning from the UV cutoff Λ. So if UV regularization is assumed to be properly implemented and comes along with a physical scale Λ, then also b refers to some physical scale.

Notice that the classical superfield $\Phi_{\rm cl}$ enters Eq. (2.47) as a new independent variable, which means that it is in principle independent of any scales that other expectation values of quantum fields are subjected to.[23] As a consequence, the supremum condition provides us with a source field $J^{\Lambda}_{{\rm sup},k}[\Phi_{\rm cl}]$, which has inherited all scale dependences from the Schwinger functional such that the expectation value (2.48) is overall scale-independent. This result allows us to resolve the explicit supremum prescription in the definition of the effective average action and write Eq. (2.47) as

$$\Gamma^{\Lambda}_{k}[\Phi_{\rm cl}] = J^{\Lambda\intercal}_{{\rm sup},k}[\Phi_{\rm cl}]\cdot\Phi_{\rm cl} - W^{\Lambda}_{k}[J^{\Lambda}_{{\rm sup},k}] - \Delta S_{k,\Lambda}[\Phi_{\rm cl}]\,. \tag{2.49}$$

As in the scale-independent case, we can obtain a functional differential equation for the effective average action by means of a few simple manipulations. We begin by evaluating the first derivative acting from the right by making use of the quantum equation of motion (2.23) from the previous section:

$$\begin{aligned}\Gamma^{\Lambda}_{k}[\Phi_{\rm cl}]\frac{\overleftarrow{\delta}}{\delta\Phi_{\rm cl}(y)} &= \left(\Gamma[\Phi_{\rm cl}]\frac{\overleftarrow{\delta}}{\delta\Phi_{\rm cl}(y)}\right)\Big|_{\Gamma=\Gamma^{\Lambda}_{k}} - \Delta S_{k,\Lambda}[\Phi_{\rm cl}]\frac{\overleftarrow{\delta}}{\delta\Phi_{\rm cl}(y)} \\ &= J^{\intercal\,\Lambda}_{{\rm sup},k}[\Phi_{\rm cl}](y) - \int_{x}\Phi^{\intercal}_{\rm cl}(x)\,R_{k,\Lambda}(x,y)\,.\end{aligned} \tag{2.50}$$

Analogously to Eq. (2.25), we can then set up a functional differential equation for the effective average action. Specifically, we obtain

$$\begin{aligned}\mathrm{e}^{-\Gamma^{\Lambda}_{k}[\Phi_{\rm cl}]} &= \mathrm{e}^{W^{\Lambda}_{k}[J^{\Lambda}_{{\rm sup},k}]-J^{\intercal\,\Lambda}_{{\rm sup},k}[\Phi_{\rm cl}]\cdot\Phi_{\rm cl}+\Delta S_{k,\Lambda}[\Phi_{\rm cl}]} \\ &= \mathcal{N}\int\mathcal{D}\Phi\;\mathrm{e}^{-S^{\Lambda}[\Phi]-\Delta S_{k,\Lambda}[\Phi]+J^{\intercal\,\Lambda}_{{\rm sup},k}[\Phi_{\rm cl}]\cdot(\Phi-\Phi_{\rm cl})+\Delta S_{k,\Lambda}[\Phi_{\rm cl}]} \\ &= \mathcal{N}\int\mathcal{D}\Phi\;\mathrm{e}^{-S^{\Lambda}[\Phi+\Phi_{\rm cl}]-\Delta S_{k,\Lambda}[\Phi]-\Phi^{\intercal}_{\rm cl}\cdot R_{k,\Lambda}\cdot\Phi+J^{\intercal\,\Lambda}_{{\rm sup},k}[\Phi_{\rm cl}]\cdot\Phi} \\ &= \mathcal{N}\int\mathcal{D}\Phi\;\exp\left(-S^{\Lambda}[\Phi+\Phi_{\rm cl}]-\Delta S_{k,\Lambda}[\Phi]+\left(\Gamma^{\Lambda}_{k}[\Phi_{\rm cl}]\frac{\overleftarrow{\delta}}{\delta\Phi_{\rm cl}}\right)\cdot\Phi\right)\,,\end{aligned} \tag{2.51}$$

where we have used that

$$\Delta S_{k,\Lambda}[\Phi+\Phi_{\rm cl}] = \Delta S_{k,\Lambda}[\Phi] + \Delta S_{k,\Lambda}[\Phi_{\rm cl}] + \Phi^{\intercal}_{\rm cl}\cdot R_{k,\Lambda}\cdot\Phi \tag{2.52}$$

after shifting in the field according to $\Phi\to\Phi+\Phi_{\rm cl}$. As the auxiliary term diverges in the limit $k\to\Lambda$, the saddle point method applied to the path integral shows that the effective average action reduces to the classical action up to a potentially infinite additive constant. In the infrared limit $k\to 0$, the effective average action agrees exactly with the generating functional of 1PI correlation functions.

$$\lim_{k\to 0}\Gamma^{\Lambda}_{k}[\Phi_{\rm cl}] = \Gamma^{\Lambda}[\Phi_{\rm cl}]\,,\qquad \lim_{k\to\Lambda}\Gamma^{\Lambda}_{k}[\Phi_{\rm cl}] = \text{const.} + S^{\Lambda}[\Phi_{\rm cl}]\,. \tag{2.53}$$

The constant contribution in the UV limit arises since the definition of the scale-dependent Schwinger functional in Eq. (2.41) makes use of the partition functional rather than the vacuum persistence amplitude, see also Eq. (2.26). That constant, however, does not carry any physical content

[23] It is nevertheless possible to simply choose the classical field to be scale-dependent in order to eventually arrive at a more general version of the fRG, which is sometimes called essential renormalization group [186] or fRG with flowing fields [187]. Notice that this idea is related to dynamical hadronization techniques that are designed to perform a rebosonization of multi-fermion interactions in every RG step, see, e.g., Refs. [188–190].

so we can ignore it in the following. Thus, the effective average action has the property that it interpolates smoothly between the classical action and the full quantum effective action as the scale k is lowered from the ultraviolet cutoff down to zero.

The non-linear functional differential equation (2.51) for the effective average action is a generalized version of Eq. (2.25) and the possibility of finding an exact solution for non-trivial situations is intensely hindered by its complexity. Since exact solutions are only realistic for some limiting cases, it is crucial to find a formulation, which permits non-perturbative approximations. We therefore make explicit use of the k-dependence of the generalized generating functionals in order to construct an RG flow equation of the effective average action. The response of the Schwinger functional to an infinitesimal variation of k is readily given by

$$\begin{aligned}
\partial_k W_k^\Lambda[J] &= \frac{1}{\mathcal{Z}_k^\Lambda[J]}\,\partial_k \mathcal{Z}_k^\Lambda[J] = \frac{1}{\mathcal{Z}_k^\Lambda[J]}\,\mathcal{N}\int \mathcal{D}\Phi\,\left(-\partial_k \Delta S_{k,\Lambda}[\Phi]\right)\,\mathrm{e}^{-S^\Lambda[\Phi]-\Delta S_{k,\Lambda}[\Phi]+J^\intercal\cdot\Phi} \\
&= \frac{1}{\mathcal{Z}_k^\Lambda[J]}\,\mathcal{N}\int \mathcal{D}\Phi\,\left(-\frac{1}{2}\Phi^\intercal\cdot\partial_k R_{k,\Lambda}\cdot\Phi\right)\,\mathrm{e}^{-S^\Lambda[\Phi]-\Delta S_{k,\Lambda}[\Phi]+J^\intercal\cdot\Phi} \\
&= -\frac{(-1)_\Psi}{2}\,\mathrm{Tr}\left\{\partial_k R_{k,\Lambda}\cdot\frac{1}{\mathcal{Z}_k^\Lambda[J]}\,\mathcal{N}\int \mathcal{D}\Phi\;\Phi\Phi^\intercal\,\mathrm{e}^{-S^\Lambda[\Phi]-\Delta S_{k,\Lambda}[\Phi]+J^\intercal\cdot\Phi}\right\} \\
&= -\frac{(-1)_\Psi}{2}\,\mathrm{Tr}\left\{\partial_k R_{k,\Lambda}\cdot\left(G_k^{(2)\Lambda}[J]+\langle\!\langle\Phi\rangle\!\rangle_{J,k}^\Lambda\langle\!\langle\Phi^\intercal\rangle\!\rangle_{J,k}^\Lambda\right)\right\} \\
&= -\frac{(-1)_\Psi}{2}\,\mathrm{Tr}\left\{\partial_k R_{k,\Lambda}\cdot G_k^{(2)\Lambda}[J]\right\}-\frac{1}{2}\,\langle\!\langle\Phi^\intercal\rangle\!\rangle_{J,k}^\Lambda\cdot\partial_k R_{k,\Lambda}\cdot\langle\!\langle\Phi\rangle\!\rangle_{J,k}^\Lambda\,.
\end{aligned}\tag{2.54}$$

Above, we have used the scale-dependent connected two-point Green's function $G_k^{(2)\Lambda}$ analogously to the definition (2.15). Also notice that we have used ∂_k to refer to a total derivative with respect to k in accordance with standard literature on RG. With this result for the behavior of the Schwinger functional with respect to a change in k, we can now write the RG flow of the effective average action (2.49) as

$$\begin{aligned}
\partial_k\Gamma_k^\Lambda[\Phi_{\mathrm{cl}}] &= \partial_k J_{\mathrm{sup},k}^{\intercal\Lambda}[\Phi_{\mathrm{cl}}]\cdot\Phi_{\mathrm{cl}}-\partial_k W_k^\Lambda[J_{\mathrm{sup},k}^\Lambda]-\frac{1}{2}\Phi_{\mathrm{cl}}^\intercal\cdot\partial_k R_{k,\Lambda}\cdot\Phi_{\mathrm{cl}} \\
&= \frac{(-1)_\Psi}{2}\,\mathrm{Tr}\left\{\partial_k R_{k,\Lambda}\cdot G_k^{(2)\Lambda}[J_{\mathrm{sup},k}^\Lambda]\right\}\,,
\end{aligned}\tag{2.55}$$

where we have used that

$$\partial_k W_k^\Lambda[J_{\mathrm{sup},k}^\Lambda] = \left(\partial_k W_k^\Lambda[J]\right)\Big|_{J=J_{\mathrm{sup},k}^\Lambda}+\partial_k J_{\mathrm{sup},k}^{\intercal\Lambda}[\Phi_{\mathrm{cl}}]\cdot\Phi_{\mathrm{cl}}\,.\tag{2.56}$$

Our next goal is to rewrite Eq. (2.55) in order to obtain a self-consistent equation for the effective average action. To this end, we compute the field-dependent 1PI two-point Green's function by differentiating Eq. (2.50) from the left:

$$\Gamma_k^{(1,1)\Lambda}[\Phi_{\mathrm{cl}}](x,y) = \frac{\overrightarrow{\delta}}{\delta\Phi_{\mathrm{cl}}^\intercal(x)}\Gamma_k^\Lambda[\Phi_{\mathrm{cl}}]\frac{\overleftarrow{\delta}}{\delta\Phi_{\mathrm{cl}}(y)} = \frac{\overrightarrow{\delta}}{\delta\Phi_{\mathrm{cl}}^\intercal(x)}J_{\mathrm{sup},k}^{\intercal\Lambda}[\Phi_{\mathrm{cl}}](y)-R_{k,\Lambda}(x,y)\,.\tag{2.57}$$

If two functions are related by a Legendre transform, their curvatures are inverses of each other. In the case of a modified Legendre transform (2.47), we observe that the source-dependent connected two-point Green's function can be represented as the inverse of the sum of the field-dependent 1PI

two-point correlator and the regulator function, i.e., it holds that

$$G_k^{(2)\Lambda}[J^\Lambda_{\mathrm{sup},k}](x,y) = \left(\frac{\overrightarrow{\delta}}{\delta J^\intercal(x)}\frac{\overrightarrow{\delta}}{\delta J(y)}W_k^\Lambda[J]\right)\Big|_{J=J^\Lambda_{\mathrm{sup},k}} = \left(\frac{\overrightarrow{\delta}}{\delta J^\intercal(x)}\langle\!\langle \Phi^\intercal(y)\rangle\!\rangle^\Lambda_{J,k}\right)\Big|_{J=J^\Lambda_{\mathrm{sup},k}}$$
$$= \left(\frac{\overrightarrow{\delta}}{\delta\langle\!\langle \Phi^\intercal(x)\rangle\!\rangle}J^{\intercal\,\Lambda}_{\mathrm{sup,k}}[\langle\!\langle\Phi\rangle\!\rangle](y)\right)^{-1}\Bigg|_{\langle\!\langle\Phi\rangle\!\rangle=\Phi_{\mathrm{cl}}} = \left(\Gamma_k^{(1,1)\Lambda}[\Phi_{\mathrm{cl}}]+R_{k,\Lambda}\right)^{-1}(x,y)\,. \quad (2.58)$$

Notice that the definition of the two-point Green's function involves two left-derivatives whereas the 1PI two-point correlator (2.57) is defined through one left- and one right-derivative. This means that directions of functional derivatives are apparently not "conserved" by the inversion process. The positivity property of the regularized connected two-point Green's function implies that its inverse must be positive definite as well.[24] This can also be seen from the pure Legendre transform

$$\check{\Gamma}_k^\Lambda[\Phi_{\mathrm{cl}}] := \sup_J\left(J^\intercal\cdot\Phi_{\mathrm{cl}} - W_k^\Lambda[J]\right) = \Gamma_k^\Lambda[\Phi_{\mathrm{cl}}] + \Delta S_{k,\Lambda}[\Phi_{\mathrm{cl}}]\,, \quad (2.59)$$

which is strictly convex per construction such that its second derivative

$$\frac{\overrightarrow{\delta}}{\delta\Phi^\intercal_{\mathrm{cl}}(x)}\check{\Gamma}_k^\Lambda[\Phi_{\mathrm{cl}}]\frac{\overleftarrow{\delta}}{\delta\Phi_{\mathrm{cl}}(y)} = \left(\Gamma_k^{(1,1)\Lambda}[\Phi_{\mathrm{cl}}]+R_{k,\Lambda}\right)(x,y) \quad (2.60)$$

is positive definite. In particular, this means the functional determinant of Eq. (2.60) is positive. At the same time, we know that the effective average action is not necessarily convex for $k>0$, i.e., analogous positivity properties do not follow for the scale-dependent 1PI two-point correlator. As a consequence, the regulator has to be at least positive definite in order to make sure that the object (2.60) is positive definite. We further remark that, due to the relation (2.58), the scale-dependent connected Green's function is often referred to as the average propagator, which makes the quantity (2.60) the inverse average propagator of the theory defined by the corresponding effective average action at the scale k.

Let us use our result to write the flow equation for the effective average action as

$$\partial_k\Gamma_k^\Lambda[\Phi_{\mathrm{cl}}] = \frac{(-1)_\Psi}{2}\,\mathrm{Tr}\left\{\partial_k R_{k,\Lambda}\cdot\left(\Gamma_k^{(1,1)\Lambda}[\Phi_{\mathrm{cl}}]+R_{k,\Lambda}\right)^{-1}\right\}\,. \quad (2.61)$$

This is a non-linear functional differential equation for the effective average action, which, compared to Eq. (2.51), comes along with no need for functional integration. Together with the UV boundary condition in Eq. (2.53), the flow equation completely determines the effective average action and therefore in particular the IR physics of a given system as defined by the classical action. The main advantages of such a formulation are its suitability for truncations of the full theory as well as its numerical accessibility [177, 182]. The Eq. (2.61) constitutes the characteristic RG flow equation of the functional renormalization group and is commonly known as the Wetterich

[24] Notice that the scale-dependent connected two-point Green's function at exactly $k=0$ is positive semi-definite but not positive definite, see Eq. (2.16). This means the connected two-point Green's function is a priori not invertible such that we would not be able to compute a meaningful 1PI two-point correlator in accordance with Eq. (2.58). This however does not automatically forbid the existence of an inverse in the limit $k\to 0$. In addition, we will often have to use approximations enabling us to solve the flow equation for the effective average action and we are going to assume that these approximations allow for a well-defined 1PI two-point correlator at all scales. For exact calculations, the relevance of zero modes of the infrared Green's function needs indeed to be addressed with care. In this context, see also Ref. [191].

equation. It has a one-loop structure, see Eq. (2.26), but is nevertheless an exact equation since the loop contains the exact average propagator. The Wetterich equation is an infrared evolution equation for the k-dependence of the effective average action and, in contrast to the Wilsonian RG, not an RG equation established by infinitesimally lowering a UV cutoff. With the initial condition at $k = \Lambda$ at hand, the ability to follow the evolution to $k = 0$ is equivalent to the ability to solve the theory completely.

Given a theory with an effective cutoff Λ, the solution of the Wetterich equation describes a trajectory towards the full quantum effective action in the space of all possible action functionals [188]. This trajectory is parameterized by the RG scale k and has its endpoints at $k = \Lambda$ and $k = 0$, as given by Eq. (2.53). The functional satisfying the Wetterich equation is, in essence, nothing but the quantum effective action but with the distinction that only quantum fluctuations with momenta $k^2 \lesssim p^2 \lesssim \Lambda^2$ are included in the corresponding path integral representation. In the UV at $k = \Lambda$, no fluctuations have been integrated out and thus we recover our microscopic theory defined by the classical action S^Λ. In the case of $0 < k < \Lambda$, we will have an effective field theory defined by the effective average action at the scale k. At the level of the path integral, this case corresponds to starting with the classical action and then successively integrating out quantum fluctuations from high to low momentum scales. When we have reached the point $k = 0$, all fluctuations that were suppressed by the regulator are now integrated out, i.e., all quantum contributions are included into the generating functional, such that we recover the full quantum effective action.

The regulator is an essential part of the Wetterich equation and the space of possible regulator functions is restricted by a set of conditions, which ensure that our renormalization group method is well-defined and that the correct physical properties are incorporated. In particular, the conditions (2.42) for the cutoff term can be translated into analogous requirements for the regulator, which ensure that the boundary conditions (2.53) for the effective average action are met. In addition, it is convenient to choose a regulator, whose derivative with respect to k provides a UV regularization for the loop integral in the Wetterich equation (2.61). If $\partial_k R_{k,\Lambda}$ sufficiently regularizes the high loop momenta, we can safely perform the continuum limit $\Lambda \to \infty$ and allow the quantum fields to fluctuate on arbitrary small length scales. A continuum formulation is often preferred for several reasons. First, it typically provides mathematically simpler expressions and allows for the inclusion of continuous spacetime symmetries. Additionally, continuum field theories can describe a wider range of physical systems, which is crucial for understanding universal behavior.[25] Taking the continuum limit eliminates the explicit UV cutoff from the fRG framework,

$$\lim_{\Lambda\to\infty} R_{k,\Lambda} = R_k \,, \qquad \lim_{\Lambda\to\infty} \Gamma_k^\Lambda = \Gamma_k \,, \tag{2.62}$$

and hence leads us to the continuum Wetterich equation:

$$\partial_k \Gamma_k[\Phi_{\mathrm{cl}}] = \frac{(-1)_\Psi}{2} \operatorname{Tr}\left\{ \partial_k R_k \cdot \left(\Gamma_k^{(1,1)}[\Phi_{\mathrm{cl}}] + R_k \right)^{-1} \right\} . \tag{2.63}$$

We have now arrived at a formulation where the auxiliary function R_k renders the loop integral implied by the trace both infrared finite and ultraviolet finite. The momentum integration is made IR finite due to the mass-like behavior of the regulator for small momenta, $p^2 \lesssim k^2$, whereas UV finiteness is achieved by the fast decay of $\partial_k R_k$ for high momenta, $p^2 \gtrsim k^2$. Therefore, only a small interval of loop momenta with $p^2 \approx k^2$ effectively contributes to the computation of the continuum

[25] In statistical physics, universality refers to the observation that apparently different physical systems can share precisely the same sets of critical exponents, meaning there are universal properties of phase transitions and critical phenomena independent of the microscopic details. Theories in a given universality class can look very different microscopically but exhibit the same macroscopic behavior near critical points. For more information, we refer to Refs. [149, 192–196].

effective average action in every RG step. In other words, in contrast to the Wilsonian case, a suitable choice of the regulator function in the fRG allows for the situation that the number of momenta contributing to the scale-dependent functional does not increase when lowering the RG scale but instead stays the same. The renormalization group flow may now be viewed as a flow through momentum shells with momenta $p^2 \approx k^2$, where each shell triggers an incremental change in the effective average action.[26] The boundary conditions (2.53) need to be adjusted according to the continuum formulation,

$$\lim_{k\to 0} \Gamma_k[\Phi_{\mathrm{cl}}] = \Gamma[\Phi_{\mathrm{cl}}]\,, \qquad \lim_{k\to\infty} \Gamma_k[\Phi_{\mathrm{cl}}] = S^{\infty}[\Phi_{\mathrm{cl}}]\,, \tag{2.64}$$

where the infinite-energy action S^{∞} is formally related to S^{Λ} by the renormalization group flow. While the requirement for the infrared behavior of the continuum effective average action is straightforward, the second boundary condition is problematic since it is a priori unclear whether a theory, which has been fixed at some finite cutoff scale, has a finite and unique UV completion up to arbitrarily high scales.[27] Even if an initial condition at infinitely high scales could be provided, it would be impractical as the RG flow could not reach low scales in any finite amount of time. We therefore adopt the strategy to fix the initial condition for the flow of the effective average action at a large yet finite scale Λ_0 and associate the corresponding functional with the microscopic action,

$$\Gamma_{\Lambda_0}[\Phi_{\mathrm{cl}}] \simeq S[\Phi_{\mathrm{cl}}]\,. \tag{2.65}$$

Exactness is not essential here since, for scales much smaller than Λ_0, the precise form of Γ_{Λ_0} is irrelevant up to the values of a few relevant couplings [176]. Therefore, although the relation above is only approximate, it is accurate enough for all practical purposes, provided that the scale Λ_0 is sufficiently large compared to all mass scales of interest [87]. Further notice that the UV scale Λ_0 is not necessarily the largest scale possible in the theory at hand.[28] It is only some scale at which we assume to know the effective average action such that we can fix the couplings of the theory.

Like 1PI $(n+m)$-point functions can be obtained from the quantum effective action by functional differentiation, see Eq. (2.28), their flow equation within the fRG is readily derived by applying corresponding derivatives to the Wetterich equation. This differential equation for the effective average action is a functional one because the trace on the right-hand side contains the second functional derivative of that scale-dependent functional. As a direct consequence, there is a general pattern that the RG flow of some $(n+m)$-point correlation function also depends on vertices of order $(n+m+1)$ and $(n+m+2)$. This means that we obtain an infinite tower of coupled flow equations by taking functional derivatives of the Wetterich equation. In most cases, we are not able to solve this system of differential equations so we need to make use of some truncation scheme. Finding reliable truncations of the effective action is the most difficult step and requires a lot of physical insight, though. Once we have chosen a truncation, its reliability has to be checked in order to estimate the truncation errors.

The results for physical quantities as obtained from $\Gamma_{k=0}$ are independent of the choice of the regulator function if the flow equation is solved exactly. We emphasize, however, that both Γ_{Λ_0} as well as the flow itself are scheme-dependent. In particular, different choices of R_k correspond

[26] Notice that this discussion is primarily about the effects of selecting a certain type of regulator and applies independently of whether we choose to take the continuum limit.

[27] This limit does in fact exist in asymptotic safe theories, see, e.g., Refs. [197–201] for more information.

[28] We would like to highlight that infrared and ultraviolet are highly context-dependent notions. Although the RG scale is introduced by the regulator insertion and carries the idea of an IR cutoff, Λ_0 is supposed to set the scale here for all those momenta that are large relative to other mass scales of the system. Therefore, Λ_0 can be safely called a UV scale.

to different trajectories in the space of possible action functional along which the unique infrared limit at $k = 0$ is reached. Once approximations are implemented, not only the trajectory and the initial condition but also the infrared results may depend on the precise definition of the regulator function. This dependence can in principle be used to study the robustness of the approximation and to estimate the approximation errors, see, e.g., Ref. [202]. Concretely, if physical observables show a highly fluctuating behavior under a variation of the regulator function, an improvement of the approximation in use should definitely be considered. On the other hand, if a certain approximation is kept fixed, an investigation of the infrared behavior under a variation of R_k can also be used to find a class of regulators under which the chosen approximation performs best.

For the remainder of this work, we agree on the following conventions regarding the functional renormalization group, which are most commonly used in the literature. Whenever we refer to *the* Wetterich equation, we mean the continuum formulation as presented in Eq. (2.63). Furthermore, we will drop the subscript that labels the input superfields of the effective average action as classical in the sense of Eq. (2.48). This means we are going to assume that the type of field used as an input variable for a functional is already clear from the context. It is nevertheless important not to confuse the quantum fields, which enter the classical action, with their source-dependent expectation values, which are relevant for the effective average action.

2.2.2 The regulator

Any concrete calculation of RG flow equations requires the specification of the regulator function R_k, which encodes the regularization scheme. Since the RG trajectory of some scale-dependent quantity depends to a great amount on how specifically the regulator function is constructed, the regulator should be considered a part of the definition of the system. The regulator is a crucial ingredient of the Wetterich equation, which is why we need to elaborate more on its construction and properties.

Because the regulator is introduced to the path integral in order to provide better control over the momentum modes contributing to the functional of interest, it is more convenient for the following presentation to switch to momentum space. The regulator (2.46) is expected to respect translation invariance such that we can deduce the following behavior under Fourier transformation,

$$R_k(x,y) = \widetilde{R}_k(x-y) = \int_p \mathrm{e}^{\mathrm{i}p^\intercal(x-y)}\, \widetilde{R}_k(p) = \int_p \int_q \mathrm{e}^{\mathrm{i}p^\intercal x} \mathrm{e}^{-\mathrm{i}q^\intercal y}\, R_k(p,q)\,, \tag{2.66}$$

where the structure from Eq. (2.46) translates to

$$\begin{aligned} R(p,q) &= \widetilde{R}(p)\,(2\pi)^4 \delta^{(4)}(p-q) \\ &= \begin{pmatrix} \widetilde{R}^{\varphi}(p) & 0 & 0 \\ 0 & 0 & -\big(\widetilde{R}^{\psi}\big)^\intercal(-p) \\ 0 & \widetilde{R}^{\psi}(p) & 0 \end{pmatrix} (2\pi)^4 \delta^{(4)}(p-q) \\ &= R^\intercal(-q,-p)\,(-1)_\Psi\,. \end{aligned} \tag{2.67}$$

Letting the position-space regulator transform with different signs in the exponential for the p- and q-modes in Eq. (2.66) is an advantageous convention, which ensures a uniform factorization of the momentum-space regulator for bosons and fermions, as can be seen in Eq. (2.67). Notice that our requirement of translation symmetry in position space directly leads to the appearance of

a Dirac delta distribution in Fourier space, which indicates momentum conservation. In addition, the symmetry property (2.67) automatically restricts the space of possible regulator functions. The regularization term can now be represented as

$$\begin{aligned}\Delta S_k[\Phi] &= \frac{1}{2}\,\Phi^{\intercal}\cdot R_k\cdot\Phi = \frac{1}{2}\int_p\int_q \Phi^{\intercal}(-p)\,R_k(p,q)\,\Phi(q)\\ &= \frac{1}{2}\int_p \varphi(-p)\,\widetilde{R}_k^{\varphi}(p)\,\varphi(p) + \int_p \overline{\psi}(p)\,\widetilde{R}_k^{\psi}(p)\,\psi(p)\,.\end{aligned} \tag{2.68}$$

We would like to point out that the reduced regulator function $\widetilde{R}_k$ in its momentum-space representation has always the same energy dimension as the mass parameter in the matching subspace of the mass matrix M^2, see Eq. (2.32). The regulator insertion therefore imitates a mass term at the level of the classical action in the sense of Eq. (2.68), where that mass not only carries a dependence on the RG scale but is in general also momentum-dependent. Through its momentum dependence, the regulator directly participates in the process of integrating out momentum modes and influences to what extent momenta in the neighborhood of k contribute to the path integral. In general, the RG scale does not need to be the same for all field momenta, meaning that the bosonic regulator may depend on k_φ, while the fermionic regulator depends on k_ψ, see, e.g., Ref. [79]. For simplicity, however, we adopt the most common choice $k_\varphi = k_\psi = k$ throughout this work.

During the derivation of the Wetterich equation, we have come across different requirements for the regulator in order to ensure that certain boundary conditions for the effective average actions are met and that the loop integral is always finite. Since these requirements have not yet been presented very concretely, let us state them here in a more detailed form. As it is more convenient, we will often speak rather generally of *the regulator* and only be more precise about the wording if necessary.

(i) In order to provide IR regularization, the regulator function needs to screen the propagator from divergences in the limit as momenta become small compared to the RG scale. This requires the regulator to be positive in the sense of

$$\forall k>0: \qquad \lim_{\frac{p^2}{k^2}\to 0}\widetilde{R}_k^{\varphi}(p) > 0\,, \quad \lim_{\frac{p^2}{k^2}\to 0}\det\left(\widetilde{R}_k^{\psi}(p)\right) > 0\,. \tag{2.69}$$

In the case of bosons, this condition is to be understood in an operator sense, meaning that positivity is a statement about eigenvalues. The same line of argumentation does, however, not carry over to fermions. Recall, for instance, that all non-vanishing eigenvalues of the massless Dirac operator always come in pairs of opposite sign [203]. In the presence of a finite fermion mass, the eigenvalues even become complex-valued. This leads us to an understanding of positivity for fermions in the sense of a positive determinant, see also Refs. [204, 205]. With this condition fulfilled the average propagator remains finite in the low-energy limit $p^2 \to 0$ such that no infrared divergences are encountered in the presence of massless modes. The fact that the regulator does not vanish when momenta become arbitrarily small is exactly what is meant when talking about the regulator having a mass-like behavior.[29]

[29] Notice that a statement about the regulator staying finite in the limit as momenta go to zero would not be enough since eigenvalues are allowed to grow infinitely big in absolute terms.

(ii) For the effective average action to coincide with the full quantum effective action in the infrared limit $k \to 0$, the regulator must satisfy the requirement

$$\forall p \in \mathbb{R}^4 \big| \, p^2 > 0 : \qquad \lim_{k\to 0} \widetilde{R}_k^{\varphi/\psi}(p) \to 0 \, . \tag{2.70}$$

In the limit as the RG scale goes to zero, the regulator also needs to vanish such that the corresponding IR endpoint of the RG trajectory is indeed free of any explicit regulator dependence.[30]

(iii) Generally speaking, the regularization term needs to diverge at the UV cutoff of the theory such that the effective average action at that UV scale coincides with the classical action. Since we are interested in the continuum formulation, we will directly consider the fact that the UV cutoff has been sent to infinity. The requirement for the regularization term then translates to the regulator in the following way,

$$\forall p \in \mathbb{R}^4 \big| \, p^2 < \infty : \qquad \lim_{k\to\infty} \widetilde{R}_k^{\varphi}(p) \to \infty \, , \quad \lim_{k\to\infty} \det\Big(\widetilde{R}_k^{\psi}(p)\Big) \to \infty \, , \tag{2.71}$$

where, in the case of bosons, this relation is again to be understood as a statement about eigenvalues.

(iv) Lastly, in order to provide UV regularization for the flow of the effective average action, the regulator needs to satisfy

$$\forall k \in [0, \infty) : \qquad \lim_{\frac{p^2}{k^2}\to\infty} \partial_k \widetilde{R}_k^{\varphi/\psi}(p) \to 0 \, . \tag{2.72}$$

In words, this means that the k-derivative of the regulator has to vanish as momenta become large compared to the RG scale. With this requirement fulfilled, the derivative term in the numerator of the trace of the Wetterich equation decays fast enough to suppress those loop momenta that cause UV divergences.

Notice that the limit of vanishing momenta and the limit in which the RG scale goes to zero do in general not commute. We would also like to point out that the condition (i) may have to be further generalized in the presence of a finite chemical potential, see Section 2.3.2 for details.

In principle, the choice or the construction of a regulator should always be constrained by the symmetries of the unregularized theory in the sense that no symmetry should be spoiled in the presence of a cutoff scale. To be more precise, every symmetry that could be realized in a given theory should be respected by the regulator function. All symmetries of the classical action, which are respected by the regulator, are automatically also symmetries of the effective average action. However, a breakdown of symmetry induced by the regulator is a completely artificial effect, which will alter the infrared physics of the theory at hand. A particularly good strategy for constructing suitable regulator functions is to relate the structure of the regulator to the inverse propagator of the free theory,

$$S_{\text{free}}[\Phi] = \frac{1}{2}\int_p \varphi(-p)\Big[p^2 + m_\varphi^2\Big]\varphi(p) + \int_p \overline{\psi}(p)\big[-\not{p} + \mathrm{i}m_\psi\big]\psi(p) \, . \tag{2.73}$$

[30] Results as obtained from the quantum effective action at $k = 0$ can nevertheless suffer from indirect regulator dependences. If the regulator insertion explicitly violates a symmetry of the theory, then this symmetry breaking affects every subsequent RG step such that the infrared endpoint of the RG trajectory does not align with the "true" result, although the regulator is explicitly removed through the condition (2.70).

Thereby, the regulator will not only obey a majority of symmetries present in the classical theory but will also have similar positivity properties. It is worth mentioning that there are also more general approaches that relate the regulator to the inverse average propagator, see, e.g., Refs. [177, 206–208].

If we want to maintain Lorentz invariance, analyticity and, in the case of fermionic theories, chiral symmetry [209], then the requirement for these properties already predicts a very general and simple structure for the regulator. More specifically, regulator functions are commonly written as

$$\widetilde{R}_k^{\varphi}(p) \sim p^2\, r^{\varphi}\left(\frac{p^2}{k^2}\right), \qquad \widetilde{R}_k^{\psi}(p) \sim -\not{p}\, r^{\psi}\left(\frac{p^2}{k^2}\right), \tag{2.74}$$

where the dimensionless function r is known as the regulator shape function and controls the influence on loop momenta relative to the RG scale k. The shape function should be analytic and has to be constructed in accordance with constraints corresponding to the general regulator conditions (i)-(iv) above. More concretely, a translation of these conditions for the shape function is presented in the following. Here, the symbol x is used to denote some generic dimensionless variable and must not be confused with a spacetime variable.

1. Behavior in the low-energy limit:

$$\forall s \geq 1: \qquad r^{\varphi}(x) = \mathcal{O}\left(\frac{1}{x^s}\right), \qquad r^{\psi}(x) = \mathcal{O}\left(\frac{1}{x^{s/2}}\right) \qquad \text{as } x \to 0^+ . \tag{2.75}$$

2. Behavior in the IR limit:

$$\lim_{x\to\infty} r^{\varphi/\psi}(x) \to 0 . \tag{2.76}$$

3. Behavior in the UV limit:

$$\lim_{x\to 0^+} r^{\varphi/\psi}(x) \to \infty . \tag{2.77}$$

4. Condition for rendering the flow UV finite:

$$\forall s > 1: \qquad r^{\varphi}(x) = \mathcal{O}\left(\frac{1}{x^s}\right), \qquad r^{\psi}(x) = \mathcal{O}\left(\frac{1}{x^{s/2}}\right) \qquad \text{as } x \to \infty . \tag{2.78}$$

Notice that condition 3 follows from 1 and that condition 2 follows from 4 such that the introduction of a shape function as in Eq. (2.74) reduces the number of remaining conditions to two. We emphasize that these requirements do not uniquely determine the regulator shape function such that many functions are possible. Frequently given examples for possible candidates are the exponential shape function

$$r^{\varphi}_{\text{exp}}(x) = \frac{1}{1-\mathrm{e}^{-x}} - 1, \qquad r^{\psi}_{\text{exp}}(x) = \frac{1}{\sqrt{1-\mathrm{e}^{-x}}} - 1 \tag{2.79}$$

and also the Litim [210] shape function

$$r^{\varphi}_{\text{Litim}}(x) = \left(\frac{1}{x} - 1\right)\theta(1-x), \qquad r^{\psi}_{\text{Litim}}(x) = \left(\frac{1}{\sqrt{x}} - 1\right)\theta(1-x) \tag{2.80}$$

with θ denoting the Heaviside step function. The Litim shape function is a non-analytic function, which is optimized in the sense that it ensures the flow of the effective average action in the leading

order derivative expansion to have optimal convergence and stability properties [210–213]. We would like to point out that x-dependent terms of the shape functions above are constructed such that condition 1 is satisfied with $s = 1$. This then implies a finite low-energy limit,

$$\lim_{x\to 0^+} x\, r^{\varphi}(x) = 1 \qquad \Rightarrow \qquad \lim_{\frac{p^2}{k^2}\to 0} \widetilde{R}_k^{\varphi}(p) \sim k^2 \,, \tag{2.81}$$

$$\lim_{x\to 0^+} \sqrt{x}\, r^{\psi}(x) = 1 \qquad \Rightarrow \qquad \lim_{\frac{p^2}{k^2}\to 0} \widetilde{R}_k^{\psi}(p) \sim k \,, \tag{2.82}$$

i.e., the mass-like behavior of the regulator becomes quantitatively accurate. In principle, constructions that satisfy the low-energy condition with $s > 1$ are allowed but the resulting divergence of the regulator as momenta become small is usually less convenient in practical situations. Notice, however, that the typical mass-like behavior as shown above comes at the cost of analyticity for the fermionic regulator. Concretely, the square root present in the fermionic shape function gives rise to a jump discontinuity of the fermionic regulator at $p = 0$. As a consequence, cases in which the analyticity of the theory constitutes a crucial feature for the phenomena of interest need to be handled with a lot of care and insight.

Let us briefly come back to the continuum limit that has been formally performed in Eq. (2.62). Using the representation of the regulator in terms of a shape function, we can now see more concretely how a finite cutoff can be taken to infinity. For illustrative purposes, we consider an exponential regulator. Having a finite UV cutoff Λ, the general regulator for bosons is given by

$$R_{k,\Lambda}^{\varphi}(p) \sim p^2\, r_{k,\Lambda}^{\varphi}(p) \,, \tag{2.83}$$

where the corresponding exponential shape function is frequently written as

$$r_{k,\Lambda}^{\varphi}(p) = \frac{1}{\exp\left(\frac{p^2}{k^2}\right) - \exp\left(\frac{p^2}{\Lambda^2}\right)} \,. \tag{2.84}$$

If we take the cutoff to infinity, we observe this shape function reduce to the standard shape function as presented above,

$$\lim_{\Lambda\to\infty} r_{k,\Lambda}^{\varphi}(p) := r_k^{\varphi}(p) = r_{\text{exp}}^{\varphi}\left(\frac{p^2}{k^2}\right) \,. \tag{2.85}$$

The presentation of the continuum limit for fermionic regulators is completely analogous. We remark, however, that the generalized regulator shape functions do not need to be unique, meaning that there may be several possible extensions to the case of having a finite UV cutoff.

The mass-like behavior of the regulator term for small momenta makes our framework perfectly suitable for dealing with theories that are plagued by infrared problems in perturbation theory. On the contrary, the mass-like behavior seems to be a major issue for gauge theories. Whereas the regulator insertion is generally not problematic in scalar field theories, gauge theories in the presence of a regulator inevitably suffer from an explicit breakdown of gauge symmetry. Even though the regularization term may not be gauge-invariant,[31] our formalism can in fact be applied to gauge theories. Independently of any RG approach, the computation of observables from gauge theories requires us to fix a particular gauge and hence break gauge symmetry by hand. At the same time, Ward-Takahashi identities get introduced, which need to be resolved in the end in order to recover gauge-invariant results. The explicit breaking of gauge symmetry as induced by

[31] For manifestly gauge-invariant formulations, see, e.g., Refs. [214–219].

the fermionic regulator then leads to scale-dependent corrections to the usual Ward-Takahashi identities and these corrections vanish in the limit $k \to 0$ [220–226]. Alternatively, one may use so-called background-field methods to study gauge theories within the RG as proposed in Refs. [120, 126, 227].

As we have seen so far, the regulator needs to satisfy the conditions (i)-(iv) in order to to ensure that the flow equation (2.63) for the effective average action is well-defined. In addition, the regulator is supposed to respect all those properties of the theory as given by the classical action which are associated with physical content. Among those properties, Lorentz invariance, chiral symmetry, and analyticity are often the most prominently discussed examples since their breakdown can be a severe issue for the reliability and predictive power of infrared results. However, also properties like charge conjugation [81] or causality [82, 228] need in principle to be maintained in the presence of a regulator. Moreover, it is also beneficial to impose certain "convenience conditions" on the regulator in order to allow for more accessible flows. A specific type of regulator may for instance be chosen depending on its potential to simplify analytical calculations or based on the stability properties of the flow of interest. Altogether, it is not unlikely to find that the regulator is overconstrained in practice, i.e., that different conditions compete with each other. Consequently, some constraints have to be prioritized while others need to be relaxed.

A prominently used class of regulators is given by those regulator functions that couple only to the spatial momentum modes of the loop integral while leaving the time-like modes unaffected. These so-called spatial regulators can be easily obtained from Eq. (2.74) by the replacement $p \to \vec{p}$ and thus follow the structure

$$\widetilde{R}_k^{\varphi}(\vec{p}) \sim \vec{p}^{\,2}\, r^{\varphi}\left(\frac{\vec{p}^{\,2}}{k^2}\right), \qquad \widetilde{R}_k^{\psi}(\vec{p}) \sim -\vec{\not{p}}\, r^{\psi}\left(\frac{\vec{p}^{\,2}}{k^2}\right). \tag{2.86}$$

Spatial regulators do not introduce additional poles to the complex plane associated with the time-like momentum mode of the analytically continued propagator. As a consequence, spatial regularization schemes immensely reduce the efforts in studying spectral properties of particles, see, e.g., Refs. [82, 208, 229, 230]. More generally, spatial regulators are specifically attractive since they often allow us to analytically evaluate loop integrals to a great extent. In particular, they usually allow for an analytic evaluation of Matsubara sums which arise in quantum field theory at finite temperature, see Section 2.3. This feature not only highly improves the accessibility of correlation functions in general but makes it even possible to obtain analytical RG flow equations, see, e.g., Refs. [231–234].

Notice that all the aforementioned benefits of spatial regularization schemes come at the cost of violating Lorentz invariance. By treating time-like and spatial momentum modes differently, the use of spatial regulators immediately leads to an explicit breakdown of Lorentz symmetry. If the system is in a medium, the presence of a heat bath or a finite chemical potential breaks the Lorentz symmetry down to rotations among spatial coordinates anyway. Therefore, additional Lorentz symmetry breaking as induced by the regulator might seem innocuous such that spatial regularization schemes appear to be a suitable choice. Although this has been confirmed in specific examples [229, 230], it is a priori unclear whether the influence of additional Lorentz symmetry breaking ends up being mild on the observable of interest. Recall that any symmetry breaking induced by the regulator is a completely artificial effect that potentially leads to a distortion of the RG flow. In accordance with our discussion of the Wetterich equation, spatial regulators lead to an RG flow in which only a small interval of loop momenta with $k^2 \approx \vec{p}^{\,2}$ contributes in every RG step. Such an RG flow is local in the spatial momenta but takes into account all time-like modes at every scale k.

This loss of locality in the time-like direction of momentum space can then lead to complications in the construction of a meaningful truncation scheme for the effective average action [235]. Furthermore, the different treatment of loop momenta causes an ambiguity in the calculation of vacuum wavefunction renormalizations Z. While intact Lorentz invariance predicts a unique wavefunction renormalization, spatial regulators enforce the wavefunction renormalization to split up into components $Z^{\parallel}$ and $Z^{\perp}$ that are parallel and perpendicular to the time-like direction, respectively. In principle, one may solve this problem by taking care of the symmetry-violating terms with the aid of corresponding Ward identities such that the theory remains Lorentz-invariant in the vacuum limit [236]. In practice, however, these efforts are rarely made since spatial regularization schemes get primarily deployed in model studies which focus on a phenomenological understanding of the physical mechanisms rather than high-precision calculations of observables.

Mostly based on symmetry considerations, we were able to present the general structure of regulator functions. Although demanding exactness for the relations (2.74) and (2.86) is completely fine in principle, choosing a non-trivial proportionality factor is often more convenient in practice. In the case of a Lorentz-invariant regularization scheme, we write

$$\widetilde{R}_k^{\varphi}(p) = Z_{\varphi,k}\, p^2\, r^{\varphi}\left(\frac{p^2}{k^2}\right), \qquad \widetilde{R}_k^{\psi}(p) = -Z_{\psi,k}\, \not{p}\, r^{\psi}\left(\frac{p^2}{k^2}\right), \tag{2.87}$$

where the appearance of bosonic and fermionic wavefunction renormalizations, Z_φ and Z_ψ, allow for a factorization of Z-factors in the regularized kinetic operator of the effective average action, see Eq. (2.36). Recall that the wavefunction renormalizations are dimensionless quantities. In the case of spatial regulators, the incorporation of wavefunction renormalizations is entirely analogous.

At last, we would like to comment on the statement that the endpoint Γ of the RG trajectory for the effective average action as described by the Wetterich equation is independent of the regulator. When stated in this form, it is based on the implicit assumptions that the flow equation can be solved exactly and especially that we only choose from a set of regulators that all satisfy the formal as well as physical constraints. In practice, however, neither can the Wetterich equation be solved exactly for interacting theories, nor is there a universally good regulator function. Computability of RG flows frequently gets into conflict with at least one of the regulator conditions. As a result, certain constraints eventually need to be lifted, leading to regulators that restrict the reliability of infrared results to a certain degree. In order to minimize these artificial effects, regulator functions have to be strategically chosen depending on the theory under consideration, the truncations in use, and the physical quantity of interest. Generally speaking, regulators that explicitly break a symmetry of the theory will lead the RG flow to a different infrared point than regulators that respect this symmetry. A collection of regulator functions that all respect a certain set of symmetries or other properties is called a regulator class. Another important thing to mention is that the quantitative meaning of the RG scale changes with the regulator. In a loop integral, the scale k parameterizes the extent to which the suppression of momentum modes is enforced by the regulator. Notice, however, that it highly depends on the regulator function how smooth or sharp this suppression is actually realized within the loop. Therefore, the amount of momenta contributing to a loop integral at a particular scale k generally changes with the regulator. Notably, the relation of the RG scale to internal scales of the system or external control parameters changes if we swap the regulator function. The same line of argumentation also applies to the initialization scale Λ_0. In order to ensure comparability of the initial condition to the RG flow at some finite UV scale between different regularization schemes, we need to adjust the value of Λ_0 according to the new regulator. Making adjustments to allow for comparability between schemes is essential in regulator studies, specifically when truncations are involved.

2.2.3 Expansion schemes

For interacting theories, the characteristic flow equation (2.63) for the effective average action can in general not be solved in closed form. We therefore have no choice but to consider truncations to the Wetterich equation in order to efficiently calculate RG flows and gain insight into the underlying physical system. Although truncations will render our results for observables generally model-dependent, we expect no qualitative deviations from exact solutions with a properly chosen truncation. The main challenge for non-perturbative systems is to find truncations that incorporate the most relevant degrees of freedom and yet ensure a set of flow equations of manageable complexity. In regard to fRG studies, all truncation methods rely on some systematic expansion scheme for the effective average action. We will thus give a presentation of commonly used expansion schemes in the following.

Vertex expansion

Most frequently, the effective average action is considered to be constructed from powers of field degrees of freedom with its $(n+m)$-point functions serving as coefficients of the construction. This so-called vertex expansion provides the formal basis for the projection of 1PI correlation functions from the corresponding generating functional. The scheme reads

$$\Gamma_k[\Phi] = \sum_{n,m=0}^{\infty} \frac{1}{(n+m)!} \prod_{i=1}^{n}\prod_{j=1}^{m} \int_{\mathbb{R}^4} \mathrm{d}^4 x_i \int_{\mathbb{R}^4} \mathrm{d}^4 y_j \\ \big(\Phi(x_i)-\Phi_0(x_i)\big)^{\intercal}\, \Gamma_k^{(n,m)}(x_1,\dots,y_m)\, \big(\Phi(y_j)-\Phi_0(y_j)\big)\ , \tag{2.88}$$

where Φ_0 denotes the ground state configuration (2.21) of the system. Implicitly, we have already made use of this vertex expansion when defining proper vertex functions, see Eq. (2.28). The structure of the Wetterich equation shows that the RG flow of some $(n+m)$-point function also depends on the flow of the $(n+m+1)$- and $(n+m+2)$-point function, leading to a set of infinitely many coupled flow equations. Since we are in general not able to solve this system of differential equations, we have to consider a truncation of the effective average action and restrict it to include only correlation functions with $N_{\max}$ external fields [185]. In other words, we restrict ourselves to a finite number of coupled flow equations by assuming that all $(n+m)$-point functions beyond a certain maximum value are simply zero. The quality of such a truncation in terms of, e.g., stability of the flow or agreement of the solution with experimental results particularly depends on the chosen value for $N_{\max}$.

Loop expansion

The Wetterich equation is an exact RG flow equation with a one-loop structure which should not be confused with a flow equation at one-loop order in perturbation theory. We can nevertheless rederive perturbation theory from the Wetterich equation in an iterative manner. Analogously to Eq. (2.26), we consider a loop expansion of the effective average action,

$$\Gamma_k[\Phi] = S[\Phi] + \Gamma_k^{\text{1-loop}}[\Phi] + \dots\ , \tag{2.89}$$

where all loop contributions are expected to vanish at high RG scales such that the initial condition (2.65) is met. This shows that, at leading order in the loop expansion, we may associate the effective average action with the scale-independent classical action. Since this equally translates to functional derivatives, we can feed back this information into the Wetterich equation. In particular, replacing the field-dependent 1PI two-point correlator in Eq. (2.63) with the corresponding

derivative of the classical action provides us with the flow of the 1-loop contribution,

$$\begin{aligned}\partial_k \Gamma_k^{\text{1-loop}}[\Phi] &= \frac{(-1)_\Psi}{2} \operatorname{Tr}\left\{\partial_k R_k \cdot \left(S^{(1,1)}[\Phi] + R_k\right)^{-1}\right\} \\ &= \frac{(-1)_\Psi}{2} \operatorname{Tr}\left\{\partial_k \operatorname{Ln}\left(S^{(1,1)}[\Phi] + R_k\right)\right\} \ . \end{aligned} \tag{2.90}$$

This flow can be formally integrated to obtain the one-loop contribution to the effective average action:

$$\Gamma_k^{\text{1-loop}}[\Phi] = \int_{\Lambda_0}^{k} \mathrm{d}k' \ \partial_{k'} \Gamma_{k'}^{\text{1-loop}}[\Phi] = \frac{(-1)_\Psi}{2} \operatorname{Tr}\left\{\operatorname{Ln}\left(\frac{S^{(1,1)}[\Phi] + R_k}{S^{(1,1)}[\Phi] + R_{\Lambda_0}}\right)\right\} \ . \tag{2.91}$$

Similarly, the result for the effective average action up to one-loop order can be reinserted into the Wetterich equation to generate higher-order contributions in the loop expansion. For practical purposes, however, we may truncate the effective average action and break off the loop expansion at a certain point. More specifically, considering only contributions up to one-loop order in the perturbative expansion is known as the one-loop approximation. In this approximation, the characteristic RG flow equation reduces to Eq. (2.90), leading to the convenient situation that flow equations for correlation functions are now decoupled.

Derivative expansion

Provided with a theory that is defined by some classical action at high scales, the RG flow towards low scales as described by the Wetterich equation generates all kinds of quantum corrections that are compatible with the symmetries of the initial action. We may therefore represent the most general ansatz for the effective average action as a series of invariants. In this regard, a prominently used ordering scheme for this series is given by the number of derivative operators. This so-called derivative expansion [176, 237] of the effective average action reads

$$\Gamma_k[\Phi] = \int_x \left(U_k\left(\Phi(x)\right) + \frac{1}{2}\Phi^\intercal(x) \ Z_k\left[-D^2\right] \ \Phi(x) + \mathcal{O}\left(D^4\right)\right) , \tag{2.92}$$

where U_k denotes the effective potential [125, 127] and Z_k the wavefunction renormalization. We would like to emphasize that the derivative expansion is not an expansion in the traditional sense of a perturbative expansion in some small quantity but rather a scheme of laying out degrees of freedom that are expected to be relevant for the phenomenon of interest. We emphasize that the variety of contributions for each order in the derivative expansion is closely linked to the number of fields and symmetries included in the theory. As the field content of our superfield Φ is rather minimalistic by construction, see Eq. (2.3), a derivative expansion of the effective average action shows a correspondingly simple structure. In the case of having a bosonic theory that not only includes multiple field degrees of freedom φ_a but also is invariant under orthogonal transformations, we observe two contributions to the derivative expansion at order ∂^2 [176]:

$$\begin{aligned}\Gamma_k[\varphi] = \int_x \Big(& U_k(\varphi(x)) + \frac{1}{2}\varphi_a(x) \ Z_{\varphi,k}\left[-\partial^2\right] \ \varphi^a(x) \\ & + \frac{1}{4!}\varphi^2(x) \ Y_{\varphi,k}\left[-\partial^2\right] \ \varphi^2(x) + \mathcal{O}\left(\partial^4\right)\Big) \ . \end{aligned} \tag{2.93}$$

Foremost, the RG flow of such a theory generates the contribution $\sim \varphi_a \partial^2 \varphi^a$ which corresponds to the first-order term in Eq. (2.92). In addition, we get the contribution $\sim \varphi^2 \partial^2 \varphi^2$ which comes with a separate wavefunction renormalization $Y_{\varphi,k}$. This second contribution may be considered

a kinetic term for the quantity $\varphi^2 = \varphi_a \varphi^a$ which denotes an invariant with respect to orthogonal transformations in field space. For fermions, a contribution of order $\not{\phi}$ which is also quartic in the fields does arise in the case of explicit chiral symmetry breaking and, as a consequence, such a term would depend explicitly on that symmetry-breaking scale. Since such a scale would spoil the association with a canonical kinetic term of the effective average action, we have neglected this scenario in the presentation of the derivative expansion above. For the sake of simplicity, we have also ignored the possibility of mixed field contributions. Lastly, it should be mentioned that the derivative expansion at each order includes contributions from all orders of the vertex expansion and may therefore be thought of as a resummation of perturbative diagrams.

Based on the derivative expansion of the effective average action, there are several truncation schemes that take only low-order contributions into account. In particular, proposing an ansatz for the effective average action which considers the effective potential as well as the first-order terms with $Z_k = 1$ and $Y_{\varphi,k} = 0$ on the r.h.s. of the flow equation is called the local potential approximation (LPA). This approximation has proven to be quite successful for, e.g., studying the thermodynamics of low-energy QCD [231, 236] or the computation of critical exponents [238, 239]. More generally, it is worth noting that the accuracy of critical exponents can be used to measure the quality of a given truncation or chosen ansatz, see, e.g., Refs. [182, 238, 240, 241]. Another opportunity to check the reliability of a chosen truncation is to perform an extension by including additional operators and then verify whether the results obtained from the new truncation are in agreement with the earlier results. If this is not the case, the chosen truncation should be reconsidered. Improvements to the LPA are straightforward and include higher-order contributions and/or non-trivial wavefunction renormalizations [239, 242].

In a momentum-space representation of the effective average action, the derivative expansion (2.92) corresponds to an expansion in terms of external momenta. We then write

$$\Gamma_k[\Phi] = \int_p \left(U_k[\Phi](p) + \frac{1}{2}\Phi^\intercal(-p)\, Z_k P^2\, \Phi(p) + \mathcal{O}\left(P^4\right) \right) , \tag{2.94}$$

where we have made use of the notation

$$P^2 = \begin{pmatrix} p^2 & 0 & 0 \\ 0 & 0 & -\not{p}^\intercal \\ 0 & -\not{p} & 0 \end{pmatrix} . \tag{2.95}$$

Notice that any expansion scheme ultimately requires the specification of an expansion point. A priori, this point is at our disposal but, for practical purposes, it should be chosen such that a low-order expansion already allows us to capture the most relevant dynamics of the system under consideration. While the expansion in Eq. (2.94) has been anchored at $P^2 = 0$, there is the possibility of bound states with a finite center-of-mass momentum. In that case, the correlation functions have non-trivial minima in momentum space and a low-order derivative expansion should be performed around the global minimum. Choosing an expansion point that does not match the lowest minimum while truncating the derivative expansion inevitably leads to a poor description of the underlying physics [243]. Furthermore, the expansion point should in principle also respect the symmetries of the theory at hand. For a discussion of the relevance of a different expansion point in the presence of a finite chemical potential, see Section 2.3.2.

$\mathcal{PF}$ expansion

If the Wetterich equation can be solved for the effective average action, correlation functions are readily obtained by applying a suitable projection based on the vertex expansion. Unless we reduce the classical fields to homogeneous backgrounds [185], solving for the effective average action is, however, a simply impossible task. A particularly convenient strategy for obtaining correlation functions from the Wetterich equation relies on an expansion in powers of field degrees of freedom. This expansion then allows us to isolate the terms relevant for the correlation function of interest. Concretely, we reparameterize the field variable Φ as a fluctuation around the ground state, i.e., we write

$$\Phi(x) = \Phi_0(x) + \Phi_{\mathrm{fl}}(x) \,, \tag{2.96}$$

where Φ_0 denotes the ground state configuration while Φ_{fl} represents the fluctuation field. In addition, we decompose the inverse average propagator in terms of a fluctuation-independent contribution $\mathcal{P}_k^{-1}$ and a fluctuation-dependent part $\mathcal{F}_k$,

$$\left(\Gamma_k^{(1,1)}[\Phi] + R_k\right)(x,y) = \mathcal{P}_k^{-1}[\Phi_0](x,y) + \mathcal{F}_k[\Phi_{\mathrm{fl}}](x,y) \,. \tag{2.97}$$

Here, the reordering of terms has been performed such that the explicit regulator dependence is completely encoded in the term $\mathcal{P}_k^{-1}$. The Wetterich equation (2.63) may therefore be rewritten as

$$\begin{aligned} \partial_k \Gamma_k[\Phi] &= \frac{(-1)_\Psi}{2} \operatorname{Tr}\left\{\widetilde{\partial}_k \operatorname{Ln}\left(\Gamma_k^{(1,1)}[\Phi] + R_k\right)\right\} \\ &= \frac{(-1)_\Psi}{2} \operatorname{Tr}\left\{\widetilde{\partial}_k \operatorname{Ln}\left(\mathcal{P}_k^{-1}[\Phi_0] + \mathcal{F}_k[\Phi_{\mathrm{fl}}]\right)\right\} \,, \end{aligned} \tag{2.98}$$

where we have used the notation $\widetilde{\partial}_k$ to refer to a derivative that only acts on the scale dependence of the regulator function. The new structure comes with the benefit that the standard Taylor series expansion of the logarithm can be associated with an expansion of the inverse average propagator in terms of fluctuations around the ground state. Assuming that the Taylor series converges,[32] it follows that [188]

$$\begin{aligned} \partial_k \Gamma_k[\Phi] &= \frac{(-1)_\Psi}{2} \operatorname{Tr}\left\{\widetilde{\partial}_k \operatorname{Ln}\left(\mathcal{P}_k^{-1}[\Phi_0] \cdot \left(\delta + \mathcal{P}_k[\Phi_0] \cdot \mathcal{F}_k[\Phi_{\mathrm{fl}}]\right)\right)\right\} \\ &= \frac{(-1)_\Psi}{2} \operatorname{Tr}\left\{\widetilde{\partial}_k \operatorname{Ln}\left(\mathcal{P}_k^{-1}[\Phi_0]\right) + \widetilde{\partial}_k \operatorname{Ln}\left(\delta + \mathcal{P}_k[\Phi_0] \cdot \mathcal{F}_k[\Phi_{\mathrm{fl}}]\right)\right\} \\ &= \frac{(-1)_\Psi}{2} \operatorname{Tr}\left\{\widetilde{\partial}_k \operatorname{Ln}\left(\mathcal{P}_k^{-1}[\Phi_0]\right)\right\} \\ &\quad + \frac{(-1)_\Psi}{2} \sum_{n=0}^{\infty} \frac{(-1)^{n+1}}{n} \operatorname{Tr}\left\{\widetilde{\partial}_k \left(\mathcal{P}_k[\Phi_0] \cdot \mathcal{F}_k[\Phi_{\mathrm{fl}}]\right)^n\right\} \,, \end{aligned} \tag{2.99}$$

[32] Let A be some complex-valued square matrix, then the matrix logarithm is defined by its Taylor series expansion

$$\operatorname{Ln}(A) = \sum_{n=1}^{\infty} \frac{(-1)^{n+1}}{n} (A - \mathbb{1})^n$$

whenever this series converges. Convergence is ensured if $\|A - \mathbb{1}\| < 1$, where $\|\ldots\|$ represents a suitably chosen matrix norm. A possible choice is given by the Hilbert-Schmidt norm defined by $\|X\|^2 = \operatorname{tr}\{X^\dagger X\}$. For more details, see, e.g., Refs. [244, 245]. Promoting this line of argumentation to matrix-valued and scale-dependent functionals B_k with inherent UV divergences, we deduce that logarithmic expressions of the form $\operatorname{Ln}(\delta + B_k)$ have a meaningful series expansion if $\operatorname{Tr}\left\{\left(\widetilde{\partial}_k B_k\right)^\dagger \cdot \widetilde{\partial}_k B_k\right\} < 1$. With this condition fulfilled for $B_k(x,y) = (\mathcal{P}_k[\Phi_0] \cdot \mathcal{F}_k[\Phi_{\mathrm{fl}}])(x,y)$, the convergence of the series in Eq. (2.99) is automatically guaranteed. Now, our assumption for this condition to be satisfied is based on the decomposition (2.97). Per construction, the quantity $\mathcal{F}_k[\Phi_{\mathrm{fl}}] \propto \Phi_{\mathrm{fl}}$ is associated with fluctuations that are supposed to be sufficiently small compared to the ground state configuration such that we obtain a correspondingly small value for the norm of B_k.

where we have used the symbol δ to display the abstract identity element with respect to matrix multiplication as well as functional multiplication. Its elements in, e.g., position space representation read $\delta_{ab}\ \delta^{(4)}(x-y)$ with a and b referring to indices of field space. The final form (2.99) is generally known as the $\mathcal{PF}$ expansion. Here, the phenomenological meaning of the quantities $\mathcal{P}_k$ and $\mathcal{F}_k$ is readily derived from the inverse average propagator, see Eq. (2.97). While $\mathcal{P}_k$ corresponds to a propagator term, the quantity $\mathcal{F}_k$ is proportional in its field argument and can therefore be directly associated with the fluctuation itself. Thus, the $\mathcal{PF}$ expansion scheme has an intuitive interpretation as an expansion of the system in terms of fluctuations around the ground state. By comparison to the original form of the Wetterich equation as presented in Eq. (2.63), the $\mathcal{PF}$ expansion also suggests that the average propagator can be understood perturbatively in the sense of a geometric series. With this scheme at hand, RG flows for $(n+m)$-point functions can be extracted from the Wetterich equation by taking the term of order $(n+m)$ from the expansion and projecting onto its coefficient in field space.

There are several things about this expansion scheme that we would like to point out. At first, notice that the $\mathcal{PF}$ expansion at zeroth order generates a fluctuation-independent tree-level contribution which is an important constituent for the thermodynamic pressure of a given theory. This contribution does, however, not matter for the computation of correlation functions and is therefore often neglected in presentations of the $\mathcal{PF}$ expansion. Secondly, by laying out infinitely many terms contributing to the average effective action, this expansion scheme simplifies the problem of inverting the full field-dependent 1PI two-point correlator to the problem of inverting only $\mathcal{P}_k^{-1}[\Phi_0]$. This inversion process can be performed rather easily by assuming the ground state to be homogeneous, which is already a huge improvement on the approximation of reducing the entire field variable to a homogeneous background. Last but not least, we remark that the presented form of the expansion (2.99) relies on the assumption that the order of summation and integration as implied by the trace can be interchanged. For a system with a finite fermion density, this assumption can in fact fail as discussed in Section 2.4.

2.2.4 Renormalization group consistency

In the following, we introduce the concept of RG consistency which is a key ingredient in assessing the reliability of results as obtained by RG methods. To this end, we will discuss the role of external parameters, e.g., temperature T or chemical potential μ, and address the matter of performing a UV extension of a fixed theory. A violation of renormalization group consistency is associated with regularization-scheme dependences of observables and can therefore significantly spoil the predictions from our RG framework. Our main line of presentation is based on Ref. [88], yet it has been slightly adapted to include new insights as well as the nuances that come with momentum-independent regulators.

In order to study a physical system by means of RG methods, we need suitable initial conditions that allow us to obtain meaningful solutions to a given set of flow equations. With regard to the functional renormalization group, such initial conditions are given by an action functional and a corresponding reference scale Λ_0. Let us consider the flow of the effective average action as described by

$$\partial_k \Gamma_k[\Phi] = f_k[\Phi]\,, \tag{2.100}$$

where the generic function f_k is determined by the Wetterich equation and some set of truncations

appropriate for the phenomenon of interest. Formally integrating this flow equation yields[33]

$$\forall k \in [0, \Lambda_0] : \qquad \Gamma_k[\Phi] = \Gamma_{\Lambda_0}[\Phi] + \int_{\Lambda_0}^{k} \mathrm{d}k' \, f_{k'}[\Phi] \, . \tag{2.101}$$

Generally speaking, the reference scale Λ_0 denotes just some RG scale at which we assume to know the effective average action. Recall that the scale k as introduced by the regulator does not necessarily refer to any physical scale of the system under consideration so, as a consequence, Λ_0 is a purely scheme-dependent quantity and has a priori no universal phenomenological meaning. Notice, however, that RG scales get related to physical scales by the regularization procedure. Given a microscopic theory S, the scale Λ_0 is usually chosen to lie somewhere within the energy range in which S is believed to be an appropriate description of the world. Then, the effective average action at $k = \Lambda_0$ can be associated with the classical action at hand, see relation (2.65). Concretely, the classical action is used to completely determine the UV structure of the effective average action. In order to arrive at a meaningful initial condition Γ_{Λ_0}, the couplings at $k = \Lambda_0$ can now be fixed based on a set of low-energy observables. This means that the values of all couplings contained in Γ_{Λ_0} get defined such that physical values for given observables are recovered from the fRG formalism in the IR limit $k \to 0$.

Notice that the scale k as appearing in the continuum fRG framework is considered to be an IR scale due to the mass-like behavior of the regulator function for low energies. Nevertheless, after integrating the flow equation from the initial scale $k = \Lambda_0$, the presence of the scale Λ_0 effectively provides UV regularization for the resulting loop integral. For a better understanding, take a look at, e.g., the one-loop contribution to the effective average action, see Eq. (2.91). Here it is illustrated that, whereas the logarithm is a naturally diverging function for infinitely large input values, the antiderivative of f_k at $k = \Lambda_0$ provides counterterms to render the overall loop integral as implied by the trace finite for $\Lambda_0 < \infty$. Therefore, the fixed reference scale Λ_0 in Eq. (2.101) truly has the meaning of a UV scale. This UV scale however does not need to be a cutoff in the strict sense that it directly couples to the loop momenta. The value for Λ_0 would ideally be chosen such that the UV scale is asymptotically large compared to at least all those physical scales that are present in the scale-fixing process. This guarantees that such scales, i.e., internal mass scales and potentially finite external parameters, can have an effect on the dynamics of the system at comparable momentum scales. On the other hand, the smaller the UV scale is relative to the physical scales, the more their influence becomes distorted by the regularization scheme, and the weaker the reliability of infrared results becomes.

The flow equation (2.100) together with some proper initial condition defines a unique trajectory, parameterized by the RG scale k, for the effective average action in a mathematical space of functionals. Once this trajectory has been established by the solution to the Wetterich equation, any point Λ on the RG trajectory can be chosen as a starting point for the RG flow at any values of external parameters. For the sake of clarity, we will explicitly display dependences on external

[33] The conventional notation in the fRG may lead to confusion in situations like these so it is worthwhile to clarify that the RG scale k appearing as a subscript indicates the dependence on a variable, $\Gamma_k \equiv \Gamma(k)$ and $f_k \equiv f(k)$, whereas every other subscript refers to fixed parameters. In particular, Γ_{Λ_0} denotes the initial condition for the effective average action at the fixed scale Λ_0 such that $\Gamma(\Lambda_0) = \Gamma_{\Lambda_0}$.

parameters $m_{\text{ext}} = \{T, \mu\}$ in the following. We have

$$\begin{aligned}\Gamma_k[\Phi](m_{\text{ext}}) &= \Gamma_{\Lambda_0, m_{\text{ext}}^{(0)}}[\Phi] + \int_{\Lambda_0}^{k} \mathrm{d}k'\, f_{k'}[\Phi](m_{\text{ext}}) \\ &= \Gamma_{\Lambda_0, m_{\text{ext}}^{(0)}}[\Phi](\Lambda, m_{\text{ext}}) + \int_{\Lambda}^{k} \mathrm{d}k'\, f_{k'}[\Phi](m_{\text{ext}}) \,, \end{aligned} \tag{2.102}$$

where $m_{\text{ext}}^{(0)}$ refers to the set of initial values for external parameters as used in the scale-fixing procedure. To be more concrete, we have made use of the flow of the effective average action between the scales Λ_0 and Λ to generate the new object

$$\Gamma_{\Lambda_0, m_{\text{ext}}^{(0)}}[\Phi](\Lambda, m_{\text{ext}}) := \Gamma_{\Lambda_0, m_{\text{ext}}^{(0)}}[\Phi] + \int_{\Lambda_0}^{\Lambda} \mathrm{d}k'\, f_{k'}[\Phi](m_{\text{ext}}) \,, \tag{2.103}$$

which has incorporated all the information about the original initial condition at $k = \Lambda_0$ and serves as a new initial condition for the flow starting at $k = \Lambda$. In the case of $\Lambda < \Lambda_0$, this approach simply means that we solve the theory at high scales and follow the flow of the effective average action from $k = \Lambda_0$ down to some lower value $k = \Lambda$. For $\Lambda > \Lambda_0$, we need to evolve the RG flow into the opposite direction and calculate a UV-extended version of the original initial condition. It should however be pointed out that an RG flow is in general not reversible. Remember that every incremental change of k down to lower values is associated with the process of integrating out field degrees of freedom in a corresponding functional integral. Once we have integrated out microscopic degrees of freedom, we cannot retrieve them from the newly generated theory without ambiguity. In the language of thermodynamics, the renormalization group flow has a dissipative character and hence leads to entropy production as well as irreversibility. For more details on this subject, see, e.g., Refs. [246–249]. Although exact RG flows are inherently irreversible, the usage of truncations often allows the integration to higher RG scales. We are therefore going to assume in the following that the equations above indeed are meaningful expressions for $\Lambda > \Lambda_0$ due to the implementation of suitable truncations like, e.g., the one-loop approximation. It may however happen that the flow cannot be integrated beyond a certain point $\Lambda_{\text{UV}} > \Lambda_0$, which characterizes the scale of, e.g., a Landau pole appearing in the loop integral. That scale Λ_{UV} then represents a strict upper bound for the RG scale in the UV extension of the theory under consideration. The emergence of such a pole demonstrates that the theory is not self-consistent and it thus signals the lack of relevant high-energy degrees of freedom. This situation applies to most effective theories for the low-energy regime of QCD, see Ref. [88] and the references therein. It is worth mentioning in this context that the value of Λ_{UV} is not unique but depends on the chosen regularization scheme.

Given some RG trajectory, the independence of infrared results with respect to the choice of the UV scale for the RG flow can be stated in the more compressed form

$$\forall \Lambda > k: \qquad \frac{\mathrm{d}}{\mathrm{d}\Lambda} \Gamma_k[\Phi](m_{\text{ext}}) = 0 \,, \tag{2.104}$$

where the concrete meaning of the scale Λ for the effective average action is determined by Eqs. (2.102)-(2.103). We would like to emphasize that the relation above should not be confused with a cutoff independence of the theory. Neither does the fRG framework in its continuum formulation have any explicit ultraviolet cutoff nor does the regulator have to directly couple to the momentum modes to implement a cutoff prescription. Only for momentum-dependent regulator functions, one may say that Eq. (2.104) expresses the situation that the effective UV cutoff for the loop integral can formally be varied such that observables remain unchanged. In that case,

the formulated independence principle is basically a restatement of Eq. (2.40) for the functional renormalization group. Nevertheless, the essence of Eq. (2.104) is that we are free to choose any point on the RG trajectory as the starting point for the flow towards lower scales.

As mentioned before, the consideration of finite external parameters leads to specific regularization scheme artifacts if those parameters become comparable in magnitude to the fixed UV scale Λ_0 of the theory.[34] In other words, the condition of an asymptotically large reference scale limits the range of values for external parameters for which we can reliably study the system.[35] If we want to consistently extend our study to a larger set of values for external parameters without amplifying regularization scheme dependences, we need to elevate the UV scale associated with the microscopic theory to higher values while respecting the given initial condition. Specifically, we perform a UV extension according to Eq. (2.103) using the initial values for external parameters. The new effective average action at scales then generically reads

$$\forall k \in [0,\Lambda]: \qquad \Gamma_k^{(\mathrm{RGc})}[\Phi](m_{\mathrm{ext}}) = \Gamma_{\Lambda_0, m_{\mathrm{ext}}^{(0)}}[\Phi](\Lambda, m_{\mathrm{ext}}^{(0)}) + \int_\Lambda^k \mathrm{d}k'\, f_{k'}[\Phi](m_{\mathrm{ext}})\,, \tag{2.105}$$

where the extension is performed up to some UV scale $\Lambda > \Lambda_0$, which is asymptotically large compared to all physical scales of interest,

$$\forall s \in m_{\mathrm{ext}}: \qquad \frac{s}{\Lambda} \ll 1\,. \tag{2.106}$$

This construction is perfectly consistent with the original RG flow (2.102) when the external parameters are set to their initial values,

$$\forall k \in [0,\Lambda_0]: \qquad \Gamma_k^{(\mathrm{RGc})}[\Phi](m_{\mathrm{ext}}^{(0)}) = \Gamma_k[\Phi](m_{\mathrm{ext}}^{(0)})\,. \tag{2.107}$$

On the other hand, if we performed the UV extension for a set of external parameters such that $s \sim \Lambda_0$, the RG flow towards lower scales would provide us with an infrared theory Γ_0^{new} that is incompatible with the low-energy observables used in the scale-fixing process. Notice that the concrete value for the new reference scale Λ is irrelevant as long as it is sufficiently large. Put differently, the condition (2.106) implies UV convergence for the backward propagation of flows at different values for external parameters. As a result, the introduction of the UV scale Λ does not lead to new artificial scale dependences:

$$\forall \Lambda \in \left\{ \Lambda > k \,|\, \forall s \in m_{\mathrm{ext}} : \frac{s}{\Lambda} \ll 1 \right\}: \qquad \frac{\mathrm{d}}{\mathrm{d}\Lambda}\Gamma_k^{(\mathrm{RGc})}[\Phi](m_{\mathrm{ext}}) = 0\,. \tag{2.108}$$

Once we have chosen some suitable value for Λ, this UV scale now sets a higher upper boundary for values of external parameters at which we can study the system without having regularization scheme artifacts spoil the results. The systematic removal of regularization scheme dependences by a UV extension which is consistent with given low-energy observables is referred to as RG consistency. In this regard, the relation (2.108) can be seen as a necessary condition for RG consistency. It is, however, important to realize that this procedure cannot suppress any scheme dependences that are already present in the system for $m_{\mathrm{ext}} = m_{\mathrm{ext}}^{(0)}$. Therefore, having the initial values $m_{\mathrm{ext}}^{(0)}$

[34] A generalization of our discussion to internal scales is straightforward but we nevertheless focus on external parameters here due to their high relevance for the studies covered in Chapter 3.

[35] How large exactly the fixed UV scale has to be compared to other relevant scales of the system in order to minimize regularization scheme artifacts, highly depends on the regularization scheme itself. Generally speaking, the smoother the suppression of high-momentum modes is implemented, the smaller the gap between the UV scale and the maximum value for external parameters can be. However, since we do not specify the regularization scheme here for the sake of generality, an asymptotically large reference scale is a safe choice.

sufficiently small compared to the initial scale Λ_0 in the first place is crucial for the reliability of results overall. The RG consistency condition closely resembles the requirement of independence with regard to the choice of the UV cutoff scale, see Eq. (2.30), but we again emphasize that these conditions are only directly comparable for momentum-dependent regulators. More generally, the RG consistency condition refers to the situation that the theory does not depend on the UV scale at which we start the RG flow as long as a certain hierarchy of scales is maintained.

The UV extension may in principle be performed up to arbitrarily high scales $\Lambda < \Lambda_{\mathrm{UV}}$ in order to allow for infrared results that are free of particular regularization scheme artifacts for a wide range of values for external parameters. We would, however, like to stress that a UV extension does not automatically imply that the effective theory under consideration has predictive power for values of external parameters beyond the physical energy scale which is inherently linked to the given classical action. An exact determination of this scale is quite involved as it requires an accurate study of the fundamental dynamics at all momentum scales but we can take the UV scale Λ_0 as an estimate. In general, the phenomenological meaning of the UV extension is highly dependent on the regularization scheme, the truncations in use, as well as the theory itself. By construction, low-energy models lack some of the microscopic degrees of freedom that are relevant at momentum scales beyond Λ_0 and therefore they cannot correctly describe the physics at energies much higher than Λ_0. To give an example, effective theories of QCD such as NJL-type models [74, 75] are typically constructed without the appearance of gauge fields since they aim at an understanding of bounded low-energy states, i.e., hadrons. Consequently, these models are not appropriate to describe the strong interaction at energies at which the gluon dynamics can no longer be neglected. Generally speaking, the UV extension should primarily be thought of as a formal extension of the initial condition for the RG flow such that a certain hierarchy of scales can be maintained.

The RG consistency methodology as presented so far is not restricted to the effective average action but equally applies to directly related objects such as correlation functions. The corresponding relations are then readily obtained from Eqs. (2.103) and (2.105) by functional differentiation. Let us consider the example of the two-point function in momentum space,

$$\begin{aligned}\Gamma_k^{(1,1)}(P,Q,m_{\mathrm{ext}}) &= \left(\frac{\overrightarrow{\delta}}{\delta\Phi^{\intercal}(-P)}\Gamma_k[\Phi](m_{\mathrm{ext}})\frac{\overleftarrow{\delta}}{\delta\Phi(Q)}\right)\Bigg|_{\Phi=\Phi_0} \\ &= \tilde{\Gamma}_k^{(1,1)}(Q,m_{\mathrm{ext}})\,(2\pi)^4\delta^{(4)}(P-Q)\ , \end{aligned} \tag{2.109}$$

where the reduced correlation function reads

$$\tilde{\Gamma}_k^{(1,1)}(Q,m_{\mathrm{ext}}) = \tilde{\Gamma}^{(1,1)}_{\Lambda_0,m_{\mathrm{ext}}^{(0)}}(Q) + \int_{\Lambda_0}^{k} \mathrm{d}k'\ \tilde{f}_{k'}^{(1,1)}(Q,m_{\mathrm{ext}})\ . \tag{2.110}$$

We note that functional derivatives introduce an explicit dependence on new momentum scales and the question arises of how these scales are to be dealt with in order to obtain an RG-consistent framework. First of all, since the external momentum Q enters the loop, the requirement of physical scales being small compared to the fixed UV scale Λ_0 also applies here. Furthermore, it is essential to understand that the functional derivatives also render the initial condition generally Q-dependent.[36] As a consequence, there is no reference flow at initial values for Q to perform a UV

[36] There are exceptions in which the definition of the microscopic theory or the choice of the truncation leads to a UV value for the wavefunction renormalization associated with Q being set to exactly zero. Then, the functional differentiation does not render the initial condition for the reduced correlation function under consideration momentum-dependent. Consequently, one may reinterpret this situation as having $Q = 0$ as the initial values in the scale-fixing process and RG consistency can be performed straightforwardly to minimize regularization scheme artifacts scaling with Q. Notice, however, that a vanishing wavefunction renormalization will render the corresponding renormalized masses divergent in the UV.

extension consistent with. For that reason, Λ_0 remains a natural upper boundary for values of Q. In other words, regularization scheme artifacts scaling with temperature or chemical potential can be eliminated by the RG consistency procedure but not those scheme dependences that originate from external momenta getting close to the fixed UV scale.

In synopsis, RG consistency refers to the situation in which the infrared physics is invariant with respect to our choice for the high-energy scale at which we start the RG flow. Inherently connected to this picture is the more formal statement that RG consistency implies the absence of regularization scheme artifacts, i.e., artificial effects originating from external parameters becoming comparable in magnitude to the fixed UV scale of the system. Once the UV parameters for a theory at hand have been fixed with the aid of some low-energy observables, finite external parameters, e.g., temperature or chemical potential, can, loosely speaking, shift the meaning of "high-energy" towards larger values. As a consequence, RG consistency then requires an adjustment of initial conditions such that a certain hierarchy of scales can be maintained. Generally speaking, RG consistency should always be taken into consideration to ensure a consistent removal of scheme dependences. Notice, however, that inherent regulator artifacts, e.g., effects arising from an explicit symmetry breaking as induced by the regulator function, cannot be repaired through RG consistency.

2.3 Thermal field theory

In standard literature on quantum field theory, the theory under consideration is conventionally formulated without any dependence on external parameters, e.g., temperature T or chemical potential μ. Temperature is a macroscopic property of a statistical system but can be related to microscopic degrees of freedom of the latter by means of the equipartition theorem. More specifically, temperature can then be used to quantify the degree of thermal agitation of the particles in a system. In thermodynamics, a key property of temperature is that, if two physical systems are in thermal equilibrium, then they have the same value of T. On the other hand, the chemical potential is directly related to the number density of particles in the system. Analogously to the temperature case, two systems are in chemical equilibrium if they share the same value of μ. In contrast to temperature, however, densities are not directly controllable in the sense of an experimental parameter. In the context of, for example, Fermi gases, the chemical potential can be adjusted indirectly by means of an external field that controls the behavior of the gas within the atom trap [250, 251]. In the absence of such external parameters, i.e., at $T = \mu = 0$, a quantum field theory is meant to describe a quantum system in the vacuum. In fact, for ordinary hadronic matter as found on earth at room temperature, corresponding values of T and μ are sufficiently small compared to the relevant mass scales in the system such that assuming vacuum conditions for the quantum field theory at hand constitutes an excellent approximation. Therefore, vacuum quantum field theories have been studied in great detail for several decades and theoretical predictions in this framework are in remarkable agreement with experimental data obtained at particle colliders.

Our physical universe is at finite temperature and incorporates matter of finite density. For that reason, theoretical descriptions of nature should in general always try to include thermodynamical effects. Despite the success of quantum field theory for vacuum systems, the thermal background and the influence of a particle reservoir can no longer be neglected when external parameters become fairly high. Ultrarelativistically hot and dense matter needs to be understood in many problems ranging from early-universe cosmology [252, 253] over nuclear physics of compact stars [254–256] to the theoretical description of heavy-ion collisions [257–259]. A suitable framework

for studying the effects of finite temperature and density is thermal field theory, which can be extended to Abelian as well as non-Abelian gauge theories. In particular, the understanding of strong-interaction matter at high temperatures and densities is of great interest since QCD under extreme conditions can give rise to a wealth of interesting phenomena and leads to the prediction of various phases, see, e.g., Refs. [10, 260–262] for reviews. Most of the current theoretical efforts aim at an improvement of our understanding of non-perturbative phenomena arising in hot and dense quark matter as asymptotic regimes of the QCD phase diagram have already been exploited perturbatively. To this end, we would like to highlight that renormalization group approaches have played and still play a very important role in the investigation of the phase structure and thermodynamics of QCD, see, e.g., Refs. [42, 78, 263–265].

Phenomenologically speaking, thermal field theory deals with the behavior of a large ensemble of quantum particles in the presence of temperature and chemical potential. It should therefore be thought of as the unified framework of statistical mechanics and quantum field theory. More concretely, thermal field theory is actually a rather generic name for different approaches to quantum field theory at finite temperature and finite density. These well-developed formalisms are the imaginary-time formalism [266], the closed time path formalism of Keldysh and Schwinger [267, 268], as well as thermo field dynamics [269, 270]. Within this work, we will put our emphasis on the first mentioned approach due to its close connection to the path integral formulation of Euclidean quantum field theory. Moreover, the imaginary-time formalism is particularly suited to describe the equilibrium thermodynamics of a given system and renders the calculation of bulk properties like pressure, entropy and other thermodynamical potentials relatively simple. Therefore, we begin by presenting the most important aspects of this formalism in the following. In addition, we discuss the influence of external parameters such as temperature and chemical potential on the calculation of correlation functions. For general and extensive literature on thermal field theory, we refer the reader to Refs. [121, 271–276].

2.3.1 Imaginary-time formalism

For everything that follows, we will assume that the physical system under consideration can be described by a Hamiltonian that has no explicit time dependence. The imaginary-time formalism is based on the formal analogy between the time evolution operator of a given real-time quantum theory and the corresponding statistical operator. With the introduction of complex times by analytic continuation, we can switch from dynamics to statistics,

$$\exp\left(-\mathrm{i}t\hat{H}\right) \xrightarrow{t\to-\mathrm{i}\beta} \exp\left(-\beta\hat{H}\right) , \tag{2.111}$$

where $\beta = 1/T$ denotes the inverse equilibrium temperature. Both operators share the properties of Markovian time evolution and locality of the evolution for short time intervals such that their matrix elements can be represented by path integrals [105]. Based on the path integral, powerful methods developed in quantum field theory and statistical physics have become closer and closer over the last decades. In particular, the renormalization group not only represents a non-perturbative approach to renormalization theory but also provides a natural framework in which to understand universality. Moreover, the concept of "spontaneous symmetry breaking" with its origin in condensed-matter physics was successfully transferred to particle physics [74, 75, 277, 278] in order to help understand phase transitions. The path integral description can even be used in polymer physics where it has proven to be an ideal tool for studying statistical fluctuations of line-like physical objects [104, 279, 280]. More generally, the relation above hints at a deep connection between the frameworks of quantum and statistical physics. In fact, it is observed that every quantum field theory in d spacetime dimensions corresponds to a statistical system in a space of $d-1$

dimensions [272]. In the same way, there is a correspondence between the correlation functions of a quantum field theory and those of a related statistical system, with quantum fluctuations being replaced by thermal fluctuations. For more information on the connection between statistical physics and quantum field theory, we refer to Refs. [281–287].

The relation (2.111) shows that, from the point of view of a real-time quantum theory, the parameter β in the statistical operator plays the role of a real-valued time in the imaginary direction of the complex t-plane. Our approach to thermal field theory, which is built upon this very relation, is therefore referred to as the imaginary-time formalism. Since we have traded the time variable for temperature by analytic continuation, the imaginary-time formalism is well suited to describe static physical systems in thermal equilibrium.[37] On the other hand, if the primary focus is on dynamical, non-equilibrium effects then methods which allow for additional evolution in real time are necessary, see, e.g., Refs. [104, 129, 289–291] for further discussions. Moreover, notice that the relation (2.111) has the implication that a quantum statistical system in thermodynamical equilibrium is mathematically equivalent to an Euclidean quantum theory. For this reason, Euclidean quantum field theory provides us with a natural framework to describe the equilibrium thermodynamics of a given quantum system.

Let us consider a generic quantum system with a constant number of particles for each particle species in the system. In the operator formalism, the corresponding Hamiltonian then has the structure

$$\hat{H} = \hat{H}_0 - \sum_i \mu_i \hat{N}_i \,, \tag{2.112}$$

where the summation index i runs over the number of particle species. The chemical potentials $\mu_i \in \mathbb{R}$ enter the theory as Lagrange multipliers and determine the average number of particles in the system for each species. Accordingly, every chemical potential gets paired with the corresponding particle number operator $\hat{N}_i$ in the description above. At vanishing chemical potential, the Hamiltonian coincides with the Hamiltonian $\hat{H}_0$ of the canonical ensemble. Furthermore, consistency requires that the construction of the Hamiltonian with non-zero chemical potentials is constrained by the relation $\left[\hat{H}, \hat{N}_i\right] = 0$, which implies particle number conservation. Assuming fields to be the relevant degrees of freedom for the quantum system under consideration, the grand canonical partition function can be expressed as

$$\begin{aligned} \mathcal{Z}(T, \{\mu_i\}) &= \operatorname{tr}\left\{ \mathrm{e}^{-\beta\left(\hat{H}_0 - \sum_i \mu_i \hat{N}_i\right)} \right\} \\ &= \mathcal{N} \oint \mathcal{D}\Phi \, \exp\left(- \int_{\vec{x}} \int_0^\beta \mathrm{d}x^0 \left(\mathcal{L}_0\big(\Phi(x), \partial_\mu \Phi(x)\big) - \mathrm{i} \sum_i \mu_i \, \mathcal{N}\big(\Phi_i(x), \partial_0 \Phi_i(x)\big) \right) \right) . \end{aligned} \tag{2.113}$$

At the classical level, Lagrange multipliers couple to conserved Noether charges such that, in the case of the chemical potential, $\mathcal{N}$ denotes the charge density which corresponds to a $U(1)_\mathrm{V}$ symmetry of the theory. From symmetry arguments, it then follows that a chemical potential can only couple to complex-valued field degrees of freedom. Let us therefore consider the example of a theory of Dirac fermions.[38] Here, the invariance of the theory under the simultaneous transformations

$$\forall \theta \in \mathbb{R}: \qquad \psi \to \mathrm{e}^{\mathrm{i}\theta} \, \psi \,, \qquad \overline{\psi} \to \overline{\psi} \, \mathrm{e}^{-\mathrm{i}\theta} \tag{2.114}$$

[37] It is possible to study near-equilibrium physics by introducing a real-time dependence through analytic continuation after the result has been obtained from the imaginary-time formalism [288].

[38] Notice that a theory of massive Majorana fermions is not $U(1)_\mathrm{V}$-symmetric. Majorana neutrinos allow for a neutrinoless double beta decay which leads to a violation of lepton number conservation, see, e.g., Ref. [292].

implies a conserved charge, namely the fermion number F, which is given by

$$F = \int_{\vec{x}} \mathcal{N}\left(\overline{\psi}(x), \psi(x)\right) = \int_{\vec{x}} \overline{\psi}(x)\, \gamma^0\, \psi(x) = \#\text{fermions} - \#\text{antifermions}\,. \tag{2.115}$$

In quantum electrodynamics, the fermion number conservation automatically implies the conservation of the electric charge. In quantum chromodynamics, the conserved charge is commonly associated with the total baryon number

$$B = \sum_q \left(N_q B_q + N_{\bar{q}} B_{\bar{q}}\right) = \sum_q \left(N_q - N_{\bar{q}}\right)\, \frac{1}{N_\mathrm{c}} = \frac{F}{N_\mathrm{c}}\,, \tag{2.116}$$

where the summation index q runs over the values of some suitably chosen quantum number, e.g., flavor or color. Whereas N_q denotes the number of fermions with quantum number q, B_q stands for the corresponding fermion baryon number. As usual, the bar notation indicates the appearance of antifermions and their quantum number. Moreover, the quantity N_c refers to the number of color degrees of freedom of which there are three in nature. Notice that the theory of the strong interaction conserves the numbers of each flavor and color individually so there are in general independent chemical potentials for each internal quark degree of freedom, see, e.g., Refs. [293–295]. It is important to mention that the introduction of a finite chemical potential leads to an explicit breakdown of charge conjugation symmetry. Under charge conjugation, the Noether charge undergoes a change in sign, encouraging the interpretation of "swapping" particles and antiparticles:

$$\mathcal{N}\left(\Phi_i(x), \partial_0 \Phi_i(x)\right) \to \mathcal{N}\left(\Phi_i^C(x), \partial_0 \Phi_i^C(x)\right) = -\mathcal{N}\left(\Phi_i(x), \partial_0 \Phi_i(x)\right)\,. \tag{2.117}$$

Although the chemical potential is not directly affected by charge conjugation, its presence explicitly breaks the invariance of the classical action under charge conjugation transformations. In addition, it immediately follows from Eq. (2.117) that theories which are invariant under charge conjugation at zero chemical potential have the property of producing physical observables invariant under the transformation $\mu_i \to -\mu_i$. It should further be noted that Euclidean time evolution introduces an additional factor of the imaginary unit to the part of the exponential that includes the chemical potentials, see Eq. (2.113). This can be thought of as the result of analytically continuating the Minkowskian number density to Euclidean spacetime, see Appendix A.4 for our conventions regarding Euclidean quantum field theory.

There are several things about the partition function and its path integral representation that we would like to point out. First of all, the interaction vertices of the theory at finite external parameters are exactly the same as for the vacuum theory. In fact, the only difference from the vacuum theory is the form of the propagator which carries all the dependence on temperature and chemical potential. Also notice that the partition function can be promoted to a functional by inserting a source term. Analogous to the vacuum case, see Eqs. (2.4)-(2.8), we write

$$\begin{aligned}\mathcal{Z}[J](T, \{\mu_i\}) &= \mathrm{tr}\left\{\hat{T}\; \mathrm{e}^{-\beta \hat{H}} \mathrm{e}^{J^\intercal \cdot \hat{\Phi}}\right\} \\ &= \mathcal{N} \oint \mathcal{D}\Phi\; \exp\left(-S[\Phi]\big|_{T,\{\mu_i\}} + \int_{\vec{x}} \int_0^\beta \mathrm{d}x^0\, \left(J^\intercal\right)_\alpha(x)\, \Phi^\alpha(x)\right)\,.\end{aligned} \tag{2.118}$$

The construction of regularized generating functionals for thermodynamic correlation functions now exactly follows the methodology presented for the vacuum case. We will thus not elaborate on such matters anymore and instead focus on the effects of finite external parameters within the imaginary-time formalism. As before, ordinary thermodynamic correlation functions can then be

obtained from the partition functional by functional differentiation and proper normalization. In particular, the two-point function reads

$$G^{(2)}_{T,\{\mu_i\}}(x,y) = \langle \Phi(x)\, \Phi^\intercal(y)\rangle_{T,\{\mu_i\}} = \frac{1}{\mathcal{Z}(T,\{\mu_i\})}\, \mathrm{tr}\left\{\hat{T}\; \mathrm{e}^{-\beta\hat{H}}\; \hat{\Phi}(x)\; \hat{\Phi}^\intercal(y)\right\}\,, \tag{2.119}$$

which is the generalization of the two-point correlator as shown in Eq. (2.10) to finite temperature and chemical potential. Making use of the time evolution of field operators in the Heisenberg picture,

$$\hat{\Phi}(x^0,\vec{x}) = \mathrm{e}^{-\beta\hat{H}}\; \hat{\Phi}(0,\vec{x})\; \mathrm{e}^{\beta\hat{H}}\,, \tag{2.120}$$

as well as the cyclic properties of the trace, we obtain

$$G^{(2)}_{T,\{\mu_i\}}(x,y) = (-1)_\Psi\; G^{(2)}_{T,\{\mu_i\}}(x,y^0+\beta,\vec{y})\,. \tag{2.121}$$

In words, the Green's function exhibits the feature of being (anti)periodic in time with period β. This is known as the Kubo-Martin-Schwinger (KMS) relation [296–298] and is an example of the detailed-balance principle of statistical physics, ensuring stability of thermal equilibrium under fluctuations. Since the KMS relation is a statement about the two-point function, it can be used to help define thermal propagators. Nevertheless, it is also possible to promote this relation to higher n-point functions [299]. It is important to realize that the KMS relation directly implies periodic and antiperiodic boundary conditions for thermal boson and fermion fields, respectively,

$$\Phi(x^0,\vec{x}) = (-1)_\Psi\; \Phi(x^0+\beta,\vec{x})\,. \tag{2.122}$$

As the imaginary-time formalism shows, finite temperature leads to a compactification of the time dimension and gives rise to periodicity constraints in the time-like direction imposed on the field variables. Technically speaking, the Euclidean space for the thermal fields has the topology of a cylinder with time as a periodic variable. These (anti)periodicity conditions ensure time-translation invariance of the finite-temperature theory and therefore play a crucial role in the definition of the closed path integral (2.113). More specifically, the functional integral representation of the partition function needs to take into account all field configurations that satisfy the (anti)periodicity relation above. Notice that the translation invariance of the action allows us to impose the boundary conditions (2.122) for the path integral at any point in time, e.g., $x^0 = 0$ or $x^0 = -\frac{\beta}{2}$. Both choices are equivalent but the widespread convention of constraining the time-like direction of spacetime to values $[0,\beta]$ rather than $[-\frac{\beta}{2},\frac{\beta}{2}]$ immediately leads to the necessity of boundary conditions for fields evaluated at $x^0 = 0$. In the zero-temperature limit, $\beta\to\infty$, either choice is still valid but only the second case leads to a path integral description which is explicitly time-translation invariant [105, 121] and consistent with our vacuum formulation, see Eq. (2.5). Due to the periodicity of the time variable in position space, the time-like direction of momentum space is not continuous anymore but is reduced to an infinite set of equidistant points, so-called Matsubara frequencies. In particular, the Fourier series expansion reads

$$\Phi(x) = \int_{\vec{p}} \frac{1}{\beta}\sum_{n\in\mathbb{Z}} \mathrm{e}^{\mathrm{i}\varpi_n x^0}\, \mathrm{e}^{\mathrm{i}\vec{p}^\intercal\vec{x}}\; \Phi_n(\vec{p})\,, \tag{2.123}$$

where the Matsubara frequencies [266] are defined as

$$\varpi_n^{(a)} = \frac{2\pi}{\beta}\left(n+\frac{1+a}{4}\right)\,, \qquad \omega_n = \varpi_n^{(-1)}\,, \qquad \nu_n = \varpi_n^{(1)} \tag{2.124}$$

for bosons ($a=-1$) and fermions ($a=1$), respectively. The infinite series over Matsubara frequencies is generally referred to as a Matsubara sum. For a full presentation of the behavior under

Fourier transformations, see Appendix A.5. Interestingly, the Matsubara zero mode is exactly zero for bosons but finite for fermions. At $n = 0$, we get $\omega_0 = 0$, which is responsible for infrared divergences in thermal field theories for massless bosons. On the other hand, finite temperature naturally screens such a divergence in fermionic propagators since $\nu_0 = \pi T$.

Any continuum formulation of a relativistic quantum field theory should be Lorentz-invariant in the vacuum limit, i.e., at $T = \mu = 0$. Nevertheless, the introduction of finite temperature or finite chemical potential leads to an explicit breakdown of Lorentz symmetry.[39] Both external parameters treat the time-like direction of spacetime differently from the others such that Lorentz symmetry breaks down to the invariance of spatial coordinates under $SO(3)$ transformations. Whereas finite temperature spoils the invariance of the integral measure under Lorentz transformations, a finite chemical potential is accompanied by a charge density that constitutes a Lorentz vector directed in the time-like direction of spacetime. From a phenomenological point of view, finite temperature introduces a preferred Lorentz frame where the plasma of particles and antiparticles, which constitutes the heat bath, is at rest. Analogously, the presence of a particle reservoir as indicated by a finite chemical potential implies the existence of a preferred reference frame for the formulation of physical laws. It should again be mentioned that this symmetry-breaking process in thermal field theory is entirely physical and that it must not be confused with a regulator-induced loss of symmetry which, on the other hand, is completely artificial. Despite the deforming behavior of external parameters towards Lorentz symmetry we would like to highlight that a finite chemical potential also gives rise to a new invariance principle of a zero-temperature field theory, the Silver-Blaze symmetry. This symmetry leads to a peculiar behavior of observables with respect to the chemical potential, which is known as the Silver-Blaze property.

2.3.2 The Silver-Blaze property

In order to study a physical system at finite density, the vacuum theory has to be modified by the insertion of a chemical potential and an associated Noether charge such that the resulting description is consistent with the statistics of a grand canonical ensemble of corresponding many-particle systems. For simplicity, we will consider a theory of only a single particle species in the following. A non-zero chemical potential μ alters the spectrum of the kinetic operator relative to the $\mu = 0$ case, leading to the expectation that the partition function and related quantities change as well. This, however, turns out to be not the case at zero temperature. As an anecdote to one of Arthur Conan Doyle's stories, this phenomenon has been labeled as the Silver-Blaze property [304]. Specifically, the Silver-Blaze property refers to the fact that the partition function of a system at $T = 0$ does not exhibit any dependence on the chemical potential, i.e., it remains as that of the vacuum, unless the chemical potential exceeds a critical value μ_{SB}. As a consequence, the chemical potential needs to be increased beyond this threshold in order to excite any states at zero temperature. The critical value is closely connected to the vacuum pole mass of the particles coupling to the chemical potential. This means that the charge density associated with the $U(1)_{\mathrm{V}}$ symmetry of the theory stays zero as long as the chemical potential has not overcome the particle mass. From the standpoint of statistical physics, this behavior may in fact not be too surprising. For a better understanding, we consider the standard thermodynamic relation

$$\mu = \frac{1}{V}\left(\frac{\partial F_{\mathrm{H}}}{\partial n}\right)\bigg|_{T,V}, \tag{2.125}$$

[39] This breakdown of symmetry at finite temperature or chemical potential is in fact independent of how these parameters themselves transform under a Lorentz boost. For a discussion on relativity and thermodynamics, see, e.g., Refs. [300–303].

where n denotes the number density of particles and V the spatial volume in which the physical system under consideration is confined. In words, the chemical potential is nothing but the change in Helmholtz free energy when particles are added to or removed from the system. In thermal field theory, the Helmholtz free energy is generally given by

$$F_{\mathrm{H}} = \frac{1}{\beta} \ln(\mathcal{Z}) = -\frac{1}{\beta} \Gamma[\Phi_0] \,. \tag{2.126}$$

Phenomenologically speaking, the relation (2.125) implies that we cannot expect any feedback from the system if the chemical potential is not large enough to induce the addition of a single particle. Once the chemical potential overcomes the energy associated with the particle, the behavior of the system will deviate from the vacuum case. Overall, the Silver-Blaze property is a quite generic feature of physical systems at zero temperature and has been studied in the context of QCD [81, 304–307] as well as scalar field theories [308–311].

Let us have a look at a generic fermonic theory at zero temperature but finite density as given by an action with the structure

$$S[\overline{\psi}, \psi]\big|_{\mu} = \int_x \overline{\psi}(x) \big[\mathrm{i}\partial\!\!\!/ - \mathrm{i}\gamma^0 \mu + \mathrm{i} m_\psi \big] \psi(x) \; + \; S_{\mathrm{int}}[\overline{\psi}, \psi] \,, \tag{2.127}$$

where S_{int} has no μ-dependence but contains all multi-fermion interactions of the theory. Since the theory is built from fermion bilinears, it follows that the action is invariant under the simultaneous transformations

$$\forall \alpha \in \mathbb{R}: \qquad \psi(x) \to \mathrm{e}^{\mathrm{i}\alpha x^0} \psi(x) \,, \qquad \overline{\psi}(x) \to \overline{\psi}(x) \, \mathrm{e}^{-\mathrm{i}\alpha x^0} \,, \qquad \mu \to \mu + \mathrm{i}\alpha \,, \tag{2.128}$$

where the continuous transformation parameter α has the physical dimensions of energy. The invariance of the fermionic theory with respect to these transformations is referred to as the Silver-Blaze symmetry.[40] This may be considered some kind of local gauge symmetry with the chemical potential acting as a constant gauge field. Unlike true gauge fields, however, the chemical potential is an external control parameter and does not get integrated over in the path integral. Therefore, the Silver-Blaze symmetry is not a symmetry in the sense of Noether in which only the field degrees of freedom are subjected to a transformation. Correspondingly, there is no conserved charge associated with this invariance principle. Although we started with a purely fermionic action, fermions may not be the relevant degrees of freedom of the system at low energies. Instead, bosonic bound states become more important and may condense, giving rise to, e.g., Cooper pairs in condensed-matter physics or hadrons in QCD. It can therefore be beneficial to perform a bosonization procedure and thereby introduce effective bosonic degrees of freedom,

$$\phi \sim \overline{\psi} \, \psi \,, \qquad \Delta \sim \psi^{\mathsf{T}} \, \psi \,, \qquad \Delta^* \sim \overline{\psi} \, \overline{\psi}^{\mathsf{T}} \,. \tag{2.129}$$

In the context of strong-interaction matter, ϕ refers to a meson while Δ and Δ^* denote diquark states [25, 27, 28, 305, 312]. For more details on bosonization, see Appendix B. It is now important to realize that, due to their internal fermionic degrees of freedom, the effective boson

[40] Strictly speaking, the Silver-Blaze symmetry relies on a set of more general transformations. Considering a time-dependent transformation parameter $\alpha(x^0)$, the generalized transformations read

$$\psi(x) \to \mathrm{e}^{\mathrm{i}\alpha(x^0)} \psi(x) \,, \qquad \overline{\psi}(x) \to \overline{\psi}(x) \, \mathrm{e}^{-\mathrm{i}\alpha(x^0)} \,, \qquad \mu \to \mu + \mathrm{i}\partial_0 \alpha(x^0) \,.$$

The special case as presented in the main text can easily be recovered by considering $\alpha(x^0) = \alpha \, x^0$ with α being some real-valued constant. Notice, however, that the (anti)periodic boundary conditions imposed on the field degrees of freedom at finite temperature enforce such a factorization anyway so, for reasons of consistency, we decide to stick with the more simple presentation also at zero temperature.

fields can also couple to the same chemical potential μ and behave as follows under a Silver-Blaze transformation,

$$\phi(x) \to \phi(x)\,, \qquad \Delta(x) \to \Delta(x)\,\mathrm{e}^{\mathrm{i}2\alpha x^0}\,, \qquad \Delta^*(x) \to \Delta^*(x)\,\mathrm{e}^{-\mathrm{i}2\alpha x^0}\,. \tag{2.130}$$

In order to include the new boson fields into our formalism, we adapt the definition of the superfield Φ, see Eq. (2.3), by identifying[41]

$$\varphi(x) = \begin{pmatrix} \phi(x) \\ \Delta(x) \\ \Delta^*(x) \end{pmatrix} = \int_p \mathrm{e}^{\mathrm{i}p^\intercal x} \begin{pmatrix} \phi(p) \\ \Delta(p) \\ \Delta^*(p) \end{pmatrix} = \int_p \mathrm{e}^{\mathrm{i}p^\intercal x}\,\varphi(p)\,. \tag{2.131}$$

This allows for the general statement that a field contained in the general field variable Φ transforms in accordance with its fermion content,

$$\Phi_j(x) \to \Phi_j(x)\,\exp\left(\mathrm{i}F_j\alpha x^0\right)\,, \tag{2.132}$$

where F_j is the fermion number associated with the field Φ_j. In momentum space, the Silver-Blaze transformations for the fields are realized by a shift in the time-like momentum:

$$\Phi_j(p) \to \Phi_j(p^0 - F_j\alpha, \vec{p})\,. \tag{2.133}$$

After having worked out the generalized symmetry property of a fermionic theory that comes along with a finite chemical potential, let us investigate its implications on the partition function and related objects. At zero temperature and finite chemical potential, the partition function of a system of fermions and bosons may generally be written as

$$\mathcal{Z}(\mu) = \mathcal{N}\int \mathcal{D}\Phi\;\mathrm{e}^{-S[\Phi]|_\mu} = \mathcal{N}\exp\left(-S[\Phi_\mathrm{c}]\big|_\mu - \frac{(-1)_\Psi}{2}\,\mathrm{Tr}\left\{\mathrm{Ln}\left(S^{(1,1)}[\Phi_\mathrm{c}]\big|_\mu\right)\right\} - \ldots\right)\,, \tag{2.134}$$

where the fixed field configuration Φ_c is determined by[42]

$$\forall x \in \mathbb{R}^4: \qquad \left(\frac{\vec{\delta}}{\delta\Phi(x)}S[\Phi]\big|_\mu\right)\bigg|_{\Phi=\Phi_\mathrm{c}} = 0\,. \tag{2.135}$$

As the path integral measure is invariant under Silver-Blaze transformations, we find that the partition function is periodic in the chemical potential with period $\mathrm{i}\alpha$. Put differently, the partition function is invariant under a shift of the chemical potential along the imaginary axis:

$$\mathcal{Z}(\mu) = \mathcal{Z}(\mu + \mathrm{i}\alpha)\,. \tag{2.136}$$

Assuming that the partition function is analytic, it follows that the partition function does not depend on the chemical potential at all. More specifically, we can perform an analytic continuation

[41] To consistently introduce the two complex-valued diquark fields as independent bosonic degrees of freedom, it must hold that

$$\Delta^*(x) = [\Delta(x)]^*\,, \qquad \Delta^*(p) = [\Delta(-p)]^*\,.$$

[42] In the literature, Φ_c is often referred to as the classical field since it represents a solution to the classical equation of motion as derived from the variational principle of classical physics. Notice, however, that Φ_c must not be confused with the classical field as defined in Eq. (2.20), where the latter is an expectation value taking into account all quantum fluctuations.

of the transformation parameter $\alpha \to \mathrm{i}\mu$ and conclude that $\mathcal{Z}(\mu) = \mathcal{Z}(0)$ as long as our assumption holds true.[43] This means the partition function remains at the vacuum value until the chemical potential μ leaves the domain of analyticity for $\mathcal{Z}$. To understand why the partition function is not analytic for all values of μ, notice that a finite chemical potential couples to the time-like direction of the kinetic operator, see Eq. (2.127). In particular, it acts like an external momentum of Minkowski spacetime. As a consequence, introducing a finite chemical potential leads to a pole in the propagator or, equivalently, a root in the inverse propagator for $\mu \geq \mu_{\mathrm{SB}}$. This critical value μ_{SB} is determined by the vacuum pole mass of the lowest-lying state with non-vanishing fermion number. The pole in the propagator of the theory is integrable but nevertheless restricts the domain of analyticity to values of the chemical potential satisfying $\mu < \mu_{\mathrm{SB}}$.[44] Within this domain, the partition function remains constant. Beyond this domain, the partition function becomes a non-analytic function of the chemical potential and thus differs from the vacuum value.[45] This is known as the Silver-Blaze property. This feature translates to all other quantities that are derived from the classical action, meaning that zero-temperature observables are generally independent of the chemical potential unless its value exceeds the threshold μ_{SB}.

Analogous to the Silver-Blaze property of the partition function, a more general invariance principle can be formulated for generating functionals,

$$\mathcal{Z}[J](\mu) = \mathcal{Z}\left[\mathrm{e}^{-\mathrm{i}\alpha\mathscr{F}x^0} J\right](\mu + \mathrm{i}\alpha)\,, \qquad \Gamma[\Phi]|_\mu = \Gamma\left[\mathrm{e}^{\mathrm{i}\alpha\mathscr{F}x^0}\Phi\right]\Big|_{\mu+\mathrm{i}\alpha}\,, \tag{2.137}$$

where $\mathscr{F}$ denotes a matrix in field space carrying all the fermion numbers F_j for the fields Φ_j on its diagonal. Evaluating the functionals at the ground state of the system, i.e., at vanishing external sources, lets us recover Eq. (2.136). The implications of the Silver-Blaze property on correlation functions are now readily obtained by functional differentiation. Due to its relevance in the context of the functional renormalization group, we will focus on the quantum effective action and its correlation functions in the following. In particular, the two-point vertex function at zero temperature now satisfies

$$\begin{aligned}\left(\frac{\overrightarrow{\delta}}{\delta\Phi_i(x_1)}\,\Gamma[\Phi]\big|_\mu\,\frac{\overleftarrow{\delta}}{\delta\Phi_j(x_2)}\right)\Big|_{\Phi=\Phi_0} &= \left(\frac{\overrightarrow{\delta}}{\delta\Phi_i(x_1)}\,\Gamma\left[\mathrm{e}^{\mathrm{i}\alpha\mathscr{F}x^0}\Phi\right]\Big|_{\mu+\mathrm{i}\alpha}\,\frac{\overleftarrow{\delta}}{\delta\Phi_j(x_2)}\right)\Big|_{\Phi=\Phi_0} \\ &= \left(\frac{\overrightarrow{\delta}}{\delta\Phi'_i(x_1)}\,\Gamma\left[\Phi'\right]\big|_{\mu+\mathrm{i}\alpha}\,\frac{\overleftarrow{\delta}}{\delta\Phi'_j(x_2)}\right)\Big|_{\Phi'=\mathrm{e}^{\mathrm{i}\alpha\mathscr{F}x^0}\Phi_0} \mathrm{e}^{\mathrm{i}\alpha\left(F_i x_1^0 + F_j x_2^0\right)}\,.\end{aligned} \tag{2.138}$$

[43] One might be wondering why we did not initially consider a complex-valued parameter α, which would directly result in translation invariance of the partition function in the chemical potential along the real axis. In that case, the Silver-Blaze transformations of the fields in position space, see Eq. (2.132), could not be associated with phase rotations but rather with exponential scalings. Additionally, having $\alpha \in \mathbb{C}$ implies a shift of time-like momenta along the imaginary direction, see Eq. (2.133), which only makes sense if the field degrees of freedom can be analytically continued. Overall, while it is possible to start with a complex-valued parameter, it does not eliminate the need for analytic continuation and would lead to an unconventional presentation of the Silver-Blaze property.

[44] The logarithmic expression $\mathrm{Ln}(S^{(1,1)}[\Phi_c])$ in Eq. (2.134) becomes ill-defined when the propagator develops a pole. However, logarithmic functions diverge slowly enough such that the area under their curve remains finite near the singularity, meaning that infinite logarithmic discontinuities are integrable. As a result, the loop integral $\mathrm{Tr}\left\{\mathrm{Ln}(S^{(1,1)}[\Phi_c])\right\}$ remains finite and continuous at and beyond the critical value for the chemical potential. Nevertheless, the existence of such a critical value renders the behavior of an integrand qualitatively different for $\mu < \mu_{\mathrm{SB}}$ and $\mu > \mu_{\mathrm{SB}}$, resulting in an integral being non-differentiable at $\mu = \mu_{\mathrm{SB}}$.

[45] In the presence of a finite chemical potential, the associated pole for $\mu \geq \mu_{\mathrm{SB}}$ renders the multi-integral $\mathrm{Tr}\left\{\mathrm{Ln}(S^{(1,1)}[\Phi_c])\right\}$ generally μ-dependent. Since the partition function is real-valued, the Silver-Blaze symmetry implies that the partition function can only depend on the real part $\mathfrak{Re}\{\mu\}$. The real part, however, is not a holomorphic function because it does not satisfy the Cauchy-Riemann equations.

Notice that a Silver-Blaze-symmetric system in particular has a ground state configuration Φ_0 that respects this symmetry. This means that such a system requires fields with non-zero fermion numbers to either vanish or keep a time dependence at the ground state. Therefore, assuming a finite and homogeneous ground state for, e.g., diquarks automatically spoils the Silver-Blaze property of the observable of interest. If the quantum effective action is analytic for $\mu < \mu_{\mathrm{SB}}$, we can perform an analytic continuation of the transformation parameter $\alpha \to \mathrm{i}\alpha$ as long as $\mu - \alpha < \mu_{\mathrm{SB}}$. Setting $\alpha = \mu$ leads us to

$$\Gamma^{(1,1)}_{i,j}(x_1,x_2)\big|_\mu = \Gamma^{(1,1)}_{i,j}(x_1,x_2)\, \mathrm{e}^{-\mu\left(F_1 x_1^0 + F_2 x_2^0\right)} \,. \tag{2.139}$$

The general implication is that, in position space, the dependence of correlation functions on the chemical potential is given by the vacuum correlation functions and the multiplication of an appropriate exponential factor. In momentum space, this translates to

$$\begin{aligned}
\Gamma^{(1,1)}_{i,j}(p_1,p_2)\big|_\mu &= \int_{x_1}\int_{x_2} \mathrm{e}^{-\mathrm{i}p_1^\intercal x_1}\, \Gamma^{(1,1)}_{i,j}(x_1,x_2)\big|_\mu\, \mathrm{e}^{\mathrm{i}p_2^\intercal x_2} \\
&= \Gamma^{(1,1)}_{i,j}(p_1^0 - \mathrm{i}F_i\mu, \vec{p}_1, p_2^0 + \mathrm{i}F_j\mu, \vec{p}_2) \\
&= \tilde{\Gamma}^{(1,1)}_{i,j}(p_1^0 - \mathrm{i}F_i\mu, \vec{p}_1)\, (2\pi)^4 \delta^{(4)}\left(p - q - \mathrm{i}\mu(F_i + F_j)\right) \,.
\end{aligned} \tag{2.140}$$

We emphasize that the Dirac delta distribution cannot be analytically continued to complex-valued arguments. In other words, energy conservation implies that the two-point function only exists for $F_i = -F_j$. For the field degrees of freedom as covered in this thesis, the possible two-point functions are given by

$$\tilde{\Gamma}^{(1,1)}_{\bar{\psi},\psi}(p)\big|_\mu = \tilde{\Gamma}^{(1,1)}_{\bar{\psi},\psi}(p^0 + \mathrm{i}\mu, \vec{p}) \,, \tag{2.141}$$

$$\tilde{\Gamma}^{(1,1)}_{\phi,\phi}(p)\big|_\mu = \tilde{\Gamma}^{(1,1)}_{\phi,\phi}(p^0, \vec{p}) \,, \tag{2.142}$$

$$\tilde{\Gamma}^{(1,1)}_{\Delta^*,\Delta}(p)\big|_\mu = \tilde{\Gamma}^{(1,1)}_{\Delta^*,\Delta}(p^0 + \mathrm{i}2\mu, \vec{p}) \,. \tag{2.143}$$

We observe that the zero-temperature vertex functions in momentum space can for $\mu < \mu_{\mathrm{SB}}$ be obtained from the corresponding vacuum correlation functions by shifting the time-like mode of the external momentum into the imaginary direction. The absolute magnitude of the shift here depends on the fermion content of the fields involved. The relations above further display that the vertex functions for fields with non-zero fermion numbers are generally complex-valued for finite external momenta. Nevertheless, the overall partition function as well as the quantum effective action remain real-valued. It should also be mentioned that, although we have restricted the explicit presentation to the two-point function for illustrative purposes, the discussion of consequences of the Silver-Blaze property is in fact quite general and applies to correlation functions of arbitrary order.

We would also like to stress that the Silver-Blaze property is only present at zero temperature. Finite temperature leads to a compactification of the time direction, which imposes periodicity constraints on the field degrees of freedom entering the path integral, see Eq. (2.122). This periodicity in position space translates to a discretization of time-like modes in momentum space, giving rise to Matsubara frequencies. Accordingly, the periodicity constraints for thermal fields also enforce a discretization of the transformation parameter α in Eq. (2.127). As a result, the Silver-Blaze transformations at finite temperature and finite chemical potential read

$$\Phi_j(x) \to \Phi_j(x)\, \mathrm{e}^{\mathrm{i}F_j\alpha_n x^0} \,, \qquad \mu \to \mu + \mathrm{i}\alpha_n \,, \tag{2.144}$$

where the transformation parameter is now given by

$$\forall T > 0,\ \forall n \in \mathbb{Z}: \quad \alpha_n = 2\pi n T\ . \tag{2.145}$$

The Silver-Blaze symmetry at finite temperature is not continuous anymore and an analytic continuation of the discrete parameter α_n to complex values cannot be uniquely defined. Equivalently, also the Matsubara frequencies do not have a unique analytic continuation. As a consequence, the partition function generally loses its analytic properties at finite temperature and the Silver-Blaze property disappears.[46]

Let us turn to a discussion of the Silver-Blaze property in the context of the functional renormalization group. Since the regulator insertion ΔS_k is bilinear in complex-valued fields, the regulator attaches to the kinetic operator of the theory and the requirement of respecting Silver-Blaze symmetry generally renders the regulator function μ-dependent. A general regulator

$$R_k(p,q)\big|_\mu = \widetilde{R}_k(p)\big|_\mu\ (2\pi)^4 \delta^{(4)}(p-q) \tag{2.146}$$

respects the Silver-Blaze symmetry of the theory if it is analytic in μ and satisfies the conditions

$$\widetilde{R}_k^\varphi(p^0,\vec{p})\big|_\mu \overset{!}{=} \widetilde{R}_k^\varphi(p^0+|F_\varphi|\alpha,\vec{p})\big|_{\mu+\mathrm{i}\alpha}\ , \qquad \widetilde{R}_k^\psi(p^0,\vec{p})\big|_\mu \overset{!}{=} \widetilde{R}_k^\psi(p^0+\alpha,\vec{p})\big|_{\mu+\mathrm{i}\alpha}\ . \tag{2.147}$$

It follows that the reduced regulator functions need to have the following structure,

$$\widetilde{R}_k^\varphi(p^0,\vec{p})\big|_\mu = \widetilde{R}_k^\varphi(p^0+\mathrm{i}|F_\varphi|\mu,\vec{p})\ , \qquad \widetilde{R}_k^\psi(p^0,\vec{p})\big|_\mu = \widetilde{R}_k^\psi(p^0+\mathrm{i}\mu,\vec{p})\ . \tag{2.148}$$

The chemical potential naturally couples to the time-like direction of the kinetic operator for each type of field. As a result, the implementation of spatial regulators automatically renders the regularization scheme Silver-Blaze-symmetric. More specifically, spatial regulators leave the time-like direction of representation space completely untouched such that the relations (2.148) are satisfied in a trivial manner.[47]

In the context of a theory involving massless particles, a finite chemical potential leads to the screening of infrared divergences that would typically occur at the origin of momentum space. Although the pole of the propagator at $p^2 = 0$ is no longer present for $\mu > 0$, the infrared divergence has been shifted into the imaginary direction of the analytically continued p^0-mode. In order to ensure proper IR regularization in the presence of a finite chemical potential, we impose the condition

$$\lim_{\frac{p^2}{k^2}\to 0} \widetilde{R}_k^\varphi(p^0-\mathrm{i}|F_\varphi|\mu,\vec{p})\big|_\mu > 0\ , \qquad \lim_{\frac{p^2}{k^2}\to 0} \det\Big(\widetilde{R}_k^\psi(p^0-\mathrm{i}\mu,\vec{p})\big|_\mu\Big) > 0\ , \tag{2.149}$$

which consistently reduces to the standard regulator condition (i) in the vacuum limit. In fact, these conditions are identical for Silver-Blaze symmetric regulators. Nevertheless, the condition (2.149)

[46] This is to be understood in the sense that an exact independence from the chemical potential can only be present for exactly zero temperature. Any finite temperature immediately renders the system globally μ-dependent. However, if T is sufficiently small compared to the Silver-Blaze threshold μ_{SB}, then finite temperatures merely introduce a slight dependence on the chemical potential, which is in practice often indistinguishable from the zero-temperature case. Therefore, the Silver-Blaze property is often mentioned even at finite but sufficiently low temperatures.

[47] There are regulator functions that do not depend on the time-like coordinate yet have a μ-dependence. These regulators induce a decoupling of the chemical potential from the time-like modes and hence introduce explicit Silver-Blaze breaking. We do not consider them to be spatial regulators in the strict sense because they destroy the structure of the kinetic operator in the presence of a finite chemical potential. They have nevertheless proven quite successful in studies of systems with a Cooper instability, see, e.g., Refs. [30, 81, 313].

implies that regularization in the presence of a finite chemical potential is provided for loop momenta in the proximity of $p^* = (-\mathrm{i}|F|\mu, \vec{0})$ instead of the origin of momentum space. The IR condition for the regulator shape function stays the same. It is worth mentioning that the adjusted condition for IR regularization does not screen the singularity of the zero-temperature system at $\mu = \mu_{\mathrm{SB}}$. The regulator only renders the particle mass associated with the Silver-Blaze threshold μ_{SB} generally scale-dependent.

The Silver-Blaze symmetry of the theory as well as its implications for correlation functions suggest that a derivative expansion of the effective average action at finite chemical potential should be anchored around a μ-dependent expansion point [81, 307]. The expansion reads

$$\begin{aligned}
\Gamma_k[\Phi]\big|_\mu = \int_x \Big(U_k(\Phi(x))\big|_{\mathfrak{Re}\{\mu\}} &+ \bar{\psi}(x) \left[Z^{\parallel}_{\psi,k}\, \mathrm{i}\gamma^0(\partial_0 - \mu) + Z^{\perp}_{\psi,k}\, \mathrm{i}\gamma^i \partial_i \right] \psi(x) \\
&+ \Delta^*(x) \left[-Z^{\parallel}_{\Delta,k}\, (\partial_0 - 2\mu)^2 - Z^{\perp}_{\Delta,k}\, \partial_i \partial^i \right] \Delta(x) \\
&+ \frac{1}{2}\phi(x) \left[-Z^{\parallel}_{\phi,k}\, \partial_0^2 - Z^{\perp}_{\phi,k}\, \partial_i \partial^i \right] \phi(x) + \dots \Big) \\
= \int_p \Big(U_k[\Phi](p)\big|_{\mathfrak{Re}\{\mu\}} &+ \bar{\psi}(p) \left[-Z^{\parallel}_{\psi,k}\, \gamma^0(p^0 + \mathrm{i}\mu) - Z^{\perp}_{\psi,k}\, \vec{\not{p}} \right] \psi(p) \\
&+ \Delta^*(-p) \left[Z^{\parallel}_{\Delta,k}\, \left(p^0 + \mathrm{i}2\mu\right)^2 + Z^{\perp}_{\Delta,k}\, \vec{p}^{\,2} \right] \Delta(p) \\
&+ \frac{1}{2}\phi(-p) \left[Z^{\parallel}_{\phi,k}\, \left(p^0\right)^2 + Z^{\perp}_{\phi,k}\, \vec{p}^{\,2} \right] \phi(p) + \dots \Big) ,
\end{aligned} \tag{2.150}$$

where we introduced several wavefunction renormalization factors parallel and perpendicular to the particle reservoir. In the case of explicitly broken Silver-Blaze symmetry, the μ-dependent contributions in the kinetic term flow differently than the time-like component such that the incorporation of a separate wavefunction renormalization Z_μ is in general necessary, see, e.g., Refs. [88, 307]. It is important to realize that, although the mesons themselves do not couple to a chemical potential, their kinetic operator also splits into parts parallel and perpendicular to the time-like direction of representation space. Since the fermionic fields do in fact couple to the chemical potential, fermion-boson interactions will generally render the bosonic wavefunction renormalizations implicitly μ-dependent and thereby induce a decomposition of the wavefunction renormalization also for the mesons.[48] This illustrates the explicit breaking of Lorentz invariance for all field degrees of freedom in the presence of a finite chemical potential. As before, U_k denotes the effective potential which is invariant under Silver-Blaze transformations. The effective potential therefore contains fields only in $U(1)_{\mathrm{V}}$-symmetric combinations and can only depend on the real part of the chemical potential. Overall, taking into account a generally μ-dependent expansion point as shown above ensures an intact Silver-Blaze symmetry at every order of the derivative expansion.

Notice that the derivative expansion around a Silver-Blaze-adapted expansion point directly implies that projections onto couplings require setting the external momenta to $p = (-\mathrm{i}|F|\mu, \vec{0})$ after functional derivatives have been performed. Choosing a different evaluation point for the projection leads to μ-dependent contributions from higher orders of the expansion and destroys

[48] The bosonization of, for example, four-fermion interactions produce Yukawa-type interactions between fermions and bosons, i.e., vertices $\sim \bar{\psi}\phi\psi$ and $\sim \bar{\psi}\Delta\bar{\psi}^{\intercal}$. The absence of interactions would imply that fermion and boson degrees of freedom have been decoupled by hand in order to study their dynamics separately. In that case and without any other source of explicit Lorentz symmetry breaking, the parallel and perpendicular part of the meson wavefunction renormalization would indeed be identical.

the Silver-Blaze property of the quantity of interest. Even worse, RG flows can develop a non-integrable pole when insisting on the standard derivative expansion (2.92) in the presence of a finite chemical potential [81, 307]. As a result, Fermi-surface-adapted regulators have to be implemented to prevent the RG flow from being ill-defined [30, 81, 313]. Furthermore, we would like to point out the general fact that any expansion is only meaningful if the function under consideration is analytic. Since the system at zero temperature is only analytic for $\mu < \mu_{\mathrm{SB}}$, the derivative expansion generally breaks down once the chemical potential passes the Silver-Blaze threshold. In particular, correlation functions become non-analytic in external momenta for $\mu \geq \mu_{\mathrm{SB}}$. An extraction of low-energy observables which is consistent with mean-field calculations then requires the usage of iterated limits, see Section 2.4.4 for details. In addition, projections involving derivatives with respect to external momenta can lead to infinite discontinuities which restrict the predictive power of our framework. A feasible solution could be to make use of finite differences instead of derivatives, see, e.g., Appendix C of Ref. [314] for a possible projection for wavefunction renormalizations.

The Silver-Blaze property is not restricted to systems with a single chemical potential but is also present if multiple particle species couple to different chemical potentials. Analogously, there then is a region in a phase diagram spanned by all the chemical potentials in which the system stays in its vacuum state. However, this Silver-Blaze region generally has a non-trivial topology because the effect of the chemical potentials on the structure of the propagator highly depends on the particle species and the interactions among them.

2.4 Subtleties at finite temperature and chemical potential

In order to correctly capture the physical principles underlying quantum as well as relativistic systems, the framework of quantum field theory combines concepts from different branches of mathematics, including functional analysis, differential geometry, and advanced calculus. Not only the conceptual challenges of quantum field theory but in particular its mathematical complexity makes it infamously difficult to obtain analytical and closed-form predictions for interacting systems. With the ambition to make calculations more accessible, physicists have come up with clever methods, which are based on interchanging the order of mathematical operations such as integration, taking a derivative, and taking a limit. Despite the great success of this approach and its indisputable benefit to modern research, it is in principle important to verify whether the operations indeed commute in the situation of interest. In the following, we present several scenarios as encountered in the context of quark-meson-type models at finite temperature and/or finite chemical potential in which a change of order is not valid. We would like to highlight that the technicalities occurring in the calculation of loop integrals and associated correlation functions are independent of any matters of regularization. We will therefore aim at a rather general presentation of the relevant mathematics before giving concrete examples related to physics. For simplicity, we consider the finite chemical potential always to be positive, $\mu \in \mathbb{R}^+$.

A major part of the following presentation relies on a powerful residue technique from the field of complex analysis, the Cauchy residue theorem. Let $D \subseteq \mathbb{C}$ be open, $G \subseteq D$ be a simply connected region, which is enclosed by a piecewise continuously differentiable curve γ. Further, let A be a finite subset of D with $A \cap \gamma = \varnothing$,[49] and let the function f be holomorphic on $D \setminus A$. The residue

[49] The residue theorem in its most straightforward form assumes that the function under consideration has a finite number of isolated singularities in order to guarantee convergence for the sum of residues. In general, however, the set A does not need to be finite. In fact, the Matsubara formalism relies on an extension of Cauchy's residue theorem to a countably infinite number of poles, see, e.g., Section 2.4.3.

theorem then states that the contour integral of f along γ equals a weighted sum of residues for isolated singularities $a \in A$, which lie in the region enclosed by the curve:

$$\oint_\gamma \mathrm{d}z\, f(z) = 2\pi\mathrm{i} \sum_{a \in A \cap G} \mathrm{ind}_\gamma(a)\ \mathrm{Res}(f,a)\ . \tag{2.151}$$

Here, $\mathrm{int}_\gamma(a)$ not only counts in absolute values how many times γ winds around $z = a$ but also takes the orientation of the curve into account. The usefulness of the theorem now stems from the fact that it is often possible to determine the residues without an explicit evaluation of contour integrals. In particular, for a pole of order $n \in \mathbb{N}$, the corresponding residue is given by the formula

$$\mathrm{Res}(f,a) = \frac{1}{(n-1)!} \lim_{z \to a} \frac{\mathrm{d}^{n-1}}{\mathrm{d}z^{n-1}} \left[(z-a)^n\, f(z)\right]\ . \tag{2.152}$$

In order to apply the Cauchy residue theorem for the evaluation of integrals, a closed integration contour in the complex plane has to be chosen. Since we are primarily interested in integral expressions appearing in the context of physics, it is most advantageous to consider an interval on the real axis and then close the contour with a semi-circle in the upper (or lower) half of the complex plane. In the following, we agree on the convention that C denotes such a contour, where the radius R of the corresponding semi-circle is taken to infinity. Provided that the integral along C exists, we write

$$\oint_C \mathrm{d}z\, f(z) \coloneqq \lim_{R \to \infty} \left(\int_{[R,R]} \mathrm{d}z\, f(z) + \int_{\mathcal{C}_0^+(R)} \mathrm{d}z\, f(z) \right)\ , \tag{2.153}$$

where

$$\mathcal{C}_d^+(r) = \{z \in \mathbb{C} |\, \Im\mathrm{m}\{z\} > 0 \wedge |z-d| = r\} \tag{2.154}$$

describes a semi-circle in the upper half of the complex plane around the point $d \in \mathbb{R}$ with radius $r > 0$. In our convention, C is positively oriented and winds around an isolated singularity of f only once at most. Furthermore, if f is uniformly convergent to zero on $\mathcal{C}_0^+(R)$ as R tends to infinity, i.e., if

$$\forall \varphi \in (0,\pi): \quad \lim_{R \to \infty} R\, f(R\, \mathrm{e}^{\mathrm{i}\varphi}) = 0\ , \tag{2.155}$$

then the integral along the semi-circle vanishes. As a consequence, the contour integral simplifies to

$$\oint_C \mathrm{d}z\, f(z) = \int_{\mathbb{R}} \mathrm{d}z\, f(z) = 2\pi\mathrm{i} \sum_{a \in A} \mathrm{Res}(f,a)\ \theta(\Im\mathrm{m}\{a\})\ . \tag{2.156}$$

Notice that, compared to Eq. (2.151), we sum over all singularities here. Due to the presence of the Heaviside step function, however, we consistently take into account only residues at those singular points that lie in the closed contour. Loosely speaking, the Heaviside step function acts an as on/off switch, letting a residue only contribute if the corresponding singularity lies in the upper half of the complex plane. In general, expressing integrals along the real axis in terms of contour integrals allows us to apply techniques of complex analysis. This approach has proven to be highly successful in simplifying the evaluation of integrals occurring in the natural sciences.

2.4.1 Order of integration

At zero temperature, the introduction of a finite chemical potential comes along with a pole in the propagator for $\mu \geq \mu_{\mathrm{SB}}$. This pole can destroy the Lebesgue-integrability of functions f in a loop integral:

$$\forall \mu \geq \mu_{\mathrm{SB}} : \qquad \int \mathrm{d}^4 p \;\; |f(p)| \to \infty \; . \tag{2.157}$$

Provided that the multiple integral converges, the failure of absolute convergence generally indicates that the integrand is singular somewhere on the integration domain and that the integration procedure leads to a process in which diverging contributions counter each other. However, the absolute value prescription interferes with this mechanism and hence causes a divergence. The absence of Lebesgue-integrability suggests that the value of the multiple integral may not be uniquely defined and instead depends on the method of integration. In many applications, a multiple integral is evaluated by computing an iterated integral. It is then essential to realize that the cancellation of infinities during the integration process is sensitive to the order in which the iterated integral is performed. In other words, the presence of a pole as induced by the chemical potential can spoil the applicability of Fubini's theorem such that the order of integrating out momentum modes becomes important. For illustrative purposes, we consider the simple function

$$f(p^0, q) = \left(\frac{1}{(p^0 + \mathrm{i}\mu)^2 + q^2 + m^2} \right)^2 , \tag{2.158}$$

whose basic structure is reminiscent of a propagator for massive fermions in one spatial dimension. We now have the opportunity to perform the integration of momentum modes in the corresponding loop integral in two different orders:

$$\int_{\mathbb{R}} \mathrm{d}q \int_{\mathbb{R}} \mathrm{d}p^0 \; f(p^0, q) = \frac{\pi}{m^2} \left(1 - \theta(\mu - m) \frac{\sqrt{\mu^2 - m^2}}{\mu} \right) , \tag{2.159}$$

$$\int_{\mathbb{R}} \mathrm{d}p^0 \int_{\mathbb{R}} \mathrm{d}q \; f(p^0, q) = \frac{\pi}{m^2} \left(1 - \theta(\mu - m) \frac{\mu}{\sqrt{\mu^2 - m^2}} \right) . \tag{2.160}$$

With the Silver-Blaze threshold being given by the mass parameter, $\mu_{\mathrm{SB}} = m$, we observe that the integrals above do in fact coincide in the vacuum, i.e., for $\mu < \mu_{\mathrm{SB}}$, but differ beyond the critical value, $\mu > \mu_{\mathrm{SB}}$. Although both integrals approach the same limit as μ becomes asymptotically large, it is important to realize that their behavior is significantly different for values of the chemical potential close to the Silver-Blaze threshold. More specifically, the result (2.160) diverges for $\mu - m \to 0^+$ while the first integral remains finite and continuous.

As demonstrated, switching the order of integration does not need to leave the result invariant if Lebesgue-integrability has broken down. In the context of zero-temperature quantum field theory, this means that the order of integration in a loop integral generally becomes important once the value of the chemical potential exceeds the Silver-Blaze threshold. However, despite this observation, there is a priori no way to decide which order of integration is correct from a physical point of view. Let us therefore take a step back and consider the evolution operators in relation (2.111). These operators show an explicit dependence on inherently time-like variables which implies that the time-like direction of spacetime has already been integrated out. In fact, this is a quite general feature of equilibrium systems and holds for finite as well as zero temperature. For that reason, we take this as a basis for our understanding of integration in which the time-like coordinate is to

be integrated out first. To be explicit, we use

$$\int_x := \int_{\vec{x}} \int_{\mathbb{R}} \mathrm{d}x^0 \,, \qquad \int_p := \int_{\vec{p}} \int_{\mathbb{R}} \frac{\mathrm{d}p^0}{2\pi} \,, \tag{2.161}$$

which translates to analogous prescriptions for finite temperature.

2.4.2 Differentiation under the integral sign

Let $Y \subset \mathbb{R}$ be an open set, $h : \mathbb{C} \times Y \to \mathbb{C}$ as well as $g : Y \to \mathbb{C}$ differentiable functions. Furthermore, let h be analytic on $\mathbb{C}$. For $n \in \mathbb{N}$ we consider the combined function

$$f(z,y) = \frac{h(z,y)}{(z-g(y))^n} \,, \tag{2.162}$$

which is singular in all points $(z,y) \in \mathbb{C} \times Y$ that satisfy the equation $z = g(y)$. Now, let $\gamma : I \to \mathbb{C}$ be a simple closed curve in the complex plane. Then, the function F as given by the parameter integral

$$F(y) = \oint_\gamma \mathrm{d}z \, f(z,y) \tag{2.163}$$

is differentiable on $Y \setminus U$, where U is defined by

$$U = \{y \in Y \,|\, \exists s \in I : \; \gamma(s) = g(y)\} \,. \tag{2.164}$$

Notice that elements of U are parametric representations of the singularity condition $z = g(y)$ for z lying on the integration contour. The Cauchy-type integral (2.163) is not defined at points at which the pole of the integrand lies on the integration contour and hence F is not differentiable on U. In the following, we shall assume that $U = \partial U$,[50] meaning that U only contains isolated points such that F is differentiable almost everywhere on Y. Making use of the Leibniz notation

$$\forall i,j \in \mathbb{N}_0 : \quad h^{(i,j)}(z,y) = \frac{\partial^i}{\partial z^i} \frac{\partial^j}{\partial y^j} h(z,y) \,, \tag{2.165}$$

we define

$$\forall y^* \in U : \quad c_{y^*} := \left| h^{(n-1,0)}(g(y^*), y^*) \right| \,, \tag{2.166}$$

which is related to the boundary value of the function F as $y \to y^*$. In particular, if g passes through the contour at $y = y^*$, it follows from the Sokhotski-Plemelj theorem that

$$\lim_{\varepsilon \to 0^+} \left| F(y^* + \varepsilon) - F(y^* - \varepsilon) \right| = \frac{2\pi \, c_{y^*}}{(n-1)!} \,. \tag{2.167}$$

If and only if $c_{y^*} = 0 \; \forall y^* \in U$, we find that

$$\int_Y \mathrm{d}y \left(\frac{\mathrm{d}}{\mathrm{d}y} F(y) - \oint_\gamma \mathrm{d}z \, \partial_y f(z,y) \right) = 0 \,. \tag{2.168}$$

[50] For $n = 1$, our discussion can be consistently extended to cases in which this assumption fails, i.e., when U contains intervals. More specifically, we can impose the Cauchy principal value on the contour integral such that Eq. (2.163) becomes well-defined on U. The parameter integral F is then differentiable on $Y \setminus S$ with $S = \bigcup_{B \in U} \partial B \cap Y = \partial S$.

In words, whenever the parameter integral is continuous, a derivative with respect to y does in fact commute with the contour integration. However, if c_{y^*} is finite, we expect the generalized derivative to generate finite contributions at the non-differentiable point y^*, spoiling the commutativity of differentiation and contour integration.

For a better understanding of the ideas described above, let us take a look at the exemplary function $f_t : \mathbb{R}^{d+1} \to \mathbb{C}$ with

$$\forall n \in \mathbb{N}: \quad f_t(p) = \left(\frac{1}{(p^0 + \mathrm{i}\mu)^2 + x_t^2(\vec{p})} \right)^n , \tag{2.169}$$

where $x_t : \mathbb{R}^d \to \mathbb{R}$ with $d \in \mathbb{N}$ denotes some continuous function of spatial momenta. The function f_t is supposed to mimic the characteristics of an integrand relevant for correlation functions as obtained from the multiplication of n fermion propagators. The real-valued parameter t is rather generic and can refer to, e.g., the RG scale k, a mass parameter m or an external momentum Q. If μ exceeds the Silver-Blaze threshold

$$\mu_{\mathrm{SB}}(t) = \min_{\vec{p}} |x_t(\vec{p})| , \tag{2.170}$$

then the function f_t has a pole of order $n \in \mathbb{N}$ in $p = p^*(t) = (0, \vec{p}^{\,*}(t))$, where $\vec{p}^{\,*}(t) \in \Omega$ are the real-valued roots of $1/f_t$ at $p^0 = 0$:

$$\Omega = \{ \vec{p} \in \mathbb{R}^d \,\big|\, x_t^2(\vec{p}) - \mu^2 = 0 \} . \tag{2.171}$$

In the following, we compute the integral of the function f_t with respect to the time-like momentum along the real number line $\mathbb{R}$. The integrand can be analytically continued in p^0 and for a better comparison with Eq. (2.162) we rewrite the function into the form

$$f_t(p) = \frac{h_t(p)}{(p_0 - g_t(\vec{p}))^n} \tag{2.172}$$

with the functions h_t and g_t given by

$$h_t(p) = \left(\frac{1}{p^0 + \mathrm{i}(|x_t(\vec{p})| + \mu)} \right)^n , \qquad g_t(\vec{p}\,) = \mathrm{i}(|x_t(\vec{p})| - \mu) . \tag{2.173}$$

The contour integral of f_t along C, see Eq. (2.153), yields

$$\begin{aligned} F_t(\vec{p}) &= \oint_C \frac{\mathrm{d}p^0}{2\pi} \, f_t(p) = \int_{\mathbb{R}} \frac{\mathrm{d}p^0}{2\pi} \, f_t(p) \\ &= \frac{\mathrm{i}}{(n-1)!} \, h^{(n-1,0)}(g_t(\vec{p}), \vec{p}) \; \theta\left(\Im\mathrm{m}\{g_t(\vec{p})\}\right) \\ &= \binom{2n-2}{n-1} \left(\frac{1}{2|x_t(\vec{p})|} \right)^{2n-1} \theta(|x_t(\vec{p})| - \mu) , \end{aligned} \tag{2.174}$$

which is discontinuous on

$$U = \{ \vec{p} \in \mathbb{R}^d \,\big|\, \Im\mathrm{m}\{g_t(\vec{p})\} = 0 \} = \Omega . \tag{2.175}$$

The appearance of the Heaviside step function θ in Eq. (2.174) reflects the fact that F_t is not differentiable at those spatial momenta for which the pole g_t hits the real axis. Moreover, since

$$\forall \vec{p}^{\,*} \in U: \quad c_{\vec{p}^{\,*}} \propto \left(\frac{1}{2\mu} \right)^{2n-1} > 0 \tag{2.176}$$

for all finite μ, we observe that the generalized derivative with respect to t does not commute with the process of integrating out the p^0-modes. In the following, we denote the derivative with respect to t by ∂_t.

$$\int_{\vec{p}} \partial_t F_t(\vec{p}\,) - \int_p \partial_t f_t(p) = \binom{2n-2}{n-1}\left(\frac{1}{2\mu}\right)^{2n-1} \underbrace{\int_{\vec{p}} \partial_t |x_t(\vec{p}\,)|\ \delta(|x_t(\vec{p}\,)|-\mu)}_{\sim\, \theta(\mu-\mu_{\mathrm{SB}}(t))} . \tag{2.177}$$

Beyond the Silver-Blaze threshold, there exist vectors $\vec{p}$ for which g_t lies in the upper half of the complex p^0-plane such that the pole contributes to the contour integral. This contribution is associated with a finite discontinuity at the Fermi surface to which generalized derivatives are sensitive. As a result, the order of carrying out derivatives and integration becomes important for $\mu \geq \mu_{\mathrm{SB}}(t)$. Notice that this has far-reaching consequences for the calculation of correlation functions by a projection procedure. More specifically, projection operators that involve derivatives ∂_t can in general not be pulled inside the integral when the zero-temperature system is at finite density.

2.4.3 Zero-temperature ambiguity

We consider an analytic function $f : \mathbb{R} \to \mathbb{C}$, which has an asymptotic expansion at infinity such that

$$f(x) = \mathcal{O}\left(\frac{1}{x^s}\right) \quad \text{as} \quad x \to \infty \quad \text{with} \quad s > 1 . \tag{2.178}$$

In a context related to relativistic physics, this function may represent the integrand of a zero-temperature correlation function with x having the meaning of a time-like momentum p^0. We therefore intend to compute its integral over the real numbers. In order to apply the Cauchy residue theorem, we perform an analytic continuation, meaning we consistently extend the original domain of the function to an open subset of $\mathbb{C}$. We are going to assume that this function is meromorphic and let P denote the set of all poles of f. The property (2.178) together with analyticity implies that the contour integral along a semi-circle in the upper half of the complex plane vanishes, see Eq. (2.155). As a result, the integral of f is readily written as a sum of residues:

$$\int_{\mathbb{R}} \mathrm{d}x\ f(x) = 2\pi\mathrm{i} \sum_{a\in P} \mathrm{Res}(f,a)\ \theta(\Im\mathrm{m}\,\{a\}) . \tag{2.179}$$

Considering a discretization of the x-axis with nodes $x = m \in \mathbb{Z}$, the integral turns into an infinite series. The existence of this series is guaranteed by the asymptotic behavior (2.178) of f for large input values [315]. Since f is analytic, we can apply the Matsubara formalism [266, 273, 286, 316] to determine the value of the series. We remark that, although the original work of Matsubara [266] is an operator description of the imaginary-time formalism, we always refer to the Matsubara-frequency summation technique as it is commonly used in modern thermal field theory. This technique allows us to evaluate infinite sums in a systematic fashion by applying Cauchy's residue theorem in reverse. The problem of calculating the value of the series is then transformed into the problem of constructing an integrand whose cumulative residues equal the original sum. With the aid of an exponential weighting function, a suitable construction is readily found:

$$\sum_{m\in\mathbb{Z}} f(m) = 2\pi\mathrm{i} \sum_{a\in P} \mathrm{Res}\left(f\ \frac{1}{\mathrm{e}^{-2\pi\mathrm{i}\,\cdot}-1}, a\right) . \tag{2.180}$$

It is worth mentioning that this formula even holds if f has poles on the real axis, as long as $\mathbb{Z} \cap P = \emptyset$.

Let us now turn to a more specific scenario and consider a function explicitly depending on $\nu_m(\beta) = \frac{2\pi}{\beta}(m + \frac{1}{2})$ with $\beta > 0$. Such a situation is often encountered in thermal field theory, where the introduced parameter has the meaning of the inverse temperature, i.e., $\beta = 1/T$. In this context, ν_m is called the fermionic Matsubara frequency, see Eq. (2.124). We then obtain

$$\sum_{m\in\mathbb{Z}} f(\nu_m(\beta)) = -\mathrm{i}\beta \sum_{a\in P} \mathrm{Res}\left(f \, \frac{1}{\mathrm{e}^{-\mathrm{i}\beta\,\cdot} + 1}, a \right) . \tag{2.181}$$

Notice that the auxiliary exponential function involved in the summation of residues can be related to the Fermi-Dirac distribution,

$$n_{\mathrm{F}}(x) = \frac{1}{\mathrm{e}^x + 1} . \tag{2.182}$$

This distribution function shows a non-uniform convergence in the zero-temperature limit,

$$\mathbb{M} = \{ z \in \mathbb{C} \mid z \notin \mathrm{i}\mathbb{R} \setminus \{0\} \} , \tag{2.183}$$

$$\forall z \in \mathbb{M} : \quad \lim_{\beta\to\infty} n_{\mathrm{F}}(\beta z) = 1 - \theta(\mathfrak{Re}\{z\}) , \tag{2.184}$$

and even loses its complex differentiability in this limit as $\mathfrak{Re}\{z\}$ is not holomorphic. Nevertheless, we observe that we can interchange derivatives and the zero-temperature limit in the sense that

$$\forall z \in \mathbb{M},\ \forall x \in \mathbb{R},\ \forall n \in \mathbb{N}_0 : \quad \lim_{\beta\to\infty} \frac{\mathrm{d}^n}{\mathrm{d}z^n} n_{\mathrm{F}}(\beta z) = \left[\frac{\mathrm{d}^n}{\mathrm{d}x^n} \lim_{\beta\to\infty} n_{\mathrm{F}}(\beta x) \right]\Bigg|_{x=\mathfrak{Re}\{z\}} . \tag{2.185}$$

The limit as β tends to infinity is associated with $\nu_m(\beta)$ becoming continuous such that the infinite series turns into an integral again. For that reason, we will now investigate the consistency between the results (2.179) and (2.181) for some meromorphic function f with $P \subset \mathrm{i}\mathbb{M}$. In the context of thermal field theory, this means that our further analysis is concerned with the consistency between correlation functions as obtained at zero as well as finite temperature. In order to allow for a comparison, we need to rescale the infinite series before performing the zero-temperature limit. We find the limit

$$\lim_{\beta\to\infty} \frac{2\pi}{\beta} \sum_{m\in\mathbb{Z}} f(\nu_m(\beta)) = 2\pi\mathrm{i} \sum_{a\in P} \mathrm{Res}\left(f \;\theta(\mathfrak{Im}\{\cdot\}), a \right) , \tag{2.186}$$

where we have used that

$$\lim_{R\to\infty} \int_{\mathcal{C}_0^+(R)} \mathrm{d}x\; f(x) = 0 \quad \Rightarrow \quad \mathrm{Res}(f, \infty) = 0 \quad \Rightarrow \quad \sum_{a\in P} \mathrm{Res}(f, a) = 0 . \tag{2.187}$$

Recall that the calculation of residues for a pole of order n involves a $(n-1)$-th derivative, see Eq. (2.152). As a consequence, the limit (2.186) of the Matsubara sum only agrees with the integral (2.179) if all poles in the upper half of the complex plane are of order $n = 1$.[51] For poles of higher order, the residues involve complex derivatives which are to be understood as

$$0 \leq k \leq n-1 : \quad \left[\frac{\mathrm{d}^k}{\mathrm{d}x^k} \theta(x) \right]\Bigg|_{x=\mathfrak{Im}\{z\}} \tag{2.188}$$

[51] In more general scenarios, in which the poles a can depend on further parameters, see, e.g., the function g_t in Eq. (2.173), the results (2.179) and (2.186) also agree if no pole crosses the real axis for all parameters of interest.

when acting on the Heaviside function. These generalized derivatives then generate terms involving Dirac delta distributions which are absent in Eq. (2.179). The implication for quantum field theory is that the zero-temperature limit of a finite-temperature calculation may lead to local contributions that are missing if we work at zero temperature right from the beginning. As correlation functions for processes occurring in relativistic theories are given by a multiple integral, terms involving Dirac delta distributions can eventually generate finite contributions to physical observables. Therefore, it does in general make a difference whether the zero-temperature results have been obtained by a zero-temperature limit or not.

We would like to render the relationship between the zero- and finite-temperature results more concrete. To this end, we again consider the exemplary function as given by Eq. (2.169), which can be written as the function

$$\tilde{f}_t(p) = \frac{1}{(p^0 + \mathrm{i}\mu)^2 + x_t^2(\vec{p})} \tag{2.189}$$

raised to the power $n \in \mathbb{N}$ such that $f_t(p) = D_t^{n-1}\, \tilde{f}_t(p)$ with the differential operator D_t^n defined by

$$\forall n \in \mathbb{N}_0 : \quad D_t^n = \frac{(-1)^n}{n!} \left(\frac{1}{\partial_t x_t^2(\vec{p})}\, \partial_t \right)^n . \tag{2.190}$$

Because the function $\tilde{f}_t$ has a finite set of poles in p^0, taking temperature-independent derivatives and Matsubara summation commutes for all $T > 0$, see Appendix C for details. The zero-temperature limit of the Matsubara sum then yields

$$\begin{aligned} \lim_{\beta\to\infty} \frac{1}{\beta} \sum_{m\in\mathbb{Z}} f_t(\nu_m(\beta), \vec{p}) &\overset{(C.51)}{=} \lim_{\beta\to\infty} D_t^{n-1}\, \frac{1}{\beta} \sum_{m\in\mathbb{Z}} \tilde{f}_t(\nu_m(\beta), \vec{p}) \\ &\overset{(2.185)}{=} D_t^{n-1} \lim_{\beta\to\infty} \frac{1}{\beta} \sum_{m\in\mathbb{Z}} \tilde{f}_t(\nu_m(\beta), \vec{p}) = D_t^{n-1} \int_{\mathbb{R}} \frac{\mathrm{d}p_0}{2\pi}\, \tilde{f}_t(p) . \end{aligned} \tag{2.191}$$

Consistency between Matsubara summation and contour integration would require that the order of carrying out the derivatives and evaluating the integral can be interchanged. However, it follows from Section 2.4.2 that

$$\forall n \geq 2 \ \wedge \mu \geq \mu_{\mathrm{SB}}(t) : \quad \int_{\vec{p}} D_t^{n-1} \int_{\mathbb{R}} \frac{\mathrm{d}p^0}{2\pi}\, \tilde{f}_t(p) \neq \int_p D_t^{n-1}\, \tilde{f}_t(p) . \tag{2.192}$$

This illustrates once more that the zero-temperature limit of a calculation at finite temperature has always at least as many terms incorporated as the corresponding computation at zero temperature.

From a mathematical point of view, our findings are simply a matter of fact and ambiguities do not arise once the order of performing mathematical operations is well-defined. For the calculation of physical observables at zero temperature, however, there is a priori no way to decide which approach will yield the physically correct results. Since thermal fluctuations prevent us from reaching exactly $T = 0$ in every experimental situation, it is reasonable to calculate zero-temperature observables by starting from a finite-temperature framework. Aside from this phenomenological argumentation, we will see in the example section 2.4.5 that the strategy of preferring finite-temperature computations in the fRG can be based on more formal grounds.

2.4.4 Static and plasmon limit

Let $f : \mathbb{R}^2 \to \mathbb{C}$ be a function and $(x_0, y_0) \in \mathbb{R}^2$ an accumulation point, then the expressions

$$\lim_{x\to x_0} \lim_{y\to y_0} f(x,y) \quad \text{and} \quad \lim_{y\to y_0} \lim_{x\to x_0} f(x,y) \tag{2.193}$$

are called iterated limits, which in general do not need to exist. We emphasize that these repeated one-variable limits are distinct from the double limit

$$\lim_{(x,y)\to(x_0,y_0)} f(x,y)\,, \tag{2.194}$$

which is the important limit concept in the definition of, e.g., continuity and differentiability for bivariate functions. Most statements relating both types of limits to each other are formulated under quite strong conditions and are therefore of only small practical value, see, e.g., Refs. [317–319]. We add, however, that the double limit does not exist, if both iterated limits exist but do not agree.

The use of iterated limits is nothing new in the context of finite-temperature field theory. For example, it has been addressed that the momentum-dependent self-energy $\Pi(Q)$ of a bosonic or fermionic system at finite temperature is discontinuous at the origin such that approaching the point $Q = (Q^0, \vec{Q}) = (0, \vec{0})$ from different directions of momentum space may result in different outcomes, see, e.g., Refs. [230, 273, 320]. Phenomenologically speaking, finite temperature introduces a preferred Lorentz frame, where the plasma of particles and antiparticles, which constitutes the heat bath, is at rest. As a consequence, Lorentz invariance is broken explicitly and the self-energy is not a function of the squared four-momentum but instead a function of $|Q^0|$ and $|\vec{Q}|$, separately, which then allows for the existence of different limits. In general, the limit prescription taking the time-like momentum Q^0 to zero first is known as the static limit, whereas letting the spatial momenta vanish first is called the plasmon limit:

$$\text{static limit:} \qquad \lim_{Q\to 0}^{(\mathrm{st})} \Pi(Q) := \lim_{\vec{Q}\to\vec{0}} \lim_{Q^0\to 0} \Pi(Q)\,, \tag{2.195}$$

$$\text{plasmon limit:} \qquad \lim_{Q\to 0}^{(\mathrm{pl})} \Pi(Q) := \lim_{Q^0\to 0} \lim_{\vec{Q}\to\vec{0}} \Pi(Q)\,. \tag{2.196}$$

When applied to the momentum-dependent self-energy, the static limit provides us with the dynamical curvature masses for the quantum fields in the system while the other limit leads to so-called plasmon masses associated with the damping of oscillations in a plasma. The curvature and plasmon masses may agree, but in general they do not. Notice that finite temperature leads to a discretization of the time-like direction in momentum space such that Q^0 is not a continuous variable. The limit as Q^0 goes to zero is then to be understood in the sense of an analytic continuation. For the static limit, this is equivalent to setting the external Matsubara index associated with Q^0 to zero.

To our knowledge, a discussion of iterated limits for external momenta in the context of quantum field theory has only been made for the case of finite temperature and zero chemical potential. In the following, we demonstrate that a disagreement between the static and plasmon limits even occurs at zero temperature and finite chemical potential. To start with a rather generic example, let us consider the function $\xi : \mathbb{R}^{d+1} \times \mathbb{R}^{d+1} \to \mathbb{C}$, which imitates the structure of the two-point function of a fermionic system. Based on Eq. (2.189) , we write

$$\xi(p,Q) = \tilde{f}(p)\,\tilde{f}(p+Q) = \frac{1}{(p^0+\mathrm{i}\mu)^2 + x^2(\vec{p})}\,\frac{1}{(p^0+\mathrm{i}\mu+Q^0)^2 + x^2(\vec{p}+\vec{Q})}\,. \tag{2.197}$$

The integral of ξ with respect to p^0 is obtained through analytic continuation and is denoted by

$$\begin{aligned}\Xi(\vec{p},Q) &= \int_{\mathbb{R}} \frac{\mathrm{d}p^0}{2\pi}\, \xi(p,Q) = \oint_C \frac{\mathrm{d}p^0}{2\pi}\, \xi(p,Q) \\ &= -\frac{1}{2}\left(\frac{1}{|\tilde{x}_0|}\, \frac{\theta(|\tilde{x}_0|-\mu)}{(|\tilde{x}_0|-\mathrm{i}Q^0)^2-\tilde{x}^2(\vec{Q})} + \frac{1}{|\tilde{x}(\vec{Q})|}\, \frac{\theta(|\tilde{x}(\vec{Q})|-\mu)}{(|\tilde{x}(\vec{Q})|+\mathrm{i}Q^0)^2-\tilde{x}_0^2} \right), \end{aligned} \tag{2.198}$$

where have assumed $Q \neq 0$ and made use of the short-hand notation

$$\tilde{x}(\vec{Q}) := x(\vec{p}+\vec{Q})\,, \qquad \tilde{x}_0 := \tilde{x}(\vec{0}) = x(\vec{p})\,. \tag{2.199}$$

Now, the terms contributing to the function Ξ individually show a divergent behavior in the limit of vanishing external momenta. To be more precise, the residues of ξ in $p^0 = a_i$ each become singular at those external momenta Q for which the corresponding poles of ξ,

$$a_1 = \mathrm{i}(|\tilde{x}_0|-\mu)\,, \qquad a_2 = \mathrm{i}(|\tilde{x}(\vec{Q})|-\mu)-Q^0\,, \tag{2.200}$$

coincide. If the two simple poles suddenly merge to a single pole of second order, the behavior of the contour integral at finite chemical potential is not continuous anymore. It is essential to recognize that the presence of a chemical potential has a significant impact on the weighting of the residues such that the isolated singularity of Ξ at $Q = 0$ is not removable for $\mu > 0$. As a consequence, the integral (2.198) is discontinuous at the origin of the vector space spanned by Q. Nevertheless, it is possible to approach this point of discontinuity by a limit procedure and yet obtain a finite result because the divergences in Ξ contribute with different signs. Concretely, the iterated limits yield

$$\lim_{Q\to 0}^{(\mathrm{st})} \Xi(\vec{p},Q) = \frac{1}{4\tilde{x}_0^2}\left(\frac{\theta(|\tilde{x}_0|-\mu)}{|\tilde{x}_0|} - \delta(|\tilde{x}_0|-\mu) \right), \tag{2.201}$$

$$\lim_{Q\to 0}^{(\mathrm{pl})} \Xi(\vec{p},Q) = \frac{1}{4|\tilde{x}_0|^3}\, \theta(|\tilde{x}_0|-\mu)\,. \tag{2.202}$$

Interestingly, the static limit generates a local contribution in the form of a Dirac delta distribution which is absent in the plasmon limit. We would like to point out that the same principles also apply if ξ had a more complicated pole structure. For our purposes, however, the schematic function (2.197) is already sufficient to demonstrate the emergence of different iterated limits.

From the point of view of relativistic physics, the function ξ can be connected to a two-point correlator at zero temperature. More specifically, this correlation function would be obtained by further integrating Ξ with respect to internal spatial momenta,

$$\Pi(Q) \sim \int_{\vec{p}} \Xi(\vec{p},Q)\,. \tag{2.203}$$

Lorentz invariance at $\mu = 0$ implies that this correlation function at $\mu > 0$ is an even function in both Q^0 and $\vec{Q}$, but not a function of the squared four-momentum. The explicit breakdown of Lorentz symmetry as induced by the chemical potential thus allows for the appearance of different iterated limits as external momenta tend to zero. Notice the similarity to the argumentation in the case of finite temperature and zero chemical potential. Therefore, different iterated limits are in general to be expected whenever Lorentz invariance is explicitly broken by either temperature or chemical potential. This observation is not limited to two-point functions, meaning that different iterated limits can equally well appear for higher-order correlation functions.

We would like to emphasize that our results for the static and plasmon limits at zero temperature are consistent with finite-temperature calculations since every pole of ξ is of order $n = 1$, provided that $Q \neq 0$. Specifically, we have

$$\overset{(\mathrm{st/pl})}{\lim_{Q\to 0}} \int_{\mathbb{R}} \frac{\mathrm{d}p^0}{2\pi}\, \xi(p,Q) = \overset{(\mathrm{st/pl})}{\lim_{Q\to 0}} \lim_{\beta\to\infty} \frac{1}{\beta} \sum_{m\in\mathbb{Z}} \xi(\nu_m(\beta),Q) = \lim_{\beta\to\infty} \overset{(\mathrm{st/pl})}{\lim_{Q\to 0}} \frac{1}{\beta} \sum_{m\in\mathbb{Z}} \xi(\nu_m(\beta),Q)\,. \tag{2.204}$$

Nevertheless, it follows from Section 2.4.3 that the first equality is in general going to break down once we let ξ acquire poles of higher order.

Recall that the iterated limits (2.201) and (2.202) do not coincide at the Fermi surface, where $\mu = |\tilde{x}_0|$. Consequently, the double limit as $Q \to 0$ applied to Ξ cannot exist for $\mu \geq \mu_{\mathrm{SB}}$. Notice, however, that ξ itself is continuous in $Q = 0$ for all $p \neq (0, \vec{p}^{\,*})$, where the values $\vec{p}^{\,*}$ are defined as the solutions to $\mu = |\tilde{x}_0|$, see Eq. (2.171). This means that the operations of integrating out the p^0-modes and taking the limit of vanishing external momenta do not commute simply because that limit cannot be uniquely defined outside of the integral. It is nevertheless possible to realize this limit after performing the integral by choosing the correct iterated limit. In particular, we observe that the plasmon limit leads to the same result as integrating ξ at zero external momenta:

$$\overset{(\mathrm{pl})}{\lim_{Q\to 0}} \int_{\mathbb{R}} \frac{\mathrm{d}p^0}{2\pi}\, \xi(p,Q) = \int_{\mathbb{R}} \frac{\mathrm{d}p^0}{2\pi} \lim_{Q\to 0} \xi(p,Q)\,. \tag{2.205}$$

Setting the external momenta to zero in ξ leads to poles of higher order in the analytically continued variable p^0 such that the equation above does not translate to finite temperature. We instead observe that the finite-temperature computation at $Q = 0$ reproduces the static limit in the sense that

$$\overset{(\mathrm{st})}{\lim_{Q\to 0}} \frac{1}{\beta} \sum_{m\in\mathbb{Z}} \xi(\nu_m(\beta),Q) = \frac{1}{\beta} \sum_{m\in\mathbb{Z}} \lim_{Q\to 0} \xi(\nu_m(\beta),Q)\,. \tag{2.206}$$

In fact, provided that it is possible in the first place to realize the limit of zero external momenta after the Matsubara summation, the static limit is the only unique limit option left ensuring consistency with Eqs. (2.204) and (2.205). It is worth noting that our two findings above also hold true in more general scenarios, e.g., if we allow ξ to have poles of higher order,

$$\forall n_1, n_2 \in \mathbb{N}: \quad \xi(p,Q) = \tilde{f}^{n_1}(p)\, \tilde{f}^{n_2}(p+Q)\,. \tag{2.207}$$

This is because the validity of Eqs. (2.205) and (2.206) originates from both how the poles of ξ contribute to the integral/series and how the components of Q affect the positions of poles relevant for the integration/summation process. While the former is determined by the analytic properties of ξ, the latter is fixed by Lorentz symmetry in the vacuum limit.

2.4.5 Relevance for the quark-meson model

In the following, we demonstrate the relevance of the subtleties discussed above in the context of the quark-meson model. Concretely, we consider a theory of massless quarks with $N_{\mathrm{f}} = 2$ flavors and N_{c} color degrees of freedom that can interact with boson fields through a Yukawa-type term with interaction strength h. These bosons under consideration are the scalar meson σ as well as pseudoscalar pions $\vec{\pi}$, which can be collected into a common field variable ϕ. The ground state of the chiral system is realized along the σ-direction of field space and is linked to the constituent quark mass by the relation $h|\sigma_0| = m_q$. For more details about this quark-meson model, we refer to Section 3.1.1. We only mention here that this model has been studied extensively

in the past and is well-understood at leading order in a loop expansion of the effective action. Therefore, it can provide additional, physical reasoning for our endeavor to resolve ambiguities in the computation of correlation functions. We will make use of the Wetterich equation (2.63) and compute the effective action of our model as well as mesonic two-point correlators in a one-loop approximation, taking into account only purely fermionic loops. We again emphasize that the subtleties as encountered in the calculation of loop integrals are of a rather general nature and not specific to a certain regularization scheme. In fact, it has already been observed in the context of dimensional regularization that an evaluation of loop integrals for different orders of integration can lead to different results [321]. In our RG approach to quantum field theory, we choose a regulator function that allows for a clean and easily accessible presentation of loop integrals. To this end, we will make use of a spatial regularization scheme,

$$\widetilde{R}_k^{\psi}(\vec{p}) = -\not{p}\, r\left(\frac{\vec{p}^{\,2}}{k^2}\right) . \tag{2.208}$$

The regulator shape function will mostly remain unspecified for the sake of generality. We will further agree on the convention to suppress the momentum dependence of the shape function and let the RG-scale dependence appear in the form of an index. This leads to the convenient notation r_k for the shape function as presented above.

Homogeneous backgrounds

By evaluating the scalar fields on a homogeneous background, we arrive at the following RG-scale dependent effective action

$$\begin{aligned}\frac{1}{V_4}\Gamma_k(\phi)\big|_\mu &= \frac{1}{V_4}\Gamma_{\Lambda_0}(\phi) - 4N_c \int_p \ln\left((p^0+\mathrm{i}\mu)^2 + \vec{p}^{\,2}(1+r_{k'})^2 + h^2\phi^2\right)\Big|_{k'=\Lambda_0}^{k'=k} \\ &= \frac{1}{V_4}\Gamma_{\Lambda_0}(\phi) - 4N_c \int_{\vec{p}} \left[\left(\sqrt{\vec{p}^{\,2}(1+r_{k'})^2 + h^2\phi^2} - \mu\right)\, \theta\left(\sqrt{\vec{p}^{\,2}(1+r_{k'})^2 + h^2\phi^2} - \mu\right)\right]\Big|_{k'=\Lambda_0}^{k'=k} ,\end{aligned} \tag{2.209}$$

where Λ_0 refers to some UV scale at which we assume to know the effective action. It is not necessarily the largest scale possible in the theory at hand but only some scale at which we fix the couplings of the theory. Furthermore, V_4 denotes the spacetime volume. We note that the usage of homogeneous backgrounds lets all terms in a derivative expansion of the effective action vanish with the exception of the effective potential, see Eq. (2.150). Therefore, the scale-dependent effective action weighted by the spacetime volume as shown above is nothing but the meson effective potential. We would like to highlight that logarithmic functions, even in the presence of infinite discontinuities, have the remarkable property that their integral is continuous and absolute convergent. It therefore holds that

$$\begin{aligned}\int_{\Lambda_0}^{k} \mathrm{d}k' \int_p \partial_{k'} \ln\left((p^0+\mathrm{i}\mu)^2 + \vec{p}^{\,2}(1+r_{k'})^2 + h^2\phi^2\right) \\ = \int_p \ln\left((p^0+\mathrm{i}\mu)^2 + \vec{p}^{\,2}(1+r_{k'})^2 + h^2\phi^2\right)\Big|_{k'=\Lambda_0}^{k'=k} .\end{aligned} \tag{2.210}$$

The meson curvature masses are now readily obtained by a suitable projection applied to the effective potential. In particular, this projection includes a second-order derivative and the evaluation at the ground state of the system. In geometric terms, these masses represent the curvature of the

effective potential at its global minimum along different directions of field space.

$$
\begin{aligned}
m_\phi^2(\mu) &= \begin{pmatrix} m_\sigma^2(\mu) & \vec{0}^\intercal \\ \vec{0} & m_\pi^2(\mu)\,\mathbb{1}_{3\times3} \end{pmatrix} = \left(\frac{\mathrm{d}}{\mathrm{d}\phi^\intercal} \frac{\mathrm{d}}{\mathrm{d}\phi} \frac{\Gamma(\phi)\big|_\mu}{V_4} \right)\Bigg|_{\phi=\phi_0} \\
&= \frac{1}{V_4}\Gamma^{(2)}_{\Lambda_0}\left(\frac{m_q}{h}\right) - 2N_c h^2 \int_{\vec{p}} \Bigg[\frac{2E_k^2(\vec{p})\,\mathbb{1}_{4\times4} - m_q^2\,(\mathbb{1}_{4\times4}+\eta)}{E_k^3(\vec{p})}\,\theta\left(E_k(\vec{p})-\mu\right) \\
&\qquad + \frac{m_q^2\,(\mathbb{1}_{4\times4}+\eta)}{E_k^2(\vec{p})}\,\delta\left(E_k(\vec{p})-\mu\right) \Bigg]\Bigg|_{k'=\Lambda_0}^{k'=0} .
\end{aligned}
\tag{2.211}
$$

The ground state of the system is given by $\phi_0^\intercal = (\sigma_0, \vec{0}^\intercal)$. To improve readability, we have introduced the short-hand notation

$$
E_k^2(\vec{p}) = \vec{p}^{\,2}(1+r_k)^2 + m_q^2 \tag{2.212}
$$

with E_k standing for the regularized energy of the quark degrees of freedom. In general, the quark mass depends on external parameters such as temperature and chemical potential as well, i.e., $m_q \equiv m_q(T,\mu)$. For simplicity, however, we drop any dependences here as they are irrelevant for our discussion of non-commuting operations. Additionally, η refers to the Lorentz matrix which immediately emerges in field space once we consider a finite fermion mass.[52] In our quark-meson model, the quark mass is dynamically generated by the Yukawa interaction and is directly linked to a finite meson condensate. In the absence of explicit symmetry breaking, this condensate is chosen such that the scalar mesons acquire a finite mass whereas the pions remain massless.[53] In this way, an action functional constructed from fluctuations around the finite ground state in field space has intact isospin symmetry but broken chiral symmetry. This choice is in particular consistent with the chiral limit of a theory with explicitly broken symmetry, in which the ground state gets naturally aligned to the σ-direction of field space. Therefore, a non-zero quark mass always leads to a distinction of the σ-direction of field space. In any case, we emphasize that the Lorentz matrix in this context does not arise as the metric of spacetime, it only precisely captures the sign structure of the mesonic two-point correlator.

The contribution from the term including the Dirac delta distribution to the curvature mass of the σ meson in Eq. (2.211) is essential since it ensures the incorporation of effects resulting from the quark chemical potential μ passing the Silver-Blaze threshold. Notice, however, that this contribution vanishes for the pseudoscalar field degrees of freedom. In general, the term including the Dirac delta distribution cannot arise if the projection is directly applied onto the logarithmic integrand in Eq. (2.209). Since the effective action at zero temperature is non-analytic for $\mu \geq \mu_{\mathrm{SB}}$, integration and differentiation must not be interchanged. It is therefore important not to change the order of integrating out the time-like modes and applying the projection if one is interested in the behavior of the system for large densities. There is also another way to think about this situation. If the effective action is a non-analytic function in field space, then it is not possible by definition to capture the entire information about the system by an expansion in field degrees of freedom. Nevertheless, we are still allowed to consider an expansion of the integrand in terms of homogeneous deviations from the ground state. In the multi-index notation, the Taylor expansion

[52] We follow the mostly-minus convention, see also Appendix A.1.

[53] Strictly speaking, it is the other way around, meaning that the scalar and pseudoscalar mesons get defined as the massive meson and the Goldstone bosons, respectively, once a finite ground state in field space has been chosen.

reads

$$\int_p \ln\left(f(p)+h^2\phi^2\right) = \int_p \sum_{|\alpha|\geq 0} c_\alpha(p)\ \phi_{\mathrm{fl}}^\alpha\ , \tag{2.213}$$

$$c_\alpha(p) = \frac{1}{\alpha!}\left[\partial^\alpha \ln\left(f(p)+h^2(\sigma_0+\sigma_{\mathrm{fl}})^2+h^2\vec{\pi}_{\mathrm{fl}}^{\,2}\right)\right]\Big|_{\phi_{\mathrm{fl}}=0}\ , \tag{2.214}$$

where ϕ_{fl} denotes a fluctuation. Now, summation and integration in Eq. (2.213) do not commute if the integral is non-analytic. Interchanging the order of summation and integration anyway is equivalent to applying the projection for the curvature mass directly onto the integrand and yields an incorrect result.

In order to give a general estimate of the relevance of the term including the Dirac delta distribution for the curvature mass of the σ meson, we analytically evaluate this contribution through the implementation of a sharp cutoff [177, 314]. This regularization prescription can be realized by the shape function

$$\forall x>0: \quad r(x) = \lim_{b\to\infty}\sqrt{1+\frac{1}{x^b}}-1\ . \tag{2.215}$$

Concretely, the contribution of the term which has the Dirac delta distribution included reads

$$\begin{aligned}
&\left(\int_{\vec{p}}\frac{\mathrm{d}^2}{\mathrm{d}m^2}\int_{\mathbb{R}}\frac{\mathrm{d}p^0}{2\pi}-\int_p\frac{\mathrm{d}^2}{\mathrm{d}m^2}\right)\ln\left((p^0+\mathrm{i}\mu)^2+\vec{p}^{\,2}(1+r_{k'})^2+m^2\right)\Big|_{k'=\Lambda_0}^{k'=k}\\
&=\int_{\vec{p}}\left[\frac{m^2}{\vec{p}^{\,2}(1+r_{k'})^2+m^2}\ \delta\left(\sqrt{\vec{p}^{\,2}(1+r_{k'})^2+m^2}-\mu\right)\right]\Big|_{k'=\Lambda_0}^{k'=k}\\
&=\frac{4\pi}{(2\pi)^3}\ \theta(\mu^2-m^2-k^2)\ m^2\ \frac{\sqrt{\mu^2-m^2}}{\mu}\ ,
\end{aligned} \tag{2.216}$$

where we have assumed in the last step that Λ_0 is the largest scale in the system. We observe that the Dirac delta term generates a finite contribution to the curvature mass of the σ meson for values of the chemical potential beyond the scale-dependent Silver-Blaze threshold $\mu_{\mathrm{SB}}(k)=\sqrt{m^2+k^2}$. This contribution grows with increasing μ and can therefore not be neglected in regions of high density.

The mean-field result for the curvature masses at zero temperature, see Eq. (2.211), is perfectly consistent with the zero-temperature limit of a corresponding finite-temperature calculation as it should be. More specifically, there is no discrepancy between these results because, on the one hand, the zero-temperature masses have been obtained by applying the projection after performing the integral with respect to the time-like momentum modes, and on the other hand, the integrand has only simple poles at most.

$$m_\phi^2(\mu) = \lim_{T\to 0}\left(\frac{\mathrm{d}}{\mathrm{d}\phi^{\intercal}}\frac{\mathrm{d}}{\mathrm{d}\phi}\frac{\Gamma(\phi)\big|_{T,\mu}}{V_4}\right)\Big|_{\phi=\phi_0}\ . \tag{2.217}$$

Notice that, at finite temperature, the projection for the curvature masses does in fact commute with the Matsubara summation. Although the zero-temperature and finite-temperature results agree when employing homogeneous background fields, this consistency can no longer be maintained if we take finite external momenta into account. Then, the propagator of the theory can

in general not be evaluated in a closed form such that flow equations for correlation functions of interest would be canonically obtained by some expansion in field degrees of freedom. As a consequence, finite-temperature results in the zero-temperature limit will not coincide with results obtained at exactly zero temperature. This will be shown explicitly in the following.

Full momentum dependence

We introduce a generalized four-momentum ζ_k, which has already regularization for the spatial modes incorporated:

$$\zeta_k(p) = \begin{pmatrix} p^0 \\ \vec{p}(1+r_k) \end{pmatrix} . \tag{2.218}$$

Recall that the regulator shape function r_k also carries a momentum dependence which we have suppressed for convenience. A generalization to covariant regularization is straightforward but we will stick with spatial regulators here for reasons of simplicity. We again take the Wetterich equation as our starting point for the calculation of flow equations for correlation functions and perform an expansion in fluctuation fields according to Eq. (2.99). We are further going to assume that the ground state is homogeneous, i.e., free of spacetime dependences, as this allows us to perform calculations analytically to a great extent. For a discussion of inhomogeneous ground states, the interested reader is referred to Refs. [322–325]. The flow for the momentum-dependent two-point function is then obtained through functional differentiation according to

$$\begin{aligned} \partial_k \Gamma_k^{(1,1)}(P,Q)\big|_{T,\mu} &= \left(\frac{\overrightarrow{\delta}}{\delta \phi_{\mathrm{fl}}^{\intercal}(-P)} \, \partial_k \Gamma_k[\phi]\big|_{T,\mu} \, \frac{\overleftarrow{\delta}}{\delta \phi_{\mathrm{fl}}(Q)} \right)\Bigg|_{\phi_{\mathrm{fl}}=0} \\ &= \frac{1}{4} \frac{\overrightarrow{\delta}}{\delta \phi_{\mathrm{fl}}^{\intercal}(-P)} \, \mathrm{Tr}\left\{ \partial_k \Big(\mathcal{P}_k(\phi_0) \cdot \mathcal{F}[\phi_{\mathrm{fl}}] \Big)^2 \right\}\Big|_{T,\mu} \, \frac{\overleftarrow{\delta}}{\delta \phi_{\mathrm{fl}}(Q)} \\ &= \partial_k \tilde{\Gamma}_k^{(1,1)}(Q)\big|_{T,\mu} \, \beta \delta_{P^0 Q^0} \, (2\pi)^3 \delta^{(3)}(\vec{P}-\vec{Q}) \, . \end{aligned} \tag{2.219}$$

At zero temperature, the flow of the reduced two-point function is given by

$$\partial_k \tilde{\Gamma}_k^{(1,1)}(Q)\big|_{\mu} = -8 N_{\mathrm{c}} h^2 \int_p \partial_k \frac{\zeta_k^{\intercal}(p^0 + \mathrm{i}\mu, \vec{p}) \, \zeta_k(p^0 + \mathrm{i}\mu + Q^0, \vec{p} + \vec{Q}) \, \mathbb{1}_{4\times 4} - m_q^2 \, \eta}{\Big(\zeta_k^2(p^0 + \mathrm{i}\mu, \vec{p}) + m_q^2 \Big) \Big(\zeta_k^2(p^0 + \mathrm{i}\mu + Q^0, \vec{p} + \vec{Q}) + m_q^2 \Big)} \, , \tag{2.220}$$

where we have made use of a common shorthand notation for the inner product, $\zeta_k^2 := \zeta_k^{\intercal} \, \zeta_k$. In the case of vanishing external momentum $Q = (Q^0, \vec{Q})$, the flow equation above provides us with the RG flow for the different zero-temperature meson masses. However, the two-point function is generally non-analytic at $Q = 0$ in the presence of a finite chemical potential. As a result, the case of having zero external momentum has to be realized by an iterated limit. The static limit, where the time-like momentum Q^0 tends to zero first, is supposed to provide us with the curvature mass, while the plasmon limit, in which the spatial components $\vec{Q}$ vanish first, is associated with

the plasmon mass. At zero temperature, the static and plasmon limits yield the following results:

$$\lim_{Q\to 0}^{(\mathrm{st})} \partial_k \tilde{\Gamma}_k^{(1,1)}(Q)\big|_\mu = -2N_c h^2 \int_{\vec{p}} \left[\partial_k \frac{2E_k^2(\vec{p})\,\mathbb{1}_{4\times4} - m_q^2\,(\mathbb{1}_{4\times4}+\eta)}{E_k^3(\vec{p})}\,\theta(E_k(\vec{p})-\mu) \right.$$
$$\left. + \partial_k \frac{m_q^2\,(\mathbb{1}_{4\times4}+\eta)}{E_k^2(\vec{p})}\,\delta\left(E_k(\vec{p})-\mu\right) \right], \tag{2.221}$$

$$\lim_{Q\to 0}^{(\mathrm{pl})} \partial_k \tilde{\Gamma}_k^{(1,1)}(Q)\big|_\mu = -2N_c h^2 \int_{\vec{p}} \partial_k \frac{2E_k^2(\vec{p})\,\mathbb{1}_{4\times4} - m_q^2\,(\mathbb{1}_{4\times4}+\eta)}{E_k^3(\vec{p})}\,\theta(E_k(\vec{p})-\mu)\,. \tag{2.222}$$

We observe that the static limit produces a result with structural similarity to the curvature mass as obtained from the mean-field calculation, see Eq. (2.211). Notice, however, that the mass-like quantity, which we would get from integrating the flow (2.221) with respect to the RG scale, does in general not coincide with the curvature mass. Instead, the result produced by the static limit above lacks local contributions that are present in our mean-field computation. The reason for this discrepancy is that non-commuting mathematical operations have been interchanged in the derivation of Eq. (2.221). To be more specific, the flow equation (2.220) has been obtained from the $\mathcal{PF}$ expansion at zero temperature although non-analytic properties of the zero-temperature theory render this expansion invalid for values of the chemical potential beyond the Silver-Blaze threshold. A plasmon mass does not arise in mean-field theory so we cannot directly compare Eq. (2.222) to corresponding calculations done before. Nevertheless, we deduce that there is a systematic error underlying the construction of the momentum-dependent two-point correlator at zero temperature, which spoils the consistency between the mean-field results and the static limit.

At finite temperature, the flow of the reduced two-point correlator as obtained from the $\mathcal{PF}$ expansion reads

$$\partial_k \tilde{\Gamma}_k^{(1,1)}(Q)\big|_{T,\mu} = -8N_c h^2 \int_{\vec{p}} \frac{1}{\beta} \sum_{n\in\mathbb{Z}} \partial_k \frac{\zeta_k^{\intercal}(\nu_n(\beta)+\mathrm{i}\mu,\vec{p})\,\zeta_k(\nu_n(\beta)+\mathrm{i}\mu+Q^0,\vec{p}+\vec{Q})\,\mathbb{1}_{4\times4} - m_q^2\,\eta}{\left(\zeta_k^2(\nu_n(\beta)+\mathrm{i}\mu,\vec{p})+m_q^2\right)\left(\zeta_k^2(\nu_n(\beta)+\mathrm{i}\mu+Q^0,\vec{p}+\vec{Q})+m_q^2\right)}\,. \tag{2.223}$$

Notice that the derivative with respect to the RG scale increases the order of poles in the time-like momentum variable beyond one. We therefore emphasize already at this point that the flow of the finite-temperature two-point correlator does not reduce to the zero-temperature flow (2.220) in the zero-temperature limit. Since the two-point correlators we have found at zero and finite temperature are genuinely different, any quantities we can extract from these correlation functions will in general not be consistent at zero temperature either. This shall now be explicitly shown through the calculation of meson curvature masses. In the static and plasmon limits, we obtain

$$\lim_{T\to 0} \lim_{Q\to 0}^{(\mathrm{st})} \partial_k \tilde{\Gamma}_k^{(1,1)}(Q)\big|_{T,\mu} = -2N_c h^2 \int_{\vec{p}} \partial_k \left[\frac{2E_k^2(\vec{p})\,\mathbb{1}_{4\times4} - m_q^2\,(\mathbb{1}_{4\times4}+\eta)}{E_k^3(\vec{p})}\,\theta(E_k(\vec{p})-\mu) \right.$$
$$\left. + \frac{m_q^2\,(\mathbb{1}_{4\times4}+\eta)}{E_k^2(\vec{p})}\,\delta\left(E_k(\vec{p})-\mu\right) \right], \tag{2.224}$$

$$\lim_{T\to 0} \lim_{Q\to 0}^{(\mathrm{pl})} \partial_k \tilde{\Gamma}_k^{(1,1)}(Q)\big|_{T,\mu} = -2N_c h^2 \int_{\vec{p}} \partial_k \left[\frac{2E_k^2(\vec{p})\,\mathbb{1}_{4\times4} - m_q^2\,(\mathbb{1}_{4\times4}+\eta)}{E_k^3(\vec{p})}\,\theta(E_k(\vec{p})-\mu) \right]. \tag{2.225}$$

Provided that we allow the chemical potential to acquire values with $\mu \geq \mu_{\mathrm{SB}}(k)$, these results differ from Eqs. (2.221) and (2.222) that have been calculated directly at zero temperature. In addition,

the static limit of the reduced finite-temperature two-point correlator successfully reproduces the mean-field result (2.211) in the zero-temperature limit:

$$\partial_k m^2_{\phi,k}(\mu) = \lim_{T\to 0} \lim_{Q\to 0}^{(\mathrm{st})} \partial_k \tilde{\Gamma}_k^{(1,1)}(Q)\big|_{T,\mu} \,. \tag{2.226}$$

To summarize, the momentum-dependent two-point correlator at zero temperature is not consistent with its finite-temperature pendant and does not reproduce the mean-field result for the meson curvature masses in the static limit. Instead, only the finite-temperature correlator leads to a curvature mass that is physical within the scope of our truncations. In the same spirit, we deduce that Eq. (2.225) provides us with the correct zero-temperature plasmon mass while Eq. (2.222) lacks relevant local contributions.

We would like to point out that the functional renormalization group is in principle free of mathematical ambiguities since the order of all operations is determined by the Wetterich equation.[54] Inconsistencies between results within the fRG only arise if the calculation of observables in a certain situation is based on methods that assume a commutation of mathematical operations even if it is not allowed. To give an example, we have demonstrated that summation and integration do not commute anymore if the integral under consideration is not analytic, see Eq. (2.213) and the corresponding discussion. As mentioned earlier, a finite chemical potential induces a pole in the propagator of the theory at zero temperature, rendering the effective action non-analytic once the quark chemical potential exceeds the Silver-Blaze threshold. In particular, this implies that the $\mathcal{PF}$ expansion at zero temperature is not legitimate for $\mu \geq \mu_{\mathrm{SB}}$. Beyond this threshold, the expansion in fluctuation fields cannot capture the entire information of the underlying physical system. If we nevertheless insist on an expansion in field degrees of freedom, we inevitably miss out on relevant contributions. At finite temperature, however, the pole in the fermion propagator gets screened by thermal fluctuations, see Eq. (2.124), such that perturbative treatments of generating functionals are well-defined in our truncation scheme and lead to the desired consistency with mean-field calculations. Therefore, our analysis makes clear that the computation of correlation functions in the presence of a finite chemical potential at zero temperature requires great care to ensure consistency with corresponding finite-temperature calculations.

In order to arrive at the correct zero-temperature results from the fRG formalism at $T = 0$, we can still employ the $\mathcal{PF}$ expansion if we also compensate for the error introduced by the expansion for $\mu \geq \mu_{\mathrm{SB}}$. More specifically, for the momentum-dependent two-point correlator (2.220), it suffices to change the order in which we apply the RG derivative and perform the integration of time-like modes. As detailed above, this step systematically leads to consistency with the zero-temperature limits, see Eqs. (2.224) and (2.225), but is, strictly speaking, not allowed. This strategy can be further generalized to higher-order correlation functions. In particular, the integrand f of a zero-temperature correlator is to be written in terms of a function $\tilde{f}$, which is allowed to have only simple poles, and a suitable derivative operator, see the example at the end of Section 2.4.3. Now, performing the integral of $\tilde{f}$ with respect to the time-like modes before applying the derivative operator leads to a result that is consistent with the zero-temperature limit of a result obtained at $T > 0$.

[54] The order of integration in an iterated integral is not determined by the Wetterich equation. In order to give a reasonable definition of integral expressions as appearing throughout relativistic physics, criteria from outside the fRG have to be employed, see Section 2.4.1.

3

SCHEME DEPENDENCE OF CHIRAL OBSERVABLES

Based on the building blocks of quantum field theory and the functional renormalization group as discussed in the previous chapter, we will now turn to more concrete applications. To this end, we would like to highlight once again that every study of a quantum field theory requires the introduction of a suitable regularization procedure. Modern RG approaches render the theory under consideration infrared finite through the use of a regulator function that enters the inverse propagator. In practice, every single regulator comes along with individual advantages and disadvantages. In other words, regulator functions are not universally applicable but instead need to be chosen carefully and optimized for the current research objective. Intuitively, one may expect that theoretical studies of relativistic systems make extensive use of covariant regulators since Lorentz symmetry is one of the most important symmetry principles of quantum field theory in the vacuum limit. On the contrary, however, covariant regulators are employed only rarely in the presence of finite external parameters.[1] We emphasize that, whereas covariant regularization schemes treat all momentum modes on equal footing, temperature or chemical potential enforces a natural distinction of the time-like modes. As a result, this opposing behavior leads to the tendency to further complicate the evaluation of loop integrals. It is often argued that the breakdown of Lorentz invariance caused by finite external parameters is strong enough to dominate any regulator-induced Lorentz symmetry breaking, rendering spatial regularization schemes unlikely to qualitatively affect the infrared physics. Put differently, Lorentz symmetry in the vacuum limit gets declared as being relatively unimportant for the observables of interest, justifying the implementation of regulators that allow for less intricate computations while breaking Lorentz symmetry. Although this argumentation may indeed be correct in special cases and although spatial regulators have proven to be undeniably successful in improving our understanding of phenomena that do not primarily rely on intact Lorentz symmetry, it remains in general unclear whether an explicit breaking of Lorentz symmetry by the regulator can lead to significant artificial effects.

The main goals of the following work are to present possible implementations of covariant regularization for the fRG and discuss their characteristics as well as the challenges that come with the chosen regulators. In particular, we will consider a standard regulator with polynomial shape

[1] For a study which employs a covariant regulator at finite temperature, see Ref. [326].

functions as well as a momentum-independent regulator named after Callan [327] and Symanzik [328]. Both types of regulators can be used to establish a covariant regularization scheme in which we follow the RG flow of the effective average action towards the infrared. Based on mesonic two-point correlators, we will then assess the applicability and relevance of these regularization schemes. To be more concrete, we will perform a detailed analysis of meson curvature masses and spectral functions, which encode essential information about the phase structure of low-energy QCD. The computation of these quantities is also appealing as it allows to access transport coefficients, thereby establishing a direct link between theory and experiment. For simplicity, we are not going to work directly with the theory of the strong interaction but rather consider a quark-meson model in which the dynamics of non-Abelian gauge fields as well as ghosts is not resolved. The quark-meson model serves as a low-energy effective theory for QCD which renders the low-energy physics of the latter more accessible and significantly simplifies the investigation of the phase diagram of strong-interaction matter. Generally speaking, low-energy effective theories are simplified models that describe the physics of a system at energies much lower than the characteristic scale of the underlying fundamental theory. These effective theories capture the relevant degrees of freedom and interactions in a given low-energy regime while ignoring high-energy details that are considered irrelevant for the quantities of interest. Even though they are approximate, effective theories can offer precise predictions within their domain of validity.

3.1 Methodology

Before we begin with our regulator studies, we would like to give an introduction to the concrete model we will be working with for the rest of the chapter. We then proceed by giving a brief presentation of the specific RG framework as well as the truncations we consider in order to calculate infrared observables later on. For simplicity, we will restrict our discussion to the zero-temperature case.

3.1.1 The quark-meson model

In order to study the physics of the strong interaction in the low-energy regime, we are going to employ an NJL-type model, see, e.g., Refs. [28, 76, 77] for reviews. Inspired by the BCS theory of superconductivity [329, 330], the NJL model [74, 75] was originally developed as a theory of interacting nucleons with the goal to describe the mechanism of dynamical mass generation for hadrons. As the fermionic degrees of freedom are nowadays reinterpreted as quarks, four-fermion models such as the NJL model are predominantly used as models for QCD at low energies. Compared to the theory of the strong interaction, corresponding low-energy effective theories typically lack gauge degrees of freedom. In particular, effective theories of QCD are usually considered the result of integrating out high-energy degrees of freedom from the path integral description of the system. In QCD, multi-fermion interactions are dynamically generated by quark-gluon interactions and the process of integrating out gluon fields transforms the remaining couplings to absorb the information associated with the gluon sector. Therefore, the four-fermion couplings in NJL-type models are assumed to be effective couplings, generated by the more fundamental interactions between quarks and gluons. At sufficiently low energies, QCD under vacuum-like conditions is dominated by non-perturbative effects such as quark confinement and the formation of bound states.[2] Therefore, four-fermion models serve as an effective but still microscopic description at intermediate energy scales between the weakly coupled high-energy regime of QCD, where quarks

[2] It is worth mentioning that the QCD vacuum is believed to be also characterized by gluon condensates [331–334] as well as instantons [335–337]. These phenomena will, however, be of no relevance for our studies.

and gluons are the relevant degrees of freedom, and the strongly coupled low-energy regime of QCD, in which hadrons dominate the dynamics. In general, it is of primary importance that effective theories share all those properties with the more fundamental theory that are believed to be relevant for the phenomenon of interest. For our purposes, the chiral symmetry of massless QCD is one of the most important features since it is essential for the understanding of the lightest hadrons. The NJL-type models have proven to be particularly useful in this context since they allow us to systematically study the behavior of the system, in particular the formation of quark condensates, as driven by various interaction channels that respect chiral symmetry. Recall that, by construction, every effective theory has built in a certain set of strategic approximations which lead to benefits in some areas of research, but also to shortcomings in other areas. In the case of the NJL model, the fact that the interactions between quarks are point-like in character causes the field theory to be non-renormalizable. This means that the model does not have a UV completion up to arbitrarily high energy scales due to the emergence of a Landau pole. This does, however, not pose a problem for our RG approach to quantum field theory if RG consistency can be ensured within the range of external parameters that we consider relevant. Furthermore, the local interactions in the NJL model do not give rise to quark confinement. In many situations, however, the mechanism that confines quarks into bound states may not be important. For example, the interaction of hadrons below the threshold for producing free quarks may not depend on the details of how the confinement is produced.

In the following, we consider a quark-meson model which is a special, partially bosonized NJL-type model. At zero temperature, our model is given by the action

$$\begin{aligned} S[\Phi]\big|_{\mu} = \int_x \Big(& \overline{\psi}(x)\big[\mathrm{i}\partial\!\!\!/ - \mathrm{i}\gamma^0\mu\big]\psi(x) + \mathrm{i}h\,\overline{\psi}(x)\big(\sigma(x) + \mathrm{i}\gamma^5\tau^i\pi_i(x)\big)\psi(x) \\ & + \frac{1}{2}\phi^{\intercal}(x)\big[-\partial^2 + m^2\big]\phi(x) - H\,\sigma(x)\Big) \\ = \int_p \int_q \Big(& \overline{\psi}(p)\big[-p\!\!\!/ - \mathrm{i}\gamma^0\mu\big](2\pi)^4\delta^{(4)}(p-q)\,\psi(q) + \mathrm{i}h\,\overline{\psi}(p)\big(\sigma(p-q) + \mathrm{i}\gamma^5\tau^i\pi_i(p-q)\big)\psi(q) \\ & + \frac{1}{2}\phi^{\intercal}(-p)\big[p^2 + m^2\big](2\pi)^4\delta^{(4)}(p-q)\,\phi(q) \\ & - H\,(2\pi)^4\delta^{(4)}(p)\,(2\pi)^4\delta^{(4)}(p-q)\,\sigma(q)\Big)\,, \end{aligned} \tag{3.1}$$

where fermionic as well as bosonic field degrees of freedom have been collected into the superfield Φ on the left-hand side. We take only the lightest quarks into account, i.e., we set $N_{\mathrm{f}} = 2$, but consider the physical number of color degrees of freedom, $N_{\mathrm{c}} = 3$. Furthermore, the fermions couple to the quark chemical potential,

$$\mu \equiv \mu_q = \frac{1}{2}\,(\mu_{\mathrm{u}} + \mu_{\mathrm{d}})\ . \tag{3.2}$$

We assume $SU(2)$ isospin symmetry such that the masses as well as chemical potentials of the lightest quarks are taken to be degenerate. The bosonic fields, σ and $\vec{\pi}$, do not carry an internal charge, e.g., flavor or color. Phenomenologically speaking, these scalar and pseudoscalar fields

carry the quantum numbers of the sigma[3] meson and the pions[4], respectively.

$$\phi = \begin{pmatrix} \sigma \\ \vec{\pi} \end{pmatrix} , \qquad \sigma \sim \overline{\psi}\psi , \qquad \vec{\pi} \sim \overline{\psi}\, \mathrm{i}\gamma^5 \vec{\tau}\, \psi . \tag{3.3}$$

In the interaction channel, h denotes the Yukawa coupling between the quarks and the mesons. The τ^i with $i \in \{1,2,3\}$ are the Pauli matrices which couple the quark spinors in flavor space. Furthermore, the scalar parameter $H \geq 0$ controls the amount of rotation symmetry breaking in the boson sector. With no explicit symmetry breaking, the pions will turn out to be Goldstone bosons [277, 278] in the hadronic phase, meaning they acquire no mass. However, if this parameter H is chosen to be finite, the auxiliary term $\sim H\sigma$ will render the pions massive in the regime of low temperatures and low densities. Since this mass will be small relative to other mesons in nature, massive pions are typically referred to as pseudo-Goldstone bosons.

First, let us comment on the decision to take only two quark flavors into account. Our expectations for the QCD phase diagram as a function of temperature and chemical potential are predominantly shaped by the symmetries of the underlying theory of the strong interaction. At low energies, a strongly interacting system in the hadronic phase is characterized by quark condensates which indicate that chiral symmetry is not present at the ground state. Massless QCD predicts that finite external parameters can trigger a transition to a different phase in which the symmetry becomes apparent again. In nature, however, the presence of massive quarks spoils chiral symmetry and hence obscures the mechanisms behind the chiral phase transition. Current quark masses quantify the extent of explicit chiral symmetry breaking and the effects of otherwise intact chiral symmetry on a specific quark flavor become more and more suppressed the larger the corresponding quark mass is. The strange quark mass is already of the same order of magnitude as the chiral phase transition temperature [340] and heavier quarks are barely influenced by otherwise intact chiral symmetry. As a result, the chiral phase transition of QCD is most relevant for the lightest quark flavors, i.e., the up and down quarks. Therefore, considering the case of $N_\mathrm{f} = 2$ is indeed a rather crude approximation to the real world but it is truly useful for the investigation of chiral symmetry patterns that underlie the phase diagram of QCD. For reviews on the chiral phase transition, we refer to, e.g., Refs. [326, 341, 342].

In the context of the phase diagram of QCD, we would like to add a word of caution regarding phenomenological descriptions that often accompany the introduction of the chiral phase transition. Let us consider again the regime of low temperatures and low density, in which the quark-gluon interactions generate bound color-singlet states, the hadrons. As temperature rises, thermal fluctuations induce a transition of the low-density system into the quark-gluon plasma in which color is screened rather than confined. At low temperatures, high densities are expected to force quark matter into a color superconducting state, a Higgs phase characterized by massive gluons and the formation of diquark condensates. These last statements about transitions to a separate phase of matter are perfectly fine by themselves but are, strictly speaking, distinct from the chiral phase transition. Our simple quark-meson model is not capable of describing quark confinement and lacks diquark degrees of freedom which are important to accurately describe the color superconducting phases of quark matter. Although the phenomenological descriptions are hugely valuable for physical context, the deconfinement transition at high temperatures and the color

[3] The scalar meson σ is also known as the $f_0(500)$ resonance [338, 339].

[4] The standard model of particle physics identifies three types of pions, which are π^0, π^+, and π^- [339]. However, since our quark-meson model assumes isospin symmetry of flavor space and does not account for electroweak interactions, we are not able to tell the different pions apart.

superconductor transition at high densities cannot be predicted by the quark-meson model. In principle, these transitions do not need to exactly align with the chiral phase transition such that separated or mixed phases are possible. For more information, see, e.g., Refs. [343–345].

In addition, we would like to point out the fact that dynamical bosons do not appear in the NJL model. More specifically, the process of partial bosonization introduces the bosons as auxiliary fields without a corresponding kinetic operator, see Appendix B. This is consistent with the idea that hadrons in QCD are emergent bound states rather than elementary fields with their own independent dynamics. Generally speaking, the dynamical behavior of hadrons in nature arises from the underlying dynamics of quarks and gluons. That the NJL model comes without contributions, which can be phrased as an effective kinetic term for the bosons, is simply part of the truncation inherent to the model. In contrast to this, the quark-meson model has a kinetic term for the boson fields included, meaning it formally treats the mesons as fundamental fields that have their own dynamics. Although the quark-meson model may be considered less close to QCD from a phenomenological point of view, the presence of the kinetic term for mesons allows for a more accurate description of low-energy hadronic physics. To give an example, the kinetic term improves the description of meson propagation which is essential for the investigation of spectral properties such as pole masses. For the sake of completeness, it should also be mentioned that bosonized NJL models include meson fields up to only second order, see again Appendix B, while quark-meson models allow for boson self-interactions of higher orders. Overall, the quark-meson model has proven to be a very valuable tool for the investigation of the chiral phase transition and the low-energy properties of light mesons in a regime not too far away from the hadronic phase. For related studies of the quark-meson model, see, e.g., Refs. [79, 178, 209, 232, 293, 346–351]. We would like to highlight, though, that our quark-meson model still is an overly simple approximation to the theory of the strong interaction. For more comprehensive studies of the low-energy physics of QCD, several extensions to the simple quark-meson model are possible. One may, for instance, include a Polyakov loop potential [306, 352–357], consider more meson degrees of freedom [358–362], incorporate additional diquark fields [88, 305, 312, 363] or introduce a rotating frame [364]. Since we are ultimately more interested in the role of covariant regularization than high-precision calculations, we will work with the model defined by Eq. (3.1) for simplicity.

Generally speaking, the low-energy physics predicted by the quark-meson model heavily relies on chiral symmetry and in particular how it is realized in the system. To this end, we will now review the most important aspects of chiral symmetry [365–367]. Fermion fields allow for the linear decomposition

$$\psi(x) = \psi_{\mathrm{L}}(x) + \psi_{\mathrm{R}}(x)\,, \tag{3.4}$$

where the two components are defined in terms of a suitable projection,

$$\psi_{\mathrm{L}}(x) = \frac{1-\gamma^5}{2}\,\psi(x)\,, \qquad \psi_{\mathrm{R}}(x) = \frac{1+\gamma^5}{2}\,\psi(x)\,. \tag{3.5}$$

By construction, these projection operators are orthogonal, idempotent, and satisfy the completeness relation. Notice that the two components are eigenstates to the chirality operator γ^5 with eigenvalues ± 1,

$$\gamma^5\psi_{\mathrm{L}}(x) = -\psi_{\mathrm{L}}(x)\,, \qquad \gamma^5\psi_{\mathrm{R}}(x) = \psi_{\mathrm{R}}(x)\,. \tag{3.6}$$

As a result, ψ_{L} is called the left-handed and ψ_{R} the right-handed component of the fermion field ψ. For the Dirac adjoint $\overline{\psi}$, the procedure is completely analogous. Now, a fermionic theory is

said to exhibit chiral symmetry if the left- and right-handed components of the fermion fields can be rotated independently in flavor space without changing the physics. To be more precise, chiral symmetry is present if the action of a fermionic system is invariant under chiral transformations, i.e., elements of the product group $SU(N_\mathrm{f})_\mathrm{L} \times SU(N_\mathrm{f})_\mathrm{R}$. More explicitly, the chiral transformations read

$$\begin{aligned} SU(N_\mathrm{f})_\mathrm{L}: \quad & \psi_\mathrm{L}(x) \to \exp\left(-\frac{\mathrm{i}}{2}\tau^i\Theta_{\mathrm{L},i}\right)\,\psi_\mathrm{L}(x)\,, \qquad \psi_\mathrm{R}(x) \to \psi_\mathrm{R}(x)\,, \\ & \overline{\psi}_\mathrm{L}(x) \to \overline{\psi}_\mathrm{L}(x)\,\exp\left(\frac{\mathrm{i}}{2}\tau^i\Theta_{\mathrm{L},i}\right)\,, \qquad \overline{\psi}_\mathrm{R}(x) \to \overline{\psi}_\mathrm{R}(x)\,, \end{aligned} \tag{3.7}$$

$$\begin{aligned} SU(N_\mathrm{f})_\mathrm{R}: \quad & \psi_\mathrm{L}(x) \to \psi_\mathrm{L}(x)\,, \qquad \psi_\mathrm{R}(x) \to \exp\left(-\frac{\mathrm{i}}{2}\tau^i\Theta_{\mathrm{R},i}\right)\,\psi_\mathrm{R}(x)\,, \\ & \overline{\psi}_\mathrm{L}(x) \to \overline{\psi}_\mathrm{L}(x)\,, \qquad \overline{\psi}_\mathrm{R}(x) \to \overline{\psi}_\mathrm{R}(x)\,\exp\left(\frac{\mathrm{i}}{2}\tau^i\Theta_{\mathrm{R},i}\right)\,, \end{aligned} \tag{3.8}$$

where the matrices τ^i with $i \in \{1,\ldots,N_\mathrm{f}^2-1\}$ are associated with the generators of the flavor group $SU(N_\mathrm{f})$. In the case of $N_\mathrm{f}=2$, the τ^i correspond to the standard Pauli matrices. The transformation parameters Θ_L and Θ_R are assumed to be continuous and real-valued. Intact chiral symmetry gives rise to conserved currents, the vector current as well as the axial-vector current. In accordance with these conserved charges, chiral transformations can be expressed in terms of vector transformations and axial-vector transformations. Those apply to the entire field variables instead of the chiral components.

$$SU(N_\mathrm{f})_\mathrm{V}: \quad \psi(x) \to \exp\left(-\frac{\mathrm{i}}{2}\tau^i\Theta_{\mathrm{V},i}\right)\,\psi(x)\,, \qquad \overline{\psi}(x) \to \overline{\psi}(x)\,\exp\left(\frac{\mathrm{i}}{2}\tau^i\Theta_{\mathrm{V},i}\right)\,, \tag{3.9}$$

$$X_\mathrm{A}: \quad \psi(x) \to \exp\left(-\frac{\mathrm{i}}{2}\gamma^5\tau^i\Theta_{\mathrm{A},i}\right)\,\psi(x)\,, \qquad \overline{\psi}(x) \to \overline{\psi}(x)\,\exp\left(-\frac{\mathrm{i}}{2}\gamma^5\tau^i\Theta_{\mathrm{A},i}\right)\,. \tag{3.10}$$

These two types of transformations can be understood as linear combinations of the left- and right-handed transformations. In particular, the transformation parameters are connected through the relations

$$\Theta_\mathrm{V} = \frac{\Theta_\mathrm{L}+\Theta_\mathrm{R}}{2}\,, \qquad \Theta_\mathrm{A} = \frac{\Theta_\mathrm{L}-\Theta_\mathrm{R}}{2}\,. \tag{3.11}$$

From this second but equivalent perspective, chiral symmetry is present if the action of a fermionic system is invariant under vector and axial-vector transformations. Since our studies do not take any physics of the weak interaction into account, there is no benefit in decomposing our fermion fields into their chiral components. Therefore, it will be more convenient to work with the vector and axial-vector transformations in the following. In any case, as our model includes no explicit mass term for the fermion fields, the fermion sector has chiral symmetry.

The set of ordinary vector transformations in flavor space, $SU(N_\mathrm{f})_\mathrm{V}$, is a subgroup of the chiral product group. We emphasize, however, that the axial-vector transformations do not form a group. More specifically, the set of axial-vector transformations as denoted by X_A is not a group because the condition of closure under a binary group operation is not satisfied. To illustrate this, we will make use of the Baker-Campbell-Hausdorff (BCH) formula [368–371], see also Refs. [245, 372, 373] for an in-depth and more modern treatment of the formula. With the matrices

$$A = \gamma^5 \otimes \tau^i\Theta_i^{(A)}\,, \qquad B = \gamma^5 \otimes \tau^i\Theta_i^{(B)} \tag{3.12}$$

at hand, we consider the following product of matrix exponentials,

$$\mathrm{e}^{-\frac{\mathrm{i}}{2}A}\,\mathrm{e}^{-\frac{\mathrm{i}}{2}B} = e^{-\frac{\mathrm{i}}{2}C}\,. \tag{3.13}$$

This mimics the situation in which two subsequently applied axial-vector transformations are combined to a new transformation. The resulting exponential is again an axial-vector transformation only if C can be brought into the form

$$C \stackrel{!}{=} \gamma^5 \otimes \tau^i f_i\left(\Theta^{(A)}, \Theta^{(B)}\right) \tag{3.14}$$

with f denoting some suitable function. According to the BCH formula, the matrix C has the series representation

$$\begin{aligned} C &= A + B - \frac{\mathrm{i}}{4}[A,B] + \mathcal{O}\left(\Theta^3\right) \\ &= \gamma^5 \otimes \tau^i \left(\Theta_i^{(A)} + \Theta_i^{(B)}\right) - \frac{\mathrm{i}}{4} \mathbb{1}_{\mathrm{D}} \otimes \left[\tau^i, \tau^j\right] \Theta_i^{(A)} \Theta_j^{(B)} + \mathcal{O}\left(\Theta^3\right) . \end{aligned} \tag{3.15}$$

Since the commutator of $SU(N_\mathrm{f})$ generators does in general not vanish and because all orders in transformation parameters are linearly independent, the even orders in this series expansion are diagonal in Dirac space. As a consequence, it is impossible for C to take the form as proposed in Eq. (3.14). This means that two subsequent axial-vector transformations do together not describe a pure axial-vector transformation anymore but instead lead to a new transformation that is not part of X_A. Thus, the set of axial-vector transformations is not a group.

Theories of fermions that respect chiral symmetry should remain symmetric also after bosonization. The realization of chiral symmetry in the space of boson fields, however, differs from that of the fermions. Since the bosons in our quark-meson model are to be understood as effective degrees of freedom resulting from a reparameterization of multi-fermion interactions, we can investigate the impact of chiral symmetry on these mesons by applying the chiral transformations on their associated fermion content. Taking the transformation parameters to be infinitesimally small, we find that the vector transformations lead to isospin rotations in the pion subspace,

$$\sigma(x) \to \sigma(x) , \qquad \vec{\pi}(x) \to \vec{\pi}(x) + \mathrm{d}\vec{\Theta}_\mathrm{V} \times \vec{\pi}(x) , \tag{3.16}$$

and that the different mesons are rotated into each other under the axial-vector transformations,

$$\sigma(x) \to \sigma(x) - \mathrm{d}\vec{\Theta}_\mathrm{A}^\intercal \, \vec{\pi}(x) , \qquad \vec{\pi}(x) \to \vec{\pi}(x) + \mathrm{d}\vec{\Theta}_\mathrm{A} \, \sigma(x) . \tag{3.17}$$

This means that intact chiral symmetry manifests itself as an $O(4)$ symmetry in the meson sector. The requirement of chiral symmetry therefore constraints possible extensions of the bosonized NJL model to those whose meson sector is invariant under orthogonal transformations,

$$\forall Q \in O(4): \qquad \phi(x) \to Q \, \phi(x) . \tag{3.18}$$

In particular, chiral symmetry restricts the effective potential of the meson sector to be a function of the $O(4)$-invariant quantity ϕ^2. This further implies that a finite ground state is degenerate in field space and that we are free to choose a specific configuration. Notice that this freedom of choice leaves physical observables unaffected as long as chiral symmetry is intact.

Now, the term $\sim H\sigma$ in the action of our quark-meson model (3.1) is not invariant under rotations in mesonic field space. More specifically, this additional term represents a linear implementation of explicit $O(4)$ symmetry breaking in the meson sector.[5] From the perspective of an effective field variable, the term $\sim H\sigma$ does not remain invariant under axial-vector transformations of the associated quark content and can therefore also be associated with explicit chiral symmetry

[5] For a discussion of quadratic symmetry breaking, see, e.g., Ref. [121].

breaking. To make this connection more explicit, we remark that the auxiliary term is related to a current quark mass term by means of a Hubbard-Stratonovich transformation,

$$-H\,\sigma(x) \mathrel{\hat{=}} \overline{\psi}(x)\,\mathrm{i}m_{\mathrm{curr}}\,\psi(x)\,. \tag{3.19}$$

In words, the linear boson term in our quark-meson model is a reformulation of explicit chiral symmetry breaking in the quark sector. This formulation allows us to study the effects of a finite quark mass directly at the boson level. The symmetry-breaking term leads to an immediate distinction of the σ-direction of field space and thereby leads to a uniquely defined ground state. The superfield for our quark-meson model reads

$$\Phi(x) = \begin{pmatrix} \phi(x) \\ \psi(x) \\ \overline{\psi}^{\mathsf{T}}(x) \end{pmatrix}, \qquad \phi(x) = \begin{pmatrix} \sigma(x) \\ \vec{\pi}(x) \end{pmatrix} \tag{3.20}$$

such that the ground state of the system with explicitly broken chiral symmetry has the structure

$$\Phi_0 = \begin{pmatrix} \phi_0 \\ 0 \\ 0 \end{pmatrix}, \qquad \phi_0 = \begin{pmatrix} \sigma_0 \\ \vec{0} \end{pmatrix}. \tag{3.21}$$

For everything that follows, we will assume the ground state to be homogeneous. A discussion of inhomogeneous phases in the phase diagram of NJL-type models can be found in, e.g., Refs. [322–325]. For $H > 0$, it follows from the minimization of the effective potential that $\sigma_0 > 0$. We emphasize that the symmetry-breaking term leaves the isospin symmetry of the system intact, meaning that all directions of the pion subspace are still being treated equally. Moreover, since our quark-meson model renders the fermions massless at high energies, the ground state of the system is directly related to the constituent quark mass by

$$m_q(\mu) = -\frac{\mathrm{i}}{V_4} \lim_{Q\to 0}^{(\mathrm{st})} \left(\frac{\overrightarrow{\delta}}{\delta\overline{\psi}(Q)}\,\Gamma[\Phi]\big|_\mu \frac{\overleftarrow{\delta}}{\delta\psi(Q)} \right)\Bigg|_{\Phi=\Phi_0} = h\sigma_0(\mu)\,. \tag{3.22}$$

For consistency with the chiral limit, $H \to 0$, the ground state of a system with no explicit chiral symmetry breaking is canonically chosen to agree with Eq. (3.21). However, there is still a residual freedom of choice at $H = 0$ left because chiral symmetry gives rise to a $\mathbb{Z}_2$ symmetry along the σ-direction of field space. Therefore, the relation between the ground state and the quark mass slightly changes for a chiral system to $m_q = h|\sigma_0|$.

3.1.2 Our fRG framework

For the investigation of low-energy QCD and in particular its non-perturbative features that underlie the phase diagram of strongly interacting matter, we take a renormalization group approach to quantum field theory and make extensive use of functional RG methods. More specifically, we will employ the Wetterich equation, a characteristic RG flow equation for the effective average action, and apply a suitable truncation scheme to gain access to the IR physics of the two-flavor quark-meson model. A presentation of all considered truncations as well as their implications is given in the following.

We shall consider the Wetterich equation in a one-loop approximation which allows for a convenient computation of the scale-dependent effective action. We remark that this approximation is specifically valuable as it allows us to integrate flow equations to higher RG scales without ambiguity. As a consequence, we will be able to perform an RG-consistent UV completion of the initial condition Γ_{Λ_0} and thereby remove regularization scheme artifacts that are associated with finite external parameters becoming comparable to the value of the reference scale Λ_0. Furthermore, we will restrict our analysis to Feynman diagrams with purely fermionic loops for simplicity. The absence of bosonic loop contributions implies that we neglect the running of the wavefunction renormalization for the quarks, i.e., $Z_{\psi,k} \equiv 1$, as well as the running of the Yukawa coupling, i.e., we assume that $h_k \equiv h$. With these truncations implemented, the Wetterich equation takes the simplified form

$$\partial_k \Gamma_k^{\text{1-loop}}[\phi]\big|_\mu = -\operatorname{Tr}\left\{\partial_k R_k^\psi \cdot \left(S^{(1,1)}_{\bar\psi,\psi}[\phi] + R_k^\psi\right)^{-1}\right\}\Big|_\mu , \tag{3.23}$$

where the second derivative of the classical action reads

$$\begin{aligned} S^{(1,1)}_{\bar\psi,\psi}[\phi](p,q)\big|_\mu &= \frac{\overrightarrow{\delta}}{\delta\bar\psi(p)} S[\Phi]\big|_\mu \frac{\overleftarrow{\delta}}{\delta\psi(q)} \\ &= \left[-\not{p} - \mathrm{i}\gamma^0\mu\right](2\pi)^4\delta^{(4)}(p-q) + \mathrm{i}h\left(\sigma(p-q) + \mathrm{i}\gamma^5\tau^i\pi_i(p-q)\right) . \end{aligned} \tag{3.24}$$

We would like to highlight that, since the term associated with explicit symmetry breaking is linear in the fields, the inverse propagator above is independent of the corresponding symmetry-breaking parameter. More generally, it follows from a loop expansion of the effective average action that its second functional derivative is always independent of the symmetry-breaking term. As a consequence, the Wetterich equation does not generate corrections to the initial value of the symmetry-breaking parameter, which means that $H_k \equiv H$. In other words, the information about explicit symmetry breaking does not enter the Wetterich equation but only becomes relevant at the ultraviolet scale where the boundary condition for the effective average action is fixed. This further implies that, as long as the regulator respects chiral symmetry, the loop contributions generated by the Wetterich equation will also have chiral symmetry.[6] In addition, we note that the second derivative of the classical action does not have a dependence on the RG scale. Therefore, we can formally integrate the RG flow equation (3.23) to obtain the effective average action up to the one-loop order. The integration process yields

$$\begin{aligned} \Gamma_k^{(0+1)\text{-loop}}[\Phi]\big|_\mu &= \Gamma_{\Lambda_0}[\Phi] + \int_{\Lambda_0}^{k} \mathrm{d}k'\,\partial_{k'}\Gamma_{k'}^{\text{1-loop}}[\phi]\big|_\mu \\ &= \Gamma_{\Lambda_0}[\Phi] - \operatorname{Tr}\left\{\operatorname{Ln}\left(S^{(1,1)}_{\bar\psi,\psi}[\phi] + R_{k'}^\psi\right)\Big|_{k'=\Lambda_0}^{k'=k}\right\}\Big|_\mu , \end{aligned} \tag{3.25}$$

where we set $\Gamma_{\Lambda_0} = S$. The reference scale Λ_0 denotes the RG scale at which we fix the coupling parameters of our theory. Notice that the UV boundary condition to the Wetterich equation is employed at zero external parameters, meaning that all coupling parameters at high scales are fixed under vacuum conditions. For convenience, we will now drop the superscript of the truncated effective average action for everything that follows.

[6] In general, the chiral symmetry of the classical action may not transfer to the average effective action despite an optimal regulator choice. For theories, which include a coupling between fermions and gauge bosons, the path integral measure spoils the chiral symmetry and leads to the so-called axial anomaly. This quantum anomaly is, however, not present in our studies since the quark-meson model does not take gauge fields into account. For more information about the anomaly, see, e.g., Refs. [374–377].

For the investigation of the chiral phase transition, we will often be interested in low-energy observables such as curvature masses. A particularly convenient method for calculating low-energy observables is to evaluate the field degrees of freedom on a homogeneous background,

$$\Phi(x) = \Phi \,, \qquad \Phi(p) = \Phi\ (2\pi)^4 \delta^{(4)}(p) \ . \tag{3.26}$$

As a result, the functional of 1PI correlation functions turns into an ordinary function and becomes directly relatable to the effective potential:

$$\Gamma_k(\Phi)\big|_\mu = V_4\ U_k(\Phi)\big|_\mu \,, \tag{3.27}$$

where V_4 denotes the four-dimensional spacetime volume. This hugely simplifies the calculation of loop integrals and makes the IR physics more accessible but comes at the cost of neglecting any momentum transfer. Considering homogeneous backgrounds, the UV effective action for our quark-meson model reads

$$\frac{1}{V_4}\Gamma_{\Lambda_0}(\Phi) = \mathrm{i}h\ \overline{\psi}\left(\sigma + \mathrm{i}\gamma^5 \tau^i \pi_i\right)\psi + \frac{1}{2} m_{\Lambda_0}^2 \phi^2 - H\,\sigma \ . \tag{3.28}$$

Moreover, we introduce an auxiliary function to parameterize the loop integral of the Wetterich equation,

$$L_k(\Lambda_0, \phi)\big|_\mu = \frac{1}{8 N_\mathrm{c} V_4}\ \mathrm{Tr}\left\{ \mathrm{Ln}\left(S^{(1,1)}_{\bar{\psi},\psi}(\phi) + R^{\psi}_{k'} \right)\Big|_{k'=\Lambda_0}^{k'=k} \right\}\Big|_\mu \ , \tag{3.29}$$

where the additional factor in the denominator compensates for the tracing over Dirac, flavor, and color space, i.e., $N_\mathrm{D} N_\mathrm{f} N_\mathrm{c} = 8 N_\mathrm{c}$. We highlight that our model does not incorporate interactions that couple the quarks in color space. Therefore, all loop integrals associated with this model will give rise to a global factor of N_c. Moreover, recall that, in our truncation scheme, the symmetry-breaking parameter H does not enter the Wetterich equation. As a result, the loop function L_k is a function of the $O(4)$-invariant ϕ^2 if the regulator respects chiral symmetry. Altogether, by evaluating the classical fields on a homogeneous background, we can phrase the scale-dependent effective action (3.25) as

$$\frac{1}{V_4}\Gamma_k(\Phi)\big|_\mu = \frac{1}{V_4}\Gamma_{\Lambda_0}(\Phi) - 8 N_\mathrm{c}\, L_k(\Lambda_0, \phi)\big|_\mu \ . \tag{3.30}$$

Once the regularization scheme is specified, the loop function can be presented more concretely. With the average effective action at hand, the quantum effective action is readily obtained in the infrared limit, $\Gamma \equiv \Gamma_0$. Meson curvature masses are then given by

$$\begin{pmatrix} m_\sigma^2(\mu) & \vec{0}^\intercal \\ \vec{0} & m_\pi^2(\mu)\ \mathbb{1}_{3\times 3} \end{pmatrix} = \left(\frac{\mathrm{d}}{\mathrm{d}\phi^\intercal} \frac{\mathrm{d}}{\mathrm{d}\phi} \frac{\Gamma(\Phi)\big|_\mu}{V_4} \right)\Big|_{\Phi=\Phi_0} \ . \tag{3.31}$$

As mentioned earlier, these masses represent the curvature of the effective potential at its global minimum along different directions of field space. We stress that projections onto physical observables always include an evaluation at the ground state Φ_0. Since the effective potential for a physical system is bounded from below,[7] the ground state satisfies the minimum condition

$$\left(\frac{\mathrm{d}}{\mathrm{d}\Phi^\intercal} U(\Phi)\big|_\mu \right)\Big|_{\Phi=\Phi_0} = 0 \ . \tag{3.32}$$

[7] Recall the quantum effective action as defined in Eq. (2.17) is convex, implying boundedness. Truncations such as the one-loop approximation, however, lead to a functional which does not need to be convex. In fact, canonical explanations of dynamical mass generation involve the effective potential taking the form of a "Mexican hat", which is non-convex. Nevertheless, a physical theory predicts the effective potential to be bounded from below and the loop expansion of the effective action does not destroy this property.

As the effective potential in general depends on external parameters such as temperature and chemical potential, the ground state will also inherit a dependence on those parameters. Since a physical ground state is zero along the fermionic directions of field space, see Eq. (3.21), and because our studies mostly focus on the computation of bosonic observables, the fermionic contributions at the reference scale Λ_0 will be of no relevance for what follows. We will therefore drop the terms involving fermion fields in the boundary condition of the average effective action and write

$$\Gamma_{\Lambda_0}[\phi] = \int_x \left(\frac{1}{2} \phi^\intercal(x) \left[-Z_{\Lambda_0} \partial^2 + m^2_{\Lambda_0} \right] \phi(x) - H\,\sigma(x) \right) , \tag{3.33}$$

$$\frac{1}{V_4} \Gamma_{\Lambda_0}(\phi) = \frac{1}{2} m^2_{\Lambda_0} \phi^2 - H\,\sigma \ . \tag{3.34}$$

The minimum condition along different directions of meson field space then takes the form of

$$\left(m^2_{\Lambda_0} \sigma - 8 N_c \frac{\mathrm{d}}{\mathrm{d}\sigma} L_0(\Lambda_0, \phi)\big|_\mu \right) \Big|_{\phi=\phi_0} = H \ , \tag{3.35}$$

$$\left(m^2_{\Lambda_0} \vec{\pi} - 8 N_c \frac{\mathrm{d}}{\mathrm{d}\vec{\pi}^\intercal} L_0(\Lambda_0, \phi)\big|_\mu \right) \Big|_{\phi=\phi_0} = \vec{0} \ . \tag{3.36}$$

As long as the symmetry-breaking parameter H is finite, the ground state σ_0 will also remain finite for all values of external parameters. In particular, a non-zero value for H makes it possible to pass smoothly from a situation in which the origin mass is positive to a situation in which it is negative. In our terminology, the origin mass denotes the curvature of the effective potential at the origin of field space,

$$m_0^2 = \left(\frac{\mathrm{d}^2}{\mathrm{d}\sigma^2} U(\phi) \right) \Big|_{\phi=0} = \left(\frac{\mathrm{d}^2}{\mathrm{d}|\vec{\pi}|^2} U(\phi) \right) \Big|_{\phi=0} \ . \tag{3.37}$$

However, if instead the symmetry-breaking parameter vanishes, the ground state also vanishes for $m_0^2 > 0$ but assumes a non-trivial value when the origin mass is negative. For $H = 0$, observables exhibit a non-analytic behavior when $m_0^2 = 0$, indicating a phase transition. This point of vanishing origin mass can then be translated to a divergence of the four-fermion coupling of a corresponding fermionic theory [185].

More generally, our analysis of the quark-meson model will focus on the calculation of bosonic two-point correlation functions. When considering their full momentum dependence, we will employ the $\mathcal{PF}$ expansion, see Eq. (2.99), to obtain these correlators from the Wetterich equation. To this end, we decompose the bosonic field variable into the ground state configuration and a corresponding fluctuation. It is worth mentioning again that we assume the ground state of the system to be homogeneous, i.e., it is uniform across all of spacetime. Accordingly, we write

$$\begin{pmatrix} \sigma(x) \\ \vec{\pi}(x) \end{pmatrix} = \begin{pmatrix} \sigma_0(\mu) \\ \vec{0} \end{pmatrix} + \begin{pmatrix} \sigma_{\mathrm{fl}}(\mu, x) \\ \vec{\pi}_{\mathrm{fl}}(x) \end{pmatrix} \ . \tag{3.38}$$

Notice that, since the ground state depends on external parameters, so do the fluctuation fields. However, the dependences of fluctuation fields on temperature and chemical potential are of no relevance within the fRG approach such that we choose to drop them in the following. The $\mathcal{PF}$ expansion relies on rewriting the inverse average propagator as a sum of two functionals, which are given by

$$\mathcal{P}_k^{-1}[\phi_0](p,q)\big|_\mu = \left[-\not{p} - \mathrm{i}\gamma^0 \mu + \mathrm{i} h \sigma_0(\mu) \right] (2\pi)^4 \delta^{(4)}(p-q) + R_k^\psi(p,q)\big|_\mu \ , \tag{3.39}$$

$$\mathcal{F}[\phi_{\mathrm{fl}}](p,q) = \mathrm{i} h \left(\sigma_{\mathrm{fl}}(p-q) + \mathrm{i}\gamma^5 \tau^i \pi_{\mathrm{fl},i}(p-q) \right) . \tag{3.40}$$

We emphasize that, in our truncation scheme, σ_0 always refers to the global minimum of the effective potential along the σ-direction of field space at $k = 0$. In general, the effective potential will have a non-trivial RG flow, meaning that the minimum of the scale-dependent effective potential also carries a scale dependence. However, as we are more interested in infrared observables rather than their RG flow, we take σ_0 to be scale-independent for convenience. Altogether, the full two-point correlator is given by

$$\begin{aligned}\Gamma^{(2)}(P,Q)\big|_\mu &= \tilde{\Gamma}^{(2)}(Q)\big|_\mu\,(2\pi)^4\delta^{(4)}(P-Q)\\ &= \left(\frac{\delta}{\delta\phi^\intercal(-P)}\frac{\delta}{\delta\phi(Q)}\Gamma[\phi]\big|_\mu\right)\Big|_{\phi=\phi_0}\\ &= \left(\frac{\delta}{\delta\phi_{\mathrm{fl}}^\intercal(-P)}\frac{\delta}{\delta\phi_{\mathrm{fl}}(Q)}\Gamma[\phi_0+\phi_{\mathrm{fl}}]\big|_\mu\right)\Big|_{\phi_{\mathrm{fl}}=0}\\ &= \Gamma^{(2)}_{\Lambda_0}(P,Q)+\frac{1}{2}\frac{\delta}{\delta\phi_{\mathrm{fl}}^\intercal(-P)}\frac{\delta}{\delta\phi_{\mathrm{fl}}(Q)}\,\mathrm{Tr}\left\{\left(\mathcal{P}_k[\phi_0]\big|_\mu\cdot\mathcal{F}[\phi_{\mathrm{fl}}]\right)^2\Big|_{k=\Lambda_0}^{k=0}\right\}\,,\end{aligned} \tag{3.41}$$

where it follows from Eq. (3.33) that

$$\begin{aligned}\Gamma^{(2)}_{\Lambda_0}(P,Q) &= \tilde{\Gamma}^{(2)}_{\Lambda_0}(Q)\,(2\pi)^4\delta^{(4)}(P-Q)\\ &= \left(Z_{\Lambda_0}Q^2+m^2_{\Lambda_0}\right)\mathbb{1}_{4\times4}\,(2\pi)^4\delta^{(4)}(P-Q)\,.\end{aligned} \tag{3.42}$$

Recall that the direction of functional differentiation does not matter when differentiating with respect to boson fields. We have therefore switched to a simpler notation for the mesonic two-point correlator,

$$\Gamma^{(2)}\equiv\Gamma^{(1,1)}=\Gamma^{(0,2)}=\Gamma^{(2,0)}\,. \tag{3.43}$$

We would also like to remark that the two-point correlator as presented above does not arise from the standard $\mathcal{PF}$ expansion of the Wetterich equation, see Eq. (2.99), since, at zero temperature and finite chemical potential, we find that

$$\int_{\Lambda_0}^{0}\mathrm{d}k\;\mathrm{Tr}\left\{\partial_k\left(\mathcal{P}_k[\phi_0]\big|_\mu\cdot\mathcal{F}[\phi_{\mathrm{fl}}]\right)^2\right\}\neq\mathrm{Tr}\left\{\left(\mathcal{P}_k[\phi_0]\big|_\mu\cdot\mathcal{F}[\phi_{\mathrm{fl}}]\right)^2\Big|_{k=\Lambda_0}^{k=0}\right\}\,. \tag{3.44}$$

Instead, our prescription for the correlation function in Eq. (3.41) includes corrections that compensate for error that is made when employing the $\mathcal{PF}$ expansion although the effective average action is non-analytical. Therefore, our formula also ensures consistency between the momentum-dependent two-point correlator at zero temperature and its finite-temperature pendant in the zero-temperature limit. For a more detailed discussion, we refer to Section 2.4. With the momentum-dependent two-point correlation function at hand, curvature masses can be recovered in the static limit,

$$\begin{pmatrix} m^2_\sigma(\mu) & \vec{0}^\intercal \\ \vec{0} & m^2_\pi(\mu)\,\mathbb{1}_{3\times3}\end{pmatrix}=\lim_{\vec{Q}\to\vec{0}}\lim_{Q^0\to0}\tilde{\Gamma}^{(2)}(Q)\big|_\mu\,. \tag{3.45}$$

This directly opens up the opportunity to cross-check the results for the curvature masses as computed from the effective potential and the two-point correlator.

The propagator of the theory is readily obtained from the momentum-dependent two-point function by inversion. The propagator admits a Källén-Lehmann (KL) spectral representation [378, 379],[8]

$$\frac{1}{\tilde{\Gamma}^{(2)}(Q)\big|_\mu} = \int_{\mathbb{R}} \frac{\mathrm{d}\lambda}{2\pi} \, \frac{\lambda}{(Q^0)^2+\lambda^2} \, \rho(\lambda,\vec{Q})\big|_\mu \,, \tag{3.46}$$

where ρ denotes the matrix-valued spectral (density) function. For more information about the derivation of the spectral representation, we refer the reader to Refs. [274, 380, 381]. Notice that the KL representation directly implies the spectral function to be an odd function in its first argument,

$$\rho(-\lambda,\vec{Q})\big|_\mu = -\rho(\lambda,\vec{Q})\big|_\mu \,. \tag{3.47}$$

Given Eq. (3.46), the spectral function can now be obtained using the discontinuity of the analytically continued propagator at the imaginary frequency axis,[9]

$$\rho(\omega,\vec{Q})\big|_\mu = 2 \lim_{\varepsilon\to 0^+} \mathfrak{Im} \left\{ \frac{1}{\tilde{\Gamma}^{(2)}(\mathrm{i}(\omega+\mathrm{i}\varepsilon),\vec{Q})\big|_\mu} \right\} \,. \tag{3.48}$$

Here, ω is defined along the imaginary axis of the complex Q^0-plane and can be associated with an energy variable of Minkowskian momentum space. A spectral function ρ represents the distribution of states in a quantum system as a function of energy ω and spatial momentum $\vec{Q}$. It encodes a variety of information on, for example, particle masses and decay processes, see, e.g., Refs. [229, 382, 383]. At some fixed momentum, the spectral functions will be presented as functions of the energy variable in the following sections. Resonance peaks in those functions indicate particle states whose masses are directly related to the corresponding value of ω_{res}. The resonance width is given by the full width at half maximum (FWHM) of the peak and provides us with the decay rate for the particle under consideration. It should also be mentioned that the decay rate and the mean lifetime of a particle state are inversely related to each other. A narrow peak in the form of a Dirac delta indicates that the propagator has a pole such that the associated mass is referred to as the pole mass. A peak of this kind has no resonance width, meaning that the corresponding particle state has an infinite lifetime and is thus stable. In cases where the pole of the propagator is screened by interactions, the peak becomes broadened and assumes a Lorentzian or Breit-Wigner shape in the spectral function. The associated mass of the particle is then typically referred to as the resonance mass. A finite FWHM signals that the particle under consideration can in fact decay, meaning the particle state is unstable. We further remark that the analytically continued propagator corresponds to the retarded propagator of Minkowski spacetime since we have

$$\tilde{\Gamma}^{(2)}(\mathrm{i}(\omega+\mathrm{i}\varepsilon),\vec{Q}) = -\tilde{\Gamma}^{(2)}_{\mathrm{M}}(\omega+\mathrm{i}\varepsilon,\vec{Q}) \,. \tag{3.49}$$

For all numerical calculations, the real-valued parameter ε is kept small but finite in order to allow for a non-trivial representation of delta distributions and overall numerically stable spectral functions. To be concrete, we set the parameter to $\varepsilon = 3\,\mathrm{MeV}$.

[8] The existence of a spectral representation for the scale-dependent propagator is in general not guaranteed. However, for spatial regularization schemes as well as Callan-Symanzik regulators, the regularized propagator indeed admits a spectral representation at every RG scale [82].

[9] Although the scale-dependent propagator need in general not admit a spectral representation, the formula (3.48) can in fact be used at all RG scales to serve as a definition of the scale-dependent spectral function ρ_k.

For illustrative purposes, let us consider the theory of a free scalar boson. The inverse Klein-Gordon propagator reads

$$\tilde{\Gamma}^{(2)}(Q) = Q^2 + m^2 \,, \tag{3.50}$$

which then leads to the following spectral function:

$$\begin{aligned}\rho(\omega,\vec{Q}) &= \frac{2\pi\ \omega}{\omega^2+\vec{Q}^2+m^2}\left(\delta\left(\omega-\sqrt{\vec{Q}^2+m^2}\right)+\delta\left(\omega+\sqrt{\vec{Q}^2+m^2}\right)\right)\\ &= \frac{\pi}{\sqrt{\vec{Q}^2+m^2}}\left(\delta\left(\omega-\sqrt{\vec{Q}^2+m^2}\right)-\delta\left(\omega+\sqrt{\vec{Q}^2+m^2}\right)\right) .\end{aligned} \tag{3.51}$$

According to the discussion above, the boson under consideration has a well-defined pole mass and is therefore considered stable. At vanishing spatial momenta, the pole mass can be read off from the argument of the Dirac delta. Equivalently, the pole mass is defined as the zero of the analytically continued inverse propagator, i.e.,

$$\tilde{\Gamma}^{(2)}(\mathrm{i}m,\vec{0}) = 0 \,. \tag{3.52}$$

Notice that a non-zero spatial momentum leads to an additional shift in the pole position. When working with spectral functions, however, we will always set the spatial external momenta to zero such that the energy ω_{res} of a resonance peak can be identified exactly as the mass of the corresponding meson. We would like to remark already here that this choice is not only based on computational convenience. As we will see in Section 3.3.3, a non-zero spatial momentum can cause the two-point correlator at zero temperature but finite chemical potential to be non-analytic in Q^0 such that the definition of a pole mass as well as the construction of a corresponding spectral function would not be possible.

We emphasize that pole masses and curvature masses do in general not need to agree. While the definition of the pole mass includes the full momentum dependence of the two-point correlation function, the curvature mass is given by the momentum-independent part of that correlator in the static limit. Put differently, compared to the curvature mass, the pole mass has information about interactions included which are sensitive to a finite momentum transfer. That being said, both types of masses must indeed agree when there are no interactions at all. In fact, as we can see from the example of the free theory above, the quantity m in Eq. (3.50) plays the role of the pole mass as well as the curvature mass of the boson under consideration. To make the distinction clear also from a formal standpoint, we always use that[10]

$$\tilde{\Gamma}^{(2)}(\mathrm{i}m_{\mathrm{pole}},\vec{0}) = 0 \,, \tag{3.53}$$

$$\lim_{\vec{Q}\to\vec{0}} \tilde{\Gamma}^{(2)}(0,\vec{Q}) = m^2_{\mathrm{curv}} \,. \tag{3.54}$$

For convenience, we will usually drop the subscript for the curvature mass. We emphasize that a translation of the definition of the curvature mass to the case of finite temperature or chemical potential is straightforward while a pole mass does not need to exist at finite external parameters. In particular, thermal fluctuations can induce a screening for the pole of the zero-temperature propagator such that the notion of a pole mass no longer applies. In the context of finite external parameters, it should further be mentioned that the definition of the pole mass of a particle that

[10] Strictly speaking, the definition of physical masses is linked to the renormalized two-point correlator, see, e.g., Ref. [235]. In this work, however, we will also use the terms of pole and curvature masses for corresponding quantities that have been obtained from the unrenormalized two-point function.

couples to a finite chemical potential is anchored at the Silver-Blaze symmetric point in momentum space. As mesons have a fermion number of exactly zero, this constraint is already trivially fulfilled in Eq. (3.53). Regarding our study of the quark-meson model, recall that we will restrict our analysis to Feynman diagrams with purely fermionic loops. As a result, there will be no loop correction to the fermion propagator such that the quark pole mass is identical to the quark curvature mass in our truncation scheme. We will therefore always refer to *the* quark mass m_q in this work.

3.2 Polynomial regulators

The investigation of physical systems within a functional renormalization group framework necessitates the specification of a regulator function. We begin our analysis of the quark-meson model by employing momentum-dependent regulators of the polynomial type, see, e.g., Ref. [81]. Common strategies to reduce computational efforts in model studies involve implementing spatial regularization schemes, where the time-like direction of spacetime is artificially distinguished such that Lorentz symmetry is explicitly broken. To assess the consequences of this regulator-induced symmetry breaking, we also consider a covariant scheme that preserves Lorentz symmetry in the vacuum limit. With these schemes at hand, we present results for meson curvature masses and spectral functions, which generally provide insights into the phase structure of QCD at low energies. Computations of an observable with different regulators eventually allow us to compare the regularization schemes to each other. In particular, by comparing the predictions of our model for mesonic observables and the chiral phase transition in these different schemes, we examine the significance of covariant regularization.

3.2.1 Generalities

For our study of the quark-meson model, we consider regulators of the form

$$\widetilde{R}_k^{\psi\,(3\mathrm{d})}(\vec{p}) = -\vec{\not{p}}\; r^{\varphi}_{\mathrm{poly}}\left(\frac{\vec{p}^{\,2}}{k^2}\right), \qquad \widetilde{R}_k^{\psi\,(4\mathrm{d})}(p) = -\not{p}\; r^{\varphi}_{\mathrm{poly}}\left(\frac{p^2}{k^2}\right) \tag{3.55}$$

for spatial and covariant regularizations, respectively. A comparison of these regulators based on low-energy observables will demonstrate the impact of covariant regularization relative to the corresponding spatial regularization scheme. The regulators in Eq. (3.55) are often referred to as polynomial regulators since they contain the polynomial shape function

$$r^{\varphi}_{\mathrm{poly}}(x) = \frac{1}{1-\left(\sum_{n=0}^{N} c_n x^n\right)^{-1}} - 1 = \left(\sum_{n=1}^{N} c_n x^n\right)^{-1} \tag{3.56}$$

with $c_0 = 1$, $c_n \in \mathbb{R}_0^+$ and $N \geq 1$. If not stated otherwise, we choose

$$\forall n \in \mathbb{N}_0 : \quad c_n = \frac{1}{n!}\,. \tag{3.57}$$

This choice is based on our observation that the coefficients c_n as shown above provide an advantage regarding the numerical stability of RG flows for all $N \geq 1$. We further remark that this choice lets the polynomial regulator turn into the exponential one in the limit as N tends to infinity:

$$\lim_{N\to\infty} r^{\varphi}_{\mathrm{poly}}(x) = \lim_{N\to\infty} \frac{1}{1-\left(\sum_{n=0}^{N} \frac{x^n}{n!}\right)^{-1}} - 1 = \frac{1}{1-\mathrm{e}^{-x}} - 1 = r^{\varphi}_{\mathrm{exp}}(x)\,. \tag{3.58}$$

For our purposes, however, we aim to choose the value of N as small as possible in order to allow for analytical simplifications of loop integrals in the presence of a covariant regulator. To be specific, we mostly choose

$$N = 2\,. \tag{3.59}$$

Notice that we use the polynomial shape function as defined in Eq. (3.56) for loop integrals with only fermionic internal lines although the superscript φ indicates that such a shape function is canonically used in bosonic loops. In contrast to this, officially fermionic shape functions always have a square root included, see, e.g., Eqs. (2.79) and (2.80). In particular, the fermionic analog of Eq. (3.56) reads

$$r^{\psi}_{\text{poly}}(x) = \frac{1}{\sqrt{1-\left(\sum_{n=0}^{N} c_n x^n\right)^{-1}}} - 1\,. \tag{3.60}$$

However, it is important to realize that the presence of a square root destroys the analytic properties of the theory. As a result, a derivative expansion of the effective average action would not be well-defined and momentum-dependent correlation functions could not be analytically continued to correlators of a Minkowski quantum field theory. In the case of zero external momenta or, equivalently, in the case of using homogeneous background fields, see Eq. (3.26), observables such as curvature masses turn out to be unaffected since the regulator enters the effective potential in terms of the quantity $(1+r^{\psi})^2$ in which the square root is effectively removed. Nevertheless, we emphasize that quantities that have been obtained by enforcing a derivative expansion do not necessarily recover their analytic properties in the limit of vanishing external momenta. Wavefunction renormalizations, for example, will not exhibit the Silver-Blaze property if their projection includes derivatives along those directions of momentum space which are influenced by the fermionic regulator. To briefly summarize, we intentionally choose a canonically bosonic regulator shape function for the purely fermionic loops to allow for analytic correlation functions in the presence of finite external momenta.

After having presented the concrete regularization schemes for this section, let us now discuss some of their properties. The following discussion of polynomial regulators is, however, by no means restricted to our choice of the coefficients c_n or the degree N. A direct consequence of using the bosonic shape function for a purely fermionic loop is that the regulator function diverges in the low-energy limit:

$$\widetilde{R}^{\psi}_{k}(q) = -\not{q}\,\mathcal{O}\left(\frac{k^2}{q^2}\right) \quad \text{as} \quad \frac{q^2}{k^2} \to 0^+\,. \tag{3.61}$$

The momentum variable q here is purely generic and can be identified with a three- or four-dimensional momentum, depending on the regularization scheme. From the standpoint of the functional renormalization group, the divergence is not problematic at all since this behavior does not conflict with any requirements on the regulator function. In fact, the divergence rather enhances the property of being mass-like as the regulator now behaves like an infinitely big mass term at small momenta. Furthermore, it follows that

$$\forall k > 0: \qquad \operatorname*{arg\,min}_{|q|\geq 0}\left(|q|\left(1 + r^{\varphi}_{\text{poly}}\left(\frac{q^2}{k^2}\right)\right)\right) > 0\,, \tag{3.62}$$

which is relevant for the propagator and correlation functions in general. Specifically for three-dimensional schemes, this property indicates that a finite quark chemical potential does not simply

play the role of an IR cutoff for the spatial momenta but rather divides their domain of integration into disjoint pieces. We would like to highlight that this behavior is significantly different from standard fermionic regulator shape functions, which behave according to

$$\forall k \geq 0: \qquad \arg\min_{|q|\geq 0}\left(|q|\left(1+r^{\psi}_{\text{poly}}\left(\frac{q^2}{k^2}\right)\right)\right)=0\,. \tag{3.63}$$

Finally, we stress that the polynomial regulators respect chiral symmetry. As a result, all loop contributions generated by the Wetterich equation will be invariant with respect to rotations in meson field space.

Our first study aims at a comparison of the spatial and covariant regulators as given by Eq. (3.55) based on observables such as meson curvature masses as well as spectral functions. For the investigation of low-energy phenomena in the context of the QCD phase diagram we employ the truncated Wetterich equation (3.23) and compute the quantum effective action of our quark-meson model in a one-loop approximation. Expanding the (pseudo-)scalar fields around a homogeneous background, we arrive at the following result for the scale-dependent effective action:

$$\begin{aligned}\frac{1}{V_4}\Gamma_k(\phi)\big|_{T,\mu} &= \frac{1}{V_4}\Gamma_{\Lambda_0}(\phi) - 8N_{\text{c}}\,L_k(\Lambda_0, h^2\phi^2)\big|_{T,\mu} \\ &= \frac{1}{V_4}\Gamma_{\Lambda_0}(\phi) - 4N_{\text{c}}\int_{\vec{p}}\frac{1}{\beta}\sum_{n\in\mathbb{Z}}\ln\left(\zeta^2_{k'}(\nu_n(\beta)+\mathrm{i}\mu,\vec{p})+h^2\phi^2\right)\Big|^{k'=k}_{k'=\Lambda_0}\,.\end{aligned} \tag{3.64}$$

The time-like quantity ν_n denotes the fermionic Matsubara frequency and depends on temperature. We remark that, at $T>0$, also the four-dimensional spacetime volume carries an implicit temperature dependence, $V_4 = \beta V$. Based on Eq. (2.218), we have further introduced a generalized four-momentum ζ, which has the following meaning in the different schemes:

$$\zeta^{(3\text{d})}_k(p) = \begin{pmatrix} p^0 \\ \vec{p}\,\left(1+r^{\varphi}_{\text{poly}}\left(\frac{\vec{p}^2}{k^2}\right)\right)\end{pmatrix}, \qquad \zeta^{(4\text{d})}_k(p) = \begin{pmatrix} p^0 \\ \vec{p}\end{pmatrix}\left(1+r^{\varphi}_{\text{poly}}\left(\frac{p^2}{k^2}\right)\right). \tag{3.65}$$

As mentioned earlier, the auxiliary function

$$L_k(\Lambda_0,\chi)\big|_{T,\mu} = \frac{1}{2}\int_{\vec{p}}\frac{1}{\beta}\sum_{n\in\mathbb{Z}}\ln\left(\zeta^2_{k'}(\nu_n(\beta)+\mathrm{i}\mu,\vec{p})+\chi\right)\Big|^{k'=k}_{k'=\Lambda_0} \tag{3.66}$$

parameterizes the loop integral as implied by the trace in the Wetterich equation. All information about the tendency of the system to establish a vanishing or finite ground state in the infrared is encoded in this loop function.[11] Since we consider only fermionic loops in our calculations, the effective potential tends towards a non-trivial minimum at small RG scales. Whether or not the ground state of the system actually becomes finite at some critical scale within the RG flow, purely depends on the initial condition for the flow of the effective average action. At the UV scale Λ_0 we represent the effective average action as a quadratic form, see Eq. (3.34). In order to perform actual calculations, we need to fix the coupling parameters of the theory, i.e., the Yukawa coupling and the meson mass parameter. To be more specific, we fix the coupling parameters such that, for

[11] We remark that the polynomial shape function with $N=2$, independent of whether it is used in its fermionic or bosonic version, does not provide sufficient UV regularization for the loop function L_k in Eq. (3.64). This does, however, not pose a problem for us since we are not interested in the entire effective potential but in correlation functions which are indeed well-defined for our regulator choice. Alternatively, one may choose $N\geq 3$ to render the effective potential UV finite. Another solution would be to adjust the initial condition Γ_{Λ_0} to include a counterterm for the loop, provided that the UV divergence can be isolated analytically.

$T = \mu = H = 0$ and at the ground state of the system, we reproduce some predetermined values for the constituent quark mass m_q and the pion decay constant f_π. In the context of our quark-meson model, these quantities are assumed to satisfy the following general relations:

$$m_q = h|\sigma_0| \,, \qquad f_\pi = \frac{m_q}{h} \,. \tag{3.67}$$

For this representation of the pion decay constant, we have applied the Goldberger-Treiman relation [384] to quarks instead of nucleons. For more information on the Goldberger-Treiman relation see, e.g., Refs. [118, 121, 365, 385]. In the absence of explicit symmetry breaking, the vacuum values for the quark mass as well as the pion decay constant are specified based on low-energy experiments. In the following, we will use a hat notation to refer to these special values. The aforementioned conditions then consistently determine the Yukawa constant,

$$h = \frac{\hat{m}_q}{\hat{f}_\pi} \,, \tag{3.68}$$

as well as the meson mass in the UV,

$$\left(\frac{\mathrm{d}}{\mathrm{d}\phi}\Gamma(\phi)\big|_{H=0}\right)\Big|_{\phi=\hat{\phi}_0} \stackrel{!}{=} 0 \quad \wedge \quad \hat{\phi}_0 \neq 0 \tag{3.69}$$

$$\Rightarrow \quad m_{\Lambda_0}^2 = 16 N_\mathrm{c} h^2 \left(\frac{\mathrm{d}}{\mathrm{d}\chi} L_0(\Lambda_0, \chi)\right)\Big|_{\chi=\hat{m}_q^2} \,. \tag{3.70}$$

We remark here that the value for the ground state is implicitly set by the specified quark mass and the Yukawa constant. For the three-dimensional and covariant regularization scheme, we can also give a more concrete representation of the mass parameter:

$$m_{\Lambda_0}^{2\,(3\mathrm{d})} = \frac{N_\mathrm{c}}{\pi^2} h^2 \int_0^\infty \mathrm{d}y \, \sqrt{y} \left(\frac{1}{\sqrt{y + \hat{m}_q^2}} - \frac{1}{\sqrt{y\left(1 + r_{\mathrm{poly}}^{\varphi}\left(\frac{y}{\Lambda_0^2}\right)\right)^2 + \hat{m}_q^2}} \right) , \tag{3.71}$$

$$m_{\Lambda_0}^{2\,(4\mathrm{d})} = \frac{N_\mathrm{c}}{2\pi^2} h^2 \int_0^\infty \mathrm{d}x \, x \left(\frac{1}{x + \hat{m}_q^2} - \frac{1}{x\left(1 + r_{\mathrm{poly}}^{\varphi}\left(\frac{x}{\Lambda_0^2}\right)\right)^2 + \hat{m}_q^2} \right) . \tag{3.72}$$

We would like to emphasize that we did not need to use any information about the scale dependence of the quark mass but only its infrared value. In addition, since our calculation is based on the full effective average action, the necessity to specify a certain ansatz for the effective potential does not emerge. Once the coupling parameters are fixed, the information about all phenomena of the quark-meson model is encoded in the initial condition Γ_{Λ_0} and the loop function L. How well this information is encoded, depends on the approximation scheme that has been used.

Guided by the Refs. [88, 231, 386], we fix our couplings according to

$$\Lambda_0 = 1\,\mathrm{GeV} \,, \qquad \hat{m}_q = 300\,\mathrm{MeV} \,, \qquad \hat{f}_\pi = 88\,\mathrm{MeV} \,. \tag{3.73}$$

As a result, the coupling parameters assume the following values:

$$h \approx 3.41 \,, \qquad m_{\Lambda_0}^{2\,(3\mathrm{d})} \approx 4.99\ \Lambda_0^2 \,, \qquad m_{\Lambda_0}^{2\,(4\mathrm{d})} \approx 4.01\ \Lambda_0^2 \,. \tag{3.74}$$

Notice that, for both regularization schemes, the meson mass parameter is larger than the UV cutoff scale Λ_0. We would like to stress that this situation does not conflict with RG consistency and is therefore not problematic for the functional renormalization group. The coupling constants of the ultraviolet action are nothing but mathematical parameters that are fixed to ensure that our theory produces physically meaningful results in the infrared. In particular, the UV values of the running couplings vary with the regularization scheme as demonstrated above. From a practical standpoint, a large UV mass for the mesons can actually be advantageous since it favors the approximation of neglecting terms $\sim \partial_\mu \phi$ in the action Γ_{Λ_0}. It generally holds that the larger the mass of a particle, the more suppressed the dynamics of that particle becomes. Therefore, the larger the UV values for the meson mass parameter, the better the initial condition (3.34) as employed in the context of homogeneous background fields.

We would like to highlight once more that the quark-meson model as defined by Eq. (3.1) renders the fermions massless in the UV. Nevertheless, the scale fixing above has been performed such that there exists a critical RG scale $k_{\text{crit}} < \Lambda_0$ below which the quarks obtain a finite constituent mass. This mass is dynamically generated along the RG flow from high to low scales by the Yukawa interaction between the quarks and the mesons. The constituent mass enters the quark propagator and breaks chiral symmetry at the ground state of the physical system. It should be emphasized, however, that the system as a whole and for $H = 0$ still has chiral symmetry, i.e., the dynamically generated mass contribution in the RG flow is not associated with explicit chiral symmetry breaking. In contrast to this, a finite value for H leads to a non-trivial ground state in field space at all RG scales and therefore implements explicit symmetry breaking. To be more specific, the parameter induces a breakdown of $O(4)$ symmetry among the meson degrees of freedom. Moreover, the parameter H does not directly affect any loop calculations since the symmetry-breaking term is only linear in the scalar field by construction. So far, the constant H has been treated as an external parameter, which we have set to zero in order to fix the Yukawa coupling as well as the meson mass parameter. With these fixed couplings at hand, let us now turn to fixing the symmetry-breaking parameter. This parameter gets fixed such that we obtain a specific pole mass for the pions under vacuum conditions. At $T = \mu = 0$, the pole mass can either be read off from the Dirac-delta peak of the spectral function or directly from the zero of the analytically continued inverse propagator,

$$\tilde{\Gamma}^{(2)}_{\pi}(\mathrm{i}\hat{m}_{\text{pole},\pi}, \vec{0}) = 0 \,. \tag{3.75}$$

For pion pole mass, we choose the value [88]

$$\hat{m}_{\text{pole},\pi} = 138\,\text{MeV} \tag{3.76}$$

and thus obtain[12]

$$H^{(3\text{d})} = 5\ 699\ 313\,\text{MeV}^3, \qquad H^{(4\text{d})} = 5\ 004\ 334\,\text{MeV}^3 \,. \tag{3.77}$$

We would like to point out the fact that a finite value for H results in a vacuum quark mass that is greater compared to the constituent mass we have fixed at $H = 0$. Recall that the symmetry-breaking term in the meson sector is related to a mass term in the quark sector, see Eq. (3.19). Therefore, choosing $H > 0$ leads to a finite current mass for the quarks which increases the corresponding constituent mass. From a geometric point of view, the symmetry-breaking parameter induces a tilt of the effective potential along the σ of field space such that the ground state gets

[12] In accordance with the action of the quark-meson model, the values for the symmetry-breaking parameter have been worked out with the initial value $Z_{\Lambda_0} = 1$ for the mesonic wavefunction renormalization in the ansatz (3.33). In the case of $Z_{\Lambda_0} \to 0$, which reproduces an NJL model, we find $H^{(3\text{d})} = 3\ 882\ 400\,\text{MeV}^3$ and $H^{(4\text{d})} = 3\ 206\ 960\,\text{MeV}^3$.

shifted to higher values. As a result, the quark mass increases accordingly, see Eq. (3.22). To be more concrete, we obtain the following constituent quark masses:

$$T=\mu=0: \qquad m_q^{(3\mathrm{d})} \approx 322.05\,\mathrm{MeV}\,, \qquad m_q^{(4\mathrm{d})} \approx 320.70\,\mathrm{MeV}\,. \tag{3.78}$$

These values are undeniably close to each other and not too far off from the physical value which is of the order of 350 MeV for the up and down quarks [1, 339]. With a larger quark mass, the pion decay constant increases as well:

$$T=\mu=0: \qquad f_\pi^{(3\mathrm{d})} \approx 94.47\,\mathrm{MeV}\,, \qquad f_\pi^{(4\mathrm{d})} \approx 94.07\,\mathrm{MeV}\,. \tag{3.79}$$

For comparison, the experimental value reads $f_\pi \approx 93\,\mathrm{MeV}$ [118, 385], meaning that our results for the pion decay constant are realistic.

3.2.2 Curvature masses

Curvature masses are crucial for an understanding of the thermodynamic and dynamical properties of low-energy QCD. As an example, they allow us to access the (pseudo-)critical external parameters for the chiral phase transition and therefore provide direct insights into the structure of the QCD phase diagram. In the following, we investigate the curvature masses of the sigma meson as well as the pions at finite temperature and finite chemical potential. In particular, we aim at a comparison of the spatial and covariant regularization schemes based on the meson curvature masses. To this end, we will illustrate the results obtained in these different schemes and compare their predictions.

As already discussed earlier, the meson curvature masses can be obtained from the quantum effective action by a projection which includes a second-order derivative and an evaluation at the ground state of the system. Using our result for the effective potential, see Eq. (3.64), we obtain

$$\begin{aligned}\begin{pmatrix} m_\sigma^2(T,\mu) & \vec{0}^\intercal \\ \vec{0} & m_\pi^2(T,\mu)\,\mathbb{1}_{3\times3}\end{pmatrix} &= \left(\frac{\mathrm{d}}{\mathrm{d}\phi^\intercal}\frac{\mathrm{d}}{\mathrm{d}\phi}\frac{\Gamma(\phi)\big|_{T,\mu}}{V_4}\right)\Bigg|_{\phi=\phi_0} \\ &= m_{\Lambda_0}^2\,\mathbb{1}_{4\times4} - 8N_\mathrm{c}\,h^2\int_{\vec{p}}\frac{1}{\beta}\sum_{n\in\mathbb{Z}}\frac{\zeta_k^2(\nu_n(\beta)+\mathrm{i}\mu,\vec{p})\,\mathbb{1}_{4\times4} - m_q^2(T,\mu)\,\eta}{\left(\zeta_k^2(\nu_n(\beta)+\mathrm{i}\mu,\vec{p})+m_q^2(T,\mu)\right)^2}\Bigg|_{k=\Lambda_0}^{k=0}\,,\end{aligned} \tag{3.80}$$

where η denotes the Lorentz matrix in meson field space. Again, this matrix structure is not used to describe the spacetime metric here but naturally arises in field space once we consider a finite quark mass, see our discussion in Sec. 2.4.5. We emphasize that the correct zero-temperature curvature masses cannot be obtained from this expression by simply replacing the Matsubara sum with a corresponding integral, see Section 2.4 for details. Instead, we need to take the zero-temperature limit after performing the Matsubara summation to reproduce the zero-temperature scenario. For a collection of potentially helpful relations regarding the zero-temperature limit, we refer to Appendix C.4.

For optimal numerical performance regarding the computation of loop integrals, it is crucial to evaluate the expression for the loop diagram analytically as far as possible. More specifically, we shall always perform the summation of Matsubara frequencies analytically. Nevertheless, we would like to stress that covariant momentum-dependent regulator functions make it notoriously difficult to evaluate loop integrals at finite external parameters. We therefore bring our analytical

expressions for the Matsubara sum into a simplified form which then allows for further numerical evaluation without problems. This will be demonstrated explicitly in the following.

We consider a function f which is analytic on $\mathbb{C} \setminus P$, where P denotes the set of poles of f. We further assume that this function has an asymptotic behavior in accordance with Eq. (2.178). By making use of the Matsubara formalism, the summation over Matsubara frequencies can then be cast into the general form of

$$\frac{1}{\beta}\sum_{n\in\mathbb{Z}} f(\nu_n(\beta)+\mathrm{i}\mu) = -\mathrm{i}\sum_{a\in P}\mathrm{Res}\left(n_\mathrm{F}(\beta(-\mathrm{i}\cdot-\mu))\ f, a\right) . \tag{3.81}$$

In order to apply this strategy to the computation of loop diagrams, we identify f as the integrand of the corresponding loop integral where any further dependences on, e.g., spatial momenta or the RG scale k have been suppressed for simplicity. In particular, we are now going to use this formula for the calculation of one-loop contributions to the meson curvature masses as appearing in Eq. (3.80). Since we employed a polynomial regulator function, the denominator of $f(x)$ is a polynomial in x with real-valued coefficients. Furthermore, Lorentz symmetry in the vacuum limit implies that f is a function of x^2. As a consequence, the denominator of f has an even number of different polynomial roots a. Specifically, if a is a root of that polynomial, then $-a$ is also a root. For convenience, we choose to order the set of roots according to

$$\forall i \in \{1,\dots,l\}: \quad a_{2i} = -a_{2i-1} , \tag{3.82}$$

where $l \in \mathbb{N}$ is used to parameterize the total number of different roots. The number l depends on the regularization scheme and, in the case of covariant regularization, also depends on the degree N used for the polynomial shape function, see Eq. (3.56). With all these preliminary considerations, the integrand of the loop integral in Eq. (3.80) can be written as

$$f(x) = \frac{h(x^2)}{\prod_{i=1}^{2l}(x-a_i)^2} = \frac{h(x^2)}{\prod_{i=1}^{l}\left(x^2-a_{2i-1}^2\right)^2} . \tag{3.83}$$

The analytic function h here simply denotes the numerator of f and does not need to be specified any further for our purposes. To evaluate the Matsubara sum above, we need to calculate the residues of f weighted with a Fermi-Dirac distribution. Such a residue at any second-order pole is given by

$$\begin{aligned}\mathrm{Res}\left(n_\mathrm{F}(\beta(-\mathrm{i}\cdot-\mu))\ f, a_j\right) = &-\mathrm{i}\beta n_\mathrm{F}'\left(\beta(-\mathrm{i}a_j-\mu)\right)\ h(a_j^2)\, A_j \\ &+ n_\mathrm{F}\left(\beta(-\mathrm{i}a_j-\mu)\right)\left[2a_j^2\, h'(a_j^2) - h(a_j^2)\, B_j\right]\frac{A_j}{a_j} ,\end{aligned} \tag{3.84}$$

where we have used the abbreviations

$$A_j = \left(4a_j^2\prod_{i=1,i\neq g(j)}^{l}\left(a_j^2-a_{2i-1}^2\right)^2\right)^{-1} , \tag{3.85}$$

$$B_j = 1 + 4a_j^2\sum_{i=1,i\neq g(j)}^{l}\frac{1}{a_j^2-a_{2i-1}^2} , \tag{3.86}$$

$$g(n) = \left\lfloor\frac{n+1}{2}\right\rfloor . \tag{3.87}$$

Notice that A_j, B_j and $h(a_j^2)$ remain invariant under $a_j \to -a_j$. Making use of this symmetry principle, the Matsubara sum takes the form

$$\begin{aligned}
&\frac{1}{\beta}\sum_{n\in\mathbb{Z}} f(\nu_n(\beta)+\mathrm{i}\mu) = -\mathrm{i}\sum_{j=1}^{2l}\mathrm{Res}\left(n_\mathrm{F}(\beta(-\mathrm{i}\cdot-\mu))\ f, a_j\right)\\
&= \beta\sum_{j=1}^{l}\frac{\sum_\pm \mathrm{sech}^2\left(\frac{\beta}{2}(-\mathrm{i}a_{2j-1}\pm\mu)\right)}{4} h(a_{2j-1}^2)\, A_{2j-1}\\
&+\mathrm{i}\sum_{j=1}^{l}\frac{\sum_\pm \tanh\left(\frac{\beta}{2}(-\mathrm{i}a_{2j-1}\pm\mu)\right)}{2}\left[2a_{2j-1}^2\, h'(a_{2j-1}^2) - h(a_{2j-1}^2)\, B_{2j-1}\right]\frac{A_{2j-1}}{a_{2j-1}}\,.
\end{aligned} \tag{3.88}$$

This exact expression for the Matsubara sum enormously simplifies any further evaluation of the loop integral for the meson curvature masses. We emphasize that our formula is quite general and in particular applies to the cases of spatial as well as covariant regularization. In any spatial regularization scheme, we find

$$l^{(3\mathrm{d})} = 1\,, \qquad a_1 = \mathrm{i}|a_1|\,, \qquad a_2 = -a_1 = a_1^*\,, \qquad B_1 = 1\,, \qquad A_1 = \frac{1}{4a_1^2}\,, \tag{3.89}$$

which then allows for even further simplifications.

For convenience, we define the quantity

$$\begin{aligned}
I_0(m)\big|_{T,\mu} &= \frac{1}{h^2}\left(\frac{\mathrm{d}}{\mathrm{d}\phi_\intercal}\frac{\mathrm{d}}{\mathrm{d}\phi}L_0(\Lambda_0, h^2\phi^2)\big|_{T,\mu}\right)\Big|_{\sigma=\frac{m}{h},\vec{\pi}=0}\\
&= \int_{\vec{p}}\frac{1}{\beta}\sum_{n\in\mathbb{Z}}\frac{\zeta_k^2(\nu_n(\beta)+\mathrm{i}\mu,\vec{p})\,\mathbb{1}_{4\times4} - m^2\,\eta}{\left(\zeta_k^2(\nu_n(\beta)+\mathrm{i}\mu,\vec{p})+m^2\right)^2}\Bigg|_{k=\Lambda_0}^{k=0}\,,
\end{aligned} \tag{3.90}$$

which simply describes the one-loop contribution in Eq. (3.80). An analysis of this integral eventually allows us to give a more concrete presentation of results for the curvature masses. Since expressions for the analytically performed Matsubara sum in the covariant scheme are too lengthy to provide additional insight into the structure of the integral I_0, we restrict our presentation of analytical results to the case of spatial regularization. Nevertheless, we emphasize that the minuend of the loop integral, i.e., the term evaluated at $k=0$, is identical in all regularization schemes that satisfy the infrared condition (2.70). Using spatial regulators, we Matsubara sum evaluates to

$$\begin{aligned}
I_0^{(3\mathrm{d})}(m)\big|_{T,\mu} = \frac{1}{16\pi^2}\int_0^\infty \mathrm{d}p\ p^2\Bigg[&\frac{2E_k^2(p)\,\mathbb{1}_{4\times4} - m^2(\mathbb{1}_{4\times4}+\eta)}{E_k^3(p)}\sum_\pm\tanh\left(\frac{E_k(p)\pm\mu}{2T}\right)\\
&+\frac{m^2(\mathbb{1}_{4\times4}+\eta)}{E_k^2(p)}\frac{1}{2T}\sum_\pm\mathrm{sech}^2\left(\frac{E_k(p)\pm\mu}{2T}\right)\Bigg]\Bigg|_{k=\Lambda_0}^{k=0}
\end{aligned} \tag{3.91}$$

with

$$E_k^2(p) = p^2\left(1+r_{\mathrm{poly}}^{\varphi}\left(\frac{p^2}{k^2}\right)\right)^2 + m^2 \tag{3.92}$$

denoting the regularized energy of the quarks. We remark here, that this expression for the loop integral I_0 is nothing but the finite-temperature version of the loop contribution to the curvature masses in Eq. (2.211) for the case of using a polynomial shape function.

We now turn to the discussion of particle masses at finite temperature and zero chemical potential. As illustrated in Fig. 3.1, the temperature dependence of the meson curvature masses and the quark mass has been investigated for both $H = 0$ and the case of explicit symmetry breaking. To begin, we focus on the results obtained from the quark-meson model in the absence of explicit symmetry breaking. Recall that we have tuned our model parameters in this scenario such that the dynamics of the system is governed by a finite ground state at low temperatures. Consequently, the pions are massless in this regime, whereas the sigma meson and the quarks acquire finite masses. As temperature increases, thermal fluctuations then drive the ground state continuously towards smaller and smaller values until it vanishes at the critical temperature T_c. From a phenomenological point of view, this temperature then marks the chiral phase transition along the temperature axis of the phase diagram. The continuous behavior of the ground state allows us to identify this transition as a second-order phase transition. Naturally, the quark mass can then serve as an order parameter to distinguish between the two separate phases of matter. Furthermore, we observe that all three particle masses vanish identically at $T = T_c$. Beyond the critical temperature, the ground state remains zero, which leads to massless quarks in this phase. In contrast to this, the meson curvature masses are finite and degenerate. Since the mesons are considered composites of fermions, the former must in fact become degenerate once the quark mass has vanished. With no matter particles left that could render the mesons massive for $T > T_c$, their finite curvature masses in this regime are purely temperature-induced.

In a system with explicitly broken symmetry, i.e., for $H > 0$, the pions acquire a finite mass even at low temperatures. This behavior can be understood by examining the effective potential. Geometrically, the linear symmetry-breaking term leads to a deformation of the otherwise symmetric effective potential, often referred to as a tilt along the σ-direction. This tilt not only leads to a unique ground state but also renders the curvatures at this point positive in all directions of field space. Accordingly, the curvature masses of both mesons are finite for $H > 0$. As before, increasing temperatures drive the ground state continuously towards lower and lower values. In contrast to the chiral limit, however, the explicit symmetry breaking prevents the ground state from actually reaching zero. This is evident from the temperature dependence of the quark mass in Fig. 3.1 (right panels), which exhibits a sigmoid shape. Since the quark mass is analytic in T and remains finite, a canonical phase transition does not occur. Instead, the system undergoes a smooth transition, a so-called crossover, between the low-temperature phase, which is governed by a finite ground state, and the high-temperature phase, in which the ground state has become sufficiently small such that the system gets dominated by thermal fluctuations. The pseudo-critical temperature T_{pc}, which quantifies this crossover, is not uniquely defined but we shall come back to this further below. At high temperatures, as the ground state diminishes, the curvature masses of the mesons become quasi-degenerate and approach the same asymptotic limit. In the intermediate regime, where the effects of the finite ground state and thermal fluctuations compete, we observe that the curvature of the sigma meson develops a finite minimum whereas the pion masses continuously grow.

Overall, we observe that our predictions for the vacuum value of the sigma curvature mass lie between 875 MeV and 974 MeV, see Table 3.1 for a more detailed overview. Values of this order of magnitude are nothing new for NJL-type models, see, e.g., Ref. [387], although these values are relatively far away from the resonance at 500 MeV associated with the scalar meson [339]. In order to ensure an outcome that is more compatible with experiment, one could extend the ansatz (3.34) to include a term $\sim \lambda(\phi^\intercal\phi)^2$ that is quartic in the fields. This would provide us with an additional parameter λ, allowing us to tune the value of the sigma mass in the vacuum limit, see, e.g., Ref. [382]. Alternatively, using regulator functions that implement less smooth UV regularization is also expected to lower the vacuum values of the meson curvature masses.

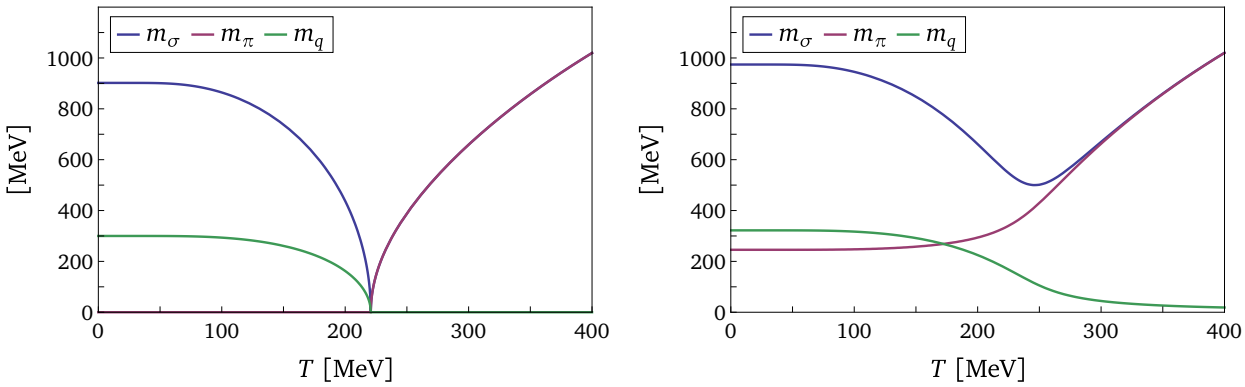

(a) Particle masses as obtained from the quark-meson model using the spatial regularization scheme.

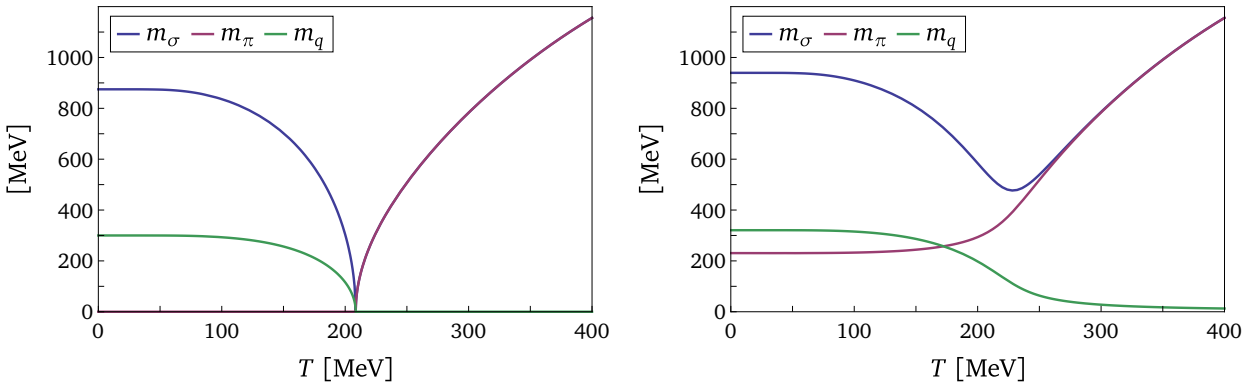

(b) Particle masses as obtained from the quark-meson model using the covariant regularization scheme.

Figure 3.1: We illustrate the temperature dependence of meson curvature masses and the quark mass at zero quark chemical potential. Using different regularization schemes, the particle masses are shown for the symmetric case, $H = 0$, (left panels) and for explicit symmetry breaking, $H > 0$, (right panels). The phase transition indicated by the minimum of m_σ is a second-order phase transition in the chiral limit and a crossover in the physical case.

For example, one may consider degrees $N > 2$ for the polynomial shape function in Eq. (3.56) to achieve this. A thorough investigation of this kind is, however, beyond the scope of this work. In any case, we would like to highlight that the curvature mass is in fact generally different from the pole mass. Recall that we have fixed the pion pole mass in the vacuum limit to 138 MeV for each scheme. Nevertheless, the corresponding values of the pion curvature mass are off by at least 93 MeV, see again Table 3.1.

A comparison of the predictions from the quark-meson model based on Fig. 3.1 shows that the spatial and covariant regularization schemes lead to qualitatively very similar behaviors of the individual particle masses with respect to temperature. We therefore now focus on the quantitative differences as observed at finite temperature and zero chemical potential. In particular, we address the critical temperature T_c associated with the chiral phase transition in the absence of explicit symmetry breaking. If the quark mass is chosen to be the order parameter of the phase transition, the critical temperature denotes the smallest temperature at which quark mass vanishes identically. Equivalently, we could determine this temperature based on one of the meson curvature masses. At the level of the effective action, the critical temperature for a second-order phase transition corresponds to the point where the one-loop effective potential becomes convex, see Fig. 3.2 (left

Scheme	m_σ [MeV]	m_π [MeV]	T_c [MeV]	μ_c [MeV]
spatial	902	0	221	398
covariant	875	0	209	390

(a) Condering the symmetric case, i.e., $H = 0$.

Scheme	m_σ [MeV]	m_π [MeV]	T_{pc} [MeV]	μ_{pc} [MeV]
spatial	974	246	246	434
covariant	940	231	229	422

(b) Considering the case of explicit symmetry breaking, $H > 0$.

Table 3.1: Rounded values of the meson curvature masses at $T = \mu = 0$ and the (pseudo-)critical external parameters as obtained from the quark-meson model when using the spatial and covariant regularization schemes.

panel). Put differently, the critical temperature T_c is characterized by a vanishing origin mass:

$$\left(\frac{\mathrm{d}}{\mathrm{d}\phi^\intercal}\frac{\mathrm{d}}{\mathrm{d}\phi}\Gamma(\phi)\Big|_{T=T_c}\right)\Big|_{\phi=0} = 0 \tag{3.93}$$

$$\Rightarrow \quad m_{\Lambda_0}^2 - 16N_c h^2\left(\frac{\mathrm{d}}{\mathrm{d}\chi}L_0(\Lambda_0,\chi)\Big|_{T=T_c}\right)\Big|_{\chi=0} = 0\,. \tag{3.94}$$

Using the spatial and covariant regularization schemes, we obtain a critical temperature of approximately 221 MeV and 209 MeV, respectively. Compared to the result of $T_c \approx 132$ MeV from lattice QCD [340], our results for the critical temperature are generally too high. Several ways to approach this issue are possible. For example, one could lift the restriction of only considering loops with internal fermionic lines and incorporate bosonic fluctuations. Bosonic loops naturally tend to make the effective potential convex and thus lower the value of the critical temperature. A more pragmatic solution would be to introduce an additional parameter to the theory by extending our ansatz for the effective action at the UV scale Λ_0 and simply use it to tune the critical temperature towards a realistic value. In this work, however, we are rather interested in the influence of the regularization prescription on observables. We therefore keep our truncation scheme as well as the initial condition for the Wetterich equation unchanged and instead investigate the dependence of the critical temperature on the regularization scheme. More specifically, we calculate the critical temperature using the polynomial regulator shape function (3.56) for different choices of the coefficients c_n, different degrees N, and different values of the initial scale Λ_0. We have assembled our results into the Table 3.2.

Our data shows that the covariant scheme systematically leads to lower values for the critical temperature than the spatial scheme. Additionally, we observe a general decrease in the critical temperature as the degree N increases. This makes it apparent that observables are indeed sensitive to how smoothly momenta get cut off from the loop by the regulator. Specifically, the sharper the cutoff becomes, the lower the value for the critical temperature turns out to be. The data further indicates that the drop in temperature tends to become less for larger degrees N. This behavior appears because the regulator gradually converges towards a limiting form as N increases, leading to less pronounced changes in the regularization scheme. In particular, the polynomial

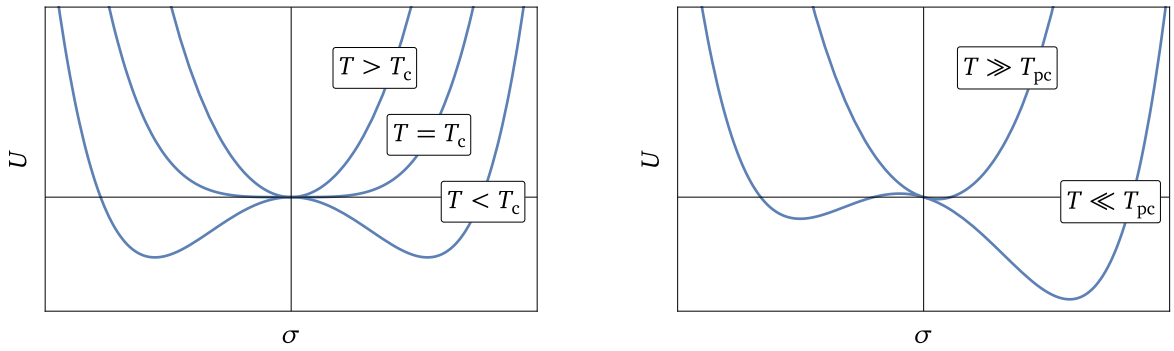

Figure 3.2: Temperature-dependent behavior of the effective potential as a function of the field variable σ in the case of $H = 0$ (left panel) as well as for explicit symmetry breaking, i.e., $H > 0$, (right panel). For the symmetric system, the critical temperature T_c refers to the temperature of the second-order phase transition. In the case of explicit symmetry breaking, one can define a pseudo-critical temperature T_{pc} indicating a crossover.

regulator approaches the exponential regulator for $c_n = 1/n!$ and converges towards a sharp regulator for $c_n = 1$. Furthermore, our results demonstrate that decreasing the initial UV scale Λ_0 also lowers the critical temperature. However, lowering Λ_0 amplifies regularization artifacts in the presence of external parameters and hence renders the results less reliable if the calculation is not RG-consistent. Our analysis makes clear that the critical temperature can in principle be tuned by suitably adjusting the polynomial regularization scheme. Nevertheless, we adhere to our original choices of $c_n = 1/n!$, $N = 2$, and $\Lambda_0 = 1\,\text{GeV}$ to ensure that loop integrals can be carried out in a covariant regularization without complications.

In contrast to the critical temperature T_c, the pseudo-critical temperature T_{pc} associated with the crossover transition is not uniquely defined. Various definitions exist, as illustrated in, e.g., Ref. [388]. Nevertheless, all consistent definitions of the pseudo-critical temperature should reduce to Eq. (3.93) in the chiral limit. Following Refs. [389, 390], we use the curvature mass of the sigma meson as an indicator to distinguish between the different phases of the quark-meson model. Specifically, we define

$$T_{pc} := \arg\max_{T>0}\left(\chi_\sigma(T)\right) = \arg\min_{T>0}\left(m_\sigma^2(T)\right)\,, \tag{3.95}$$

where $\chi_\sigma = (m_\sigma^2)^{-1}$ denotes the static susceptibility for the radial mode in field space. Our results, summarized in Table 3.1, again show that the covariant regularization scheme yields a smaller pseudo-critical temperature than the corresponding spatial scheme. Finally, we would like to remark that our reasoning regarding critical points is not limited to temperature-induced transitions. In fact, the Eqs. (3.93) and (3.95) can be adapted straightforwardly to define the (pseudo-)critical chemical potential at zero temperature. For an analysis of the behavior of the particle masses with respect to the chemical potential, we refer to Fig. 3.4 and the corresponding discussion further below.

In accordance with our discussion of RG consistency, regularization artifacts at zero chemical potential are suppressed as long as the temperatures under consideration remain sufficiently small compared to the reference scale. To make this comparison more concrete, it is useful to examine the momentum scale associated with temperature. Since the dominant contribution to the finite-temperature propagator stems from the smallest Matsubara frequency, it is reasonable to compare Λ_0 to $\nu_0(\beta) = \pi T$. Consequently, the value of Λ_0 chosen in Eq. (3.73) implies that calculations of correlation functions are generally RG-consistent for temperatures $T \lesssim 300\,\text{MeV}$. In addition, for a

Λ_0 [MeV]	Scheme	$N=2$	$N=3$	$N=4$
10^3	spatial	221	215	213
	covariant	209	202	200
600	spatial	194	188	186
	covariant	173	163	160

(a) Use of the polynomial regulator function with coefficients $c_n = 1/n!$.

Λ_0 [MeV]	Scheme	$N=2$	$N=3$	$N=4$
10^3	spatial	214	204	200
	covariant	199	186	179
600	spatial	188	179	175
	covariant	163	146	137

(b) Use of the polynomial regulator function with coefficients $c_n = 1$.

Table 3.2: Rounded values of the critical temperature T_c [MeV] for the chiral phase transition of the quark-meson model at $H = 0$ and $\mu = 0$ as obtained when using a spatial or covariant regularization scheme. In our numerical calculations, we have implemented the polynomial regulator shape function for different coefficients c_n and degrees N.

polynomial regulator with degree $N = 2$, the suppression of high-momentum modes is particularly smooth, which suggests that regularization artifacts should remain small even at somewhat higher temperatures. To quantitatively evaluate potential regularization artifacts, we have analyzed the impact of an RG-consistent calculation on the temperature-dependent behavior of particle masses, as shown in Fig. 3.3. The results for the meson curvature masses as calculated in the spatial regularization scheme in fact confirm our reasoning. Here, differences between the "naive" and the RG-consistent calculations are not visible for $T < 250\,\mathrm{MeV}$ and remain negligible for $T \lesssim 300\,\mathrm{MeV}$. In particular, RG consistency has no noticeable effect on the (pseudo-)critical temperature here. However, regularization artifacts become more severe at higher temperatures. For example, we observe a difference between the calculations of $\Delta m^{(3\mathrm{d})} \approx 120\,\mathrm{MeV}$ at $T = 400\,\mathrm{MeV}$. In the covariant scheme, regularization artifacts become already visible at $T \gtrsim 180\,\mathrm{MeV}$. Notably, considering RG consistency has the effect of raising the (pseudo-)critical temperature as computed within this scheme. More specifically, in the absence of regularization scheme artifacts, we obtain $T_c^{(4\mathrm{d})} \approx 215\,\mathrm{MeV}$ and $T_{pc}^{(4\mathrm{d})} \approx 237\,\mathrm{MeV}$. This difference in sensitivity to RG consistency stems from the different treatment of temperature by the schemes. Concretely, Λ_0 directly sets a scale for temperature in the covariant scheme. Spatial schemes, however, leave the time-like modes of the loop integral unaffected such that there is no direct coupling between temperature and the reference scale of the RG flow. As a result, the influence of regularization on the temperature-dependent behavior is weaker in the spatial schemes. Despite these differences, our results demonstrate the importance of accounting for RG consistency in studies of curvature masses at high temperatures, regardless of the chosen regularization scheme.

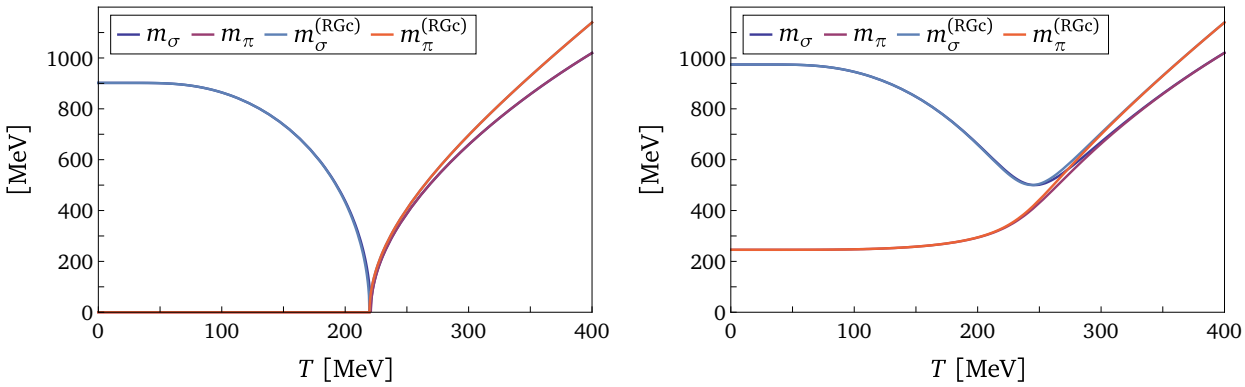

(a) Particle masses as obtained from the quark-meson model within the spatial regularization scheme.

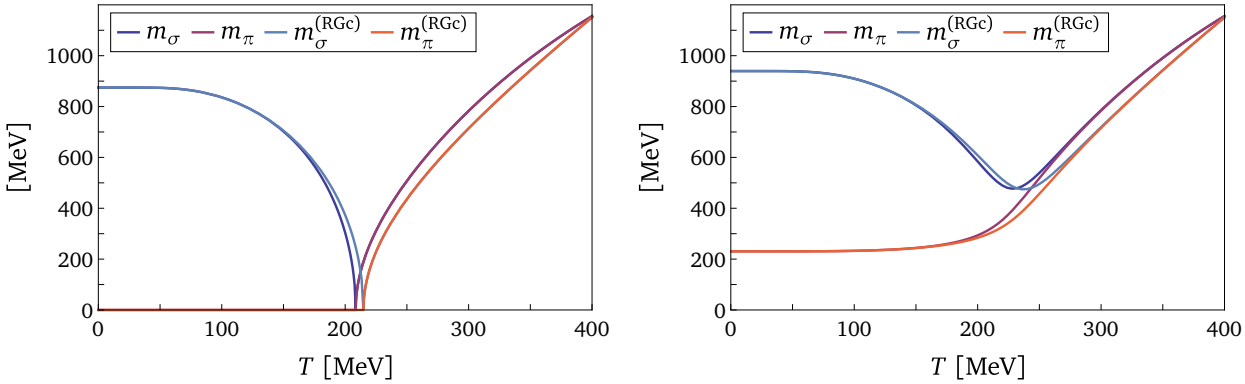

(b) Particle masses as obtained from the quark-meson model within the covariant regularization scheme.

Figure 3.3: We illustrate the impact of RG consistency on the temperature dependence of meson curvature masses at zero chemical potential as obtained from the quark-meson model. The particle masses are shown in the case of intact rotation symmetry, $H = 0$, (left panels) and for explicit symmetry breaking, $H > 0$, (right panels). We observe that regularization scheme artifacts of the non-RG-consistent calculations become apparent for $T \gtrsim 180\,\mathrm{MeV}$ in the covariant scheme but remain absent until $T \approx 250\,\mathrm{MeV}$ in the spatial scheme.

Let us extend our discussion of RG consistency to the case of zero temperature and finite chemical potential. Under these circumstances, the infrared theory is in fact automatically RG-consistent for $\mu < \Lambda_0$. This shall be explained in the following. At zero temperature and finite chemical potential, the pole structure of the integrand allows the corresponding loop integral L_k to split into a vacuum contribution, which has no explicit μ-dependence,[13] and a matter part M_k, which carries all the information about the effects of a finite chemical potential. In addition, the system exhibits the Silver-Blaze property at zero temperature, meaning it does not show any dependence on the chemical potential unless μ exceeds the Silver-Blaze threshold. This behavior is expressed as

$$M_k(\mu, \chi) \propto \theta(\mu - \mu_{\mathrm{SB}}(k, \chi)) \,. \tag{3.96}$$

Furthermore, it follows from dimensional analysis that μ cannot have any effect on the loop integral unless it is at least of the order of k. As a consequence, the loop integral at zero temperature

[13] The vacuum contribution to the loop function can, however, gain an implicit dependence on the chemical potential by evaluating the function at the μ-dependent ground state.

takes the general form

$$L_k(\Lambda_0, h^2\phi^2)\big|_\mu = L_k(\Lambda_0, h^2\phi^2) - M_{k'}(\mu, h^2\phi^2)\Big|_{k'=\Lambda_0}^{k'=k} \overset{\mu<\Lambda_0}{=} L_k(\Lambda_0, h^2\phi^2) - M_k(\mu, h^2\phi^2)\,. \tag{3.97}$$

An RG-consistent UV completion for our ansatz for the effective average action to the scale $\Lambda > \Lambda_0$ then gives rise to the new functional

$$\begin{aligned}\frac{1}{V_4}\Gamma_k^{(\mathrm{RGc})}(\phi)\big|_\mu &= \frac{1}{V_4}\Gamma_{\Lambda_0}(\phi,\Lambda) - 8N_c\, L_k(\Lambda, h^2\phi^2)\big|_\mu \\ &= \frac{1}{V_4}\Gamma_{\Lambda_0}(\phi) - 8N_c\Big[L_k(\Lambda, h^2\phi^2)\big|_\mu - L_{\Lambda_0}(\Lambda, h^2\phi^2)\Big] \\ &= \frac{1}{V_4}\Gamma_{\Lambda_0}(\phi) - 8N_c\left[L_k(\Lambda_0, h^2\phi^2) - M_{k'}(\mu, h^2\phi^2)\Big|_{k'=\Lambda}^{k'=k}\right]. \end{aligned} \tag{3.98}$$

As we can see, this expression is equivalent to the original theory, provided that the chemical potential does not exceed the reference scale.

$$\forall k < \Lambda_0: \qquad \frac{1}{V_4}\Gamma_k^{(\mathrm{RGc})}(\phi)\big|_\mu \overset{\mu<\Lambda_0}{=} \frac{1}{V_4}\Gamma_k(\phi)\big|_\mu\,. \tag{3.99}$$

In other words, the infrared results for the system at zero temperature are already RG-consistent as long as we restrict our analysis to values of the chemical potential μ which are below the reference scale Λ_0. We stress that this property is by no means restricted to polynomial regulators.

From a physical standpoint, scalar and pseudoscalar mesons are the most relevant low-energy degrees of freedom for QCD at low densities. However, they become less important with increasing chemical potential. In particular, interaction channels associated with the formation of diquark condensates dominate the regime of low temperature but high density [88, 264, 386, 391]. Since our model does not include diquark degrees of freedom, its predictions at low temperatures can be physically reliable only up to intermediate densities.[14] To ensure reliability, we restrict our study of the quark-meson model to $\mu \leq 400\,\mathrm{MeV}$. This restriction then naturally renders our zero-temperature calculations RG-consistent.

This directly leads us to the investigation of particle masses at zero temperature and finite chemical potential. As mentioned earlier, consistent results for the meson curvature masses at zero temperature can be obtained from Eq. (3.80) by first performing the Matsubara sum and then taking the zero-temperature limit. For simplicity, we will again focus on the case of spatial regularization in our presentation of analytical results. Specifically, in the limit as the temperature tends to zero, the integral presented in Eq. (3.91) takes the form

$$\begin{aligned} I_0^{(3\mathrm{d})}(m)\big|_\mu &= \lim_{T\to 0} I_0^{(3\mathrm{d})}(m)\big|_{T,\mu} \\ &= \frac{1}{8\pi^2}\int_0^\infty \mathrm{d}p\; p^2\left[\frac{2E_k^2(p)\,\mathbb{1}_{4\times4} - m^2(\mathbb{1}_{4\times4}+\eta)}{E_k^3(p)}\;\theta\left(E_k(p)-\mu\right)\right. \\ &\qquad \left. + \frac{m^2(\mathbb{1}_{4\times4}+\eta)}{E_k^2(p)}\;\delta\left(E_k(p)-\mu\right)\right]\Bigg|_{k=\Lambda_0}^{k=0}. \end{aligned} \tag{3.100}$$

[14] Although the ground state is expected to be governed by diquark condensation in the regime of high densities, calculations that do not include condensation effects are reliable, provided that the chemical potential is much larger than the scale set by the diquark gap.

The Heaviside step function with the property of $\theta(x) = 1 - \theta(-x)$, see Appendix A.1 for details, allows us to decompose the integral into a vacuum part, which is independent of μ, and a matter part, which captures the entire information about the finite chemical potential. Additionally, we have

$$\forall k > 0, p \geq 0 : \qquad p\left(1 + r^{\varphi}_{\text{poly}}\left(\frac{p^2}{k^2}\right)\right) > k \,, \tag{3.101}$$

which implies that the matter part does not depend on the reference scale Λ_0 as long as $\mu \leq \Lambda_0$. In fact, we arrive at the same conclusion when implementing a covariant regulator. This means that the matter part of the loop integral is scheme-independent for all chemical potentials of interest. As a result, the integral can be written as

$$I_0^{(3\text{d})}(m)\big|_{\mu} = I_0^{(3\text{d})}(m) - M_0^{(2)}(\mu, m) \,, \tag{3.102}$$

where the chemical potential dependent part of the loop integral is given by

$$\begin{aligned} M_0^{(2)}(\mu, m) &= \frac{1}{h^2}\left(\frac{\mathrm{d}}{\mathrm{d}\phi^{\intercal}}\frac{\mathrm{d}}{\mathrm{d}\phi} M_0(\mu, h^2\phi^2)\right)\Big|_{\sigma=\frac{m}{h},\vec{\pi}=0} \\ &= \frac{1}{8\pi^2}\int_0^{\infty} \mathrm{d}p\; p^2 \left[\frac{(2p^2+m^2)\,\mathbb{1}_{4\times4} - m^2\,\eta}{\sqrt{p^2+m^2}^{\,3}}\;\theta\left(\mu - \sqrt{p^2+m^2}\right)\right. \\ &\qquad\qquad \left. - \frac{m^2(\mathbb{1}_{4\times4}+\eta)}{p^2+m^2}\;\delta\left(\sqrt{p^2+m^2}-\mu\right)\right] \\ &= \frac{\theta(\mu-m)}{8\pi^2}\left(\mathbb{1}_{4\times4}\,\mu\sqrt{\mu^2-m^2} - \left(2\mathbb{1}_{4\times4}+\eta\right)\mathrm{m}^2\,\mathrm{arsinh}\left(\frac{\sqrt{\mu^2-m^2}}{m}\right)\right) . \end{aligned} \tag{3.103}$$

Let us now turn to the discussion of particle masses at zero temperature and finite chemical potential. Specifically, we have investigated the dependence of the meson curvature masses and the quark mass on the chemical potential for both the symmetric case and the case of explicit symmetry breaking, as shown in Fig. 3.4. Since the polynomial regulator respects the analytic properties and preserves the Silver-Blaze symmetry of the system, the behavior of particle masses at zero temperature is governed by the Silver-Blaze property at low densities. In other words, all masses remain at their vacuum values as long as the chemical potential is not larger than the Silver-Blaze threshold, $\mu < \mu_{\text{SB}}$. In our truncation scheme, the value of μ_{SB} is always determined by the vacuum quark mass. For an analysis of the behavior of the system beyond this threshold, we start by concentrating on the results obtained from the quark-meson model for $H = 0$. As in the case of finite temperature and zero chemical potential, see Fig. 3.1 (left panels), we observe a continuous decrease of the sigma and the quark masses with increasing chemical potential until all particle masses vanish identically at the critical value μ_{c}. Phenomenologically speaking, this critical value marks the chiral phase transition along the chemical potential axis of the phase diagram. Furthermore, the continuous behavior of the ground state allows us to identify this transition as a second-order phase transition, consistent with our observations at finite temperature and zero chemical potential. Interestingly, this result is in contradiction with the generally accepted notion that the phase transition at low temperatures and intermediate densities is of first order, see, e.g., Refs. [392–395]. Nevertheless, other fRG approaches to the phase diagram of QCD have in fact been successful in reproducing a first-order transition, see, e.g., Refs. [88, 178, 232, 349, 382, 396]. Our findings therefore suggest that the nature of the phase transition at low temperatures is sensitive to the regularization of the vacuum loop and that our regularization prescription is simply

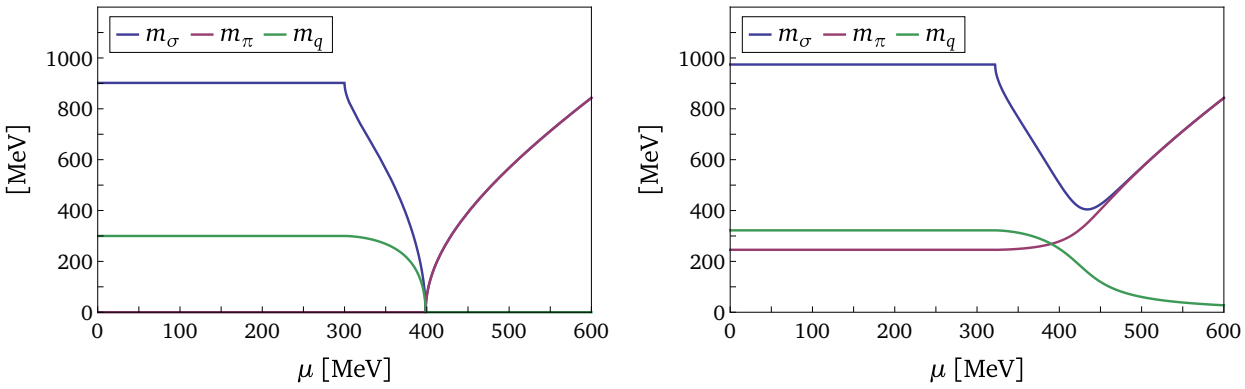

(a) Particle masses as obtained from the quark-meson model using the spatial regularization scheme.

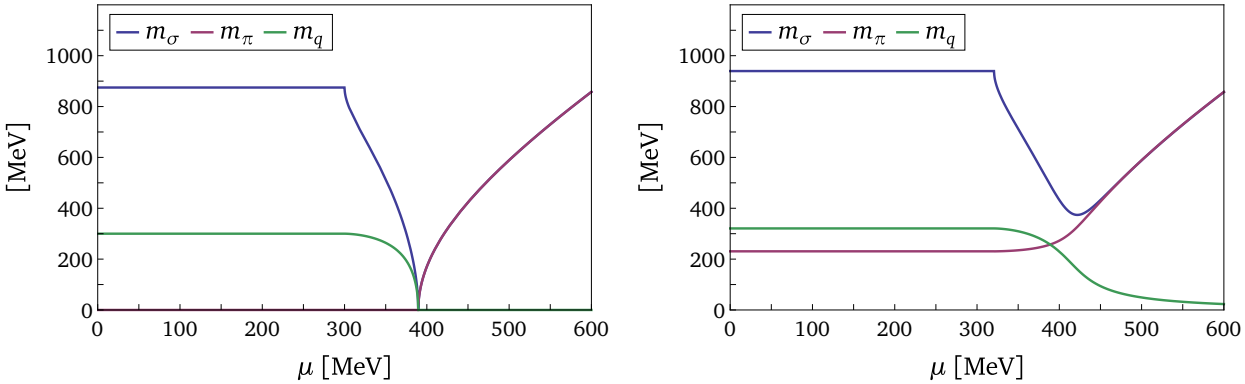

(b) Particle masses as obtained from the quark-meson model using the covariant regularization scheme.

Figure 3.4: We illustrate the chemical potential dependence of the meson curvature masses and the quark mass at zero temperature. Using different regularization schemes, the particle masses are shown for the symmetric case, $H = 0$, (left panels) and for explicit symmetry breaking, $H > 0$, (right panels). The phase transition indicated by the minimum of m_σ is a second-order phase transition in the symmetric case and a crossover in the physical case.

not suited to capture the correct low-energy behavior of QCD at those scales. Beyond the critical value μ_c, where the quark mass remains zero, the meson curvature masses become degenerate and scale with the chemical potential. When explicit symmetry breaking is included, i.e., for $H > 0$, the situation we encounter at zero temperature closely resembles the results shown in Fig. 3.1 (right panels). Once the chemical potential exceeds the Silver-Blaze threshold, the quark mass continuously decreases although never becoming zero. Between the low-density regime governed by the Silver-Blaze property and the high-density regime characterized by an almost vanishing ground state, the curvature mass of the sigma meson develops a global minimum. The value of the chemical potential associated with this minimum then defines the pseudo-critical value μ_{pc} in our setting and marks a crossover at this scale. Together with the calculations at finite temperature and zero chemical potential, our results falsely indicate that the transition line corresponding to the chiral phase transition is entirely a second-order phase transition line for $H = 0$ and a crossover line for $H > 0$. As a consequence, we will observe no critical endpoint in the phase diagram of our quark-meson model. Finally, we note that there are no qualitative differences between the results obtained from using the spatial and covariant regularization schemes. In particular, the nature of the phase transition is the same for both schemes. For a short overview of the quantitative differences, we again refer to Table 3.1. The data shows that the covariant scheme systematically predicts slightly lower values for the (pseudo-)critical chemical potential.

So far, we have compared quantities derived from the quark-meson model using a spatial and a covariant regularization scheme. However, these considerations do not allow us to directly compare the schemes themselves. Recall that the RG scale k corresponds to a spatial momentum $|\vec{p}|$ in spatial regularization schemes whereas it sets the scale for the full four-momentum in covariant schemes. Consequently, for any given finite value k, the amount of momenta contributing to a loop integral differs between the two schemes. The same reasoning applies to the initialization scale, meaning that the value of Λ_0 as chosen in Eq. (3.73) has different implications for the momentum space in each scheme. Moreover, since spatial regulators distinguish the time-like direction of momentum space, modes influenced by external parameters such as temperature and chemical potential are treated differently in spatial and covariant schemes. In order to allow for a meaningful comparison, we need to establish a point in parameter space at which both schemes agree identically. To this end, we adjust the initial condition of the effective average action in the covariant scheme such that both schemes yield the identical infrared physics at $T = \mu = 0$:

$$\frac{1}{V_4}\Gamma^{(4\mathrm{d})}_{\Lambda_0}(\phi) = \frac{1}{V_4}\Gamma^{(3\mathrm{d})}_{\Lambda_0}(\phi) - 8N_\mathrm{c}\left[L_0^{(3\mathrm{d})}(\Lambda_0, h^2\phi^2) - L_0^{(4\mathrm{d})}(\Lambda_0, h^2\phi^2)\right] . \tag{3.104}$$

This construction enables us to isolate the effects of covariant regularization in the presence of finite temperature or finite chemical potential. As mentioned before, the Silver-Blaze property governs the behavior of the zero-temperature theory at low densities. For our choice of the regulator shape function, it then follows that the predictions of this theory are identical in both regularization schemes for all chemical potentials of interest. Our comparison therefore focuses on the case of finite temperature and zero chemical potential in the following. One may be inclined to additionally consider RG consistency for our direct comparison of schemes. Recall, however, that RG consistency has the effect of eliminating scheme dependences from that part of the loop integral that depends on finite external parameters. Together with the initial condition (3.104), this means that an RG-consistent calculation would completely align the covariant scheme to the spatial scheme. As a result, this would leave us no basis for a meaningful comparison of schemes.

The temperature-dependent behavior of the meson curvature masses as obtained for spatial and covariant regularizations is shown in Fig. 3.5. While no differences are evident for $T \leq 150\,\mathrm{MeV}$, the impact of covariant regularization on the one-loop contributions to the curvature masses becomes apparent near the (pseudo-)critical temperature. Consistent with previous results, the covariant scheme systematically predicts lower transition temperatures. Beyond these critical points, the quantitative differences between the two schemes increase with temperature. Contrary to the common belief that the explicit breaking of Lorentz symmetry induced by spatial regulators is negligible at high values of external parameters, our findings suggest the opposite. For low temperatures, the space of momenta contributing to the loop integrals seems to be rather insensitive to the artificial breaking of Lorentz symmetry, hence leading to no visible differences in the particle masses obtained from the different schemes. However, at higher temperatures, the effect of thermal fluctuations being regularized in the covariant scheme whereas fully contributing at every RG scale in the spatial scheme becomes more and more prominent. Specifically, while the covariant scheme implies corrections to the (pseudo-)critical temperature of the order of 10 MeV, the meson curvature masses in the covariant scheme are $\Delta m \approx 125\,\mathrm{MeV}$ larger at $T = 400\,\mathrm{MeV}$ than those obtained in the spatial scheme. Based on these results, we conclude that the importance of covariant regularization increases with temperature, especially at temperatures above the chiral phase transition.

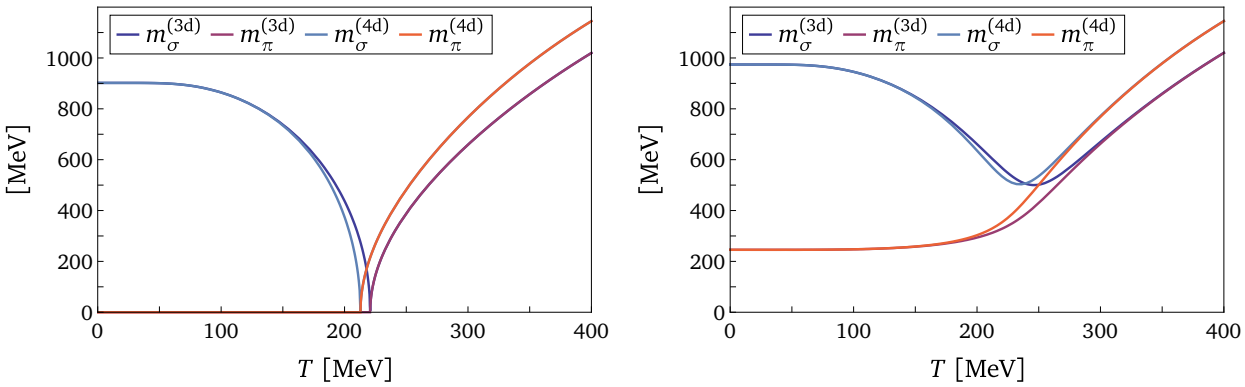

Figure 3.5: We directly compare the spatial and covariant regularization schemes based on the temperature dependence of meson curvature masses. These particle masses are shown for intact rotation symmetry, $H = 0$, (left panel) and for the case of explicit symmetry breaking, $H > 0$, (right panel). We observe that the covariant scheme leads to slightly lower transition temperatures as well as an altered high-temperature behavior. Concretely, we obtain $\Delta T_c \approx 8\,\text{MeV}$ and $\Delta T_{pc} \approx 12\,\text{MeV}$.

3.2.3 Spectral functions

Spectral functions are valuable tools in quantum field theory as they offer insights into dynamical as well as structural properties of quantum systems. Specifically, they provide access to physical observables such as pole masses, decay rates, lifetimes, and transport coefficients, thereby establishing a direct link between theory and experiment. In the context of low-energy QCD, spectral functions play an essential role in understanding the behavior of mesons and baryons, particularly under varying external conditions. In the following, we investigate the spectral functions of the sigma meson and the pions at finite external parameters. In particular, we take a first step towards a comparison of the spatial and covariant regularization schemes based on meson spectral functions.

For the computation of spectral functions, we first extract the momentum-dependent two-point correlator from the full quantum effective action. This can be done most conveniently by performing a $\mathcal{PF}$ expansion of the effective action to second order in the field degrees of freedom, see Eq. (3.41) for details. Using the ansatz given in Eq. (3.42) and choosing $Z_{\Lambda_0} = 1$, the two-point correlation function can be expressed as

$$\tilde{\Gamma}^{(2)}(Q)\big|_{T,\mu} = \left(Q^2 + m_{\Lambda_0}^2\right)\mathbb{1}_{4\times4} - 8N_c h^2\, \mathcal{I}_0\left(Q, m_q(T,\mu)\right)\big|_{T,\mu}\,, \tag{3.105}$$

where the corresponding momentum-dependent loop integral reads

$$\mathcal{I}_0\,(Q,m)\,\big|_{T,\mu} = \int_{\vec{p}} \frac{1}{\beta} \sum_{n\in\mathbb{Z}} \frac{\zeta_k^{\intercal}(\nu_n(\beta)+\mathrm{i}\mu,\vec{p})\;\zeta_k(\nu_n(\beta)+\mathrm{i}\mu+Q^0,\vec{p}+\vec{Q})\,\mathbb{1}_{4\times4} - m^2\,\eta}{\left(\zeta_k^2(\nu_n(\beta)+\mathrm{i}\mu,\vec{p})+m^2\right)\left(\zeta_k^2(\nu_n(\beta)+\mathrm{i}\mu+Q^0,\vec{p}+\vec{Q})+m^2\right)}\Bigg|_{k=\Lambda_0}^{k=0}\,. \tag{3.106}$$

Implementing a covariant regularization scheme makes it notoriously challenging to perform loop integrals analytically. Nevertheless, evaluating the Matsubara sum in closed form is crucial for ensuring numerical stability when analyzing correlation functions and spectral functions. To this end, we put forward a general formula that enables us to perform the Matsubara sum analytically and more easily.

For our approach to further evaluate the loop integral above, we can in fact follow our strategy from Section 3.2.2 regarding the general computation of screening masses. We observe that the integrand of the loop function (3.106) can be cast into the form

$$f(x,\vec{p},Q^0,\vec{Q}) = \frac{h(x,\vec{p},Q)}{\prod_{i=1}^{2l}(x-a_i(\vec{p}))\prod_{i=1}^{2l}\left(x+Q^0-a_i(\vec{p}+\vec{Q})\right)} , \tag{3.107}$$

where we have dropped any k-dependences for simplicity. Lorentz symmetry in the vacuum limit again implies that the complex poles a_i with respect to the time-like momentum variable x can be laid out with alternating signs, see Eq. (3.82). In addition, we note that the bosonic time-like momentum is not continuous at finite temperature but instead assumes only discrete values,

$$\forall N \in \mathbb{Z}: \qquad Q^0 \equiv Q_N^0 = \frac{2\pi}{\beta} N \ . \tag{3.108}$$

For convenience, however, we keep the external Matsubara index N suppressed in the following. This property implies that

$$n_{\mathrm{F}}\left(\beta(z+\mathrm{i}Q^0)\right) = n_{\mathrm{F}}(\beta z) \ , \tag{3.109}$$

meaning that temperature T and the time-like momentum Q^0 naturally decouple. Making use of Eq. (3.81) for the case of a multi-variate function and exploiting the symmetry properties of f, we arrive at the following expression for the Matsubara sum:

$$\int_{\vec{p}} \frac{1}{\beta} \sum_{n\in\mathbb{Z}} f(\nu_n(\beta)+\mathrm{i}\mu,\vec{p},Q^0,\vec{Q}) = \frac{\mathrm{i}}{2}\int_{\vec{p}} \sum_{j=1}^{l} \left(F_{2j-1}(\vec{p},Q)+F_{2j-1}(-\vec{p}-\vec{Q},Q)\right) \tag{3.110}$$

with

$$\begin{aligned} F_j(\vec{p},Q) = &\Big[\operatorname{Res}\left(f(\cdot,\vec{p},Q^0,\vec{Q}),a_j(\vec{p})\right)+\operatorname{Res}\left(f(\cdot,\vec{p},-Q^0,\vec{Q}),a_j(\vec{p})\right)\Big] \\ &\times \frac{1}{2}\sum_{\pm}\tanh\left(\frac{\beta}{2}\left(-\mathrm{i}a_j(\vec{p})\pm\mu\right)\right) . \end{aligned} \tag{3.111}$$

This formulation enormously simplifies the evaluation of the loop integral for the momentum-dependent two-point correlator within the covariant regularization scheme. Now, the process of performing the Matsubara sum essentially reduces to constructing the residue

$$\operatorname{Res}\left(f(\cdot,\vec{p},Q^0,\vec{Q}),a_j(\vec{p})\right) = \frac{h(a_j(\vec{p}),\vec{p},Q)}{2a_j(\vec{p})\prod_{i=1,i\neq g(j)}^{l}\left(a_j^2(\vec{p})-a_i^2(\vec{p})\right)\prod_{i=1}^{2l}\left(a_j(\vec{p})+Q^0-a_i(\vec{p}+\vec{Q})\right)} \tag{3.112}$$

with the function g being given by Eq. (3.87). We highlight that this formula applies to the case of spatial regularization as well as covariant regularization. In particular, using a spatial regulator and setting the spatial external momenta to zero leads us to

$$\mathcal{I}_0^{(3\mathrm{d})}(Q^0,\vec{0},m)\big|_{T,\mu} = \frac{1}{4\pi^2}\int_0^\infty \mathrm{d}p\ p^2 \left[\frac{2E_k^2(p)\,\mathbb{1}_{4\times4}-m^2(\mathbb{1}_{4\times4}+\eta)}{E_k(p)\left(4E_k^2(p)+\left(Q^0\right)^2\right)}\sum_{\pm}\tanh\left(\frac{E_k(p)\pm\mu}{2T}\right)\right]\Bigg|_{k=\Lambda_0}^{k=0} , \tag{3.113}$$

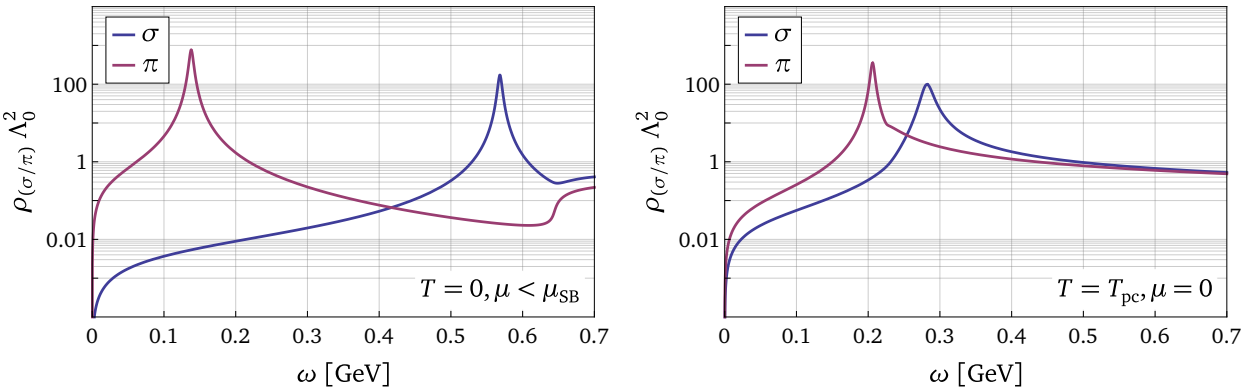

Figure 3.6: Meson spectral functions as obtained using the spatial regularization scheme. We illustrate the spectral functions in the vacuum limit (left panel) as well as for finite temperature (right panel). While the vacuum pion pole mass has been fixed to 138 MeV, the predicted vacuum pole mass of the sigma meson is $m_{\mathrm{pole},\sigma} \approx 568\,\mathrm{MeV}$.

where the regularized energy E_k is again given by Eq. (3.92). Notice that setting the time-like modes to zero here as well would provide us with the plasmon limit of the loop integral (3.106) and does not reproduce Eq. (3.91). Instead, the latter has to be obtained by considering the static limit of the momentum-dependent loop integral.

With the meson two-point correlators at hand, the corresponding spectral function can be obtained via analytic continuation, see Eq. (3.48). We present our results for the spectral functions of the scalar and pseudoscalar mesons as functions of the energy variable ω and in the presence of explicit symmetry breaking, $H > 0$. In all of our numerical studies, we will set the spatial external momenta to zero, i.e., $\vec{Q} = \vec{0}$, such that the energy ω_{res} associated with a resonance peak in the spectral function can be identified with a mass of the corresponding meson. In addition, we note that the integrand of the loop integral (3.113) develops a pole when the denominator becomes zero. After analytic continuation, $Q^0 \to \mathrm{i}\omega$, and for $\omega \leq \Lambda_0$, we find an integrable pole at

$$p^* = \sqrt{\frac{\omega^2}{4} - m^2}\,. \tag{3.114}$$

As a consequence, the corresponding loop integral becomes non-analytic at those energies where the pole enters or exits the domain of integration. For zero chemical potential, this occurs at the critical value $\omega_{\mathrm{c}} = 2m$ such that $p^* = 0$. In the context of spectral functions, the non-analytic behavior at this energy is commonly associated with a decay process into two particles of mass m each. We shall come back to this further below. Moreover, recall that the term evaluated at $k = 0$ in Eq. (3.113) is identical in both regularization schemes. Therefore, the dependence of the critical energy on the mass remains unchanged when employing a covariant regulator.

We now turn to the discussion of meson spectral functions obtained within the spatial regularization scheme. For this case, the spectral functions in the vacuum limit are shown in Fig. 3.6 (left panel). Whereas the vacuum pole mass of the pions has a value of $m_{\mathrm{pole},\pi} = \omega_{\mathrm{res},\pi} \approx 138\,\mathrm{MeV}$ by construction, the pole mass for the sigma meson is a prediction. We observe that this predicted value, $m_{\mathrm{pole},\sigma} = \omega_{\mathrm{res},\sigma} \approx 568\,\mathrm{MeV}$, is significantly closer to the expected resonance of 500 MeV than the corresponding value of the curvature mass, see Table 3.1b. Furthermore, the spectral functions exhibit more structural features than the typical peaks associated with the pole masses. For example, at $\omega \approx 644\,\mathrm{MeV}$ a kink in the spectral function of the sigma meson and a turning point in that of the pions can be observed. These structures are typically interpreted as indicating a decay of

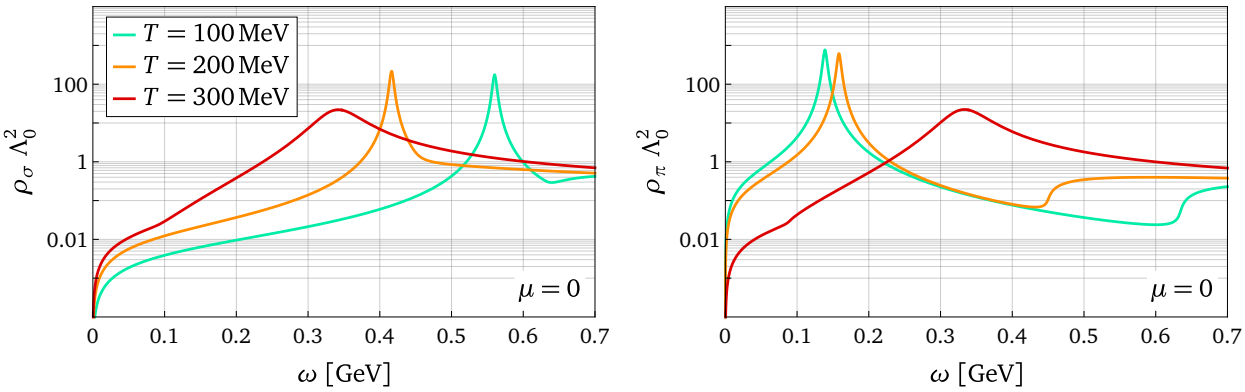

Figure 3.7: Illustration of meson spectral functions at different temperatures. More specifically, we show the sigma spectral function (left panel) as well as the pion spectral function (right panel) at $T = 100\,\mathrm{MeV}$ (turquoise curve), $T = 200\,\mathrm{MeV}$ (orange curve), and $T = 300\,\mathrm{MeV}$ (red curve).

an excited state of the meson into an energetically more favorable state. Within our model, these decays can be identified as the processes $\sigma' \to \bar{\psi}\psi$ and $\pi' \to \bar{\psi}\psi$, where the primes denote the excited states. Specifically, when we reach the energy $\omega_{\mathrm{decay}} = 2m_q$ associated with a pair of two constituent quarks with zero center-of-mass energy, it becomes favorable for the mesons to decay into these quark states. The decay scale ω_{decay} corresponds precisely to the critical value of the energy variable that we identified earlier based on the expression (3.113) for the loop integral. We would like to remark, however, that the non-analytic behavior of the spectral functions at this energy value appears to be rather smoothed out in Fig. 3.6. This is a result of the finite ε parameter which we have used in our numerical computations of spectral functions.

By increasing the temperature at zero chemical potential, we can deform the spectral functions. For an illustration of the meson spectral functions at various temperatures, we refer to Fig. 3.7. More specifically, as the quark mass decreases with rising temperature, the structures associated with the decay of the mesons into two quarks follow the relation $\omega_{\mathrm{decay}}(T) = 2m_q(T)$ and thus shift continuously to lower temperatures. Furthermore, the energy $\omega_{\mathrm{res},\pi}$ that corresponds to the pion resonance mass increases steadily with temperature. In contrast to this, the sigma resonance mass as indicated by the energy $\omega_{\mathrm{res},\sigma}$ decreases with increasing temperature until it reaches its minimum value at $T \approx 256\,\mathrm{MeV}$. Beyond this temperature, the sigma resonance mass begins to increase again and approaches the same high-temperature limit as the pion mass. The temperature-dependent behavior of the resonance masses is reminiscent of that of the curvature masses, see Fig. 3.1a (right panel).[15] For a more concrete presentation of the temperature dependence of meson resonance masses, see, for example, Refs. [235, 360, 397, 398]. At sufficiently high temperatures, where the quark mass approaches zero, the spectral functions of the scalar and pseudoscalar mesons become nearly degenerate.

Let us comment more on the shape of the spectral functions. In particular, we observe that the structural features associated with decay processes tend to become increasingly suppressed with rising temperatures. Moreover, although the peak positions ω_{res} shift with temperature, the shapes of the peaks remain unchanged at low temperatures. More specifically, the Dirac-delta peaks present in the vacuum spectral functions, which correspond to poles of the inverse two-point

[15] In principle, we could define the temperature associated with the crossover transition by the minimum of the sigma resonance mass. Nevertheless, our calculations of curvature masses as derived from effective potential in Section 3.2.2 reproduce standard mean-field results and therefore establish a direct link to Landau theory, which is an important cornerstone for the concept of phase transitions. Thus, while defining a pseudo-critical temperature using the resonance mass is feasible, this definition would be less tied to the thermodynamic properties governing the transition.

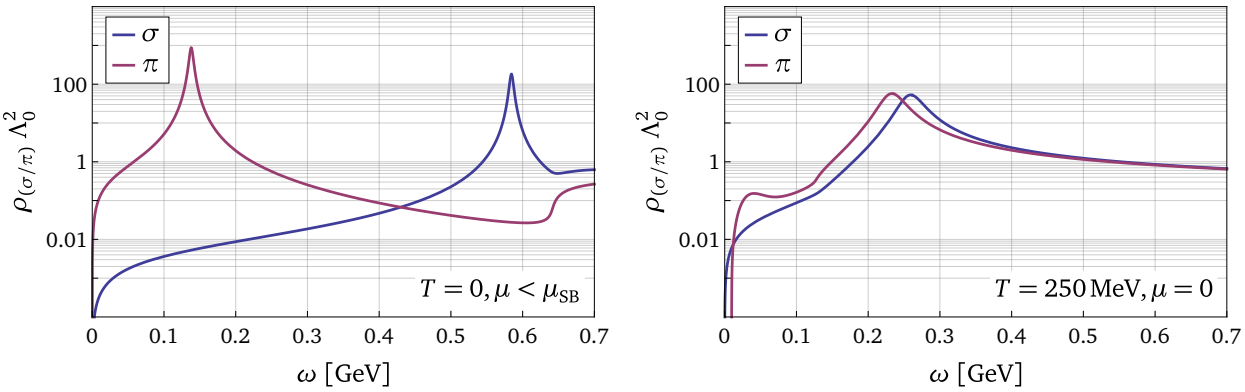

Figure 3.8: Meson spectral functions as obtained using the covariant regularization scheme. We illustrate the spectral functions in the vacuum limit (left panel) as well as for finite temperature (right panel). While the vacuum pion pole mass has been fixed to 138 MeV, the predicted vacuum pole mass of the sigma meson is $m_{\text{pole},\sigma} \approx 584\,\text{MeV}$.

function, remain Dirac-delta peaks at finite temperature provided that $\omega_{\text{res}} < \omega_{\text{decay}}$. Phenomenologically, this implies that mesons remain stable as long as their resonance mass is smaller than the energy required to trigger a decay into their constituents. At temperatures where this relation is reversed, $\omega_{\text{res}} > \omega_{\text{decay}}$, the resonance peaks not only decrease in height but also undergo a significant broadening. These effects become more pronounced with increasing temperatures and can be attributed to thermal fluctuations, which induce a screening for the pole present in the propagator of the vacuum theory. As a consequence, at such temperatures, the resonance mass associated with the peak no longer corresponds to a pole mass. Furthermore, the particle becomes unstable as the finite FWHM of its resonance peak indicates a finite average lifetime. One may define a characteristic temperature by the solution to $\omega_{\text{res}}(T) = \omega_{\text{decay}}(T)$, beyond which the destabilization process begins. We emphasize that this temperature is specific for each particle. This means that, given a certain temperature, one particle can still be stable whereas another has already become unstable. Such a scenario is illustrated in Fig. 3.6 (right panel). In particular, at the pseudo-critical temperature as derived from the effective potential, we find $\omega_{\text{res},\sigma}(T_{\text{pc}}) \approx 282\,\text{MeV}$, $\omega_{\text{res},\pi}(T_{\text{pc}}) \approx 206\,\text{MeV}$, and $\omega_{\text{decay}}(T_{\text{pc}}) \approx 227\,\text{MeV}$. Accordingly, the pion spectral function at $T = T_{\text{pc}}$ still exhibits a Dirac-delta peak, indicating the existence of a pole mass. In contrast to this, the resonance peak in the sigma spectral function is broadened, which signals that thermal fluctuations have rendered the particle unstable.

When employing a covariant regularization scheme for the computation of spectral functions, the results remain qualitatively the same at low temperatures as those obtained using the spatial scheme. The meson spectral functions in the vacuum limit as derived in the covariant scheme are shown in Fig. 3.8 (left panel). As before, the model parameters have been tuned to set the vacuum pole mass of the pions to $m_{\text{pole},\pi} = \omega_{\text{res},\pi} \approx 138\,\text{MeV}$. Interestingly, the predicted vacuum pole mass for the sigma meson, $m_{\text{pole},\sigma} = \omega_{\text{res},\sigma} \approx 584\,\text{MeV}$, is further away from the expected resonance at 500 MeV than the prediction of the quark-meson model in the spatial scheme. At the same time, pole masses and curvature mass lie closer together in the covariant scheme. The temperature-dependent behavior of peaks and decay structures in the spectral functions is the same for both regularization schemes. Nevertheless, we observe a new feature arising in the pion spectral function for $T \gtrsim 240\,\text{MeV}$. Concretely, a "bump" emerges at low energies. For illustrational purposes, we present the meson spectral functions at $T = 250\,\text{MeV}$ in Fig. 3.8 (right panel). To the best of our knowledge, this bump does not have any phenomenological interpretation. Nevertheless, our analysis indicates that this bump does not originate from numerical inaccuracies and is not an

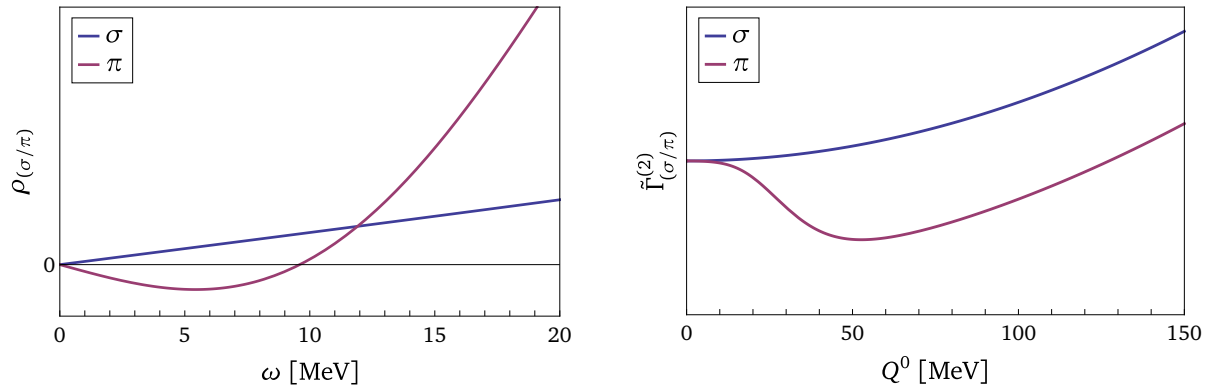

Figure 3.9: For $T = 250\,\text{MeV}$ and $\mu = 0$, we show the behavior of the meson spectral functions at low energies (left panel) as well as the two-point correlators as functions of the external time-like momentum Q^0 (right panel). Both cases here refer to calculations in which we have used the covariant regularization scheme and have chosen $\vec{Q} = \vec{0}$. For illustrative purposes, the correlators have been normalized such that they agree at the origin of momentum space.

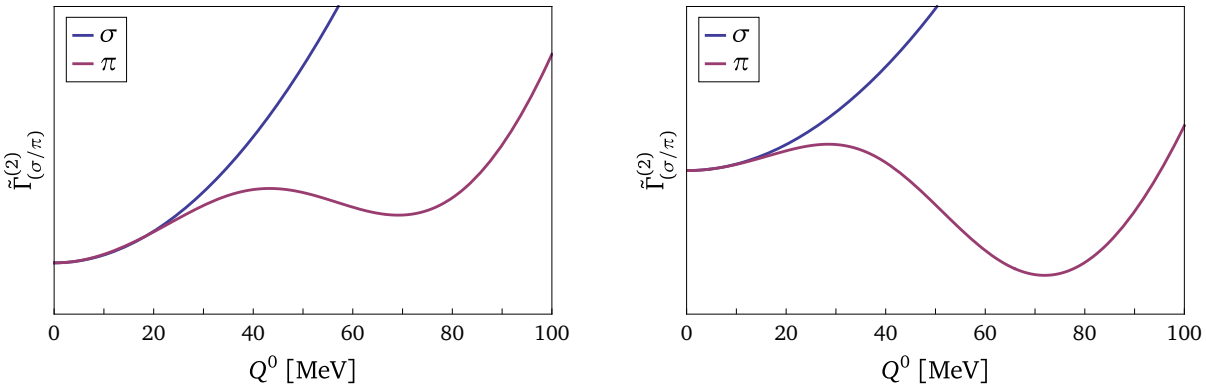

Figure 3.10: For $T = 220\,\text{MeV}$ (left panel) and $T = 225\,\text{MeV}$ (right panel), we show the behavior of the meson two-point correlation functions with respect to the external time-like momentum Q^0. Both cases here refer to calculations in which we have used the covariant regularization scheme and have chosen $\vec{Q} = \vec{0}$. Each time the correlators have been normalized such that they agree at the origin of momentum space.

artifact of the finite ϵ parameter. In fact, it is worth mentioning that this feature is absent in the chiral limit, i.e., when considering $H = 0$. This observation indicates that the bump results from the intricate interplay of several competing scales in the covariant scheme.

Furthermore, we observe that the presence of the bump structure is accompanied by the pion spectral function becoming negative at even lower energies. This behavior is illustrated more clearly in Fig. 3.9 (left panel). While the spectral functions of not (directly) observable particles can indeed assume negative values, see, e.g., Refs. [383, 399–401], the negative values of the pion spectral function render our results unphysical. Additionally, we observe the development of a finite minimum in the corresponding two-point correlator in momentum space, see Fig. 3.9 (right panel). In general, such a property may hint towards a non-trivial dispersion relation or some exotic excitation. However, neither is expected for the pions. We note that the anomalous behavior of the pion correlation function at finite temperature becomes apparent already at $T \gtrsim 210\,\text{MeV}$. Specifically, the pion correlator reveals that its minimum undergoes a temperature-induced (reversed) first-order phase transition, see Fig. 3.10. Overall, our findings suggest that the polynomial regulator in the covariant scheme significantly alters the momentum structure of the

propagator. As discussed in Refs. [82, 228], covariant regulators can lead to unphysical poles in the complex p^0-plane and can therefore spoil causality. More generally, this may lead to artificial features in certain regions of parameter space as we see in our results.

In the context of spectral functions, we would like to briefly comment on the possibility of calculating the shear viscosity. The shear viscosity is one of several so-called transport coefficients and emerges from the energy-momentum tensor of a relativistic fluid in a derivative expansion up to first order, see, e.g., Ref. [402]. Through the works of Green [403, 404], Mori [405], and Kubo [296] it became clear that transport coefficients can also be obtained from correlation functions. For more general discussions of transport coefficients in field theory, see Refs. [406–408]. By definition, transport coefficients describe how a hydrodynamical system responds to small perturbations. The feedback from the medium under consideration then provides information about, for example, mechanical resistances and conductivity properties. In particular, the shear viscosity is a measure of the resistance of a material to deformation due to shear stress. The viscosity of a system depends in detail on how the constituents of that system interact. For instance, in gases momentum is transported by molecules moving freely between collisions. In liquids, however, the momentum transport is governed by the electrodynamic forces that bind molecules together. As a result, the dynamic viscosities of liquids are typically much larger than those of gases, see, e.g., Ref. [409]. Experimental data from heavy-ion collisions suggests that the physics of the hot quark-gluon plasma can be described by a fluid model with small viscosity. Accordingly, a determination of transport coefficients of strongly interacting matter has been and still is of great interest, see, e.g., Refs. [410–416]. In QCD, the shear viscosity helps to resolve the fluid-dynamical properties of quark matter, in particular the nature of interactions. For studies of the shear viscosity in this regard, we refer to Refs. [417–421]. As shown in Ref. [422], the shear viscosity of the scalar and pseudoscalar mesons can be directly linked to their respective spectral functions. However, a computation of transport coefficients in a covariant regularization scheme is beyond the scope of this work. In any case, we expect the unphysical behavior of the pion spectral function to distort the temperature dependence of the corresponding shear viscosity.

We continue our investigation of the quark-meson model with a presentation of meson spectral function at zero temperature and finite chemical potential. As before, we begin by examining the analytical structure of the correlator. Specifically, in the zero-temperature limit, the integral presented in Eq. (3.113) becomes

$$\begin{aligned}\mathcal{I}_0^{(3\mathrm{d})}(Q^0,\vec{0},m)\big|_{\mu} &= \lim_{T\to 0}\mathcal{I}_0^{(3\mathrm{d})}(Q^0,\vec{0},m)\big|_{T,\mu}\\ &= \frac{1}{2\pi^2}\int_0^\infty \mathrm{d}p\; p^2\left[\frac{2E_k^2(p)\,\mathbb{1}_{4\times4}-m^2(\mathbb{1}_{4\times4}+\eta)}{E_k(p)\left(4E_k^2(p)+\left(Q^0\right)^2\right)}\,\theta\left(E_k(p)-\mu\right)\right]\Bigg|_{k=\Lambda_0}^{k=0}.\end{aligned} \tag{3.115}$$

After analytic continuation of the time-like momentum, $Q^0\to \mathrm{i}\omega$, the integrable pole at $p=p^*$, see Eq. (3.114), is still present. Consequently, the loop integral becomes non-analytic at energies ω which causes the pole to enter or exit the domain of integration. At zero temperature, this is the case at the critical value $\omega_\mathrm{c}=2m$, provided that $\mu<\mu_\mathrm{SB}$. As discussed before, this energy determines the position of the corresponding non-analytic structures in the spectral functions, which are associated with decay processes. Beyond the Silver-Blaze threshold, the Heaviside function in Eq. (3.115) restricts the loop momenta for the minuend to be at least as large as the Fermi momentum $p_\mathrm{F}=\sqrt{\mu^2-m^2}$. As a result, the dependence of the critical energy on the chemical potential changes to $\omega_\mathrm{c}=2\mu$ such that $p^*=p_\mathrm{F}$. Accordingly, we expect that the position of corresponding structures in the spectral functions gets shifted to higher values as we increase the chemical potential. Altogether, the zero-temperature theory implies that $\omega_\mathrm{c}=2\max(m,\mu)$.

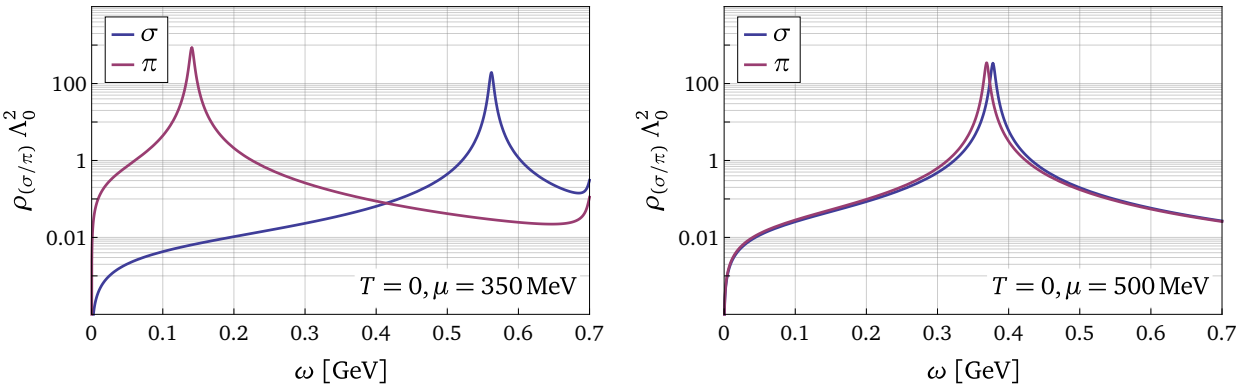

Figure 3.11: Meson spectral function obtained in the covariant regularization scheme for $T = 0$ and different values of the chemical potential. In particular, we show the case of $\mu = 350\,\mathrm{MeV}$ (left panel) and $\mu = 500\,\mathrm{MeV}$ (right panel).

Meson spectral functions at zero temperature are illustrated in Fig. 3.11 for different values of the quark chemical potential. Because the behavior of the system at zero temperature is governed by the Silver-Blaze property, we consider only the case of $\mu > \mu_{\mathrm{SB}}$ for our following presentation of spectral functions. Below the Silver-Blaze threshold, the zero-temperature spectral functions as functions of the energy ω do not change with the chemical potential. These are shown in Fig. 3.6 (left panel) for the spatial regularization scheme and in Fig. 3.8 (left panel) for the covariant scheme. Additionally, the matter part

$$\mathcal{M}_0^{(2)}(Q^0,\vec{0},\mu,m) = \frac{\theta(\mu-m)}{2\pi^2}\int_0^{\sqrt{\mu^2-m^2}} \mathrm{d}p\; p^2\; \frac{(2p^2+m^2)\,\mathbb{1}_{4\times4} - m^2\,\eta}{\sqrt{p^2+m^2}\left(4p^2+4m^2+\left(Q^0\right)^2\right)} \tag{3.116}$$

of the loop integral corresponding to the two-point correlator at zero temperature is scheme-independent for all chemical potentials of interest. As a consequence, the results for the meson spectral functions are very similar among the different schemes. In order to avoid redundancy, we will only present our results obtained within the covariant regularization scheme.

Above the Silver-Blaze threshold, we observe that the energy ω_{decay} associated with the decay of an excited meson into two quarks does not follow the chemical potential dependence of the quark mass. Instead, it increases monotonically with the chemical potential. In agreement with our discussion of the critical energy above, the position of the decay structures seen in the spectral functions behaves as $\omega_{\mathrm{decay}}(\mu) = 2\mu$. A phenomenological explanation for this phenomenon is readily given. According to the Fermi statistics, in a fermionic system at zero temperature, quantum states with energy $\omega < \mu$ are fully occupied. As a consequence, the mesons can only decay into their quark content if their excitation is high enough to produce a pair of fermions with at least the Fermi energy $\omega_{\mathrm{F}} = \mu$ each. Therefore, the decay structures observed in the spectral functions are shifted to energies $\omega_{\mathrm{decay}} = 2\omega_{\mathrm{F}}$ in the regime characterized by $\mu \geq \mu_{\mathrm{SB}}$. It is worth mentioning that, according to the relativistic energy-momentum relation, quarks with the Fermi energy $\omega_{\mathrm{F}} = \sqrt{p_{\mathrm{F}}^2 + m_q^2} = \mu$ carry the Fermi momentum $p_{\mathrm{F}} = \sqrt{\mu^2 - m_q^2}$. Moreover, we observe that the kink seen in the vacuum spectral function of the sigma meson at ω_{decay} quickly transforms into a turning point above the Silver-Blaze threshold.

Analogous to the behavior observed at finite temperature and zero chemical potential, the resonance peaks in the zero-temperature spectral functions approach each other with increasing values of the chemical potential and then follow the same isotonic μ-dependence once the corresponding

energies ω_{res} have become quasi-degenerate. However, unlike the finite-temperature case, the resonances at zero temperature remain sharply peaked and do not undergo a broadening process as the chemical potential increases. In other words, the poles of the propagator at zero-temperature remain poles at finite chemical potential such that the notion of a pole mass $m_{\text{pole}} = \omega_{\text{res}}$ remains valid. The origin of this property lies in the chemical potential dependence of the energy at which the mesons decay. More specifically, since the position of the decay structures increases with chemical potential, the relation $\omega_{\text{res}} < \omega_{\text{decay}}$ is always satisfied for both mesons. As a consequence, a broadening of the resonance peak cannot be triggered by non-analyticities intersecting the pole position. Accordingly, our model indicates that the sigma meson and the pions are stable particles at zero temperature.

We would like to highlight that, at zero temperature and finite chemical potential, the meson spectral functions and the corresponding correlation functions in the covariant scheme do not exhibit unexpected structures or anomalous behaviors. As demonstrated before, the behavior of the system under vacuum conditions is free of anomalies. Also recall that, at zero temperature, the dependence of the system on the chemical potential is given by a scheme-independent contribution to the vacuum loop integral for all chemical potentials of interest. In other words, information about the regularization scheme does not enter the matter part (3.116) unless the chemical potential is at least of the order of magnitude as the initial scale Λ_0. The absence of anomalies in Fig. 3.11 therefore again suggests that the artificial effects observed at finite temperature have been induced by the covariant regulator. Since the momentum structure of the zero-temperature propagator remains unaltered for all relevant chemical potentials, no unphysical behavior can be observed. Nevertheless, we expect artificial effects to emerge once the chemical potential is sufficiently large for the regularization scheme to affect the matter part. At zero temperature, this scheme dependence can be fully eliminated again by taking RG consistency into account.

To briefly summarize, we have been successful in computing meson spectral functions in a momentum-dependent covariant regularization scheme at finite external parameters. While we observe no qualitative discrepancies from a spatial scheme at low temperatures, unexpected behavior appears at high temperatures. For example, the spectral function for the pseudoscalar mesons can assume negative values at low energies, which is an unphysical outcome. Our analysis suggests that the anomalous behavior as observed from calculations with covariant regularization arises from an unphysical momentum structure of the propagator induced by the regulator. We therefore conclude that the covariant polynomial regulator is simply not suited to reliably study quantities such as spectral functions, which depend on finite external momenta. For an investigation of low-energy QCD based on spectral functions, we strongly recommend a regularization scheme that preserves the pole structure of the propagator with respect to the internal time-like momenta.

3.3 The Callan-Symanzik regulator

This section addresses the implementation of the Callan-Symanzik (CS) regulator function within the functional renormalization group framework to investigate low-energy QCD, focusing on curvature masses and spectral properties. Our approach builds upon a novel fRG setup introduced in Ref. [82], which derives finite functional flows for regulators that do not provide sufficient ultraviolet regularization for all loop diagrams. The CS regulator offers significant advantages, including the preservation of Lorentz symmetry and Silver-Blaze symmetry, while also avoiding the emergence of a series of poles in the propagator. Notably, this regulator often allows us to compute loop integrals analytically to a great extent. However, these benefits come with the drawback of

an unphysical breakdown of chiral symmetry in theories with fermions. Using the quark-meson model as an example of such a theory, the following work not only provides a detailed discussion of the regulator-induced symmetry breaking but also demonstrates how to handle this issue in a systematic fashion. Considering the CS regulator, we formulate an fRG framework that preserves all symmetries of the quark-meson model. Using this framework, we present results for meson curvature masses, meson spectral functions, and the phase diagram of low-energy QCD. This study represents a first step toward a comprehensive understanding of the mechanisms shaping the phase structure of QCD at low energies.

3.3.1 Generalities

In the present section, we employ a standard CS regulator which can be parameterized as

$$\widetilde{R}_k^{\psi}(p) = Z_{\psi,k}\, ik\,, \qquad \widetilde{R}_k^{\varphi}(p) = Z_{\varphi,k}\, k^2\,, \tag{3.117}$$

for the fermions and bosons, respectively. This class of regulators provides IR regularization by acting as a mass term where the RG scale k corresponds to a mass scale. More concretely, through the regulator insertion, the propagator gains an explicit mass term $\Delta m_\psi = Z_{\psi,k}k$, $\Delta m_\varphi^2 = Z_{\varphi,k}k^2$ for the fermions and bosons, respectively. We highlight that, compared to other canonically used regulator functions, the CS regulators exhibit the characteristic feature of coming without the dependence on loop momenta. As a consequence, our regularization scheme does not implement a Wilsonian-type momentum-shell integration for which the flow of the effective average action would be dominated by fluctuations with momenta $p^2 \approx k^2$. Instead, the RG flow as generated by CS regulators rather describes a flow through infrared theories associated with different masses for the fields. When considering a CS flow, all momentum shells are already integrated out at every scale k. Because of this property, the initial condition for the Wetterich equation at a given mass scale $k = \Lambda_0$ refers to an infrared theory and should not be confused with a UV action in the Wilsonian sense. It should be rather considered as an ansatz for the quantum effective action of a theory with particle masses that are at least of the order of Λ_0. This initial condition is chosen such that an action functional with specific properties at some lower scale $k < \Lambda_0$ is recovered when we solve the Wetterich equation. In our analysis, we take $k = 0$ as the point at which the effective action provides us with physical observables.

As detailed in Ref. [82], the standard CS regulator is advantageous for several reasons. It preserves the analytic properties of the theory and yields a propagator with a simple pole structure in momentum space since it does not generate additional poles in the complex plane associated with the time-like component of the four-momentum. This property ensures a spectral representation of the regularized propagator, which is of great relevance for the computation of real-time correlation functions. Furthermore, the CS regulator does not interfere with a multitude of symmetries of the theory. Specifically, the regulator not only respects Lorentz symmetry in the vacuum limit but also the Silver-Blaze symmetry in the presence of a finite chemical potential. These advantages come at a twofold cost: First of all, the CS regulator only lowers the degree of the UV divergences by two, which is not always sufficient to render all loop integrals in the RG flow finite. Hence, in general, an additional UV regularization is required. Secondly, the CS regulator for the fermions introduces an artificial source of explicit chiral symmetry breaking as the mass term $\sim \overline{\psi} k \psi$ does not remain invariant under chiral transformations. This is a major problem for studies of systems whose dynamics is governed by chiral symmetry. Consequently, the flow with respect to the fermionic mass must be examined accurately and physical contributions must be extracted with the aid of symmetry constraints. It is worth mentioning in this context that the bosonic CS regulator does in fact not spoil the $O(N)$ symmetry in the boson subspace. This is because the corresponding

mass term $\sim \varphi^\intercal k^2 \varphi$ is indeed invariant under orthogonal transformations of the fields. Suitable strategies that allow us to obtain finite and physically meaningful results in the presence of the CS regulator will be addressed in more detail further below. Lastly, we recall that our study of low-energy QCD by means of the functional renormalization group takes into account only purely fermionic loops. Nevertheless, we have also presented the bosonic version of the CS regulator in Eq. (3.117) for reasons of completeness. For works that make use of the bosonic CS regulator, we refer to Refs. [423, 424].

First, let us comment on the issue of symmetry breaking as induced by the fermionic CS regulator more concretely in the context of the quark-meson model. Our truncation scheme for the computation of the quantum effective action involves the one-loop approximation and setting $Z_{\psi,k} = 1$. Within this scheme, the Wetterich equation describing the CS flow then takes the simple form

$$\partial_k \Gamma_k^{(\mathrm{CS})}[\sigma, \vec{\pi}]\big|_{T,\mu} = -\operatorname{Tr}\left\{\partial_k \operatorname{Ln}\left(S^{(1,1)}_{\bar{\psi},\psi}\left[\sigma + \frac{k}{h}, \vec{\pi}\right]\Big|_\mu\right)\right\}\Big|_T \,, \tag{3.118}$$

making clear that the regulator R_k^ψ directly affects the σ-direction of meson field space but leaves the pion fields untouched.[16] This additional shift in the sigma field of the order of k makes the breakdown of rotation symmetry among the mesons in the loop contribution to the effective action apparent. We stress that a regulator-induced breaking of symmetry affects every RG step such that the infrared endpoint of the RG trajectory does not align with the true result, although the regulator is explicitly removed for $k \to 0$. Furthermore, since the ground state of the system is always aligned with the σ-direction by convention, Eq. (3.118) implies that the quark mass scales with k. A variation of the RG scale k can therefore be directly translated into a variation of the mass associated with the fermion fields. This again shows that the standard RG phenomenology of Wilsonian momentum shell integration does not apply anymore when considering CS regulator functions. In any case, without a procedure that removes the regulator-induced symmetry breaking at every scale, results for physical observables will be significantly spoiled by artificial effects. Such a symmetrization procedure will be the subject of the subsequent section.

The Callan-Symanzik regulator satisfies the regulator conditions (i)-(iii) but fails condition (iv). Specifically, for the fermionic regulator with $Z_{\psi,k} = 1$, we find

$$\lim_{\frac{p^2}{k^2}\to\infty} \partial_k \tilde{R}_k^\psi(p) = 1 \neq 0 \,, \tag{3.119}$$

which implies that the corresponding effective average action is still plagued by UV divergences. In order to render the RG flows in the presence of a CS regulator finite, additional UV regularization must be implemented. This may be achieved by considering the CS regulator together with an auxiliary cutoff function for the modes of high momentum, see, e.g., Refs. [82, 425]. We emphasize that such a strategy introduces an additional momentum scale into the theory which must be handled appropriately to allow for meaningful predictions. Our realization of UV finiteness relies on the introduction of counterterms that cancel the UV divergences of the quantum loop. Concretely, we employ a sharp cutoff to suppress momenta with $p^2 > \lambda^2$ and let the counterterms subtract all pathological contributions before removing the momentum scale by taking the limit $\lambda \to \infty$. Concretely, we write

$$\Gamma_k\big|_{T,\mu} = \lim_{\lambda\to\infty}\left(\Gamma_k^{(\mathrm{CS})\lambda}\big|_{T,\mu} - 8N_\mathrm{c}\, V_4\, \mathrm{CT}_k^\lambda\right) \equiv \Gamma_k^{(\mathrm{CS})}\big|_{T,\mu} - 8N_\mathrm{c}\, V_4\, \mathrm{CT}_k \,. \tag{3.120}$$

[16] One can consider an alternative version of the CS regulator, namely $R_k^\psi = Z_{\psi,k} \mathrm{i}\gamma^5 k$, for which the RG scale k does not couple to the sigma mode but instead to the pion fields. This regulator, however, not only breaks chiral symmetry but also parity.

Once again, we remark that, at $T > 0$, the four-dimensional spacetime volume carries an implicit temperature dependence, $V_4 = \beta V$. Our procedure ensures that the space of momenta contributing to the loop integral does not get deformed by the overall regularization prescription. Just as in the case of ordinary regulator functions, the construction of counterterms is in principle constrained by the symmetries of the underlying quantum field theory. The counterterms for the effective action of our quark-meson model read

$$\begin{aligned}\mathrm{CT}_k(\Lambda, h\phi) &= \frac{(k-\Lambda)(k+\Lambda+2h\sigma)}{2}\,\frac{1}{2}\frac{2\pi^2}{(2\pi)^4}\lim_{\lambda\to\infty}\left(\left[(k+h\sigma)^2+(\Lambda+h\sigma)^2+2h^2\vec{\pi}^2\right]\ln\left(\frac{\lambda}{s}\right)-\lambda^2\right)\\ &= \frac{(k-\Lambda)(k+\Lambda+2h\sigma)}{2}\lim_{\lambda\to\infty}\int_{p^2\leq\lambda^2}\frac{\mathrm{d}^4p}{(2\pi)^4}\left(\frac{(k+h\sigma)^2+(\Lambda+h\sigma)^2+2h^2\vec{\pi}^2}{2p^3\sqrt{4s^2+p^2}}-\frac{1}{p^2}\right),\end{aligned} \tag{3.121}$$

where we have used that

$$\lim_{x\to\infty}\left(\ln(x)-\operatorname{arsinh}\left(\frac{x}{2}\right)\right)=0 \tag{3.122}$$

for a most convenient representation of counterterms at the integral level. The counterterms for 1PI n-point functions with $n \geq 1$ are then readily obtained by differentiating the result above n times with respect to the fields. We highlight that our analysis of UV divergences takes Lorentz symmetry into account, leading to a description of counterterms where the cutoff parameter λ represents a momentum scale for all components of the internal four-momentum. Notably, we add that the counterterms inherit the symmetry and additivity properties of the associated loop integrals,

$$\mathrm{CT}_\Lambda(k, h\phi) = -\mathrm{CT}_k(\Lambda, h\phi)\,, \tag{3.123}$$

$$\mathrm{CT}_k(\Lambda_0, h\phi) + \mathrm{CT}_\Lambda(k, h\phi) = \mathrm{CT}_\Lambda(\Lambda_0, h\phi)\,. \tag{3.124}$$

Notice that the counterterms above do not exhibit any dependence on temperature or chemical potential, because non-vacuum parts of the loop are naturally free of UV divergences. In other words, the counterterms provide UV regularization for the vacuum theory but leave the behavior of the IR-regularized system with respect to temperature and chemical potential unaffected. Therefore our usage of counterterms to employ additional UV regularization does not destroy the Silver-Blaze symmetry. It should further be mentioned that our counterterms introduce an artificial scale dependence to the effective action. In order to perform actual calculations, we have to explicitly choose a scale s and this choice then belongs to the definition of the vacuum theory. For all practical applications, we choose the scale to be the initialization scale of the RG flow, i.e., $s = \Lambda_0$. We also add that the form of the counterterms is unique only up to finite terms in the limit $\lambda \to \infty$. Our counterterms have been chosen this way such that we obtain a non-trivial vacuum ground state in the limit $k \to 0$ when choosing the initial condition (3.34). For an ansatz of the effective action at the scale Λ_0 which contains terms of higher orders in the fields, it is possible to adjust the counterterms such that there is no need for the introduction of an additional scale s. Nevertheless, explicit calculations within such a setting are beyond the scope of this work.

We stress that the different realization of the IR and UV regularization does not lead to an overall inconsistent regularization scheme in our case. As the counterterms respect the symmetries of the underlying quantum field theory and do not alter how momenta enter the loop integrals, they are perfectly compatible with the CS regulator. In other words, the momentum modes of the vacuum

and non-vacuum contributions to the loops are treated consistently in our regularization scheme. At last, we would like to highlight that these counterterms are scale-dependent and hence are not to be considered part of the initial condition for the Wetterich equation. Instead, the counterterms constitute a necessary second ingredient to the regularization prescription that is needed to have an IR- as well as UV-regularized theory.

Ultimately, we aim at a computation of physical observables via the functional renormalization group using the Callan-Symanzik regulator. As a preliminary step in this regard, we have presented counterterms that ensure a well-defined framework. Next, we need to restore the chiral symmetry in the regularized quantum loop in order to allow for physically meaningful results.

3.3.2 Restoration of rotation symmetry

The effective potential

By expanding the meson fields about a homogeneous background, we arrive at the following result for the scale-dependent effective action:

$$\begin{aligned}\frac{1}{V_4}\Gamma_k(\phi)\big|_{T,\mu} &= \frac{1}{V_4}\Gamma_{\Lambda_0}(\phi) - 8N_{\mathrm{c}}\, L_k(\Lambda_0, h\phi)\big|_{T,\mu} \\ &= \frac{1}{V_4}\Gamma_{\Lambda_0}(\phi) - 8N_{\mathrm{c}}\Big[L_k^{(\mathrm{CS})}(\Lambda_0, h\phi)\big|_{T,\mu} + \mathrm{CT}_k(\Lambda_0, h\phi)\Big]\,, \end{aligned} \tag{3.125}$$

which is equivalent to the effective action. Here, Λ_0 denotes the reference scale at which the RG flow of the effective action is initialized. The initial condition Γ_{Λ_0} is usually used to tune the results for a given set of low-energy observables such that they assume their physical values in the vacuum limit. We shall discuss the determination of parameters present in the initial condition in more detail in Sections 3.3.4 and 3.3.5 when we consider concrete applications of our CS framework. The auxiliary function parameterizing the IR-regularized loop is given by

$$\begin{aligned} L_k^{(\mathrm{CS})}(\Lambda_0, h\phi)\big|_{T,\mu} &= \frac{1}{2}\int_{\vec{p}}\frac{1}{\beta}\sum_{n\in\mathbb{Z}}\ln\big((\nu_n + \mathrm{i}\mu)^2 + \vec{p}^{\,2} + (h\sigma + k')^2 + h^2\vec{\pi}^2\big)\Big|_{k'=\Lambda_0}^{k'=k} \\ &= \frac{1}{(2\pi)^2}\int_0^\infty \mathrm{d}p\; p^2\left\{\sqrt{p^2 + (h\sigma + k')^2 + h^2\vec{\pi}^2}\right. \\ &\qquad \left. + \frac{1}{\beta}\sum_{\pm}\ln\Big(1 + \mathrm{e}^{-\beta\left(\sqrt{p^2 + (h\sigma + k')^2 + h^2\vec{\pi}^2} \pm \mu\right)}\Big)\right\}\Bigg|_{k'=\Lambda_0}^{k'=k}\,, \end{aligned} \tag{3.126}$$

which is a more explicit representation of Eq. (3.118). As discussed earlier, a suitable IR regularization is implemented through the CS regulator by construction. This can be readily recognized from the appearance of the scale k' which acts like a fermion mass in the loop integral. In this regard, we emphasize that the scale Λ_0 should not be confused with a UV momentum cutoff of the loop integral. It also represents a mass-like scale associated with the CS regulator and enters the loop integral because the RG flow is initialized at $k' = \Lambda_0$. Therefore, this scale in general also appears in the counterterms. The result (3.126) shows, that chiral symmetry is broken by the presence of the fermionic CS regulator since the loop function is not $O(4)$-symmetric. Specifically, note that the regulator does not simply generate a linear symmetry-breaking pattern but instead leads to symmetry-breaking terms of arbitrary order in the fields. The effective potential therefore not only gets tilted along the σ-direction but rather undergoes an overall distortion. Nevertheless, we still observe an intact $O(3)$ symmetry among the pions because the regulator leaves the $SU(2)_{\mathrm{V}}$ symmetry of the theory unaffected.

Let us now discuss how the regulator-induced breaking of the chiral symmetry can be removed in a controlled and systematic fashion. To this end, we would like to point out that the Lie group $O(N)$ and its subgroup $SO(N)$ have the same generators. Thus, a scalar quantity invariant under $O(N)$ transformations is also $SO(N)$-symmetric and vice versa. Let us therefore now take a look at infinitesimal $SO(4)$ transformations in the mesonic field space. Intact chiral symmetry implies that all mesonic quantities should be invariant with respect to such rotations, i.e.,

$$\mathcal{Q}^{(\mathrm{sym})}[\phi] = \mathcal{Q}^{(\mathrm{sym})}[(1+\alpha^j X_j)\phi]\,, \tag{3.127}$$

where $\alpha^j \in \mathbb{R}$ is the j-th rotation angle parameter for all $j \in \{1,\dots,6\}$ and X_j the corresponding generator of the group $SO(4)$. This implies that

$$\forall i \in \{1,2,3\}: \quad \frac{\delta \mathcal{Q}^{(\mathrm{sym})}[\phi]}{\delta \sigma}\,\pi_i - \frac{\delta \mathcal{Q}^{(\mathrm{sym})}[\phi]}{\delta \pi_i}\,\sigma = 0\,. \tag{3.128}$$

This relation can be considered a Ward-Takahashi identity (WTI) for rotational symmetry between the σ-direction and the pionic directions of field space. Let us now consider a quantity $\mathcal{Q}$, which is not invariant with respect to $O(4)$ transformations of the meson fields. For example, such a quantity may have been obtained from the effective potential (3.125) as generated by a CS flow. In order to build a correspondingly symmetric quantity from $\mathcal{Q}$, we make the ansatz

$$\mathcal{Q}^{(\mathrm{sym})}[\phi] = \mathcal{Q}[\phi] + c[\phi] \tag{3.129}$$

and construct the additional term c such that the WTI is fulfilled. It is important to realize that our symmetrization procedure must not alter the dependence of $\mathcal{Q}$ on the pion fields since this subspace is not affected by the CS regulator. Concretely, this means that Eq. (3.128) has to be solved for c with the initial condition

$$c[\sigma = 0, \vec{\pi}] = 0\,. \tag{3.130}$$

Notice that our ansatz implies that c can be considered a counterterm for the contributions in $\mathcal{Q}$ that explicitly break the rotation symmetry. In order to ensure that the regulator-induced symmetry breaking is removed even in the presence of external parameters, e.g., temperature or chemical potential, the counterterm must in general also carry a corresponding dependence on such parameters. For convenience, let us further introduce the symmetrization operator $\mathcal{S}$ by

$$\mathcal{Q}^{(\mathrm{sym})} \equiv \mathcal{S}\,\mathcal{Q} := \mathcal{Q} + c\,. \tag{3.131}$$

We shall employ this operator for our studies below. Throughout this work, it is sufficient to consider the symmetrization of functions rather than functionals such that a generic solution for c can be readily given. For details, we refer the reader to Appendix D.

Having established a procedure for restoring rotation symmetry, we now apply our considerations to the effective action that has been generated by a CS flow. Specifically, we subject the loop function in Eq. (3.125) to the symmetrization procedure in order to remove the regulator-induced breaking of the chiral symmetry. This leads us to an average effective action, which is physically meaningful in the sense that it respects all symmetries of the classical action of our model, even for $H = 0$. Concretely, we obtain

$$\begin{aligned}\frac{1}{V_4}\Gamma_k^{(\mathrm{phys})}(\phi)\big|_{T,\mu} &= \frac{1}{V_4}\Gamma_{\Lambda_0}(\phi) - 8N_{\mathrm{c}}\,L_k^{(\mathrm{sym})}(\Lambda_0, h^2\phi^2)\big|_{T,\mu} \\ &= \frac{1}{V_4}\Gamma_{\Lambda_0}(\phi) - 8N_{\mathrm{c}}\Big(\mathcal{S}\,L_k^{(\mathrm{CS})}\big|_{T,\mu} + \mathcal{S}\,\mathrm{CT}_k\Big)(\Lambda_0, h^2\phi^2)\,,\end{aligned} \tag{3.132}$$

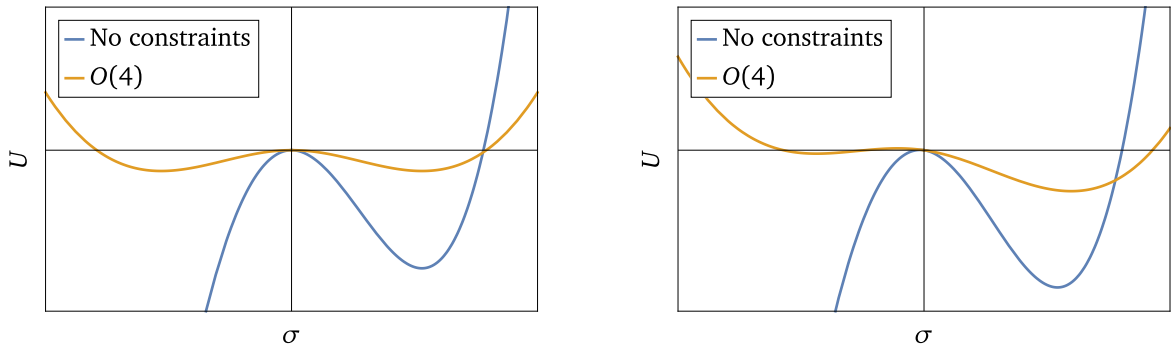

Figure 3.12: The effective potential of the quark-meson model computed at $T = \mu = 0$ from the unconstrained Callan-Symanzik scheme (blue curve) as well as the symmetrized one (orange curve). We present results for the effective potential in the absence of physical symmetry breaking, i.e., at $H = 0$, (left panel) as well as for $H > 0$ (right panel).

where

$$\begin{aligned}\left(\mathcal{S}L_k^{(\mathrm{CS})}\right)(\Lambda_0,\chi)\big|_{T,\mu} &= \frac{1}{2}\int_{\vec{p}}\frac{1}{\beta}\sum_{n\in\mathbb{Z}}\ln\left((\nu_n+\mathrm{i}\mu)^2+\vec{p}^{\,2}+k'^2+\chi\right)\Big|_{k'=\Lambda_0}^{k'=k}\\ &= \frac{1}{(2\pi)^2}\int_0^\infty \mathrm{d}p\; p^2\left\{\sqrt{p^2+k'^2+\chi}+\frac{1}{\beta}\sum_{\pm}\ln\left(1+\mathrm{e}^{-\beta(\sqrt{p^2+k'^2+\chi}\pm\mu)}\right)\right\}\Bigg|_{k'=\Lambda_0}^{k'=k}.\end{aligned} \tag{3.133}$$

A comparison with the asymmetric expression (3.125) shows that the symmetrization procedure has successfully removed the symmetry-breaking terms $\sim \sigma k$ from the integrand of the loop integral. We add that the term Γ_{Λ_0} can still contain a term that is linear in the sigma field, controlling the amount of physical explicit symmetry breaking. Otherwise, the initial condition to the Wetterich equation is invariant with respect to orthogonal transformations of the meson fields, see Eq. (3.34).

For another illustration of the impact of our symmetrization procedure, we also visually compare the effective potentials in Fig. 3.12. Concretely, we show the vacuum effective potential at $k = 0$ for the unphysical case, in which no symmetry constraints have been taken into account, as well as the $O(4)$-symmetrized scenario. The initial condition has been chosen such that it is quadratic in the fields at the most and reproduces a standard value for the quark mass. We observe that the effective potential as generated by the unconstrained CS flow is significantly affected by artificial symmetry breaking. More specifically, the regulator-induced symmetry breaking renders the effective potential unbounded from below and completely dominates the behavior of the system at the local minimum, even for $H > 0$. After the symmetrization, the effective potential takes the form as expected for a physical system. Moreover, the minima are less pronounced as for the unconstrained case.

We emphasize that it is not sufficient to restore only $\mathbb{Z}_2$ symmetry in the σ-direction since reflection symmetry for each field degree of freedom does not ensure rotation symmetry among the fields. For simplicity of notation, we drop dependences on external parameters for the following discussion. Concretely, it holds that

$$L_k^{(\mathrm{refl})}(\Lambda_0,h^2\sigma^2,h^2\vec{\pi}^2) := \frac{1}{2}\left(L_k(\Lambda_0,h\phi)+L_k(\Lambda_0,h\phi)\Big|_{\sigma\to-\sigma}\right) \neq L_k^{(\mathrm{sym})}(\Lambda_0,h^2\phi^2)\,. \tag{3.134}$$

Notice that this inequality remains true even in the absence of pion fields. Assuming the loop function to be analytic, it holds for all natural numbers n that

$$\frac{1}{2}\Big((h\sigma+k)^{2n}+(-h\sigma+k)^{2n}\Big)-\Big((h\sigma)^2+k^2\Big)^n=\sum_{\kappa=0}^{n}\left[\binom{2n}{2\kappa}-\binom{n}{\kappa}\right](h\sigma)^{2\kappa}k^{2(n-\kappa)} \tag{3.135}$$

such that

$$\forall n\in\mathbb{N}_{\geq 2}: \qquad \frac{1}{2}\Big((h\sigma+k)^{2n}+(-h\sigma+k)^{2n}\Big)\neq\Big((h\sigma)^2+k^2\Big)^n\,. \tag{3.136}$$

This means that the reflection-symmetric version of the CS loop function still has artificial scale dependences that can spoil results for physical observables. To give a concrete example, the critical temperature for the chiral phase transition as computed from the quark-meson model with a reflection-symmetric CS scheme would be different for the σ- and $\vec{\pi}$-directions of field space.

Two-point functions

Correlation functions can be conveniently obtained from an expansion of the effective action in terms of fluctuation fields $\Phi_{\mathrm{fl}}(x)=\Phi(x)-\Phi_0$ around $\Phi_{\mathrm{fl}}(x)=0$, where Φ_0 denotes the homogeneous ground state. This is often referred to as a vertex expansion, see Section 2.2.3 for details. In our truncation scheme, the vertex expansion of the vacuum effective action in momentum space reads

$$\Gamma_k[\,\phi\,]=\text{const.}+\int_P \phi_{\mathrm{fl}}^{\intercal}(-P)\;\Gamma_k^{(1)}(P)+\frac{1}{2}\int_P\int_Q \phi_{\mathrm{fl}}^{\intercal}(-P)\;\Gamma_k^{(2)}(P,Q)\;\phi_{\mathrm{fl}}(Q)+\mathcal{O}\big[\phi_{\mathrm{fl}}^3\big]\,. \tag{3.137}$$

If chiral symmetry is intact, it follows that all odd-numbered correlation functions vanish for $\phi_0=0$. However, when the invariance of the theory under axial-vector transformations is explicitly broken by the presence of a fermionic mass term, the effective action receives finite contributions from terms of all orders in the fluctuation fields. We highlight that a fermion mass leaves the $SU(N_{\mathrm{f}})_{\mathrm{V}}$ symmetry of the theory intact. Consequently, the vector-valued one-point function is always zero along the pionic directions of meson field space but may exhibit a non-zero contribution along the σ-direction. Symmetry considerations further imply that the physical meson two-point function is diagonal in field space and that its diagonal elements are identical within the subspace of the pions. In the limit of a vanishing fermion mass, this two-point function becomes degenerate among the mesons such that its matrix structure reduces to the unit matrix. Given the importance of the two-point function for the computation of curvature masses and spectral functions, we will now focus on it in more detail.

From the expansion above, it follows that the two-point correlator is in general given by

$$\Gamma_k^{(2)}(P,Q)\big|_{T,\mu}=\tilde{\Gamma}_k^{(2)}(Q)\big|_{T,\mu}\,\beta\delta_{P^0Q^0}\,(2\pi)^3\delta^{(3)}(\vec{P}-\vec{Q})=\left(\frac{\delta}{\delta\phi_{\mathrm{fl}}^{\intercal}(-P)}\frac{\delta}{\delta\phi_{\mathrm{fl}}(Q)}\Gamma_k[\,\phi\,]\big|_{T,\mu}\right)\bigg|_{\phi_{\mathrm{fl}}=0}\,. \tag{3.138}$$

For simplicity, we have suppressed external Matsubara indices $M,N\in\mathbb{Z}$ for the bosonic time-like momenta, i.e., $P^0\equiv P_M^0$ and $Q^0\equiv Q_N^0$, such that $\delta_{P^0Q^0}\equiv\delta_{MN}$. For our quark-meson model, the reduced two-point correlation function as generated by the Callan-Symanzik flow reads

$$\begin{aligned}\tilde{\Gamma}_k^{(2)}(Q)\big|_{T,\mu}&=\tilde{\Gamma}_{\Lambda_0}^{(2)}(Q)+\int_{\Lambda_0}^{k}\mathrm{d}k'\;\partial_{k'}\tilde{\Gamma}_{k'}^{(2)}\big(Q,m_q(T,\mu)\big)\big|_{T,\mu}\\&=\tilde{\Gamma}_{\Lambda_0}^{(2)}(Q)+\int_{\Lambda_0}^{k}\mathrm{d}k'\;\partial_{k'}\tilde{\Gamma}_{k'}^{(2)(\mathrm{CS})}\big(Q,m_q(T,\mu)\big)\big|_{T,\mu}-8N_{\mathrm{c}}\left(\frac{\mathrm{d}}{\mathrm{d}\phi^{\intercal}}\frac{\mathrm{d}}{\mathrm{d}\phi}\mathrm{CT}_k(\Lambda_0,h\phi)\right)\bigg|_{\phi=\phi_0}\,,\end{aligned} \tag{3.139}$$

where

$$\partial_k \tilde{\Gamma}_k^{(2)(\mathrm{CS})}(Q,m)\big|_{T,\mu} = -8N_c h^2 \int_{\vec{p}} \frac{1}{\beta} \sum_{n\in\mathbb{Z}} \partial_k \frac{p_n^{\intercal}(\beta,\mu)\,(p_n(\beta,\mu)+Q)\,\mathbb{1}_{4\times4} - (m+k)^2\,\eta}{\left(p_n^2(\beta,\mu)+(m+k)^2\right)\left((p_n(\beta,\mu)+Q)^2+(m+k)^2\right)} \tag{3.140}$$

and

$$p_n^{\intercal}(\beta,\mu) = (\nu_n(\beta) + \mathrm{i}\mu, \vec{p}^{\intercal}) \,, \qquad \beta = \frac{1}{T} \,, \qquad \eta = \mathrm{diag}(+,-,-,-) \,. \tag{3.141}$$

It is worth mentioning that our counterterms do not receive corrections in the presence of finite external momenta. Consequently, we can use Eq. (3.121) to render also the momentum-dependent correlation functions UV finite. The ground state ϕ_0 as determined by the effective potential defines the dynamical quark mass m_q. In systems with a physical source of explicit symmetry breaking, the ground state is always finite, i.e., $\sigma_0 > 0$, resulting in a positive quark mass. However, particular care is needed when determining the quark mass in the presence of the CS regulator. This is because the global minimum of the effective potential may lie at negative values in field space, see Fig. 3.12. In such cases, one may anchor the definition of the quark mass at a local minimum that is positive. Nevertheless, this local minimum does not represent the true ground state of the system such that inconsistencies may arise in the computation of observables. In any case, from the action of our quark-meson model, we would expect that the loop contribution is invariant under $m_q \to -m_q$ and that the meson two-point functions agree identically in the limit $m_q \to 0$. However, due to the presence of the CS regulator, this is clearly not the case here. Importantly, the CS regulator affects the results not only in the massless limit but also for $m_q \neq 0$. In fact, the CS regulator always gives rise to an unphysical breaking of chiral symmetry.

As in the case of the effective potential, we can systematically remove the regulator-induced breaking of the chiral symmetry to obtain meson two-point functions that respect the global $O(4)$ symmetry. We begin with a general analysis of the structure of the effective action. Intact chiral symmetry for the quantum loop implies that there exists a $\hat{\Gamma}$ such that

$$\lim_{H\to 0} \Gamma_k^{(\mathrm{phys})}[\phi] = \hat{\Gamma}_k[\phi^2] \,. \tag{3.142}$$

In contrast to the effective potential, our truncation scheme does not allow us to calculate the full effective average action for momentum-dependent fields. As a result, it is not feasible to apply our symmetrization procedure to the action functional to obtain physical momentum-dependent correlation functions through an appropriate projection. Instead, we adopt the equivalent strategy of removing the artificial symmetry breaking after the correlation function has been obtained. To this end, we consider a generalized homogeneous background

$$\overline{\varphi}^{\intercal} = (\overline{\sigma}, \overline{\pi}_1, \overline{\pi}_2, \overline{\pi}_3) \tag{3.143}$$

for the meson fields. Recall that the parameter H controlling the physical amount of explicit symmetry breaking does not explicitly enter the two-point function since a term linear the fields does not survive the second derivative. The generalized two-point function as obtained from the physical effective action can then be cast into the form

$$\Gamma_{k,\mathrm{gen}}^{(\mathrm{phys})(2)}(\overline{\varphi}) = \left(\frac{\delta}{\delta\phi^{\intercal}}\frac{\delta}{\delta\phi}\Gamma_k^{(\mathrm{phys})}[\phi]\right)\Big|_{\phi=\overline{\varphi}} = A_k^{(\mathrm{sym})}(\overline{\varphi})\,\mathbb{1}_{4\times4} + B_k^{(\mathrm{sym})}(\overline{\varphi})\,\overline{\varphi}\,\overline{\varphi}^{\intercal} \,, \tag{3.144}$$

where we have dropped any arguments indicating dependences on external momenta for convenience. The scalar functions are given by

$$A_k^{(\mathrm{sym})}(\overline{\varphi}) = 2\left(\frac{\delta}{\delta\Theta}\hat{\Gamma}_k[\Theta]\right)\Big|_{\Theta=\overline{\varphi}^2}, \qquad B_k^{(\mathrm{sym})}(\overline{\varphi}) = 4\left(\frac{\delta^2}{\delta\Theta^2}\hat{\Gamma}_k[\Theta]\right)\Big|_{\Theta=\overline{\varphi}^2}. \tag{3.145}$$

We observe that an intact chiral symmetry translates into an $O(4)$ symmetry among the field directions of the generalized background within the contributions $A_k^{(\mathrm{sym})}$ and $B_k^{(\mathrm{sym})}$. Imposing chiral symmetry is then equivalent to requiring that the two-point function assumes the form (3.144). In order to obtain the physical two-point function, i.e., the two-point function with removed regulator-induced symmetry breaking, we compute the corresponding coefficients for our CS scheme,

$$B_k(\overline{\varphi}) = \frac{h}{(h\overline{\sigma}+k)\overline{\pi}_i}\Gamma^{(2)}_{k,\sigma\pi_i}(\overline{\varphi}), \tag{3.146}$$

$$\begin{aligned} A_k(\overline{\varphi}) &= \Gamma^{(2)}_{k,\sigma\sigma}(\overline{\varphi}) - \frac{(h\overline{\sigma}+k)^2}{h^2}B_k(\overline{\varphi}) \\ &= \Gamma^{(2)}_{k,\pi_i\pi_i}(\overline{\varphi}) - \overline{\pi}_i^2\, B_k(\overline{\varphi}), \end{aligned} \tag{3.147}$$

and symmetrize their dependence on the background according to Eq. (3.131),

$$A_k^{(\mathrm{sym})} = \mathcal{S}A_k, \qquad B_k^{(\mathrm{sym})} = \mathcal{S}B_k. \tag{3.148}$$

From this, we can then reconstruct the generalized and symmetrized two-point function in accordance with Eq. (3.144). Finally, setting the generalized background equal to the ground state yields the symmetrized version of Eq. (3.139),

$$\Gamma_k^{(\mathrm{phys})(2)} = \Gamma_{k,\mathrm{gen}}^{(\mathrm{phys})(2)}(\overline{\varphi}=\phi_0). \tag{3.149}$$

Specifically, applying our line of argumentation above, we obtain the physical two-point function

$$\begin{aligned} \tilde{\Gamma}_k^{(\mathrm{phys})(2)}(Q)\big|_{T,\mu} &= \tilde{\Gamma}^{(2)}_{\Lambda_0}(Q) + \int_{\Lambda_0}^{k}\mathrm{d}k'\,\partial_{k'}\tilde{\Gamma}^{(\mathrm{phys})(2)}_{k'}\left(Q, m_q^2(T,\mu)\right)\big|_{T,\mu} \\ &= \tilde{\Gamma}^{(2)}_{\Lambda_0}(Q) + \int_{\Lambda_0}^{k}\mathrm{d}k'\,\partial_{k'}\tilde{\Gamma}^{(\mathrm{phys})(2)(\mathrm{CS})}_{k'}\left(Q, m_q^2(T,\mu)\right)\big|_{T,\mu} \\ &\quad - 8N_c\left(\frac{\mathrm{d}}{\mathrm{d}\phi^{\intercal}}\frac{\mathrm{d}}{\mathrm{d}\phi}\left(\mathcal{S}\,\mathrm{CT}_k\right)(\Lambda_0, h^2\phi^2)\right)\Big|_{\phi=\phi_0}, \end{aligned} \tag{3.150}$$

where

$$\partial_k\tilde{\Gamma}_k^{(\mathrm{phys})(2)(\mathrm{CS})}(Q,m^2)\big|_{T,\mu} = -8N_c h^2\int_{\vec{p}}\frac{1}{\beta}\sum_{n\in\mathbb{Z}}\partial_k\frac{\left(p_n^{\intercal}(\beta,\mu)\left(p_n(\beta,\mu)+Q\right)+k^2\right)\mathbb{1}_{4\times4} - m^2\,\eta}{\left(p_n^2(\beta,\mu)+k^2+m^2\right)\left((p_n(\beta,\mu)+Q)^2+k^2+m^2\right)}. \tag{3.151}$$

Compared to Eq. (3.140), the sign structure in the numerator of the two-point function has changed for the σ meson but not in the pion subspace. This demonstrates that our symmetrization procedure respects the condition (3.130), meaning it takes the fact into account that the CS regulator leaves the $SU(2)_{\mathrm{V}}$ symmetry of the theory intact. In addition, because of the restoration of global $O(4)$ symmetry, the two-point functions now agree for $m_q \to 0$ and exhibit the invariance under $m_q \to -m_q$.

As in the case of the effective potential, we always evaluate the Matsubara sum for the two-point functions analytically. This step is essential for, e.g., the investigation of spectral functions and transport coefficients. Specifically, for $\vec{Q}=\vec{0}$ it follows from Eq. (3.150) that

$$\begin{aligned}&\lim_{\vec{Q}\to\vec{0}}\partial_k\tilde{\Gamma}_k^{(\mathrm{phys})(2)(\mathrm{CS})}(Q,m^2)\big|_{T,\mu}\\&\quad=-\frac{2N_c h^2}{\pi^2}\int_0^\infty \mathrm{d}p\; p^2\;\partial_k\left[\frac{2E_k^2(p)\,\mathbb{1}_{4\times4}-m^2(\mathbb{1}_{4\times4}+\eta)}{E_k(p)\left(4E_k^2(p)+(Q^0)^2\right)}\sum_{\pm}\tanh\left(\frac{E_k(p)\pm\mu}{2T}\right)\right],\end{aligned}\tag{3.152}$$

where we have used that

$$E_k(p)=\sqrt{p^2+k^2+m^2}\,.\tag{3.153}$$

We would like to highlight that the structure of this contribution to the meson two-point function matches that of Eq. (3.113), where a spatial polynomial regulator was used. This consistency arises because, like the CS regulator, spatial regulator functions do not generate additional poles in the complex p^0-plane of the propagator. The only difference between these results lies in the scheme dependence of the regularized fermion energy E_k. In the case of the CS regulator, the k-dependence fails to render the two-point correlation functions UV finite such that additional counterterms are necessary. Analogous to our analysis in Section 3.2.3, we observe that the loop integral above, after the analytic continuation $Q^0\to \mathrm{i}\omega$, develops an integrable pole at

$$p_k^*=\sqrt{\frac{\omega^2}{4}-k^2-m^2}\,.\tag{3.154}$$

As a result, the meson two-point functions become non-analytic at those critical values ω_c for which the pole enters or exits the domain of integration. These values of the Minkowskian energy variable are then associated with decay processes of the mesons into energetically more favorable states. As before, for $k=\mu=0$, we find $\omega_c=2m$ such that $p^*=0$. At finite chemical potential and $k=T=0$, the critical value reads $\omega_c=2\max(m,\mu)$, resulting in a pole at $p^*=\theta(\mu-m)\,p_F$. For values of the chemical potential beyond the Silver-Blaze threshold $\mu_{SB}=m$, this pole position corresponds exactly to the Fermi momentum $p_F=\sqrt{\mu^2-m^2}$.

3.3.3 Analytical zero-temperature results

At finite temperature, it is not possible to calculate the entire two-point function in closed form. This means that, once the Matsubara sum has been performed analytically, the remaining integral with respect to the spatial momenta has to be evaluated numerically. In the case of zero temperature, however, the situation is different. In the following, we present analytic results from calculations performed in the symmetrized CS scheme at zero temperature and finite chemical potential, $\mu\geq 0$. For the fully momentum-dependent two-point functions of the mesons, we obtain

$$\tilde{\Gamma}_k^{(\mathrm{phys})(2)}(Q)\big|_\mu=\tilde{\Gamma}_{\Lambda_0}^{(2)}(Q)-8N_c h^2\left[\mathcal{I}_x(Q,m_q(\mu))-\mathcal{M}_x^{(2)}(Q,\mu,m_q(\mu))\right]\Big|_{x=\sqrt{\Lambda_0^2+m_q^2(\mu)}}^{x=\sqrt{k^2+m_q^2(\mu)}},\tag{3.155}$$

where we have parameterized the momentum-dependent vacuum loop contribution as

$$\begin{aligned}\mathcal{I}_x(Q,m)=\frac{1}{16\pi^2}\Bigg\{&\mathbb{1}_{4\times4}\,x^2\ln\left(\frac{x^2}{\Lambda_0^2}\right)+\frac{Q^2\,\mathbb{1}_{4\times4}+2m^2(\mathbb{1}_{4\times4}+\eta)}{4}\times\\&\times\left[2\ln\left(\frac{x^2}{\Lambda_0^2}\right)-\frac{\sqrt{Q^2+4x^2}}{Q}\ln\left(\frac{(\sqrt{Q^2+4x^2}-Q)x^2}{(\sqrt{Q^2+4x^2}+Q)(Q^2+x^2)+2Qx^2}\right)\right]\Bigg\}\,.\end{aligned}\tag{3.156}$$

In our calculation, the vacuum loop $\mathcal{I}_x$ contains the scale Λ_0, irrespective of the value of x. Accordingly, this scale dependence does not result from initializing the CS flow at $k = \Lambda_0$ but stems from our choice of the counterterms with $s = \Lambda_0$, see Eq. (3.121). The matter part corresponding to the meson two-point functions reads

$$\mathcal{M}_x^{(2)}(Q,\mu,m) = \frac{\theta(\mu-x)}{8\pi^2}\left\{\mathbb{1}_{4\times4}\left[\mu\sqrt{\mu^2-x^2} - x^2\,\mathrm{artanh}\left(\frac{\sqrt{\mu^2-x^2}}{\mu}\right)\right] + \frac{Q^2\,\mathbb{1}_{4\times4} + 2m^2(\mathbb{1}_{4\times4}+\eta)}{4}\times\right.$$
$$\times\left[\frac{\mu}{|\vec{Q}|}\ln\left(\frac{4\mu^2Q_0^2 + \left(Q^2 - 2|\vec{Q}|\sqrt{\mu^2-x^2}\right)^2}{4\mu^2Q_0^2 + \left(Q^2 + 2|\vec{Q}|\sqrt{\mu^2-x^2}\right)^2}\right) - \frac{|Q_0|}{|\vec{Q}|}\left(\arctan\left(\frac{Q^4 + 4x^2\vec{Q}^2 + 4\mu^2(Q_0^2-\vec{Q}^2)}{8|Q_0||\vec{Q}|\,\mu\sqrt{\mu^2-x^2}}\right) - \frac{\pi}{2}\right)\right.$$
$$\left.\left. + \frac{\sqrt{Q^2+4x^2}}{2Q}\ln\left(\frac{4x^4Q_0^2 + Q^2\left(Q\mu + \sqrt{\mu^2-x^2}\sqrt{Q^2+4x^2}\right)^2}{4x^4Q_0^2 + Q^2\left(Q\mu - \sqrt{\mu^2-x^2}\sqrt{Q^2+4x^2}\right)^2}\right) - 2\ln\left(\frac{\mu+\sqrt{\mu^2-x^2}}{x}\right)\right]\right\}. \tag{3.157}$$

Since we restrict the values of the chemical potential to $\mu < \Lambda_0$ in our study of the quark-meson model, the Λ_0-dependent contribution from the matter part always evaluates to zero. For the sake of completeness, it is also worth mentioning that the results for the μ-dependent part of the zero-temperature polarization tensor of QCD as found by Toimela [426] exhibit a structure that is similar to the matter part shown above.

We begin the analysis of our results by noting that the vacuum contribution $\mathcal{I}_x$ to the two-point functions of the mesons can only be expanded in powers of Q around $Q = 0$ for $x > 0$, i.e., we must have either $k > 0$ or $m_q > 0$. Notice that this property has direct implications for quantities that are commonly obtained from the effective action by means of a derivative expansion. Specifically, as the vacuum loop becomes non-analytic in Q for $k = m_q = 0$, wavefunction renormalization factors cannot be defined in this case by an expansion of the two-point functions in Q around $Q = 0$ up to second order. We will come back to this issue further below when presenting explicit expressions for the wavefunction renormalizations at zero temperature. Nevertheless, the unexpanded expressions for the vacuum two-point functions are well-defined in the limits $k \to 0$ and $m_q \to 0$, where the latter two limits also commute.

The matter part $\mathcal{M}_x^{(2)}$ of the meson two-point functions is divergent for $k = m_q = 0$, provided that external momenta are finite. In addition, the matter part exhibits non-analyticities in the momenta which cannot be avoided by a finite quark mass or a finite value of the RG scale. To be specific, we observe that the matter part for values of the external three-momentum $\vec{Q}$ with $0 < |\vec{Q}| \leq 2\sqrt{\mu^2-x^2}$ is non-analytic in $Q^0 = 0$. This property restricts the values of $\vec{Q}$ for which an analytic continuation of the zero-temperature theory back to Minkowski spacetime can be reliably performed. Notice that this aspect is of particular importance for the computation of spectral functions. In our case, taking the value $\vec{Q} = \vec{0}$ is the most convenient choice for the presentation of spectral functions in the upcoming Sections 3.3.4 and 3.3.5.
Moreover, the explicitly μ-dependent function $\mathcal{M}_x^{(2)}$ at $Q^0 = 0$ is non-analytic in $|\vec{Q}| = 2\sqrt{\mu^2-x^2}$, which renders an expansion in spatial momenta $\vec{Q}$ generally ill-defined. At $k = 0$, this value of $|\vec{Q}|$ corresponds precisely to twice the Fermi momentum for massive quarks. We would like to point out that this property is directly connected to the phenomenon of Friedel oscillations [427–429] in the context of condensed-matter physics. Friedel oscillations describe the response of the particle density to a localized perturbation in systems of degenerate fermions and occur with a characteristic frequency of $2p_F$. As our two-point functions are generated by fermionic loops,

information about Friedel oscillations is naturally contained within our results. For more details on this subject, we refer to, e.g., Refs. [80, 430–434].

In contrast to the non-analytic, yet finite behavior of the meson correlation functions that we observe at zero temperature, a divergence has been found at $Q_0 = m_q = 0$ and $|\vec{Q}| = 2\mu$ in low-dimensional Gross-Neveu-type models [435–437]. The emergence of such a different behavior in low-dimensional models may not be too surprising since the number of spatial dimensions crucially controls the behavior of the loop integrals at those values of the external parameters where the corresponding integrand has a pole along the contour of integration. In other words, the origin of the observed non-trivial behavior of the correlation functions is the same but the pole structure of the underlying integrand manifests itself differently at the level of the integral, depending on the dimensionality of the theory.

Lastly, it is important to remark that the matter part $\mathcal{M}_x^{(2)}$ is discontinuous in $(Q^0, \vec{Q}) = (0, \vec{0})$ such that the limit $Q \to 0$ does no longer exist. This discontinuity directly translates to the full meson two-point functions for values of the chemical potential beyond the (scale-dependent) Silver-Blaze threshold, i.e., for $\mu \geq \sqrt{k^2 + m^2}$. As a consequence, the case of vanishing external momenta has then to be realized by an iterated limit, see Section 2.4 for details.

Curvature masses can be obtained from the momentum-dependent two-point correlator by considering the limit of vanishing momenta. However, the presence of a finite quark chemical potential explicitly breaks Lorentz invariance, leading to a two-point function that is sensitive to the specific order of the limits $Q^0 \to 0$ and $\vec{Q} \to \vec{0}$. In order to obtain results for the curvature masses that are consistent with those derived from the effective potential, we have to take the static limit, where Q_0 is set to zero first. Accordingly, the explicit zero-temperature curvature masses read

$$\begin{pmatrix} m_{\sigma,k}^2(\mu) & \vec{0}^\intercal \\ \vec{0} & m_{\pi,k}^2(\mu)\, \mathbb{1}_{3\times3} \end{pmatrix} = \lim_{Q\to 0}^{(\mathrm{st})} \tilde{\Gamma}_k^{(\mathrm{phys})(2)}(Q)\big|_\mu \equiv \lim_{\vec{Q}\to\vec{0}} \lim_{Q_0\to 0} \tilde{\Gamma}_k^{(\mathrm{phys})(2)}(Q)\big|_\mu \,, \tag{3.158}$$

where

$$\lim_{Q\to 0}^{(\mathrm{st})} \mathcal{I}_x(Q,m) = \frac{1}{16\pi^2}\left(\mathbb{1}_{4\times4}\, x^2 \ln\left(\frac{x^2}{\Lambda_0^2}\right) + m^2\,(\mathbb{1}_{4\times4} + \eta)\left[\ln\left(\frac{x^2}{\Lambda_0^2}\right) - 2\right]\right) , \tag{3.159}$$

$$\begin{aligned} \lim_{Q\to 0}^{(\mathrm{st})} \mathcal{M}_x^{(2)}(Q,\mu,m) = \frac{\theta(\mu-x)}{8\pi^2}\Bigg(& \mathbb{1}_{4\times4}\left[\mu\sqrt{\mu^2-x^2} - x^2\,\mathrm{artanh}\left(\frac{\sqrt{\mu^2-x^2}}{\mu}\right)\right] \\ & - m^2\,(\mathbb{1}_{4\times4} + \eta)\ln\left(\frac{\mu+\sqrt{\mu^2-x^2}}{x}\right)\Bigg) . \end{aligned} \tag{3.160}$$

We would like to remark that the vacuum loop $\mathcal{I}_x$ is, in fact, insensitive to the order in which the external momenta are taken to zero. Since Lorentz symmetry remains intact in the vacuum theory, the static and the plasmon limit yield the same results in this case.

The wavefunction renormalization factors associated with the meson fields can be obtained from the corresponding two-point functions by a suitable projection. This procedure usually includes taking derivatives with respect to momenta and also taking limits. We emphasize that, at zero temperature and for $\mu \geq \sqrt{k^2 + m^2}$, it is not allowed to interchange this projection onto the wavefunction renormalizations and the integration over the time-like loop momenta. In any case, we only consider wavefunction renormalizations associated with modes perpendicular to the particle

reservoir:[17]

$$\begin{pmatrix} Z^{\perp}_{\sigma,k}(\mu) & \vec{0}^{\intercal} \\ \vec{0} & Z^{\perp}_{\pi,k}(\mu)\,\mathbb{1}_{3\times3} \end{pmatrix} = \lim_{Q\to0}^{(\mathrm{st})} \frac{1}{2}\frac{\partial^2}{\partial|\vec{Q}|^2}\tilde{\Gamma}^{(\mathrm{phys})(2)}_k(Q)\Big|_\mu \,. \tag{3.161}$$

The computation of the right-hand side of this equation requires to compute derivatives of the vacuum contribution and the chemical potential dependent contribution to the two-point functions of the mesons:

$$\lim_{Q\to0}^{(\mathrm{st})} \frac{1}{2}\frac{\partial^2}{\partial|\vec{Q}|^2}\mathcal{I}_x(Q,m) = \frac{1}{32\pi^2}\left(\mathbb{1}_{4\times4}\left(2+\ln\left(\frac{x^2}{\Lambda_0^2}\right)\right)+(\mathbb{1}_{4\times4}+\eta)\frac{m^2}{3x^2}\right), \tag{3.162}$$

$$\lim_{Q\to0}^{(\mathrm{st})} \frac{1}{2}\frac{\partial^2}{\partial|\vec{Q}|^2}\mathcal{M}^{(2)}_x(Q,\mu,m) = \frac{\theta(\mu-x)}{16\pi^2}\left(-\mathbb{1}_{4\times4}\ln\left(\frac{\mu+\sqrt{\mu^2-x^2}}{x}\right)+(\mathbb{1}_{4\times4}+\eta)\frac{m^2\,\mu}{6x^2\sqrt{\mu^2-x^2}}\right). \tag{3.163}$$

As in our computation of the curvature masses, we again need to take an iterated limit here since the behavior of the two-point functions at the origin of momentum space becomes discontinuous once we consider finite external parameters

For our analysis of results for the wavefunction renormalization factors, let us begin by considering the vacuum case. In particular, vanishing external parameters, $T=\mu=0$, lead to a restoration of Lorentz symmetry such that perpendicular and parallel wavefunction renormalizations agree. At $k=0$, we have

$$Z^{\perp}_{(\sigma/\pi)} = Z^{\parallel}_{(\sigma/\pi)} \equiv Z_{(\sigma/\pi)} \tag{3.164}$$

with

$$\begin{aligned}\begin{pmatrix} Z_\sigma & \vec{0}^{\intercal} \\ \vec{0} & Z_\pi\,\mathbb{1}_{3\times3} \end{pmatrix} &= \lim_{Q\to0}\frac{1}{2}\frac{\mathrm{d}^2}{\mathrm{d}|Q|^2}\tilde{\Gamma}^{(\mathrm{phys})(2)}_0(Q) \\ &= Z_{\Lambda_0}\,\mathbb{1}_{4\times4} + \frac{N_c h^2}{4\pi^2}\left(\mathbb{1}_{4\times4}\ln\left(1+\frac{\Lambda_0^2}{m_q^2}\right)-\frac{\mathbb{1}_{4\times4}+\eta}{3}\frac{\Lambda_0^2}{m_q^2+\Lambda_0^2}\right).\end{aligned} \tag{3.165}$$

We would like to highlight that the vacuum wavefunction renormalizations carry a logarithmic divergence in the limit $m_q\to0$. This divergence originates from the fact that our projection prescription for the wavefunction renormalization is anchored at a point in momentum space at which the meson two-point functions are non-analytic. Specifically, as the vacuum loop $\mathcal{I}_x$ for $k=m_q=0$ has no well-defined expansion in momenta around $Q=0$, applying derivatives leads to divergences at this point. In addition, we observe that

$$\lim_{m_q\to0}(Z_\pi - Z_\sigma) = \frac{N_c h^2}{6\pi^2}\lim_{m_q\to0}\frac{\Lambda_0^2}{m_q^2+\Lambda_0^2} = \frac{N_c h^2}{6\pi^2} \neq 0\,. \tag{3.166}$$

In words, the vacuum wavefunction renormalizations at $k=0$ do not agree in the chiral limit. This surprising phenomenon can be traced back to the fact that the general expression for the corresponding vacuum contribution is discontinuous in the space of fermion masses. Specifically,

[17] We may in principle also consider the wavefunction renormalization factors which are aligned parallel to the direction of momentum space that is characterized by a finite chemical potential. These quantities can be defined via the second derivative with respect to the time-like momentum Q^0. Nevertheless, a concrete examination of these wavefunction renormalizations is beyond the scope of this work. For further discussions, see, e.g., Ref. [236].

at some finite RG scale k, the second term in Eq. (3.162) is sensitive to the order in which the mass scales are taken to zero:

$$\lim_{k\to 0}\lim_{m_q\to 0}\frac{m_q^2}{k^2+m_q^2} \neq \lim_{m_q\to 0}\lim_{k\to 0}\frac{m_q^2}{k^2+m_q^2}\,. \tag{3.167}$$

When taking the limit $m_q \to 0$ before setting the RG scale to zero, the difference in the vacuum wavefunction renormalizations indeed vanishes. In fact, the difference vanishes in the chiral limit for all $k > 0$. Therefore, we classify the breakdown of chiral symmetry at $k = 0$ indicated by Eq. (3.166) as a new artifact that is specific to Callan-Symanzik-type regulator functions. We emphasize that this CS artifact does not indicate a failure of our symmetrization procedure. In fact, the unexpanded vacuum expressions for the meson two-point functions, see Eq. (3.156), are well-defined and identical in the limit as the mass scales tend to zero. Despite the appearance of this new artifact, its impact on our studies is expected to be small for two reasons. Firstly, the scenario $m_q = \mu = T = 0$ is not realized within our quark-meson model. Secondly, any finite contributions from the CS artifact are entirely overshadowed by the logarithmic divergence in Eq. (3.165) as $m_q \to 0$. After all, if both mass scales go to zero, an expansion of the two-point functions around $Q = 0$ breaks down and thus cannot provide us with a meaningful description of wavefunction renormalizations.

In the presence of a finite chemical potential, the matter part as given in Eq. (3.163) must be taken into account. The first term of this contribution to the μ-dependent wavefunction renormalization is negative since the logarithm associated with this term is positive for all $\mu > x$. This leads to a continuous decrease of the wavefunction renormalizations as we increase the chemical potential beyond the Silver-Blaze threshold. Depending on the initial value Z_{Λ_0} and the Yukawa coupling h, the wavefunction renormalizations can therefore become negative. Provided that the theory is stable, negative wavefunction renormalization factors generally indicate a non-trivial minimum of the meson two-point correlators in momentum space, see, e.g., Ref. [243]. An accurate description of the physics at the ground state of the system then in principle requires a generalization of the projection according to

$$\begin{pmatrix} Z^{\perp}_{\sigma,k}(\mu) & \vec{0}^{\intercal} \\ \vec{0} & Z^{\perp}_{\pi,k}(\mu)\,\mathbb{1}_{3\times 3}\end{pmatrix} = \lim_{\vec{Q}\to\vec{Q}_{\min}}\lim_{Q^0\to 0}\frac{1}{2}\frac{\partial^2}{\partial|\vec{Q}|^2}\tilde{\Gamma}_k^{(\mathrm{phys})(2)}(Q)\Big|_{\mu}\,. \tag{3.168}$$

However, an analysis of results obtained by this projection is beyond the scope of this work. In addition, it follows from the second term in Eq. (3.163) that the wavefunction renormalization associated with the sigma meson exhibits a singular behavior at the Fermi surface. Specifically, the relation

$$Z^{\perp}_{\sigma}(\mu) \propto \frac{N_c h^2}{6\pi^2}\frac{\mu}{\sqrt{\mu^2 - m_q^2(\mu)}}\,\theta\left(\mu - m_q(\mu)\right) \tag{3.169}$$

shows that $Z^{\perp}_{\sigma}$ diverges at $\mu = \mu_{\mathrm{SB}} = m_q(\mu = 0)$. This divergence originates from the non-analytic behavior of the matter part $\mathcal{M}^{(2)}_x$, see Eq. (3.157), in $|\vec{Q}| = 2\sqrt{\mu^2 - x^2}$ when $Q^0 = 0$. Once again, the derivative operators used in our projection procedure for the wavefunction renormalization factors generate divergences at points in parameter space where the underlying two-point correlator is not differentiable. To further address this issue, one might consider using finite differences instead of derivatives, see, e.g., Ref. [314]. Interestingly, the wavefunction renormalization associated with the pions remains well-behaved at the Fermi surface.

3.3.4 Curvature masses and spectral functions

So far, we have developed an fRG framework for the quark-meson model in which Callan-Symanzik flows are UV finite and even respect chiral symmetry. As a next step, we aim to apply this CS framework to the calculation of concrete physical observables. With a focus on the phenomenological study of the QCD phase diagram, we present results for the curvature masses and spectral functions of the sigma meson and the pions. Moreover, we emphasize the importance of a meaningful implementation of the CS regulator in theories with fermions. Therefore, we shall illustrate in detail the necessity of symmetry constraints and also demonstrate the relevance of an RG-consistent construction of the effective action for studies at finite temperature and chemical potential.

Scale fixing

In our numerical study of low-energy QCD by means of the CS framework, we need to specify not only the initialization scale Λ_0 of the RG flow but also assign concrete values to the free parameters of our theory. For the initial condition Γ_{Λ_0} of the Wetterich equation, we use the ansatz (3.33) in case of our symmetry-constrained CS scheme and choose $Z_{\Lambda_0} = 1$. Furthermore, the mass parameter $m^2_{\Lambda_0}$, the Yukawa coupling h as well as the symmetry-breaking parameter H are tuned such that a given set of low-energy observables is recovered. In the case of the Callan-Symanzik regulator, the RG scale directly corresponds to a mass scale. Therefore, when solving the Wetterich equation, we could in principle stop the fermionic CS flow at some finite value $k_{\min} > 0$ which may be associated with the physical current mass of the light quarks, $k_{\min} = m_{\text{curr}}$. In our approach, however, we always assume that the entire amount of physical explicit symmetry breaking is carried by the parameter H. Thus, we take $k = 0$ as the point at which each observable is assigned its corresponding physical value.

Our scale-fixing procedure here closely follows that of Section 3.2. Nevertheless, let us repeat the most important aspects for clarity. In the chiral limit, $H = 0$, we fix the couplings in the initial action such that we obtain specific values for the constituent quark mass and the pion decay constant at $k = T = \mu = 0$. In the context of our quark-meson model, these quantities are assumed to satisfy the following general relations:

$$m_q = h|\sigma_0| \,, \qquad f_\pi = \frac{m_q}{h} \,. \tag{3.170}$$

Again, σ_0 denotes the ground state of the system and is assumed to be homogeneous. Once specific values for the quark mass and the pion decay constant have been chosen, they consistently fix the Yukawa coupling and the meson mass parameter. As before, we will use a hat notation to refer to these special values. It then directly follows from Eq. (3.170) that the Yukawa constant is simply given by $h = \hat{m}_q/\hat{f}_\pi$. The minimum condition applied to the physical effective potential at $H = 0$ then determines the mass parameter as

$$\begin{aligned} m^2_{\Lambda_0} &= 16 N_c h^2 \left(\frac{\mathrm{d}}{\mathrm{d}\chi} L_0^{(\mathrm{sym})}(\Lambda_0, \chi) \right) \Big|_{\chi = \hat{m}_q^2} \\ &= \frac{N_c h^2}{2\pi^2} \left[\hat{m}_q^2 \, \ln\left(\frac{\hat{m}_q^2}{\Lambda_0^2} \right) - \left(\hat{m}_q^2 + \Lambda_0^2 \right) \ln\left(1 + \frac{\hat{m}_q^2}{\Lambda_0^2} \right) \right] . \end{aligned} \tag{3.171}$$

The specific values are chosen to be

$$\Lambda_0 = 500\,\mathrm{MeV} \,, \qquad \hat{m}_q = 265\,\mathrm{MeV} \,, \qquad \hat{f}_\pi = 90\,\mathrm{MeV} \,. \tag{3.172}$$

Our choice for the quark mass here may be considered less common in the context of QCD phenomenology compared to the value presented in Section 3.2. Instead, the set of values above is fine-tuned for a study of the Callan-Symanzik regulator in which effects of renormalization on physical observables are taken into account, see Section 3.3.5. Nevertheless, for the sake of consistency, we will make use of these values already here. In any case, while this parameter set may not be ideal for achieving high physical accuracy in studies of low-energy QCD, it allows us to properly assess the performance of our CS framework for the quark-meson model. With these concrete values at hand, we obtain the following coupling parameters:

$$h \approx 2.94\,, \qquad m^2_{\Lambda_0} \approx -0.89\,\Lambda_0^2\,. \tag{3.173}$$

Notice that our scale-fixing procedure results in a negative meson mass parameter, $m^2_{\Lambda_0} < 0$. Consequently, as our ansatz (3.33) for the functional form of the initial condition Γ_{Λ_0} is only bilinear in the fields, the theory at $k = \Lambda_0$ is not bounded from below. Nevertheless, solving the Wetterich equation with this initial condition, we find that the $O(4)$-symmetrized effective action is bounded from below for all scales $k < \Lambda_0$. Thus, in particular, in the limit $k \to 0$, which is associated with physical values for observables in our setting, the effective action is bounded from below. In principle, we could also add a term $\sim \lambda_{\Lambda_0}(\phi^\intercal\phi)^2$ with $\lambda_{\Lambda_0} > 0$ to our ansatz, rendering the effective action bounded from below also at the initial RG scale Λ_0. In the following, however, we shall restrict ourselves to an initial action bilinear in the fields as given by Eq. (3.33). We would like to add that the negative meson mass parameter is not the result of poorly chosen values for low-energy observables in the scale-fixing procedure. Instead, it is a characteristic feature of fermionic systems when employing the CS regulator. From Wilsonian-type RG flows, it is well known that the fermion dynamics increasingly shape the effective potential into a "Mexican-hat" form and thereby generate a finite ground state as more and more momenta are integrated out from the path integral. In the case of CS flows, however, all of those momenta are already integrated out for all k such that our effective potential has a negative curvature at all RG scales. Using an ansatz at $k = \Lambda_0$ which is bilinear in the fields thus necessarily renders the theory unstable at that scale. An RG step towards any lower scale $k < \Lambda_0$ generates terms of higher order in the fields. These quantum fluctuations then render the theory stable for $k < \Lambda_0$. We further highlight that, in our CS framework, the effective action at the initial scale Λ_0 should not be confused with a UV action describing the theory at some high momentum scale, as would be the case for Wilsonian-type RG flows. Instead, the scale-dependent effective action always describes an IR action in which the masses of the particles are increased when we increase the scale k.

The parameter H in our ansatz (3.33) for the effective action controls the physical amount of explicit symmetry breaking and is chosen such that we obtain a pion pole mass of $\hat{m}_{\mathrm{pole},\pi} = 138\,\mathrm{MeV}$ in the vacuum limit. Recall that the pole mass is determined from the momentum-dependent two-point correlator by analytic continuation, see Eq. (3.75). Specifically, we choose

$$H = 3\,668\,866\,\mathrm{MeV}^3\,. \tag{3.174}$$

Compared to the value of the quark mass that we have fixed at $H = 0$, the finite amount of explicit symmetry breaking naturally leads to an increase in the constituent quark mass. Thereby, also the pion decay constant changes. Concretely, we obtain:

$$T = \mu = 0: \qquad m_q \approx 299.19\,\mathrm{MeV}\,, \qquad f_\pi \approx 101.61\,\mathrm{MeV}\,. \tag{3.175}$$

In order to properly assess the effects of symmetrization and also RG consistency on the unconstrained CS scheme, we need to make sure that the various schemes are indeed comparable. To

this end, we adapt the initial condition of the CS scheme with no constraints ("nc") such that the physics in the vacuum limit is the same as in the case of the symmetrized scheme:

$$\frac{1}{V_4}\Gamma^{(\mathrm{nc})}_{\Lambda_0}(\phi) = \frac{1}{V_4}\Gamma_{\Lambda_0}(\phi) - 8N_\mathrm{c}\left[L_0^{(\mathrm{sym})}(\Lambda_0, h^2\phi^2) - L_0(\Lambda_0, h\phi)\right] . \tag{3.176}$$

Analogously, for the Euclidean two-point function in the unconstrained scheme, the initial condition reads

$$\tilde{\Gamma}^{(\mathrm{nc})(2)}_{\Lambda_0}(Q) = \tilde{\Gamma}^{(2)}_{\Lambda_0}(Q) + \int_{\Lambda_0}^{0} \mathrm{d}k \, \left[\partial_k \tilde{\Gamma}_k^{(\mathrm{phys})(2)}(Q, m_q^2) - \partial_k \tilde{\Gamma}_k^{(2)}(Q, m_q)\right] . \tag{3.177}$$

Note that the vacuum physics in RG-consistent and symmetrized CS calculations is already identical to the one in the symmetrized-only scheme. By construction, differences in the schemes can then become apparent in the presence of finite external parameters by propelling the system away from the vacuum. Specifically, in the case of the unconstrained CS scheme, finite external parameters hence control the amount of regulator-induced symmetry breaking.

Curvature masses

Let us begin our phenomenological study of the QCD phase diagram by computing the curvature masses of the sigma mode and the pions. These masses can then be used to pinpoint the transition from the phase governed by a finite ground state to the phase where it vanishes. The curvature masses can be extracted from the effective action as follows

$$\begin{pmatrix} m_\sigma^2(T,\mu) & \vec{0}^\intercal \\ \vec{0} & m_\pi^2(T,\mu)\, \mathbb{1}_{3\times 3} \end{pmatrix} = \left(\frac{\mathrm{d}}{\mathrm{d}\phi^\intercal} \frac{\mathrm{d}}{\mathrm{d}\phi} \frac{\Gamma^{(\mathrm{scheme})}(\phi)\big|_{T,\mu}}{V_4} \right)\Bigg|_{\phi=\phi_0} . \tag{3.178}$$

We shall compute the curvature masses for different schemes and compare the results. In particular, we will consider the standard CS scheme without symmetry constraints, the CS scheme with restored $O(4)$ symmetry, and the symmetrized as well as RG-consistent CS scheme. The initial condition for the RG flow in each case is determined by Eq. (3.176). We highlight that the ground state ϕ_0 has to be obtained from a minimization of the effective action in each case. Since observables are always computed at the ground state of the system, differences in the results for observables as obtained from our different CS schemes are strongly correlated with the differences in the behavior of the ground state as a function of the external parameters.

Let us start with the discussion of curvature masses at finite temperature and zero chemical potential in the chiral limit, $H \to 0$. Since we have tuned our model parameters such that the dynamics of the vacuum system is governed by a finite ground state, we expect the pions to be massless at $T = \mu = 0$ whereas the sigma modes and the quarks acquire a finite mass. In the absence of explicit chiral symmetry breaking, thermal fluctuations then drive the ground state continuously towards smaller and smaller values until it exactly vanishes at the critical temperature T_c. For temperatures above this critical value, the ground state remains zero, which leads to massless quarks in this phase whereas the masses of the mesons are finite and degenerate. Phenomenologically speaking, the temperature T_c then marks the chiral phase transition. The expected temperature dependence of the various masses implies that the masses of both the mesons and the quarks should vanish identically at the transition, provided that the transition is of second order. For example, the quark mass can then serve as an order parameter to distinguish between the two separate phases of matter. For finite explicit chiral symmetry breaking, however, the quark mass is differentiable and remains finite for all temperatures. Accordingly, this behavior signals

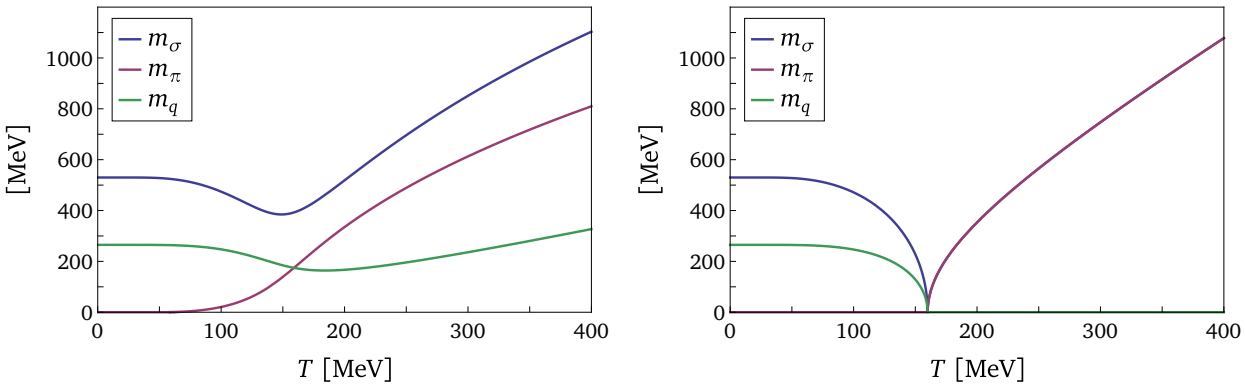

Figure 3.13: Meson curvature masses and the quark mass as functions of the temperature T at $H = \mu = 0$. In the vacuum limit, the sigma mass assumes the value of $m_\sigma \approx 530\,\text{MeV}$, whereas the curvature mass of the pion vanishes exactly. The unconstrained CS scheme (left panel) predicts a chiral crossover at $T_{\text{pc}} \approx 149\,\text{MeV}$ while the $O(4)$-constrained and RG-consistent scheme (right panel) indicates a second-order phase transition at $T_{\text{c}} \approx 160\,\text{MeV}$.

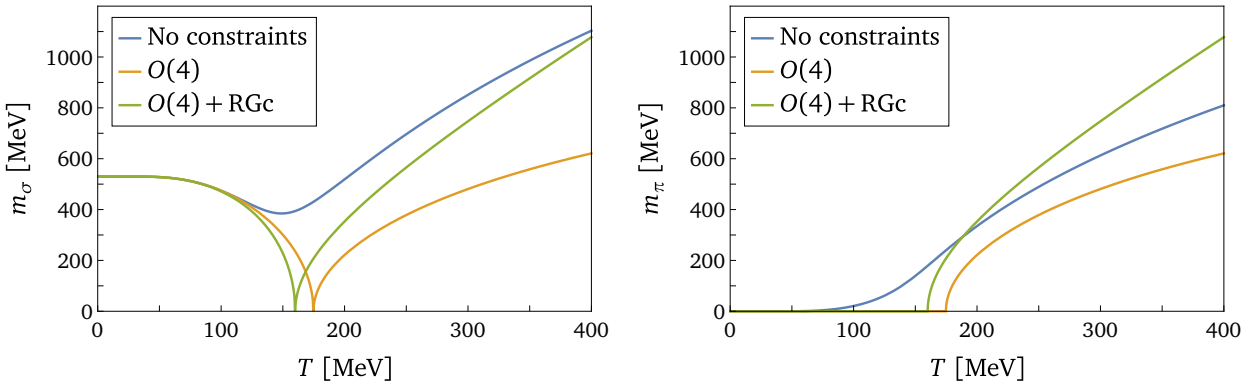

Figure 3.14: The curvature mass of the sigma meson (left panel) and the pions (right panel) as a function of the temperature T at $H = \mu = 0$. The CS scheme without constraints (blue curves) is plagued by strong regularization artifacts and gives rise to massive pions for all finite temperatures. With the restoration of $O(4)$ symmetry for CS flows (orange curves), the crossover turns into a second-order phase transition at $T_{\text{c}} \approx 175\,\text{MeV}$. Taking additional RG consistency into account (green curves), the nature of the phase transition does not change but the critical temperature receives corrections.

that the phase transition has turned into a crossover. In this case, we use the minimum of the curvature mass of the sigma mode to define a crossover temperature. We remark that the inverse of this mass can be related to the correlation length in the system. Therefore, it represents a meaningful definition for the crossover as it is associated with a maximum in the correlation length. In the chiral limit, this minimum coincides with the definition of the critical temperature in terms of the quark mass.

In Fig. 3.13, we show our results for the curvature masses as functions of the temperature for $H = \mu = 0$ as obtained from CS calculations without symmetry constraints (left panel) and from a symmetrized as well as RG-consistent CS calculation (right panel). By comparing the two panels, it becomes apparent that the regulator-induced breaking of the chiral symmetry severely spoils the results for the curvature masses, even though the unconstrained CS scheme is free of artificial symmetry breaking at $T = \mu = 0$ by construction. Recall that our ansatz (3.176) for the effective action at the initial mass scale Λ_0 has been chosen such that all schemes agree identically with the symmetrized CS scheme in the vacuum limit.

Regarding Fig. 3.13 (left panel), we observe that the quark mass at finite temperature as obtained from the unconstrained CS calculation is always finite and even increases at high temperatures, indicating that there is no phase transition at all. Contrary to that, the mass of the sigma mode as a function of the temperature exhibits a minimum which would indicate a crossover at $T_{\mathrm{pc}} \approx 149\,\mathrm{MeV}$. Moreover, not only are the meson masses not degenerate at high temperatures, the difference between them actually increases as the temperature rises. An increase in the temperature is expected to suppress the effect of a physical explicit symmetry breaking such that the meson curvature masses should approach the same high-temperature limit instead of being driven further apart. Our results for the particle masses in the unconstrained CS scheme therefore demonstrate the unphysical nature of the regulator-induced breaking of the chiral symmetry. Once this regulator-induced symmetry breaking is removed and the global $O(4)$ symmetry of the effective action is restored, we observe the expected behavior of the curvature masses, see in particular Fig. 3.14 (right panel). For example, in this case, we find that the quark mass tends to zero at $T_{\mathrm{c}} \approx 160\,\mathrm{MeV}$ and remains zero above this temperature, indicating a second-order chiral phase transition. Moreover, the meson masses also tend to zero at this temperature and then become degenerate for $T > T_{\mathrm{c}}$. Note that the results from the symmetrized and RG-consistent CS calculation differ only quantitatively but not qualitatively from those obtained from the symmetrized-only CS calculation. For example, we find $T_{\mathrm{c}} \approx 175\,\mathrm{MeV}$ for the phase transition temperature, if we do not take RG consistency into account. This is illustrated in Fig. 3.14 for the meson masses. From this figure, it also becomes clear that unconstrained CS calculations are pathological and do not have any predictive power.

We now turn to the case of a finite physical explicit symmetry-breaking term in the action, i.e., we consider $H > 0$. In this case, the ground state of the system is always finite. As a consequence, we expect to find a crossover rather than a phase transition. For sufficiently high temperatures, however, we still expect that the quark mass approaches zero. In the same way, we expect to find that the difference between the sigma and pion masses tends to zero. As can be deduced from Figs. 3.15 and 3.16, the results from the unconstrained CS calculations are again severely spoiled by the explicit regulator-induced symmetry breaking. For example, the quark mass does not tend to zero at high temperatures but rather increases, in contrast to the symmetrized CS calculation. In addition, also the predictions for the meson masses suffer strongly from the regulator-induced explicit symmetry breaking, in particular at high temperatures. Looking at the results from the symmetrized as well as RG-consistent calculations in the right panel of Fig. 3.15, we observe that the system undergoes a crossover which is associated with a pseudo-critical temperature $T_{\mathrm{pc}} \approx 183\,\mathrm{MeV}$ as defined by the minimum of the sigma mass. At high temperatures, we then find that the quark mass tends to zero continuously and the difference between the meson masses decreases, as expected. Lastly, we find that the vacuum pole mass of the pions, which we have fixed at $m_{\mathrm{pole},\pi} = 138\,\mathrm{MeV}$ by tuning the symmetry-breaking parameter H, translates into a pion curvature mass of $m_{\pi} \approx 190\,\mathrm{MeV}$.

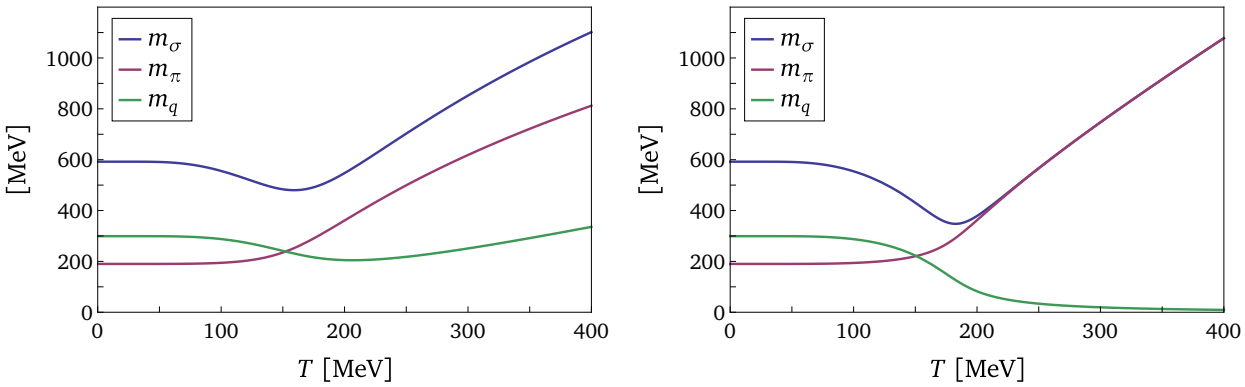

Figure 3.15: Meson curvature masses and the quark mass as functions of the temperature T at $\mu = 0$ and $H > 0$. In the vacuum limit, the meson masses read $m_\sigma \approx 592\,\text{MeV}$ and $m_\pi \approx 190\,\text{MeV}$. The unconstrained CS scheme (left panel) indicates a chiral crossover at $T_{\text{pc}} \approx 159\,\text{MeV}$ while the $O(4)$-constrained and RG-consistent scheme (right panel) predicts a pseudo-critical temperature of $T_{\text{pc}} \approx 183\,\text{MeV}$.

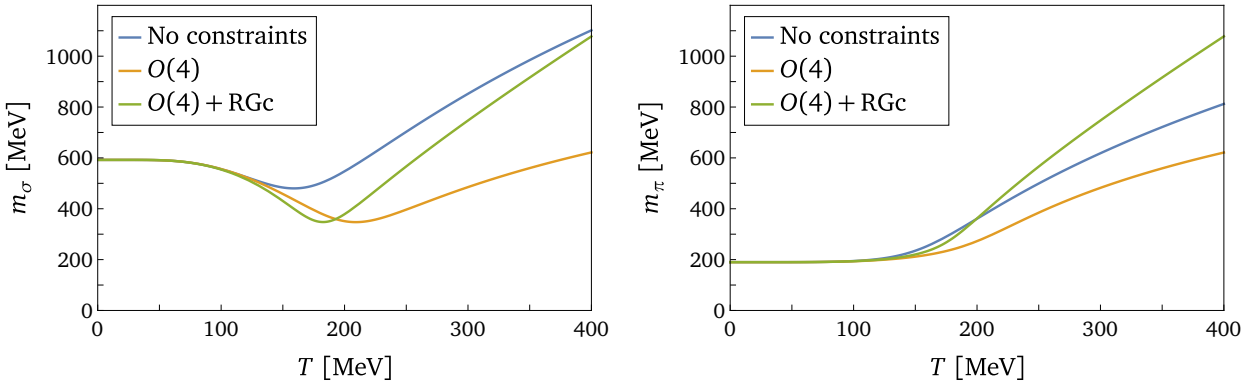

Figure 3.16: The curvature mass of the sigma meson (left panel) and the pions (right panel) as a function of the temperature T at $\mu = 0$ and $H > 0$. In the presence of physical explicit symmetry breaking, all CS schemes give rise to a crossover. Nevertheless, the unconstrained calculations (blue curves) suffer from strong regularization artifacts. The $O(4)$-constrained CS scheme (orange curves) predicts a pseudo-critical temperature of $T_{\text{pc}} \approx 209\,\text{MeV}$, additional RG consistency (green curves) then lowers this value.

In the zero-temperature limit at finite chemical potential, the dynamics of the system is governed by the Silver-Blaze property. This refers to the fact that the partition function of a physical system at $T = 0$ does not exhibit any dependence on the chemical potential μ, provided that the chemical potential remains smaller than a critical value μ_{SB}, see Section 2.3.2 for details. As the CS regulator respects the Silver-Blaze symmetry of the system, our choice for the initial conditions, see Eq. (3.176), implies that our three CS schemes at zero temperature yield the same effective action, provided that the chemical potential is smaller than its critical value. Furthermore, we restrict ourselves to the case of $\mu < \Lambda_0$ as our model is not expected to have predictive power for chemical potentials beyond that scale where, e.g., diquark condensation may become relevant, see, e.g., Refs. [264, 391]. As a result, we find that all schemes are in fact identical at $k = 0$. We shall illustrate this in the following.

At zero temperature, the loop corrections exhibit the feature that they can be separated into a vacuum part and a matter part, where only the latter has an explicit dependence on the chemical

potential. It then follows that

$$\begin{aligned}\frac{1}{V_4}\Gamma(\phi)\big|_\mu &= \frac{1}{V_4}\Gamma^{(\mathrm{nc})}_{\Lambda_0}(\phi) - 8N_\mathrm{c}\left[L_0(\Lambda_0,h\phi) - M_k(\mu,h\phi)\Big|_{k=\Lambda_0}^{k=0}\right]\\ &\overset{(3.176)}{=} \frac{1}{V_4}\Gamma_{\Lambda_0}(\phi) - 8N_\mathrm{c}\left[L_0^{(\mathrm{sym})}(\Lambda_0,h^2\phi^2) - M_k(\mu,h\phi)\Big|_{k=\Lambda_0}^{k=0}\right]\\ &\overset{(3.118)}{=} \frac{1}{V_4}\Gamma_{\Lambda_0}(\phi) - 8N_\mathrm{c}\left[L_0^{(\mathrm{sym})}(\Lambda_0,h^2\phi^2) - M\left(\mu,(h\sigma+k)^2+h^2\vec{\pi}^2\right)\Big|_{k=\Lambda_0}^{k=0}\right]\\ &\overset{\mu<\Lambda_0}{=} \frac{1}{V_4}\Gamma_{\Lambda_0}(\phi) - 8N_\mathrm{c}\left[L_0^{(\mathrm{sym})}(\Lambda_0,h^2\phi^2) - M(\mu,h^2\phi^2)\right]\\ &= \frac{1}{V_4}\Gamma_{\Lambda_0}(\phi) - 8N_\mathrm{c}\left[L_0^{(\mathrm{sym})}(\Lambda_0,h^2\phi^2) - M_0^{(\mathrm{sym})}(\mu,h^2\phi^2)\right]. \end{aligned} \tag{3.179}$$

By restricting ourselves to chemical potentials $\mu < \Lambda_0$, the matter part becomes independent of the scale Λ_0. As a result, the unconstrained CS scheme is identical to the symmetrized one at $k = T = 0$. This property of the matter part holds quite generally in Silver-Blaze-symmetric theories and is not affected by RG consistency. In other words, also the symmetrized and RG-consistent CS scheme yields the same quantum effective action for $\mu < \Lambda_0$. For more information in this regard, we refer to our general discussion around Eq. (3.99).

Since all three CS schemes are identical at zero temperature and for all chemical potentials of interest, we simply refer to the physical effective action in the following. Furthermore, the equivalence of all schemes implies the absence of regularization artifacts for $0 \leq \mu < \Lambda_0$. Let us now consider the explicit form of the effective action at zero temperature and finite chemical potential. Evaluating the effective action on a homogeneous background, we obtain

$$\begin{aligned}\frac{1}{V_4}\Gamma^{(\mathrm{phys})}(\phi)\big|_\mu &= \frac{1}{2}m^2_{\Lambda_0}\phi^2 - H\sigma - 8N_\mathrm{c}\, L_0^{(\mathrm{sym})}(\Lambda_0,h^2\phi^2)\big|_\mu\\ &= \frac{1}{2}m^2_{\Lambda_0}\phi^2 - H\sigma - 8N_\mathrm{c}\left[L_0^{(\mathrm{sym})}(\Lambda_0,h^2\phi^2) - M_0^{(\mathrm{sym})}(\mu,h^2\phi^2)\right] \end{aligned} \tag{3.180}$$

with

$$\begin{aligned}L_0^{(\mathrm{sym})}(\Lambda_0,\chi) &= \frac{1}{(2\pi)^2}\int_0^\infty \mathrm{d}p\; p^2\sqrt{p^2+\chi+k^2}\Big|_{k=\Lambda_0}^{k=0} + (\mathcal{S}\,\mathrm{CT}_0)(\Lambda_0,\chi)\\ &= \frac{1}{(2\pi)^2}\frac{1}{32}\left[\Lambda_0^2(\Lambda_0^2+2\chi) + 2\chi^2\ln\left(\frac{\chi}{\Lambda_0^2}\right) - 2(\Lambda_0^2+\chi)^2\ln\left(1+\frac{\chi}{\Lambda_0^2}\right)\right] \end{aligned} \tag{3.181}$$

and

$$\begin{aligned}M_0^{(\mathrm{sym})}(\mu,\chi) &= \frac{1}{(2\pi)^2}\int_0^\infty \mathrm{d}p\; p^2\left(\sqrt{p^2+\chi}-\mu\right)\theta\left(\mu-\sqrt{p^2+\chi}\right)\\ &= \frac{1}{(2\pi)^2}\frac{\theta(\mu-\sqrt{\chi})}{24}\left[\mu\sqrt{\mu^2-\chi}\,(5\chi-2\mu^2) - 3\chi^2\,\mathrm{arsinh}\left(\sqrt{\frac{\mu^2}{\chi}-1}\right)\right]. \end{aligned} \tag{3.182}$$

In Fig. 3.17, we illustrate the curvature masses as obtained from the physical effective action in Eq. (3.180). In accordance with our discussion of the Silver-Blaze property above, we find that all masses agree identically with their respective values in the vacuum limit for $\mu < \mu_{\mathrm{SB}}$. Here, the Silver-Blaze threshold is set by the constituent quark mass at $T = \mu = 0$. Recall that the value of the quark mass in the vacuum limit depends on whether or not we consider explicit symmetry breaking.

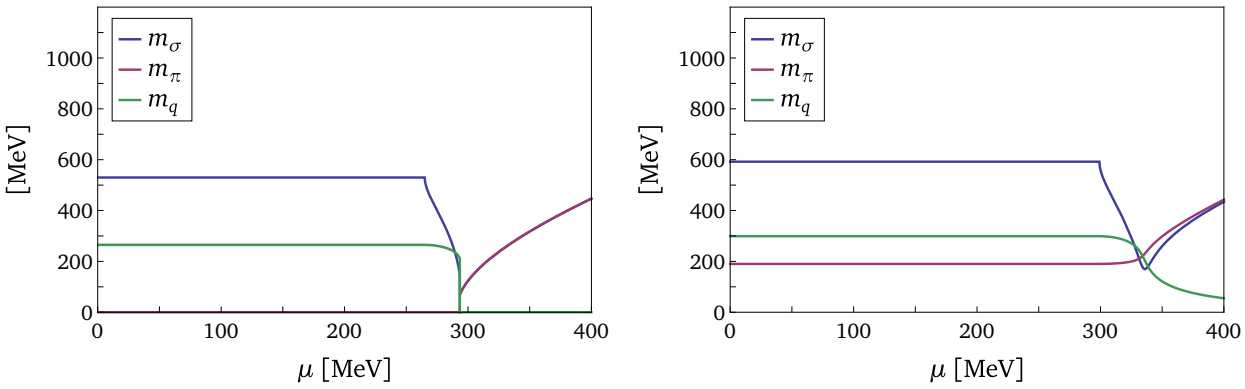

Figure 3.17: Meson curvature masses and the quark mass as functions of the quark chemical potential μ at zero temperature, $T = 0$. The particle masses as obtained from the effective action in Eq. (3.180) are presented in the absence of explicit symmetry breaking, i.e., $H = 0$, (left panel) and for the case of $H > 0$ (right panel). In the chiral limit, our CS calculations predict a first-order phase transition at $\mu_c \approx 293\,\text{MeV}$. For $H > 0$, the transition turns into a crossover occurring at the pseudo-critical value $\mu_{pc} \approx 336\,\text{MeV}$.

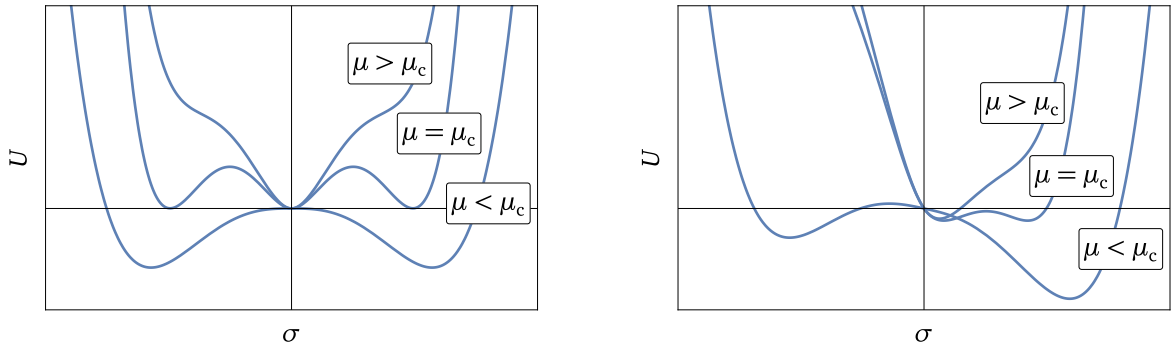

Figure 3.18: Exemplary μ-dependent behavior of an effective potential as a function of the field variable σ in the case of $H = 0$ (left panel) as well as for explicit symmetry breaking, i.e., $H > 0$, (right panel). The critical value μ_c signals a first-order phase transition and corresponds to the point where the ground state as a function of the chemical potential is discontinuous. We note that a first-order transition is not restricted to symmetric systems but is also possible in the presence of symmetry breaking. Nevertheless, our CS scheme at zero temperature produces a first-order transition only for $H = 0$.

Specifically, at $H = 0$, we have $\mu_{SB} = \hat{m}_q$. In the chiral limit, the quark mass as a function of the chemical potential exhibits a jump discontinuity at the critical value $\mu_c \approx 293\,\text{MeV}$ and becomes zero for all $\mu > \mu_c$. This discontinuous behavior at μ_c signals a first-order phase transition of the system. At the level of the effective potential, such a transition arises from the development of multiple minima which, loosely speaking, compete with each other as the chemical potential increases, see Fig. 3.18. Whereas the absolute value of the ground state is uniquely defined for small values of the chemical potential, the minima become degenerate at $\mu = \mu_c$, leading to an abrupt change in the global minimum for $\mu > \mu_c$. Further notice that, in contrast to the situation at the second-order phase transition, the meson curvature masses do not tend to zero. Instead, they also behave discontinuously at the critical chemical potential and assume the finite value

$$\min(m_\sigma) = \sqrt{m_{\Lambda_0}^2 + \frac{N_c h^2}{\pi^2}\mu_c^2}\,. \tag{3.183}$$

Choosing now H such that the pion pole mass assumes its physical value in the vacuum limit, we observe that the first-order transition turns into a crossover at $\mu_{\mathrm{pc}} \approx 336\,\mathrm{MeV}$ as indicated by the continuous behavior of the masses as functions of the chemical potential, see Fig. 3.17. Here, the pseudo-critical value μ_{pc} is defined by the minimum of the curvature mass of the sigma mode. These observations imply that, at least in our current approximation, there is no critical point in the phase diagram of the quark-meson model for physical pion masses. Consequently, our results are in disagreement with the expectation that the physical phase structure of QCD includes a critical endpoint and a first-order transition at low temperatures and intermediate densities, see, e.g., Refs. [392–395, 438]. Nevertheless, we note that a first-order transition in the presence of explicit symmetry breaking could still be realized in our model by adjusting the initial condition, as suggested by, e.g., Ref. [438]. In addition, it has been found that the appearance of the critical endpoint correlates with the value k_{min} chosen for the endpoint of the RG flow [425]. As we always choose $k_{\mathrm{min}} = 0$ in our studies, this may contribute to the outcome that a critical endpoint and the first-order phase transition cannot be observed in our results.

Spectral functions

Let us now construct meson spectral functions from the Euclidean two-point function. The CS regulator ensures the existence of the Källén-Lehman spectral representation for the regularized propagator at every scale k. For each of our CS schemes, the scale-dependent spectral function rho_k is then generally obtained by

$$\rho_k(\omega,\vec{Q})\big|_{T,\mu} = 2 \lim_{\varepsilon\to 0^+} \Im\mathfrak{m} \left\{ \frac{1}{\tilde{\Gamma}_k^{(\mathrm{scheme})(2)}(\mathrm{i}(\omega+\mathrm{i}\varepsilon),\vec{Q})\big|_{T,\mu}} \right\} . \tag{3.184}$$

Nevertheless, we will focus exclusively on the case $k = 0$ in the following. We present our results for the spectral functions of the scalar and pseudoscalar mesons as functions of the energy ω in the presence of a physical explicit symmetry breaking, $H > 0$. As above, we start by comparing the results from different treatments of the CS flow at finite temperature and zero chemical potential. In all our numerical studies, we set the spatial external momenta of the two-point function to zero, i.e., $\vec{Q} = 0$, such that the energy ω_{res} associated with a resonance peak in the spectral function can be identified exactly with the mass of the corresponding meson.

In Fig. 3.19 (left panel), we show the spectral functions of the sigma mode and the pions in the vacuum limit. The pole masses of these two mesons can be extracted from a localization of the peaks in these functions. We find $m_{\mathrm{pole},\sigma} = \omega_{\mathrm{res},\sigma} \approx 457\,\mathrm{MeV}$ for the sigma mode. For the pion spectral function, the position of the pole at $m_{\mathrm{pole},\pi} = \omega_{\mathrm{res},\pi} \approx 138\,\mathrm{MeV}$ is not a prediction in our present study as we have used the parameters of our model to tune the pion pole mass in the vacuum limit. In any case, the spectral functions exhibit more structure than the typical peaks associated with the pole masses. For example, at $\omega \approx 600\,\mathrm{MeV}$, the spectral function of the sigma meson and that of the pions displays a kink and a turning point, respectively. These structures are commonly interpreted as the decay of an excited state of the respective meson into an energetically more favorable state. Within our model study, we can identify these decays as the processes $\sigma' \to \overline{\psi}\psi$ and $\pi' \to \overline{\psi}\psi$, where the primes indicate the excited state. Concretely, when we reach the energy $\omega_{\mathrm{decay}} = 2m_q$ associated with a pair of two constituent quarks with zero center-of-mass energy, it is favorable for the mesons to decay into these quark states.[18]

[18] Recall that Λ_0 is not a UV momentum cutoff but represents a mass scale in the CS scheme. Therefore, the CS regularization does not restrict the range of external four-momenta in correlation functions. Still, this does not imply that our results necessarily have predictive power at arbitrarily high external momenta as the quark-meson model does not contain the correct degrees of freedom in these regimes.

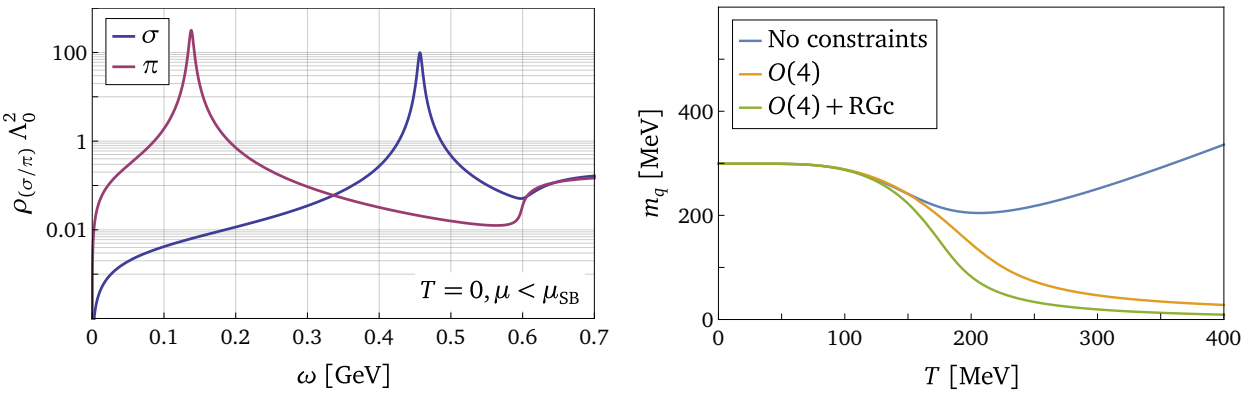

Figure 3.19: Left panel: Meson spectral functions at zero temperature and for chemical potentials below the Silver-Blaze threshold. We observe resonances associated with pole masses at $\omega_{\mathrm{res},\sigma} \approx 457\,\mathrm{MeV}$ and $\omega_{\mathrm{res},\pi} \approx 138\,\mathrm{MeV}$. Right panel: The quark mass at $\mu = 0$ as a function of the temperature T as obtained within different CS schemes.

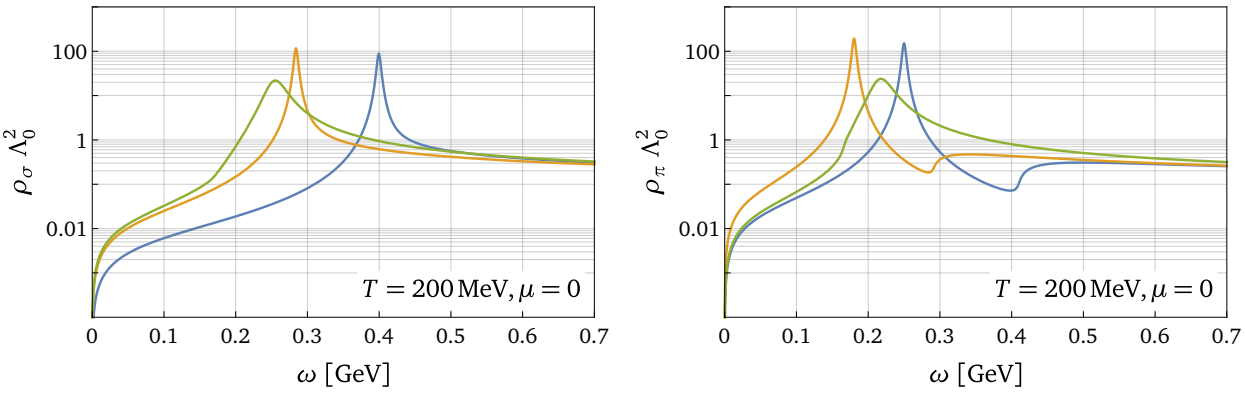

Figure 3.20: Spectral function of the sigma meson (left panel) and the pions (right panel) at $T = 200\,\mathrm{MeV}$ and $\mu = 0$ as obtained from the CS scheme with no constraints (blue curves), an $O(4)$-constrained CS calculation (orange curves), and an $O(4)$-constrained RG-consistent computation (green curves).

For an analysis of spectral functions and an associated comparison of different treatments of the CS regulator, let us start with the case of finite temperature and zero chemical potential. Since the shapes and structures of the meson spectral functions among the different CS schemes are strongly correlated with the behavior of the ground state with respect to external parameters, we also provide a direct comparison of quark masses as functions of temperature in Fig. 3.19 (right panel). Specifically, as the quark mass changes with temperature, the structures associated with the decay of the mesons in two quark states follow the temperature-dependence of the ground state, $\omega_{\mathrm{decay}}(T) = 2m_q(T)$. For temperatures associated with $\omega_{\mathrm{decay}} < \omega_{\mathrm{res}}$, the width of the resonance peaks increases with increasing temperature and their height decreases. This broadening effect is the result of thermal fluctuations screening the pole that is present in the propagator of the vacuum theory. Accordingly, the mass associated with this peak is no longer a pole mass at these temperatures but should rather be considered a resonance mass. From a more phenomenological standpoint, the broadening of the peak in a spectral function signals that the particle under consideration has become unstable. The temperature-induced instability thus crucially depends on the temperature-dependence of the quark mass, as illustrated in Fig. 3.20. Specifically, whereas the symmetrized and RG-consistent CS scheme (green curves) predicts unstable mesons at $T = 200\,\mathrm{MeV}$, the destabilization has not yet started in the other schemes. Moreover, the spectral functions of the mesons as extracted from the $O(4)$-symmetrized CS calculations (or-

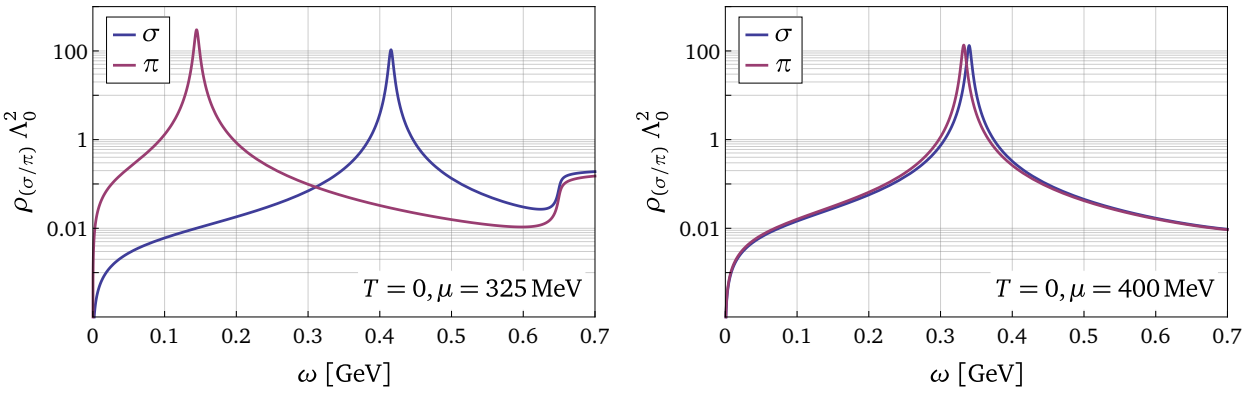

Figure 3.21: Meson spectral functions at zero temperature as obtained from our $O(4)$-constrained CS framework for different values of the chemical potential beyond the regime governed by the Silver-Blaze property. Specifically, we present results for $\mu = 325\,\mathrm{MeV}$ (left panel) and $\mu = 400\,\mathrm{MeV}$ (right panel).

ange and green curves) become more and more degenerate with increasing temperature. As this phenomenon can be traced back to an almost vanishing quark mass at high temperatures, this behavior of the spectral functions cannot be observed in our unconstrained CS calculations (blue lines). Apart from these more phenomenological aspects, we would like to emphasize that the differences in the results as obtained from our different CS schemes are not only qualitative but also quantitative. As can be deduced from Fig. 3.20, we observe that the results from the unconstrained CS calculation (blue curves) receive significant corrections from the symmetrization (orange lines) at $T = 200\,\mathrm{MeV}$ and $\mu = 0\,\mathrm{MeV}$. By ensuring RG consistency in addition to the symmetrization (green curves), the spectral functions receive additional corrections.

At zero temperature, the dynamics of the system is governed by the Silver-Blaze property, meaning that the meson spectral functions remain unchanged compared to their form in the vacuum limit up to $\mu_{\mathrm{SB}} \approx 300\,\mathrm{MeV}$. Analogously to our discussion of curvature masses at $T = 0$, the zero-temperature two-point correlators and hence also spectral functions are identical across all CS schemes for all chemical potentials of interest. As a consequence, our results for meson spectral functions at zero temperature as obtained from the $O(4)$-constrained CS framework, see Fig. 3.21, are in particular RG-consistent. Exceeding the chemical potential beyond the Silver-Blaze threshold, $\mu > \mu_{\mathrm{SB}}$, the kink-like structures of the meson spectral functions observed at $\omega_{\mathrm{decay}} = 2m_q$ in the vacuum limit are now found at $\omega_{\mathrm{decay}}(\mu) = 2\mu$. Notice that, compared to the case of finite temperature and zero chemical potential, the structures of the zero-temperature spectral functions, which are associated with meson decays, do not follow the μ-dependence of the ground state. Thus, the position of these structures is continuously shifted to larger values by increasing the chemical potential. In this regime, these kink-like structures can then be associated with a decay into two quarks where each quark carries the Fermi energy μ. In other words, the mesons can only decay into their quark content if there is enough energy to create a pair of quarks "sitting" at the Fermi surface or above. This makes sense because, in a fermionic system at zero temperature, quantum states with energy less than μ cannot be occupied due to the Pauli exclusion principle. Moreover, the kink of the sigma spectral function quickly transforms into a turning point for $\mu > \mu_{\mathrm{SB}}$, whereas the analogous structure in the pion spectral function does not change qualitatively. Additionally, when we increase the chemical potential beyond the point associated with the crossover, the sigma and pion spectral functions become degenerate, similar to the case of finite temperature and zero chemical potential. However, a key difference is that the zero-temperature spectral functions feature sharp peaks rather than broad resonances. This is due to the fact the decay energy at zero temperature increases with the chemical potential, thereby ensuring the relation $\omega_{\mathrm{decay}} > \omega_{\mathrm{res}}$ for

both mesons. As long as this relation is satisfied, the poles in the propagator of the vacuum theory remain poles even at finite external parameters.

3.3.5 Renormalization effects on physical observables

As previously shown, the Callan-Symanzik regulator can be effectively employed to obtain meaningful results for observables within the quark-meson model. Building on this, we now take a step further in the direction of investigating the phase structure of low-energy QCD by means of our CS framework and take effects of renormalization into account. More specifically, the focus of the following study lies on the computation of renormalized curvature masses and renormalized spectral functions, which requires the calculation of wavefunction renormalization factors. As discussed earlier, the regulator-induced breaking of chiral symmetry and regularization artifacts in the presence of finite external parameters can significantly influence physical observables, both qualitatively and quantitatively. Therefore, we will exclusively use the $O(4)$-constrained and RG-consistent CS scheme from here on. In addition, we will restrict our analysis to the phenomenologically most relevant case, which involves finite physical explicit symmetry breaking.

Scale fixing

Let us again begin by fixing the coupling parameters of our model in the absence of explicit symmetry breaking such that we obtain specific values for the constituent quark mass m_q and the pion decay constant f_π in the vacuum limit. In general, these quantities are defined as [76]

$$m_q = \bar{h}_\sigma |\bar{\sigma}_0| \,, \qquad f_\pi = \frac{m_q}{\bar{h}_\pi} \,, \tag{3.185}$$

where the bar notation indicates that renormalization factors have been taken into account. Specifically, the definitions of the renormalized Yukawa couplings and the renormalized ground state read

$$\bar{h}_{(\sigma/\pi)} = \frac{h}{\sqrt{Z^\perp_{(\sigma/\pi)}}} \,, \qquad \bar{\sigma}_0 = \sqrt{Z^\perp_\sigma}\, \sigma_0 \,. \tag{3.186}$$

Notice that the quark mass is invariant under renormalization in our setting,[19] i.e., we have $m_q = \bar{h}_\sigma |\bar{\sigma}_0| = h|\sigma_0|$. The bosonic wavefunction renormalizations can be obtained from the RG-consistent two-point correlator of the physical quantum effective action by a suitable projection. In particular, we make use of the standard projection prescription that involves two derivatives with respect to (spatial) momenta and the static limit. For our exact results for the wavefunction renormalization factors at zero temperature, we refer to Section 3.3.3.

Once we have chosen specific values $\hat{m}_q$ and $\hat{f}_\pi$ for the quark mass and the pion decay constant at $T = \mu = H = 0$, the relations (3.185) together with our result for the vacuum wavefunction renormalizations as presented in Eq. (3.165) consistently determine the values of the model parameters. Concretely, we find

$$h^2 = \frac{Z_{\Lambda_0}}{\left(\frac{\hat{f}_\pi}{\hat{m}_q}\right)^2 - \frac{N_c}{4\pi^2} \ln\left(1 + \frac{\Lambda_0^2}{\hat{m}_q^2}\right)} \,, \qquad m^2_{\Lambda_0} = 16 N_c\, h^2 \left(\frac{\mathrm{d}}{\mathrm{d}\chi} L_0^{(\mathrm{sym})}(\Lambda_0, \chi) \right)\Big|_{\chi = \hat{m}_q^2} \tag{3.187}$$

[19] In a more general setting, the renormalized quark mass would also include the fermionic wavefunction renormalization factor. However, in our calculations, we always choose $Z_\psi = 1$ and thus effectively consider the large-N_c limit. For more information about this limit, see, e.g., Refs. [439–442].

for the bare Yukawa coupling and meson mass parameter, respectively. Notice that the logarithmic term in the denominator of the expression for the Yukawa constant is strictly positive since $\Lambda_0 > \hat{m}_q$. As a consequence, the condition $0 < h^2 < \infty$ restricts our choices for Λ_0, $\hat{m}_q$ and $\hat{f}_\pi$. Because the values for the latter quantities as proposed in Section 3.3.4 are compatible with this restriction, we choose the same values here. This also simplifies direct comparisons of results obtained with and without the inclusion of the wavefunction renormalization factors of the mesons. To be specific, we set $\Lambda_0 = 500\,\text{MeV}$, $\hat{m}_q = 265\,\text{MeV}$ and $f_\pi = 90\,\text{MeV}$. Furthermore, we would like to remark that the general form of the meson mass parameter is still given by Eq. (3.171). We also add that our results for the bare parameters and the wavefunction renormalizations imply that renormalized couplings do not depend on Z_{Λ_0}.

We would like to mention that the renormalized vacuum Yukawa coupling associated with quark-pion interactions in the absence of explicit symmetry breaking is directly determined by the relation (3.185),

$$T = \mu = H = 0 : \qquad \bar{h}_\pi = \frac{\hat{m}_q}{\hat{f}_\pi} \approx 2.94 \,. \tag{3.188}$$

The definition of the renormalized couplings in Eq. (3.186) and the result for the wavefunction renormalizations, see Eq. (3.165), can then be used to determine the corresponding value for quark-sigma interactions,

$$T = \mu = H = 0 : \qquad \bar{h}_\sigma = \bar{h}_\pi \sqrt{\frac{Z_\pi}{Z_\sigma}} = \frac{1}{\sqrt{\left(\frac{\hat{f}_\pi}{\hat{m}_q}\right)^2 - \frac{N_c}{6\pi^2}\frac{\Lambda_0^2}{\hat{m}_q^2+\Lambda_0^2}}} \approx 3.63 \,. \tag{3.189}$$

As a result, we obtain $\bar{h}_\sigma/\bar{h}_\pi \approx 1.23$ within our present approximation. The renormalized symmetry-breaking parameter is generally defined by

$$\bar{H} = \frac{H}{\sqrt{Z_\sigma^\perp}} \tag{3.190}$$

and is fixed such that we obtain a pion pole mass of $\hat{m}_{\text{pole},\pi} = 138\,\text{MeV}$ in the vacuum limit. Concretely, we set

$$T = \mu = 0 : \qquad \bar{H} = 2\,248\,666\,\text{MeV}^3 \,. \tag{3.191}$$

In the presence of a finite symmetry breaking, we then find

$$T = \mu = 0 : \qquad m_q \approx 282.22\,\text{MeV} \,, \qquad f_\pi \approx 92.74\,\text{MeV} \,, \qquad \bar{h}_\pi \approx 3.04 \,, \qquad \bar{h}_\sigma \approx 3.79 \tag{3.192}$$

for the constituent quark mass, the pion decay constant, and the renormalized Yukawa couplings, respectively. Additionally, we now obtain $\bar{h}_\sigma/\bar{h}_\pi \approx 1.25$, whereas QCD studies have found a ratio of $\bar{h}_\sigma/\bar{h}_\pi \approx 1.5$, see Ref. [42]. In any case, we deduce from these considerations that the minimum $\bar{\sigma}_0$ of the effective potential should in general not be identified with the pion decay constant.

Curvature masses and the phase diagram

Having fixed the parameters of our model in the vacuum and chiral limit, we can now study the dynamics of the system at finite temperature and chemical potential. In particular, let us begin

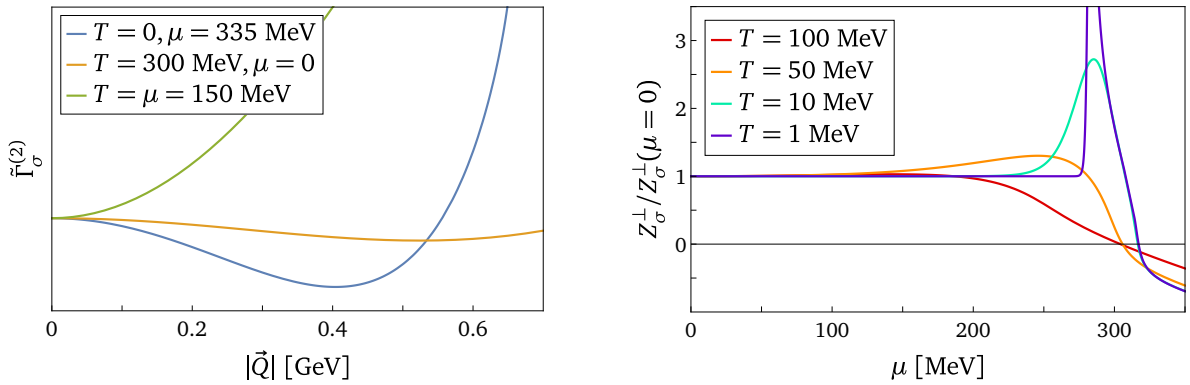

Figure 3.22: Left panel: Reduced two-point correlator of the sigma meson as a function of the spatial momentum for $Q^0 = 0$. We present the correlator for several temperatures and chemical potentials, where the results have been normalized such that all curves agree at $|\vec{Q}| = 0$. Our computations demonstrate that the momentum-dependent two-point correlator develops a non-trivial minimum in certain regions of the phase diagram. Right panel: Wavefunction renormalization of the sigma meson as a function of the quark chemical potential for several temperatures. By lowering the temperature, we observe that a pole at $T = 0$ and $\mu = \mu_{\rm SB} \approx 282\,\text{MeV}$ builds up. For $\mu > \mu_{\rm SB}$, the wavefunction renormalization continuously decreases, leading to negative values.

with a discussion of renormalized curvature masses. These are readily obtained from the bare curvature masses by

$$\bar{m}^2_{(\sigma/\pi)}(T,\mu) = \frac{m^2_{(\sigma/\pi)}(T,\mu)}{Z^\perp_{(\sigma/\pi)}(T,\mu)}\,, \tag{3.193}$$

which requires a computation of wavefunction renormalization factors at finite external parameters. Interestingly, we observe negative values of the wavefunction renormalizations in certain regions of the phase diagram. The zero-crossings of the wavefunction renormalizations inevitably lead to diverging renormalized quantities and thus limit the range of external parameters for which our results have predictive power.

A zero-crossing of a wavefunction renormalization in general indicates that the expansion of the effective action in external momenta has not been performed about the correct expansion point. In fact, as illustrated in Fig. 3.22 (left panel), the two-point correlator associated with the sigma meson indeed acquires a non-trivial minimum in momentum space in certain regions of the phase diagram. The two-point function for the pions behaves similarly but we refrain from showing this case explicitly in order to avoid redundancy. According to our definition, the wavefunction renormalization associated with a given field is nothing but the curvature of the corresponding momentum-dependent two-point function at vanishing momentum. Therefore, as the non-trivial minimum in momentum space evolves, our expressions for the wavefunction renormalizations become negative, see Fig. 3.22 (right panel). To capture the correct ground state physics of the quark-meson model, we could in principle consider a generalized definition of wavefunction renormalizations, which is always anchored at the global minimum in momentum space, see Eq. (3.168). Nevertheless, even if this definition was employed, the wavefunction renormalizations would still become zero at some points in the space of external parameters. As a consequence, although the generalized definition avoids negative values for the wavefunction renormalizations, the renormalized curvature masses would still exhibit a divergence. In addition, we would like to remark that, in the zero-temperature limit, the wavefunction renormalization associated with the sigma meson diverges at the Fermi surface, i.e., at $\mu = \mu_{\rm SB} = m_q(T = \mu = 0)$. Strictly speaking, our wavefunction

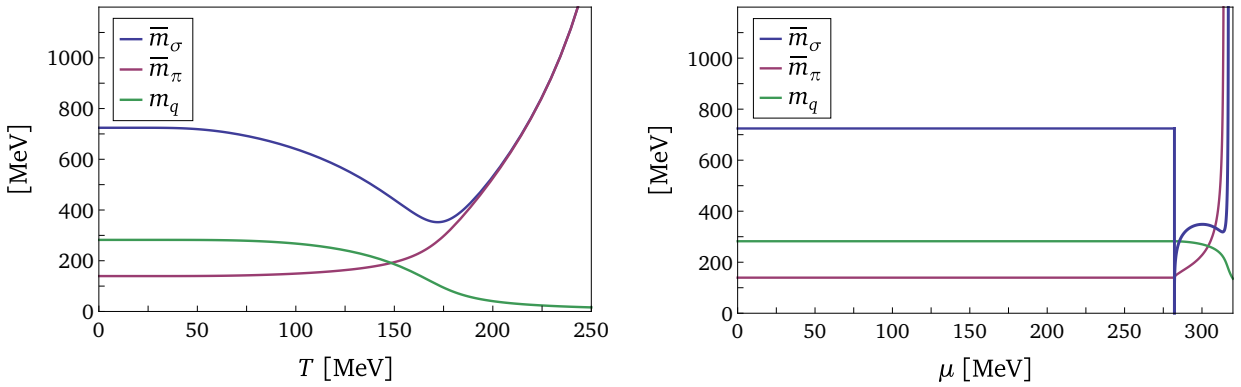

Figure 3.23: Renormalized curvature masses for the mesons and the quark mass. We present the particle masses as functions of the temperature at $\mu = 0$ (left panel) and also as functions of the chemical potential at $T = 0$ (right panel). In the vacuum limit, the renormalized meson curvature masses read $\overline{m}_\sigma \approx 724\,\text{MeV}$ and $\overline{m}_\pi \approx 140\,\text{MeV}$. Our results indicate a chiral crossover in both scenarios. Specifically, the pseudo-critical values are $T_{\text{pc}} \approx 172\,\text{MeV}$ at $\mu = 0$ and $\mu_{\text{pc}} \approx 313\,\text{MeV}$ at $T = 0$.

renormalization is ill-defined at this point since the momentum-dependent two-point correlator is non-analytic, see Eq. (3.169). As illustrated in Fig. 3.22 (right panel), this divergence at $T = 0$ already starts building up at low temperatures and hence cannot be cured by finite temperature. Notably, our zero-temperature wavefunction renormalization for the pions is well-defined at the Fermi surface.

From a more phenomenological point of view, a negative curvature of bosonic two-point functions may be considered an indication of an instability associated with the formation of an inhomogeneous ground state at low temperatures [243, 443, 444], see also Refs. [323, 349, 445] in this context. In addition, such a feature also underlies the discussion of the existence of moat regimes in the QCD phase diagram which are defined by $Z^{\perp}_{(\sigma/\pi)} < 0$, see Refs. [80, 446–450]. We will come back to this when we discuss the position of the boundaries of regimes associated with negative wavefunction renormalizations relative to the position of the chiral phase boundary in our model.

In Fig. 3.23 we show our results for the renormalized meson masses together with the quark mass. Since the wavefunction renormalization factors exhibit a zero-crossing at sufficiently high temperatures and/or large chemical potentials, our presentation of particle masses is restricted to regions of external parameters where the wavefunction renormalizations remain positive. As before, we can use the minimum of the sigma mass as a function of the temperature to quantify the chiral crossover. To be specific, for $\mu = 0$, we find that the temperature-induced crossover occurs at $T_{\text{pc}} \approx 172\,\text{MeV}$. Above the pseudo-critical temperature, the differences in the curvature masses of the mesons become rapidly suppressed by thermal fluctuations. For higher temperatures, the renormalized meson curvature masses are eventually dominated by the zero-crossing of the wavefunction renormalizations at $T \approx 284\,\text{MeV}$. At zero temperature, we identify a crossover at $\mu_{\text{pc}} \approx 313\,\text{MeV}$ as indicated by the finite minimum of the sigma mass as a function of the chemical potential. As before, our results imply that there is no critical endpoint in the phase diagram of the quark-meson model. Beyond this crossover, the behavior of the renormalized curvature masses at zero temperature is completely dominated by the zero-crossings of the wavefunction renormalizations. Additionally, it is important to note that the renormalized curvature mass of the sigma meson jumps to zero at $\mu = \mu_{\text{SB}}$. This jump discontinuity is unphysical since it stems from the divergence of the corresponding wavefunction renormalization at this point, see Fig. 3.22 (right panel). Therefore, although the renormalized curvature mass of the sigma meson at zero temperature acquires its minimal value at $\mu = \mu_{\text{SB}}$, this minimum is not linked to the chiral phase

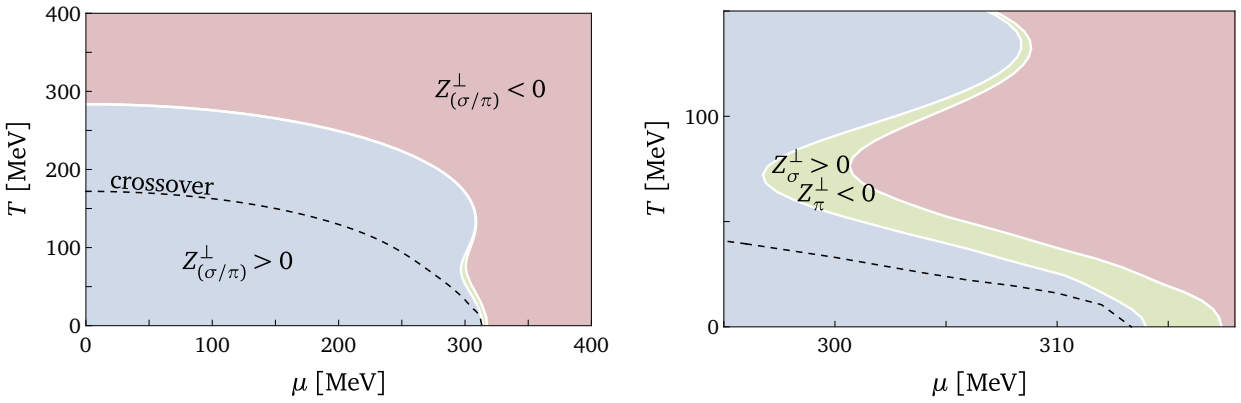

Figure 3.24: Phase diagram of the quark-meson model in the plane spanned by the temperature T and the chemical potential μ. In the blue-colored region, both wavefunction renormalizations are positive, whereas the red-colored area indicates that both wavefunction renormalizations are negative. In the small green-colored region at high densities, we find $Z^{\perp}_{\sigma} > 0$ and $Z^{\perp}_{\pi} < 0$. Accordingly, the green and red regions are identified as moat regimes. A zoom into the green-colored region is shown in the right panel. The dashed line represents the crossover line which is fully contained in the region of positive wavefunction renormalization factors.

transition. Finally, we remark that, in the vacuum limit, the renormalized curvature mass of the pion is $\overline{m}_{\pi} \approx 140\,\text{MeV}$, which is in close agreement with the fixed pole mass of 138 MeV.

With the sigma mass as a function of external parameters at hand, we can determine the entire phase boundary associated with the chiral crossover. We consider the simple case in which this phase boundary is described by a curve in the plane spanned by temperature T and chemical potential μ. Phenomenologically, this curve indicates at which points (T,μ) the correlation length for fluctuations in the chiral condensate reaches a maximum. From our analysis of results illustrated in Fig. 3.23, it already follows that the endpoints of the crossover line are located at $(T_{\text{pc}},0)$ and $(0,\mu_{\text{pc}})$. For values of the chemical potential with $0 < \mu < \mu_{\text{pc}}$, we determine the corresponding crossover temperature from the minimum of the temperature-dependent renormalized curvature mass associated with the sigma meson. Our results for the phase diagram of the quark-meson model are shown in Fig. 3.24. In addition to the presentation of the crossover line, we highlighted the normal region, in which the wavefunction renormalization factors are positive, as well as the moat regimes, where at least one wavefunction renormalization is negative. In particular, at zero chemical potential, we find that both wavefunction renormalizations exhibit a zero-crossing at $T \approx 284\,\text{MeV}$. Accordingly, this temperature then marks the transition into the moat regime at $\mu = 0$. At zero temperature, the moat transition as indicated by the zero-crossing of $Z^{\perp}_{\pi}$ occurs as $\mu \approx 314\,\text{MeV}$. Notice, however, that the wavefunction renormalization associated with the sigma meson is still positive at this point of the phase diagram. Eventually, the zero-crossing of $Z^{\perp}_{\sigma}$ at $\mu \approx 317\,\text{MeV}$ marks the second moat transition along the μ-axis beyond which both wavefunction renormalizations assume negative values. Altogether, our results demonstrate that the chiral crossover line is fully contained within the normal region of the phase diagram. Furthermore, the phase structure presented in Fig. 3.24 is corroborated by a computation in full functional QCD [80].

Spectral functions

In accordance with our previous renormalization prescription for the fields, we define the renormalized spectral functions as follows:

$$\bar{\rho}_{(\sigma/\pi)}(\omega,\vec{Q})\big|_{T,\mu} = Z^{\perp}_{(\sigma/\pi)}(T,\mu)\ \rho_{(\sigma/\pi)}(\omega,\vec{Q})\big|_{T,\mu}\,. \tag{3.194}$$

We would like to remark that the multiplication with a wavefunction renormalization does not change the behavior of the spectral function with respect to the energy ω or the spatial momentum $\vec{Q}$. This means that all energies that are associated with a certain structure found in ρ remain unchanged. In particular, pole masses are invariant under this renormalization of the spectral function.

As before, we focus on meson spectral functions at vanishing spatial momentum, i.e., we set $\vec{Q} = \vec{0}$. Our results for the renormalized spectral functions in the vacuum limit are illustrated in Fig. 3.25 (left panel). In particular, we observe that the resonance peak associated with the mass of the sigma meson is located at $\omega_{\mathrm{res},\sigma} \approx 572\,\mathrm{MeV}$. By construction, the renormalized spectral function for the pions shows that their pole mass lies at $m_{\mathrm{pole},\pi} = \omega_{\mathrm{res},\pi} \approx 138\,\mathrm{MeV}$. Moreover, the pion spectral function exhibits the familiar structure for the decay into two quarks, $\pi' \to \bar{\psi}\psi$. This structure can be observed at $\omega_{\mathrm{decay}} = 2m_q \approx 564\,\mathrm{MeV}$, which is the energy necessary to trigger the decay process. We emphasize that the vacuum limit provides us with the situation in which $\omega_{\mathrm{decay}} < \omega_{\mathrm{res},\sigma}$. Consequently, the resonance peak in the spectral function of the sigma mode does not correspond to a Dirac-delta peak and hence cannot be associated with a pole mass. However, we add that this result should be considered with caution as it may be an artifact of our choice for the initial condition. In other words, the mass resonance of the sigma meson may be lifted to higher energies by introducing additional couplings to the initial action Γ_{Λ_0}. Furthermore, due to $\omega_{\mathrm{decay}} < \omega_{\mathrm{res},\sigma}$, the structure associated with the decay of the sigma meson, $\sigma' \to \bar{\psi}\psi$, is highly suppressed and therefore not visible on the scale of the figure. At zero temperature and above the Silver-Blaze threshold, i.e., for $\mu > \mu_{\mathrm{SB}}$, this situation changes rapidly. The kink-like structures associated with the meson decay now scale as $\omega_{\mathrm{decay}}(\mu) = 2\mu$, resulting in $\omega_{\mathrm{decay}} > \omega_{\mathrm{res}}$ for both mesons, see Fig. 3.25 (right panel). Accordingly, the decay structures become clearly visible in both spectral functions. In addition, the sigma spectral function now gives rise to a Dirac-delta peak such that the notion of a pole mass applies. As mentioned in our previous studies, the behavior of the decay energy as a function of the chemical potential is readily explained by the fact that the mesons at zero temperature can only decay into their quark content if the excitation energy is high enough to create a pair of quarks carrying the Fermi energy $\omega_{\mathrm{F}} = \mu$ each.

Our results for the renormalized meson spectral functions at finite temperature and zero chemical potential are shown in Fig. 3.26. In this case, the temperature dependence of the decay structures follows that of the quark mass, $\omega_{\mathrm{decay}}(T) = 2m_q(T)$. Moreover, we find that the resonance peak in the sigma spectral function broadens rapidly with increasing temperature and that its height is continuously lowered. For temperatures $T \gtrsim 180\,\mathrm{MeV}$, the renormalized meson spectral functions eventually become more and more degenerate, see Fig. 3.26 (right panel).

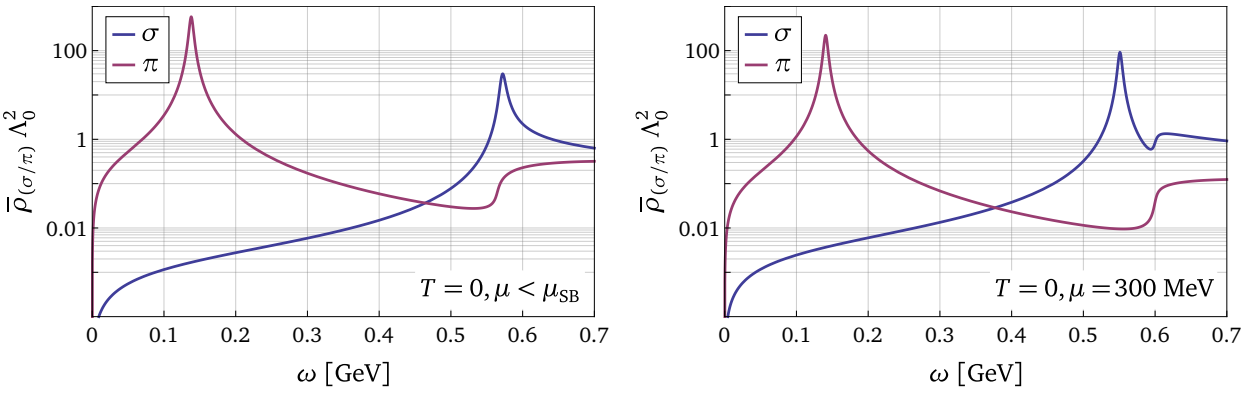

Figure 3.25: Renormalized meson spectral functions at zero temperature. For $\mu < \mu_{\mathrm{SB}} \approx 282\,\mathrm{MeV}$ (left panel), where the behavior of the system is governed by the Silver-Blaze property, we find resonances at $\omega_{\mathrm{res},\sigma} \approx 572\,\mathrm{MeV}$ and $\omega_{\mathrm{res},\pi} \approx 138\,\mathrm{MeV}$. In this case, the resonance peak in the sigma spectral function cannot be associated with a pole mass since $\omega_{\mathrm{decay}} < \omega_{\mathrm{res},\sigma}$. Above the Silver-Blaze threshold, this situation quickly changes as the energy associated with the decay of a meson into two quarks scales with the chemical potential. Specifically, for $\mu = 300\,\mathrm{MeV}$ (right panel), the resonances in both spectral functions correspond to a pole mass.

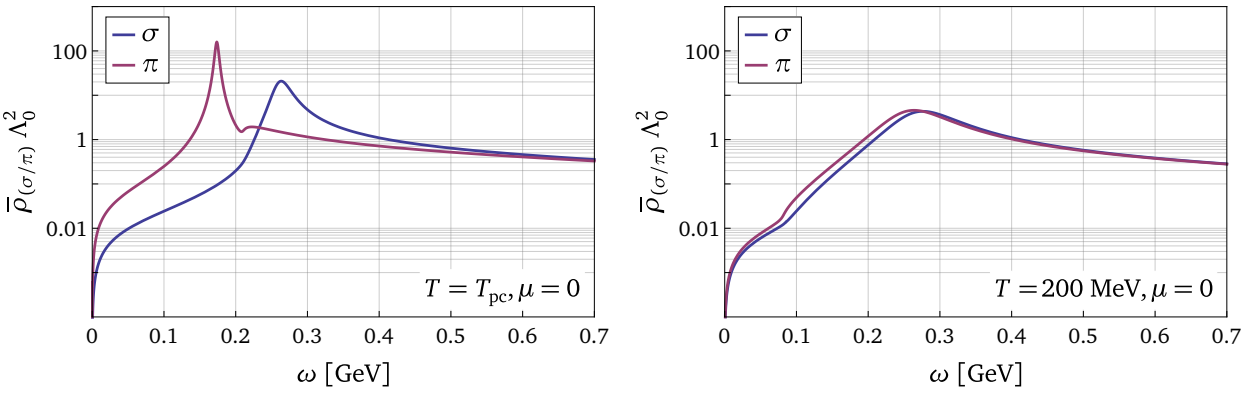

Figure 3.26: Renormalized meson spectral functions at finite temperature and zero chemical potential. At $T = T_{\mathrm{pc}} \approx 172\,\mathrm{MeV}$ (left panel), the sigma meson is already destabilized by thermal fluctuations while the spectral function of the pions still exhibits a Dirac-delta peak. At $T = 200\,\mathrm{MeV}$ (right panel), the mesons are quasi-degenerate as indicated by the almost identical spectral functions.

4

SUMMARY AND OUTLOOK

In this thesis, we have studied technical as well as phenomenological aspects of QCD at low energies and finite external parameters such as temperature T and chemical potential μ. To be more specific, we have made use of an effective theory, which considers two massless quark flavors interacting through a Yukawa term, in order to study the phase structure of quark matter and, in particular, examine the effects of artificial symmetry breaking on observables relevant for the chiral phase transition. The functional renormalization group has served as our key method, representing an ideal non-perturbative tool for the investigation of strong-interaction matter. In addition, we have collected and analyzed subtleties that appear in the calculation of correlation functions and that are specifically important in quantum field theories with fermions coupled to a chemical potential.

In our analysis of loop integrals for fermionic systems in the presence of finite external parameters, we have identified and discussed in detail scenarios in which an interchange of mathematical operations such as differentiation, integration, and limit processes leads to different results. These operations are often involved in the computation of physical observables and do, a priori, not commute. As a consequence, the non-commutative nature of different mathematical operations needs to be considered with great care to avoid ambiguities and inconsistencies in results for correlation functions. As for any well-defined framework, the fRG approach is in principle free of mathematical ambiguities since the order of all operations is determined by the Wetterich equation. Observables can then be obtained by applying suitable projection rules to the exact solution of the Wetterich equation. However, exact solutions of this equation exist only for rare, special cases. As a result, strategies for the calculation of correlation functions have been developed, which commonly rely on the assumption that at least some of the involved mathematical operations are commutative. Although many of these approaches have been applied very successfully to quantum field theories in the vacuum limit, finite external parameters such as temperature and/or chemical potential introduce several subtleties. These must be taken into account in order to obtain correct results for correlation functions. We have demonstrated in detail that calculations directly at zero temperature and at finite chemical potential are particularly delicate in this respect. Although our presentation has focused on diagrams with a one-loop structure, as only such diagrams appear within the fRG framework, our general considerations can be carried over to computations of loop diagrams of higher order as encountered in other approaches.

In addition to our general discussion of subtleties that arise in finite-temperature and finite-

density studies, we demonstrated where such subtleties are encountered in concrete calculations by employing the quark-meson model. To be specific, we calculated the curvature and plasmon masses of the sigma meson and the pions. To this end, we employed a standard expansion of the Wetterich equation in terms of field degrees of freedom and analyzed the resulting meson two-point functions. In accordance with our general considerations, we found that the zero-temperature and finite-temperature results are inconsistent in the sense that the two-point functions calculated directly at zero temperature do not agree with the corresponding finite-temperature results in the zero-temperature limit. This is the case for correlation functions evaluated at vanishing external momenta and finite external momenta. We showed that the inconsistency between results for correlation functions obtained at $T = 0$ and in the limit $T \to 0$ eventually originates from interchanging derivatives with respect to fields with the loop integration on the right-hand side of the Wetterich equation. In conjunction with the presence of a derivative with respect to the RG scale under the loop integral, this is not allowed in calculations directly at zero temperature for values of the chemical potential that exceed the Silver-Blaze threshold because of the non-analytic behavior of the loop diagrams in this regime. From our analysis, however, we deduced a systematic prescription that allows us to compute correlation functions directly at zero temperature such that they are consistent with those obtained from taking the zero-temperature limit of a finite-temperature calculation. We also showed that finite-temperature calculations of correlation functions via the aforementioned interchange of derivatives with respect to fields and loop integration are unambiguous, even at finite chemical potential.

The fRG approach to quantum field theory relies on the introduction of an auxiliary function, the regulator, which systematically modulates the amount of quantum fluctuations contributing to the theory. The regulator is in general no physically meaningful object but rather serves as an instrument to evaluate loop diagrams in a controlled fashion. In particular, the regulator should not spoil the predictions for physical observables and is therefore constrained by the symmetry properties of the theory. However, since exact calculations in quantum field theory are notoriously difficult, it is common not only to implement truncations but also to relax the symmetry constraints on the regulator function. Specifically, regulators that induce an explicit breakdown of Lorentz symmetry are predominantly favored in the presence of finite external parameters. In order to assess the impact of this artificial symmetry breaking at finite temperature and chemical potential, we have computed chiral observables from the quark-meson model in different regularization schemes. In particular, we have considered regulators that not only respect Lorentz symmetry in the vacuum limit but preserve also chiral symmetry as well as the Silver-Blaze symmetry in the presence of a quark chemical potential.

Our first study of QCD phenomenology by means of the functional renormalization group has been performed with canonical momentum-dependent regulator functions. In particular, we have considered polynomial regulators with and without explicit Lorentz symmetry breaking, allowing us to examine the scheme dependence of physical observables in the context of the chiral phase transition. To this end, we calculated meson curvature masses and meson spectral functions in the presence of finite temperature and chemical potential. We remark that, for momentum-dependent regulators, a calculation of correlation functions at finite external parameters is significantly more difficult in covariant regularization schemes than in spatial ones. Nevertheless, based on symmetry properties and an analysis of the pole structure of the regularized propagator, we were able to evaluate loop integrals analytically to a great extent in both schemes.

Our analysis of results for curvature masses as obtained within the spatial and covariant schemes suggests that the impact of Lorentz symmetry breaking is, in fact, mild in the regime governed by

a finite quark mass. Along the T-axis and the μ-axis of the phase diagram, both schemes give rise to a second-order phase transition in the absence of explicit chiral symmetry breaking, which turns into a crossover in the physical case. Interestingly, the momentum-dependent covariant regulator systematically leads to slightly lower values of curvature masses in the vacuum limit as well as (pseudo-)critical external parameters. Differences in the results obtained within the two schemes then grow bigger with increasing temperatures, specifically for temperatures beyond the phase transition or crossover. Our results further demonstrate that regularization scheme artifacts, which are associated with external parameters becoming comparable in size to the initial RG scale Λ_0, are also sensitive to the treatment of Lorentz symmetry.

As a second step in our investigation of scheme dependences, we have computed spectral functions for the sigma meson and the pions in the presence of explicit chiral symmetry breaking. Our results for the meson spectral functions again show that, for values of external parameters below the chiral crossover, the choice of a momentum-dependent covariant regulator over a spatial one only results in quantitative and no qualitative differences. However, this situation changes for temperatures beyond the pseudo-critical temperature. While the meson spectral functions as obtained within the spatial scheme still behave as expected from QCD phenomenology, unphysical structures arise in the pion spectral function as calculated within the covariant scheme. More specifically, the finite-temperature spectral function becomes negative at low energies and gives rise to an additional small peak that has no physically meaningful interpretation. Our analysis indicates that the polynomial regulator in the covariant scheme significantly alters the pole structure of the propagator in momentum space, which can lead to an unphysical behavior in regions of the phase diagram where multiple physical scales compete with each other. Despite this observation, we highlight that the spectral function of the sigma meson as computed in the covariant scheme is free of anomalies.

Possible future efforts in the context of covariant polynomial regulators could involve a fine-tuning of coefficients c_n for some given polynomial degree N such that unphysical effects in the calculation of, e.g., spectral functions are minimized. However, we generally advise against this step as the complexity as well as the numerical stability of corresponding loop integrals is highly sensitive to those parameters. Overall, we come to the conclusion that spatial regulators, which explicitly break Lorentz symmetry, are in fact well suited to study the mechanisms of low-energy QCD that underlie the chiral phase transition. However, for values of external parameters beyond the chiral phase boundary, the different treatment of momentum modes by the spatial regulator becomes more apparent such that we expect effects associated with artificial Lorentz symmetry breaking to increase. For a comprehensive and accurate study of the phase diagram, we therefore recommend a symmetry-constrained regularization scheme which also preserves the pole structure of the propagator.

In the final part of this thesis, we discussed Callan-Symanzik flows of chiral fermion-boson models within the functional RG framework. Unlike canonically used regulator functions, the CS regulator is independent of loop momenta. As a consequence, CS flows do not describe the evolution of a given theory from some high-momentum regime down to a low-momentum regime, as in RG flows of the Wilsonian type. Instead, they specify the dependence of a given effective action on a mass scale, e.g., the fermion mass. The CS regulator has several advantages: it allows for Lorentz-invariant renormalization group flows in the vacuum limit, preserves the Silver-Blaze symmetry of quantum field theories in the presence of a finite chemical potential, and leaves the momentum structure of the propagator unchanged. Nevertheless, besides the fact that CS flows require an additional UV regularization, the fermionic CS regulator introduces an explicit fermion mass in

the form of the RG scale to the theory such that chiral symmetry becomes explicitly broken. We emphasize that this symmetry breaking is unphysical and significantly spoils any results for chiral observables. To address this issue, we derived Ward-Takahashi identities for a global chiral symmetry of the theory. In our case, these identities are partial differential equations that we solved to obtain a symmetry-constrained effective action in which all unphysical symmetry-breaking terms are removed. In essence, the Ward-Takahashi identities give rise to a symmetrization procedure, which we implemented to render the computation of physical quantities from the corresponding effective action meaningful. In our framework, physical explicit chiral symmetry breaking is realized by a linear source term for the field associated with the sigma meson.

We demonstrated the application of our symmetrized CS framework by computing several quantities such as meson curvature masses, the phase diagram, momentum-dependent two-point functions of the mesons, and corresponding spectral functions within the quark-meson model. In particular, by comparing results from our CS framework with those obtained from unconstrained CS flows, we demonstrated the strong impact of the regulator-induced explicit breaking of the chiral symmetry on physical observables. With our symmetrized CS framework at hand, we analyzed the phase diagram of our quark-meson model in the plane spanned by the temperature and the quark chemical potential together with the meson two-point functions. In general, we find that our results are in accordance with results from previous studies of related models. Furthermore, we highlight that the CS regulator generally allows us to perform calculations analytically to a great extent and thus renders the mechanisms underlying the phase diagram of low-energy QCD more accessible. Specifically, our exact one-loop results provide the opportunity for an analytic understanding of intriguing phenomena potentially existing in different regimes of the phase diagram, such as the emergence of moat regimes and Friedel oscillations at finite chemical potential. From a field-theoretical standpoint, our exact results for the meson two-point functions at zero temperature allow us to analyze the limits of the application of derivative expansions of the effective action, both at vanishing and finite chemical potential.

The Callan-Symanzik framework developed in this present work is an enormously promising approach toward the low-energy physics of QCD as it respects all symmetries of the underlying theory and does not alter the pole structure of the propagator. Therefore, our CS framework sets the methodological stage for future non-perturbative studies of thermodynamic as well as spectral properties of chiral fermion-boson models. Since we restricted our computations to purely fermionic loops for simplicity, a natural next step would be to employ our CS framework for computations which also take bosonic fluctuations into account. Whereas effects from bosonic fluctuations may be suppressed at very low temperatures along the chemical potential axis, they are known to be highly relevant for an analysis of the phase diagram at finite temperature and chemical potential. In particular, it will be very interesting to make use of our CS framework to improve our understanding of the critical endpoint in the QCD phase diagram and also to study the potential emergence of inhomogeneous phases.

Appendices

A

CONVENTIONS

A.1 Basic conventions

All calculations are performed in four spacetime dimensions, i.e., $d = 4$. The standard Dirac matrices then are complex $n \times n$ matrices with $n = 2^{\lfloor \frac{d}{2} \rfloor} = 4$. Furthermore, we always consider the physical number of color degrees of freedom, i.e., we set

$$N_c = 3 \,. \tag{A.1}$$

Our Lorentz matrix follows the mostly-minus convention, i.e., we have

$$\eta = \mathrm{diag}(+,-,-,-) \,. \tag{A.2}$$

The Lorentz matrix is used to describe the metric of Minkowski spacetime in Sec. A.4. In the main part of this work, however, we use the Lorentz matrix to capture the sign structure of the mesonic two-point correlator.

An indispensable aid in the representation of discontinuities is the Heaviside step function. It can be generally defined as

$$\forall x \in \mathbb{R}: \qquad \theta_c(x) = \begin{cases} 1, & x > 0 \\ c, & x = 0 \\ 0, & x < 0 \end{cases} \,, \tag{A.3}$$

where the constant c can be chosen at will. For our purposes, setting $c = \frac{1}{2}$ is the most reasonable choice. Thus, we define

$$\theta(x) := \theta_{\frac{1}{2}}(x) \,. \tag{A.4}$$

This directly implies that the Heaviside function θ satisfies the following relation:

$$\theta(-x) = 1 - \theta(x) \,. \tag{A.5}$$

In words, the values of the Heaviside function at some point x and its negative counterpart $-x$ always sum to exactly one. For any other choice of c, this property would not hold at $x = 0$.

A.2 Units

For simplicity of notation, we shall choose a unit system in which selected physical constants are set to unity. For example, the speed of light c may be set to unity such that the conversion of the (invariant) mass of a particle and the associated energy becomes trivial. Specifically, we choose

$$c = \hbar = k_B = 1 \,, \tag{A.6}$$

meaning that we employ the so-called natural units. In this unit system, the physical dimensions of all quantities can be expressed in terms of dimensions of energy:

$$[\text{length}]^{-1} = [\text{time}]^{-1} = [\text{temperature}] = [\text{momentum}] = [\text{mass}] = [\text{energy}] \,. \tag{A.7}$$

To be more concrete, Eq. (A.6) implies the following conversions:

$$\begin{aligned} 1\,\text{m} &\approx 5,07 \times 10^{12}\,\text{MeV}^{-1} \,, & 1\,\text{s} &\approx 1,52 \times 10^{21}\,\text{MeV}^{-1} \,, \\ 1\,\text{kg} &\approx 5,61 \times 10^{29}\,\text{MeV} \,, & 1\,\text{K} &\approx 8,62 \times 10^{-11}\,\text{MeV} \,. \end{aligned} \tag{A.8}$$

In natural units, the physical dimensions of a quantity take the form $[\text{energy}]^{\varepsilon}$, where ε denotes the so-called energy dimension of that quantity. The energy dimension depends in general on the number d of spacetime dimensions. To give an example, we consider a bosonic n-point correlation function.

Bosonic correlator	$\varepsilon(d)$	$\varepsilon(4)$
$\tilde{\Gamma}^{(n)}(Q_1,\ldots,Q_{n-1})$	$n\,\frac{2-d}{2} + d$	$4-n$

It follows that the bosonic two-point correlation function ($n = 2$) in four spacetime dimensions ($d = 4$) has an energy dimension of $\varepsilon = 2$. A more comprehensive overview of quantities and their energy dimension can be found in Table A.1.

When it is necessary to compare results from theory and experiment, factors of c, $\hbar$, and k_B can easily be reintroduced in order to convert the units of the prediction into the units of the data. More concretely, if our result has the energy dimension ε and the physical units for the result should be $[\text{mass}]^{\alpha}\,[\text{length}]^{\beta}\,[\text{time}]^{\gamma}\,[\text{temperature}]^{\delta}$, then consistency requires that

$$\varepsilon = \alpha - \beta - \gamma + \delta \tag{A.9}$$

and the conversion is accomplished by

$$\begin{aligned} &\big(\text{answer in } [\text{mass}]^{\alpha}\,[\text{length}]^{\beta}\,[\text{time}]^{\gamma}\,[\text{temperature}]^{\delta}\big) \\ &\quad = (\text{answer in } [\text{energy}]^{\varepsilon})\; c^{\delta-\varepsilon-\alpha-\gamma}\,\hbar^{\alpha+\delta-\varepsilon}\,k_B^{-\delta} \,. \end{aligned} \tag{A.10}$$

Quantity	$\varepsilon(d)$	$\varepsilon(4)$
$\phi(x)$	$\frac{d-2}{2}$	1
$\phi(p)$	$-\frac{d+2}{2}$	-3
$\frac{\delta}{\delta\phi(x)}$, H	$\frac{d+2}{2}$	3
$\frac{\delta}{\delta\phi(p)}$	$\frac{2-d}{2}$	-1
$\psi(x)$, $\overline{\psi}(x)$	$\frac{d-1}{2}$	$\frac{3}{2}$
$\psi(p)$, $\overline{\psi}(p)$	$-\frac{d+1}{2}$	$-\frac{5}{2}$
$\frac{\delta}{\delta\psi(x)}$, $\frac{\delta}{\delta\overline{\psi}(x)}$	$\frac{d+1}{2}$	$\frac{5}{2}$
$\frac{\delta}{\delta\psi(p)}$, $\frac{\delta}{\delta\overline{\psi}(p)}$	$\frac{1-d}{2}$	$-\frac{3}{2}$
$\Gamma[\Phi]$	0	0
$U(\Phi)=\Gamma(\Phi)/V_d$	d	4
m_ϕ, m_ψ, μ	1	1
h	$2-\frac{d}{2}$	0
$\rho(\omega,\vec{Q})$	-2	-2

Table A.1: Overview of quantities and their energy dimension ε, which is a function of the number d of spacetime dimensions. In addition to the general case, we also considered the special case $d=4$. The energy dimensions of ψ and its adjoint $\overline{\psi}$ are always the same.

A.3 Shorthand notations

Throughout this work, we adopt the following notations.

- Shorthand notation for integrals:

$$\int_x \equiv \int_{\mathbb{R}^4} \mathrm{d}^4x \equiv \int_{\mathbb{R}^3} \mathrm{d}^3x \int_{\mathbb{R}} \mathrm{d}x^0 \,, \qquad \int_{\vec{x}} \equiv \int_{\mathbb{R}^3} \mathrm{d}^3x \,, \tag{A.11}$$

$$\int_p \equiv \int_{\mathbb{R}^4} \frac{\mathrm{d}^4p}{(2\pi)^4} \equiv \int_{\mathbb{R}^3} \frac{\mathrm{d}^3p}{(2\pi)^3} \int_{\mathbb{R}} \frac{\mathrm{d}p^0}{2\pi} \,, \qquad \int_{\vec{p}} \equiv \int_{\mathbb{R}^3} \frac{\mathrm{d}^3p}{(2\pi)^3} \,. \tag{A.12}$$

- We make use of the Einstein summation convention in which a summation is implied whenever a pair of matching upper and lower indices appears:

$$a^i \; b_i \equiv \sum_i a_i \; b_i \,. \tag{A.13}$$

- It is often possible to express a function of more than one variable in terms of a reduced function, which depends on fewer arguments. In order to formally distinguish between these functions, we denote the reduced function with a tilde. For example, the regulator function can be written as

$$R_k(p,q) = \widetilde{R}_k(p)\,(2\pi)^4\delta^{(4)}(p-q) \,. \tag{A.14}$$

- For logarithmic expressions, we use the notation $\ln(a)$ when the input $a \in \mathbb{C}$ is a scalar, and $\mathrm{Ln}(A)$ if $A \in M_n(\mathbb{C})$ has matrix structure.

- The trace tr of a linear operator A is defined as

$$\mathrm{tr}\{A\} = \sum_i \sum_j A_{ij}\, \delta_{ij} = \sum_i A_{ii} \tag{A.15}$$

and denotes the sum over diagonal elements. Notice that the elements $A_{ij} = \langle i|A|j\rangle$ depend on the choice for the vector space basis $\{|i\rangle\}$, whereas the trace itself is basis-independent. In analogy to the case of countably many basis vectors, we define the trace Tr of an operator-valued bi-variate function A as

$$\mathrm{Tr}\{A\} = \int_x \int_y \mathrm{tr}\{A\}(x,y)\, \delta^{(4)}(x-y) = \int_x \mathrm{tr}\{A\}(x,x)\,. \tag{A.16}$$

Here, the trace Tr is also independent of the basis such that a representation in momentum space is straightforward.

$$\mathrm{Tr}\{A\} = \int_p \int_q \mathrm{tr}\{A\}(p,q)\, (2\pi)^4 \delta^{(4)}(p-q) = \int_p \mathrm{tr}\{A\}(p,p)\,. \tag{A.17}$$

Furthermore, it is worth mentioning that integration and the process of evaluating the trace tr are commutative operations.

A.4 Minkowski and Euclidean quantum field theory

If we aim to describe processes occurring in nature, we need a mathematical structure, that allows us to specify the location of an object in space and time, as well as to establish the notion of a scalar based on transformations between different frames of reference. Introductory literature on relativistic physics naturally provides the concept of Minkowski spacetime, i.e., a manifold $\mathbb{R}^4$ equipped with the Lorentzian metric, which serves as a topological basis for a Poincaré-invariant formulation of the theory content. In this work, we deal with systems of quantum particles in the absence of strong gravitational fields so that, from the standpoint of general relativity, the usage of Minkowski spacetime is physically reasonable even over arbitrarily large spacetime distances.

Throughout this thesis, we use the framework of quantum field theory as defined on Euclidean spacetime[1], which is related to its Minkowski counterpart by analytic continuation. Euclidean field theory was first brought forward by Schwinger [451–453] and also Nakano [454], and has since then gained more and more interest, particularly through the work of Symanzik [455–457] and Nelson [458, 459]. Over time, it has developed into a powerful and immensely valuable tool for modern research. The advantage of working in the Euclidean formulation is reflected by the fact that its (vacuum) correlators are real-analytic functions, while their Minkowski counterparts are distributions.[2] Moreover, Euclidean path integrals benefit from exponential suppression of large field values, whereas the corresponding Minkowski integrals are oscillatory in nature and hence more difficult to work with.[3] This has important consequences for practical calculations as

[1] Notice that purists often refer to it as Euclidean *space* since former temporal and spatial coordinates are treated equally by the Euclidean metric. However, we will use the term *spacetime* as the incorporation of finite temperature or a finite chemical potential by means of the imaginary-time formalism inherently leads to the distinction of one Euclidean direction, see Section 2.3.

[2] Correlation functions of a Minkowski quantum field theory are often declared to be tempered distributions but several extensions have been proposed in order to include a wider class of test functions, allowing for modified locality properties and non-renormalizable interactions. Noteworthy works suggest the use of ultradistributions [460, 461], (Fourier) hyperfunctions [462–469], and further generalizations, see, e.g., Refs. [470–472].

[3] Although significant progress has been made in controlling the real-time functional integrals arising in quantum mechanics, the situation for real-time functional integrals relevant to quantum field theory is much less developed. For an accounting of both, see, e.g., Ref. [473].

the convergence properties of the Euclidean path integrals allow for first-principle computations of correlation functions on a spacetime lattice by numerical Monte-Carlo methods. Furthermore, the path integral formalism reveals a formal connection between Euclidean quantum physics and classical statistical physics such that Euclidean field theory also provides a suitable framework for studying the equilibrium thermodynamics of relativistic quantum systems.

For practical purposes, it can be convenient to construct an interacting quantum field theory within the Euclidean framework, i.e., without prior knowledge that the generated Euclidean Green's functions arose from a Minkowski quantum field theory. In order to claim any physical relevance for the results obtained from the Euclidean field theory, the Euclidean construction must be built upon a system of conditions, which not only justifies an analytic continuation to Minkowski spacetime but also ensures that the analytic continuation yields a sensible quantum field theory that suffices fundamental physical principles. Such a system indeed exists in various forms and stages of refinement, see, e.g., Refs. [101, 474–482], and it is based on the Osterwalder-Schrader axioms [474, 475].[4] The several formulations of the Osterwalder-Schrader axioms differ on a technical level but their relationship is, at least conceptually, well understood. Despite these differences, they are all built upon the same central idea of enabling an Euclidean equivalent of relativistic quantum field theory.[5] Following the core reasoning of the Osterwalder-Schrader construction, we notice that in the Euclidean framework, the Lorentz group $SO^+(1,3)$ translates into the rotation group $SO(4)$, unitarity becomes reflection positivity, and cluster decomposition remains cluster decomposition. Analytic correlation functions of an Euclidean quantum field theory with those properties are then related to real-time correlators of a corresponding Minkowski quantum field theory by analytic continuation. This sets the stage for our "heuristic" study of quantum field theory and we do not aim to give a more detailed or more rigorous presentation of its mathematical foundations. Mathematical quantum field theory is a wide and ongoing area of research, which plays an important role since its developments benefit mathematics as well as physics. Nevertheless, it is severely handicapped by the fact that it is hardly possible to obtain results in quantum field theory, which are both interesting and rigorous. For an overview of the current efforts in mathematical quantum field theory, see, e.g., Refs. [482, 492–497].

In the following, we present more concretely how Euclidean and Minkowski quantum field theory are related. We start with the latter and perform an analytic continuation of the time variable such that the new time axis is rotated by an angle $\theta \in (-\pi, 0)$ into the complex plane, i.e., $x^0 \to \mathrm{e}^{\mathrm{i}\theta} x^0$. This procedure, commonly known as Wick rotation [498], is based on the assumption that there are no singularities in the covered region of the complex time plane. We choose $\theta = -\pi/2$ and hence let $x^0 \in \mathbb{R}$ parameterize time along the purely imaginary direction. The spatial components of the coordinate four-vector remain unchanged.

$$x^0 \to -\mathrm{i} x^0 \,. \tag{A.18}$$

[4] Notice that, prior to Osterwalder and Schrader, Nelson [483] offered a probabilistic solution for the reconstruction of Minkowski quantum field theory and presented an axiomatic system based on the construction of a Markov field. This has led to studies of the interplay between constructive quantum field theory and classical statistical mechanics, see, e.g., Refs. [282, 283]. Moreover, it soon became clear that Nelson's axiomatic system is stronger than the one given by Osterwalder and Schrader [484]. Nelson's method relies on scalar fields to have a Markovian structure, which turned out to be exceedingly difficult to verify for interacting fields, and cannot include fermion fields due to their Grassmann nature such that the Osterwalder-Schrader scheme is generally considered to be more worthwhile [282, 485].

[5] Constructing an axiomatic system for Euclidean quantum field theory that enables a well-defined transition to Minkowski spacetime implies having an analogous system of axioms for Minkowski quantum field theory in the first place. Indeed, a great amount of pioneering work in the endeavor to establish a consistent mathematical basis for Minkowski quantum field theory has been provided by Wightman [117, 486], Lehmann, Symanzik, and Zimmermann [487, 488], Ruelle [489] as well as Haag and Kastler [490, 491].

As a consequence, the metric of Minkowski spacetime, $g_{\mathrm{M}} = \eta$, effectively gets converted into the metric of Euclidean spacetime, $g_{\mathrm{E}} = \mathbb{1}_{4\times4}$, up to a global minus sign. To see this, we examine how a Lorentz scalar in position space transforms under the analytic continuation (A.18):

$$x^{\intercal}\, g_{\mathrm{M}}\, x = \left(x^0\right)^2 - \vec{x}^2 \;\rightarrow\; -\left(x^0\right)^2 - \vec{x}^2 = -x^{\intercal}\, g_{\mathrm{E}}\, x \;. \tag{A.19}$$

As for any Euclidean vector space, it is common practice to omit g_{E} in the matrix product such that $x^{\intercal}\, g_{\mathrm{E}}\, x \equiv x^{\intercal}\, x$. In order to obtain a consistent analytic continuation of the Fourier transform, the Wick rotation of the Minkowskian energy variable p^0 has to be performed in the opposite direction compared to its position space analog. A clockwise Wick rotation of the Minkowskian time variable, see Eq. (A.18), then implies a counterclockwise Wick rotation of the Minkowskian energy variable. In contrast to this, a clockwise Wick rotation of the Minkowskian energy variable would be problematic anyway since the Feynman propagator with the $\mathrm{i}\varepsilon$-prescription has poles in the fourth and second quadrant of the complex energy plane. As before, the spatial components of the four-momentum remain the same.

$$p^0 \rightarrow \mathrm{i}p^0 \;. \tag{A.20}$$

This gives rise to the (negative) Euclidean metric in momentum space, analogous to relation (A.19). Let us consider a general object ϑ, which can stand for a four-vector or a four-gradient in Euclidean spacetime. It becomes clear there is no distinction between contravariant and covariant components of ϑ, i.e.,

$$\vartheta^{\mu} = g_{\mathrm{E}}^{\mu\nu}\, \vartheta_{\nu} = \delta^{\mu\nu}\, \vartheta_{\nu} = \vartheta_{\mu} \;. \tag{A.21}$$

The same principle also applies to tensors of higher order. Notice that, nowadays, the term Wick rotation is used rather generically for the transition between Minkowski and Euclidean quantum field theory without necessarily referring to the traditional approach of keeping the metric fixed and changing the timelike component. A more general formulation is based on the vielbein formalism and extends the notion of Wick rotation as presented above to curved Minkowski spacetimes, see, e.g., Refs. [108, 499, 500].

In the second step, we show how field degrees of freedom in Euclidean and Minkowski quantum field theory are related. For the sake of clarity, quantities in Minkowski spacetime are labeled with a subscript M and quantities in Euclidean spacetime with a subscript E. In the case of a scalar field theory, the bosonic fields obey the relations

$$\phi_{\mathrm{E}}(x^0, \vec{x}) = \phi_{\mathrm{M}}(-\mathrm{i}x^0, \vec{x}) \;, \qquad \phi_{\mathrm{E}}(p^0, \vec{p}) = \mathrm{i}\phi_{\mathrm{M}}(-\mathrm{i}p^0, \vec{p}) \tag{A.22}$$

such that the analytic continuation translates the action functional into the Euclidean action and a global factor i:

$$\begin{aligned} S_{\mathrm{M}}[\phi_{\mathrm{M}}] &= \int_x \left(\phi_{\mathrm{M}}(x)\, \frac{1}{2}\left[-\partial_{\mathrm{M}}^2 - m_\phi^2\right]\, \phi_{\mathrm{M}}(x) - V\left(\phi_{\mathrm{M}}\right)(x) \right) \\ &\rightarrow \mathrm{i} \int_x \left(\phi_{\mathrm{E}}(x)\, \frac{1}{2}\left[-\partial_{\mathrm{E}}^2 + m_\phi^2\right]\, \phi_{\mathrm{E}}(x) + V\left(\phi_{\mathrm{E}}\right)(x) \right) \coloneqq \mathrm{i}\, S_{\mathrm{E}}[\phi_{\mathrm{E}}] \;. \end{aligned} \tag{A.23}$$

The appearance of the imaginary unit is essential as it turns the oscillatory factor of the path integral into a damping factor:

$$\mathcal{N}_{\mathrm{M}} \int \mathcal{D}\phi_{\mathrm{M}}\, \mathrm{e}^{\mathrm{i}S_{\mathrm{M}}[\phi_{\mathrm{M}}]} \;\rightarrow\; \mathcal{N}_{\mathrm{E}} \int \mathcal{D}\phi_{\mathrm{E}}\, \mathrm{e}^{-S_{\mathrm{E}}[\phi_{\mathrm{E}}]} \;. \tag{A.24}$$

For fermionic field theories, the Wick rotation is a little more subtle since properties of spinor representations of the Lorentz group are sensitive to the metric signature of spacetime. There have been several approaches to Euclidean fermions, see, e.g., Refs. [108, 500–504], but we follow the line of argumentation by Wetterich [108] and relate our Grassmann fields by

$$\begin{aligned} \psi_{\mathrm{E}}(x^0,\vec{x}) &= \psi_{\mathrm{M}}(-\mathrm{i}x^0,\vec{x})\,, & \psi_{\mathrm{E}}(p^0,\vec{p}) &= \mathrm{i}\psi_{\mathrm{M}}(-\mathrm{i}p^0,\vec{p})\,, \\ \overline{\psi}_{\mathrm{E}}(x^0,\vec{x}) &= -\mathrm{i}\overline{\psi}_{\mathrm{M}}(-\mathrm{i}x^0,\vec{x})\,, & \overline{\psi}_{\mathrm{E}}(p^0,\vec{p}) &= \overline{\psi}_{\mathrm{M}}(-\mathrm{i}p^0,\vec{p})\,. \end{aligned} \tag{A.25}$$

Furthermore, we impose the following relations for the Dirac matrices,

$$\gamma^0_{\mathrm{E}} = \gamma^0_{\mathrm{M}}\,, \qquad \gamma^i_{\mathrm{E}} = -\mathrm{i}\gamma^i_{\mathrm{M}} \qquad \forall i \in \{1,2,3\}\,, \qquad \gamma^5_{\mathrm{E}} = \gamma^5_{\mathrm{M}}\,, \tag{A.26}$$

which leads to the Euclidean Dirac algebra

$$\left\{\gamma^\mu_{\mathrm{E}}, \gamma^\nu_{\mathrm{E}}\right\} = 2\delta^{\mu\nu} \qquad \forall \mu,\nu \in \{0,1,2,3\}\,. \tag{A.27}$$

Notice that the relations (A.26) also imply self-adjoint Euclidean Dirac matrices, i.e.,

$$\left(\gamma^\alpha_{\mathrm{E}}\right)^\dagger = \gamma^\alpha_{\mathrm{E}} \qquad \forall \alpha \in \{0,1,2,3,5\}\,. \tag{A.28}$$

We now have all the necessary components to derive the Euclidean action for the fermionic quantum field theory:

$$\begin{aligned} S_{\mathrm{M}}\left[\overline{\psi}_{\mathrm{M}},\psi_{\mathrm{M}}\right] &= \int_x \left(\overline{\psi}_{\mathrm{M}}(x)\,\left[\mathrm{i}\partial\!\!\!/_{\mathrm{M}} - m_\psi\right]\,\psi_{\mathrm{M}}(x) - V_{\mathrm{M}}\left(\overline{\psi}_{\mathrm{M}},\psi_{\mathrm{M}}\right)(x)\right) \\ &\to \mathrm{i}\int_x \left(\overline{\psi}_{\mathrm{E}}(x)\,\left[\mathrm{i}\partial\!\!\!/_{\mathrm{E}} + \mathrm{i}m_\psi\right]\,\psi_{\mathrm{E}}(x) + V_{\mathrm{E}}\left(\overline{\psi}_{\mathrm{E}},\psi_{\mathrm{E}}\right)(x)\right) := \mathrm{i}\,S_{\mathrm{E}}\left[\overline{\psi}_{\mathrm{E}},\psi_{\mathrm{E}}\right]\,. \end{aligned} \tag{A.29}$$

Thus, the path integral then transforms according to

$$\mathcal{N}_{\mathrm{M}}\int \mathcal{D}\overline{\psi}_{\mathrm{M}}\mathcal{D}\psi_{\mathrm{M}}\,\mathrm{e}^{\mathrm{i}S_{\mathrm{M}}\left[\overline{\psi}_{\mathrm{M}},\psi_{\mathrm{M}}\right]} \to \mathcal{N}_{\mathrm{E}}\int \mathcal{D}\overline{\psi}_{\mathrm{E}}\mathcal{D}\psi_{\mathrm{E}}\,\mathrm{e}^{-S_{\mathrm{E}}\left[\overline{\psi}_{\mathrm{E}},\psi_{\mathrm{E}}\right]}\,. \tag{A.30}$$

Together, all of the relations above ensure that statements about the Minkowski quantum field theory translate consistently to analogous statements about the Euclidean quantum field theory and vice versa. However, we will not be overly strict in our use of language and will often refer to $SO(4)$ symmetry as Lorentz symmetry to emphasize the actual physical meaning of the rotation group within the framework of Euclidean quantum field theory. Since we exclusively employ Euclidean spacetime throughout this thesis, labels specifying quantities as Euclidean will be dropped outside this section.

A.5 Fourier transforms

Whenever we want to express a quantity in terms of its conjugate variable, the change of representation has to be done by a Fourier transform. To switch from position space to momentum space and vice versa, we impose the following conventions. For zero temperature we have

$$\phi(x) = \int_p \mathrm{e}^{\mathrm{i}p^\intercal x}\,\phi(p)\,, \qquad \phi(p) = \int_x \mathrm{e}^{-\mathrm{i}p^\intercal x}\,\phi(x)\,, \tag{A.31}$$

$$\psi(x) = \int_p \mathrm{e}^{\mathrm{i}p^\intercal x}\,\psi(p)\,, \qquad \psi(p) = \int_x \mathrm{e}^{-\mathrm{i}p^\intercal x}\,\psi(x)\,, \tag{A.32}$$

$$\overline{\psi}(x) = \int_p \mathrm{e}^{-\mathrm{i}p^\intercal x}\,\overline{\psi}(p)\,, \qquad \overline{\psi}(p) = \int_x \mathrm{e}^{\mathrm{i}p^\intercal x}\,\overline{\psi}(x)\,. \tag{A.33}$$

In order to include temperature dependence, we make use of the imaginary-time formalism of thermal field theory. The Fourier transforms of the boson and fermion fields are then given by

$$\phi(x) = \int_{\vec{p}} \frac{1}{\beta} \sum_{n\in\mathbb{Z}} \mathrm{e}^{\mathrm{i}\omega_n x^0} \mathrm{e}^{\mathrm{i}\vec{p}^{\intercal}\vec{x}}\ \phi_n(\vec{p}\,)\,, \qquad \phi_n(\vec{p}\,) = \int_{\vec{x}} \int_0^\beta \mathrm{d}x^0\ \mathrm{e}^{-\mathrm{i}\omega_n x^0} \mathrm{e}^{-\mathrm{i}\vec{p}^{\intercal}\vec{x}}\ \phi(x)\,, \tag{A.34}$$

$$\psi(x) = \int_{\vec{p}} \frac{1}{\beta} \sum_{n\in\mathbb{Z}} \mathrm{e}^{\mathrm{i}\nu_n x^0} \mathrm{e}^{\mathrm{i}\vec{p}^{\intercal}\vec{x}}\ \psi_n(\vec{p}\,)\,, \qquad \psi_n(\vec{p}\,) = \int_{\vec{x}} \int_0^\beta \mathrm{d}x^0\ \mathrm{e}^{-\mathrm{i}\nu_n x^0} \mathrm{e}^{-\mathrm{i}\vec{p}^{\intercal}\vec{x}}\ \psi(x)\,, \tag{A.35}$$

$$\overline{\psi}(x) = \int_{\vec{p}} \frac{1}{\beta} \sum_{n\in\mathbb{Z}} \mathrm{e}^{-\mathrm{i}\nu_n x^0} \mathrm{e}^{-\mathrm{i}\vec{p}^{\intercal}\vec{x}}\ \overline{\psi}_n(\vec{p}\,)\,, \qquad \overline{\psi}_n(\vec{p}\,) = \int_{\vec{x}} \int_0^\beta \mathrm{d}x^0\ \mathrm{e}^{\mathrm{i}\nu_n x^0} \mathrm{e}^{\mathrm{i}\vec{p}^{\intercal}\vec{x}}\ \overline{\psi}(x)\,, \tag{A.36}$$

where $\beta = 1/T$ denotes the inverse equilibrium temperature. Due to the periodicity properties of the field variables at finite temperature, their mode expansion in the Euclidean time direction comes along with discrete frequencies, the so-called Matsubara frequencies. For bosons and fermions, the Matsubara frequencies read

$$\forall n \in \mathbb{Z}: \qquad \omega_n = 2n\,\frac{\pi}{\beta}\,, \qquad \nu_n = (2n+1)\,\frac{\pi}{\beta}\,, \tag{A.37}$$

respectively.

B

BOSONIZATION

The path integral formulation of quantum field theory provides a convenient framework for the application of analytical tools such as bosonization. This term refers to a set of techniques that aim at reformulating a field theory defined in terms of microscopic fermion and gauge degrees of freedom as an effective theory of collective boson fields. Considering the partition function $\mathcal{Z}$ for a given theory S, bosonization can be understood as the following transformation:

$$\mathcal{Z} \propto \int \mathcal{D}\overline{\psi}\, \mathcal{D}\psi\, \mathcal{D}A^{\mu}\, \mathrm{e}^{-S[\overline{\psi},\psi,A^{\mu}]} \quad \rightarrow \quad \int \mathcal{D}\phi\, \mathcal{D}V^{\mu} \ldots\, \mathrm{e}^{-S_{\mathrm{b}}[\phi,V^{\mu},\ldots]} \,. \tag{B.1}$$

The new theory of bosons is physically equivalent to the original theory, only the description of the system in terms of field degrees of freedom and corresponding symmetry patterns has changed. In fact, all parameters of the bosonized theory S_{b} are related to parameters of the original theory by the bosonization procedure. It is worth mentioning that bosonization is not an RG transformation and, therefore, is not associated with a change in scale. Bosonization techniques have proven to be extremely valuable in quantum field theory and many-body physics as they allow for a representation of the system in terms of relevant low-energy degrees of freedom from the very beginning. This leads to a simplification of Feynman diagrams, thereby enhancing our understanding of physics at larger length scales. For more general information on the subject of bosonization, see, e.g., Refs. [505–511].

In the following, we consider an NJL-type model and demonstrate the process of partial bosonization. This is a type of bosonization in which the fermion degrees of freedom do not get completely eliminated. Instead, partial bosonization allows us to phrase multi-fermion interactions in terms of fermion-boson interactions. This does not only simplify analytical treatments in general but is particularly beneficial when studying the properties of bosons for which fermion dynamics play an essential role. The extended two-flavor (vacuum) NJL model under consideration reads

$$\mathcal{L}\left(\overline{\psi},\psi\right) = \overline{\psi}\left[\mathrm{i}\partial\!\!\!/ + \mathrm{i}m_{\mathrm{curr}}\right]\psi + \mathcal{L}_{\mathrm{int}}\left(\overline{\psi},\psi\right) \,, \tag{B.2}$$

$$\begin{aligned}\mathcal{L}_{\mathrm{int}}\left(\overline{\psi},\psi\right) = \frac{G_{\mathrm{S}}}{2}\left[\left(\overline{\psi}\psi\right)^2 - \left(\overline{\psi}\,\gamma^5\vec{\tau}\,\psi\right)^2\right] - \frac{G_{\mathrm{V}}}{2}\left(\overline{\psi}\,\gamma^{\mu}\,\psi\right)^2 \\ + G_{\mathrm{D}}\left(\overline{\psi}\;\gamma^5\tau_2 T^A\,\psi^C\right)\left(\overline{\psi}^C\;\gamma^5\tau_2 T_A\;\psi\right) \,,\end{aligned} \tag{B.3}$$

where we have suppressed the dependence of the fields on spacetime coordinates for simplicity. Working in the isospin-symmetric case, the fermion mass $m_{\mathrm{curr}} = m_{\mathrm{u}} = m_{\mathrm{d}}$ refers to the current

mass of the up and down quarks. The interaction Lagrangian $\mathcal{L}_{\text{int}}$ of the NJL model contains four-fermion interactions which may be classified according to the bosonic condensates they can give rise to. More specifically, our model takes into account the scalar as well as pseudoscalar channel, a vector channel and a diquark channel. At low temperatures and large densities, the latter is dynamically rendered the most dominant channel and constitutes a crucial ingredient in the emergence of color superconducting phases of quark matter [30, 264]. The implied sum over the color index A in the diquark channel runs only over the antisymmetric color generators T^A in the fundamental representation. In accordance, this channel suggests the formation of a scalar condensate, which behaves as an antitriplet under $SU(3)$ transformations in color space. Moreover, we have made use of the charge-conjugated fields

$$\psi^C = \mathcal{C}\,\overline{\psi}^{\intercal}, \qquad \overline{\psi}^C = \psi^{\intercal}\,\mathcal{C} \tag{B.4}$$

with $\mathcal{C} = \mathrm{i}\gamma^2\gamma^0$ denoting the charge conjugation matrix. The coupling parameters G_{S}, G_{V} and G_{D} for the corresponding four-fermion interactions are all assumed to be real-valued and positive.

At the heart of every path integral bosonization lies the Hubbard-Stratonovich transformation [512, 513], a systematic procedure of rewriting an interacting theory in terms of auxiliary field variables. In the case of the NJL model, the Hubbard-Stratonovich transformation is used to replace a four-quark interaction with a Yukawa-type coupling between the quarks and a collective boson field. In general, we start by making use of the Gaussian-type path integral

$$\mathcal{N}_\phi \mathcal{N}_V \mathcal{N}_\Delta \int \mathcal{D}\phi\ \mathcal{D}V^\mu\ \mathcal{D}\Delta_B^*\ \mathcal{D}\Delta^B\ \exp\left(-\int_x \left(\frac{1}{2}m_\phi^2\,\phi^2 + \frac{1}{2}m_V^2 V^2 + m_\Delta^2\,\Delta_A^*\Delta^A\right)\right) = 1\,, \tag{B.5}$$

where different fields have been introduced for the bosonization of each interaction channel. For completeness, it should be mentioned that the field variable ϕ has four components, which are denoted by σ and $\vec{\pi}$ in the following. Although all of these field variables are in principle purely generic at this point, they will acquire physical meaning when linking them to our model by means of the Hubbard-Stratonovich transformation. This transformation relies on a strategic shift of field variables. In particular, we consider shifting the fields according to

$$\begin{aligned} &\sigma \to \sigma + \alpha_\sigma\ \overline{\psi}\psi + c_\sigma\,, \qquad \vec{\pi} \to \vec{\pi} + \alpha_\pi\ \overline{\psi}\,\gamma^5\vec{\tau}\,\psi\,, \qquad V^\mu \to V^\mu + \alpha_V\ \overline{\psi}\,\gamma^\mu\,\psi\,, \\ &\Delta_A \to \Delta_A + \alpha_\Delta\ \overline{\psi}^C\ \gamma^5\tau_2 T_A\,\psi\,, \qquad \Delta_A^* \to \Delta_A^* - \alpha_\Delta^*\ \overline{\psi}\ \gamma^5\tau_2 T_A\,\psi^C\,. \end{aligned} \tag{B.6}$$

The transformations now indicate the fermion content and quantum numbers of the auxiliary field variables. As a result, the fields ϕ, V^μ, and Δ_A can be associated with collective bosons as appearing in the context of low-energy QCD. To be more concrete, ϕ contains the scalar meson σ and the pseudoscalar pions $\vec{\pi}$. The omega meson associated with the isoscalar-vector channel is denoted by V^μ, whereas Δ_A refers to the complex-valued diquark field with an open color index. The mass parameters for the boson fields are real-valued such that Eq. (B.5) is well-defined. Apart from this constraint, the masses are arbitrary here but have to be eventually fixed in order to calculate low-energy observables.[1] We further demand that

$$\frac{1}{2}m_\phi^2\ \alpha_\sigma^2 = -\frac{G_{\text{S}}}{2}\,, \qquad \frac{1}{2}m_\phi^2\ \alpha_\pi^2 = \frac{G_{\text{S}}}{2}\,, \qquad \frac{1}{2}m_V^2\ \alpha_V^2 = \frac{G_{\text{V}}}{2}\,, \qquad m_\Delta^2|\alpha_\Delta|^2 = G_{\text{D}}\,, \tag{B.7}$$

as well as

$$m_\phi^2\ \alpha_\sigma c_\sigma = -\mathrm{i}m_{\text{curr}}\,. \tag{B.8}$$

[1] We could in principle introduce different mass parameters for the scalar mesons, m_σ^2 and m_π^2. Nevertheless, chiral symmetry of the scalar interaction channel requires that $m_\sigma^2 = m_\pi^2 = \mathrm{m}_\phi^2$.

The conditions (B.7) ensure the partial bosonization of the interaction channels, while the requirement (B.8) leads to the bosonization of the fermionic mass term. Under the transformations of field degrees of freedom, the Gaussian integral behaves as follows:

$$
\begin{aligned}
& \mathcal{N}_\phi \mathcal{N}_V \mathcal{N}_\Delta \int \mathcal{D}\phi\ \mathcal{D}V^\mu\ \mathcal{D}\Delta_B^*\ \mathcal{D}\Delta^B\ \exp\left(-\int_x \left(\frac{1}{2}m_\phi^2\phi^2 + \frac{1}{2}m_V^2 V^2 + m_\Delta^2 \Delta_A^* \Delta^A\right)\right) \\
\to\ & \mathcal{N}_\phi \mathcal{N}_V \mathcal{N}_\Delta \int \mathcal{D}\phi\ \mathcal{D}V^\mu\ \mathcal{D}\Delta_B^*\ \mathcal{D}\Delta^B\ \exp\left(-\int_x \left(\frac{1}{2}m_\phi^2\phi^2 + \frac{1}{2}m_V^2 V^2 + m_\Delta^2 \Delta_A^* \Delta^A\right)\right) \\
& \times \exp\left(-\int_x \left(m_\phi^2\, \overline{\psi}\left[\alpha_\sigma \sigma + \alpha_\pi \gamma^5 \tau^i \pi_i\right]\psi + m_\phi^2 c_\sigma \sigma + \frac{1}{2}m_\phi^2 c_\sigma^2 + m_V^2\, \alpha_V\, \overline{\psi}\,\gamma^\mu V_\mu\, \psi\right)\right) \\
& \times \exp\left(-\int_x \left(m_\Delta^2\, \alpha_\Delta \overline{\psi}^C\, \gamma^5 \tau_2 T^A \Delta_A^* \psi - m_\Delta^2\, \alpha_\Delta^*\, \overline{\psi}\,\gamma^5 \tau_2 T^A \Delta_A \psi^C\right)\right) \\
& \times \exp\left(-\int_x \left(-\overline{\psi}\, \mathrm{i} m_{\mathrm{curr}}\, \psi - \mathcal{L}_{\mathrm{int}}\left(\overline{\psi}, \psi\right)\right)\right) .
\end{aligned}
\tag{B.9}
$$

Terms that are constant with respect to any field variable do not affect the dynamics of the physical system. Consequently, the corresponding exponential factor can simply be absorbed into the normalization,

$$
\mathcal{N}_\phi' = \mathcal{N}_\phi\ \exp\left(-\int_x \frac{1}{2}m_\phi^2 c_\sigma^2\right) . \tag{B.10}
$$

Notice that the conditions (B.7) do not uniquely determine the transformation parameters. The specific choice of sign is then a matter of convention, which leaves the physics unchanged. We follow the conventions of Refs. [305, 514] and choose

$$
\alpha_\sigma = \mathrm{i}\sqrt{\frac{G_{\mathrm{S}}}{m_\phi^2}}\,, \qquad \alpha_\pi = -\sqrt{\frac{G_{\mathrm{S}}}{m_\phi^2}}\,, \qquad \alpha_V = \sqrt{\frac{G_{\mathrm{V}}}{m_{\mathrm{V}}^2}}\,, \qquad \alpha_\Delta = \sqrt{\frac{G_\Delta}{m_\Delta^2}} = \alpha_\Delta^*\,, \tag{B.11}
$$

which also leads to

$$
c_\sigma = -\frac{m_{\mathrm{curr}}}{m_\phi^2}\sqrt{\frac{m_\phi^2}{G_{\mathrm{S}}}}\,. \tag{B.12}
$$

For convenience, we further introduce the parameters

$$
h_\phi := m_\phi^2\sqrt{\frac{G_{\mathrm{S}}}{m_\phi^2}}\,, \qquad h_V := m_V^2\sqrt{\frac{G_{\mathrm{V}}}{m_V^2}}\,, \qquad h_\Delta := m_\Delta^2\sqrt{\frac{G_{\mathrm{D}}}{m_V^2}}\,, \tag{B.13}
$$

which will serve as couplings in the partially bosonized formulation of our extended NJL model. In addition, we define

$$
H := m_{\mathrm{curr}}\sqrt{\frac{m_\phi^2}{G_{\mathrm{S}}}} = \frac{m_{\mathrm{curr}}\, m_\phi^2}{h_\phi}\,. \tag{B.14}
$$

Since this parameter is linear in the current quark mass, it can likewise serve as a measure of explicit chiral symmetry breaking.

In short, we have made use of the fact that the unit element has a path integral representation with different types of fields as integration variables. A transformation of these fields with suitably chosen transformation parameters then allows us to connect the fields in the integral relation to the fermionic system under consideration. Applying this procedure to the path integral representation of the partition function gives rise to a new Lagrangian:

$$\begin{aligned}\mathcal{Z} &= \mathcal{N}\int \mathcal{D}\overline{\psi}\;\mathcal{D}\psi\;\mathrm{e}^{-\int_x \mathcal{L}(\overline{\psi},\psi)}\\ &= \mathcal{N}\,\mathcal{N}_\phi\mathcal{N}_V\mathcal{N}_\Delta\int \mathcal{D}\overline{\psi}\;\mathcal{D}\psi\;\mathcal{D}\phi\;\mathcal{D}V^\mu\;\mathcal{D}\Delta_B^*\;\mathcal{D}\Delta^B\;\mathrm{e}^{-\int_x\left(\mathcal{L}(\overline{\psi},\psi)+\frac{1}{2}m_\phi^2\phi^2+\frac{1}{2}m_V^2V^2+m_\Delta^2\Delta_A^*\Delta^A\right)}\\ &\to \mathcal{N}_{\mathrm{pb}}\int \mathcal{D}\overline{\psi}\;\mathcal{D}\psi\;\mathcal{D}\phi\;\mathcal{D}V^\mu\;\mathcal{D}\Delta_B^*\;\mathcal{D}\Delta^B\;\mathrm{e}^{-\int_x \mathcal{L}_{\mathrm{pb}}(\overline{\psi},\psi,\phi,V^\mu,\Delta_A^*,\Delta_A)}\,. \end{aligned}\tag{B.15}$$

The new normalization constant reads

$$\mathcal{N}_{\mathrm{pb}} = \mathcal{N}\,\mathcal{N}_\phi'\mathcal{N}_V\mathcal{N}_\Delta \tag{B.16}$$

and the partially bosonized version of our NJL model is given by the Lagrangian

$$\begin{aligned}\mathcal{L}_{\mathrm{pb}}\left(\overline{\psi},\psi,\phi,V^\mu,\Delta_A^*,\Delta_A\right) = \overline{\psi}\left[\mathrm{i}\partial\!\!\!/ + \mathrm{i}h_\phi\left(\sigma+\mathrm{i}\gamma^5\tau^i\pi_i\right)+h_V\,V\!\!\!/\right]\psi\\ + h_\Delta\;\overline{\psi}^C\,\gamma^5\tau_2T^A\Delta_A^*\psi - h_\Delta\;\overline{\psi}\,\gamma^5\tau_2T^A\Delta_A\,\psi^C\\ + \frac{1}{2}m_\phi^2\phi^2 - H\sigma + \frac{1}{2}m_V^2V^2 + m_\Delta^2\Delta_A^*\Delta^A\,.\end{aligned}\tag{B.17}$$

It now becomes clear that h denotes the coupling for a Yukawa-type interaction between the quark and boson degrees of freedom. The parameter H can be associated with a fixed source field for the scalar meson. In the context of spin models, for example, this would correspond to a fixed external magnetic field. Also notice that, whereas a finite quark mass spoils the invariance of the fermionic theory under axial-vector transformations, the parameter H introduces a linear breaking of $O(4)$ symmetry in the meson sector.

We would like to highlight that the Hubbard-Stratonovich transformation is an exact transformation and does not involve any approximations for the original functional integral. Since normalization factors of the path integral do not contribute to correlation functions, observables calculated from the Lagrangian (B.2) and from its partially bosonized form (B.17) are identical. In this sense, both formulations are equivalent descriptions of the underlying physical system.
Lastly, it is worth mentioning that there is a second way of carrying out the Hubbard-Stratonovich transformation. After having arrived at the transformed Gaussian integral (B.9), one can rearrange the purely fermionic terms to arrive at a path integral identity for the theory under consideration,

$$\begin{aligned}1 &= \mathcal{N}_\phi'\mathcal{N}_V\mathcal{N}_\Delta\int \mathcal{D}\phi\;\mathcal{D}V^\mu\;\mathcal{D}\Delta_B^*\;\mathcal{D}\Delta^B\;\exp\left(-\int_x\ldots\right)\mathrm{e}^{-\int_x\left(-\overline{\psi}\,\mathrm{i}m_{\mathrm{curr}}\psi-\mathcal{L}_{\mathrm{int}}\left(\overline{\psi},\psi\right)\right)}\\ \Leftrightarrow\quad \mathrm{e}^{-\int_x\left(\overline{\psi}\,\mathrm{i}m_{\mathrm{curr}}\psi+\mathcal{L}_{\mathrm{int}}\left(\overline{\psi},\psi\right)\right)} &= \mathcal{N}_\phi'\mathcal{N}_V\mathcal{N}_\Delta\int \mathcal{D}\phi\;\mathcal{D}V^\mu\;\mathcal{D}\Delta_B^*\;\mathcal{D}\Delta^B\;\exp\left(-\int_x\ldots\right).\end{aligned}\tag{B.18}$$

In words, the exponential factor containing the fermionic mass term and interaction channels can be rewritten in terms of collective boson fields. Applying this identity to the path integral representation of the partition function and using the transformation parameters as previously defined, the resulting Lagrangian exactly coincides with Eq. (B.17).

C

RELATIONS RELEVANT AT FINITE TEMPERATURE

C.1 Hyperbolic functions

Hyperbolic functions and their inverses naturally arise in quantum field theory. To give an example, hyperbolic functions directly emerge as the result of Matsubara summation in finite-temperature field theory. In order to achieve optimal numerical performance in the computation of observables, the ability to formally manipulate hyperbolic functions is essential. We therefore collect some of their most important properties in the following.

C.1.1 Definitions

The hyperbolic sine and cosine functions are given by

$$\forall\, x \in \mathbb{R}: \qquad \sinh(x) := \mathrm{i}\sin(-\mathrm{i}x) = \frac{\mathrm{e}^{x}-\mathrm{e}^{-x}}{2} = \sum_{n=0}^{\infty} \frac{x^{2n+1}}{(2n+1)!}\,, \tag{C.1}$$

$$\forall\, x \in \mathbb{R}: \qquad \cosh(x) := \cos(\mathrm{i}x) = \frac{\mathrm{e}^{x}+\mathrm{e}^{-x}}{2} = \sum_{n=0}^{\infty} \frac{x^{2n}}{(2n)!}\,. \tag{C.2}$$

Every other hyperbolic function can now be defined in terms of sinh and cosh:

$$\forall\, x \in \mathbb{R}: \qquad \tanh(x) := \frac{\sinh(x)}{\cosh(x)} = \frac{\mathrm{e}^{x}-\mathrm{e}^{-x}}{\mathrm{e}^{x}+\mathrm{e}^{-x}} = \frac{\mathrm{e}^{2x}-1}{\mathrm{e}^{2x}+1} = 1-\frac{2}{\mathrm{e}^{2x}+1}\,, \tag{C.3}$$

$$\forall\, x \in \mathbb{R}\setminus\{0\}: \qquad \coth(x) := \frac{\cosh(x)}{\sinh(x)} = \frac{\mathrm{e}^{x}+\mathrm{e}^{-x}}{\mathrm{e}^{x}-\mathrm{e}^{-x}} = \frac{\mathrm{e}^{2x}+1}{\mathrm{e}^{2x}-1} = 1+\frac{2}{\mathrm{e}^{2x}-1}\,, \tag{C.4}$$

$$\forall x \in \mathbb{R}: \qquad \operatorname{sech}(x) := \frac{1}{\cosh(x)} = \frac{2}{\mathrm{e}^{x}+\mathrm{e}^{-x}}\,, \tag{C.5}$$

$$\forall x \in \mathbb{R}\setminus\{0\}: \qquad \operatorname{csch}(x) := \frac{1}{\sinh(x)} = \frac{2}{\mathrm{e}^{x}-\mathrm{e}^{-x}}\,. \tag{C.6}$$

Due to the analytic properties of the exponential function, the hyperbolic functions can be analytically continued to the complex plane. However, for simplicity, we assume real-valued arguments unless stated otherwise.

C.1.2 Basic properties

Asymptotic behavior:

$$\lim_{x\to\pm\infty} \sinh(x) = \pm\infty \,, \qquad \lim_{x\to\pm\infty} \cosh(x) = +\infty \,, \tag{C.7}$$

$$\lim_{x\to\pm\infty} \tanh(x) = \pm 1 \,, \qquad \lim_{x\to\pm\infty} \coth(x) = \pm 1 \,, \tag{C.8}$$

$$\lim_{x\to\pm\infty} \operatorname{sech}(x) = 0 \,, \qquad \lim_{x\to\pm\infty} \cosh(x) = 0 \,. \tag{C.9}$$

Derivatives:

$$\frac{\mathrm{d}}{\mathrm{d}x}\sinh(x) = \cosh(x) \,, \qquad \frac{\mathrm{d}}{\mathrm{d}x}\cosh(x) = \sinh(x) \,, \tag{C.10}$$

$$\frac{\mathrm{d}}{\mathrm{d}x}\tanh(x) = \operatorname{sech}^2(x) \,, \qquad \frac{\mathrm{d}}{\mathrm{d}x}\coth(x) = -\operatorname{csch}^2(x) \,, \tag{C.11}$$

$$\frac{\mathrm{d}}{\mathrm{d}x}\operatorname{sech}(x) = -\operatorname{sech}(x)\tanh(x) \,, \qquad \frac{\mathrm{d}}{\mathrm{d}x}\operatorname{csch}(x) = -\operatorname{csch}(x)\coth(x) \,. \tag{C.12}$$

Identities:

$$\cosh(x) \pm \sinh(x) = \mathrm{e}^{\pm x} \,, \tag{C.13}$$

$$\cosh^2(x) - \sinh^2(x) = 1 \,, \tag{C.14}$$

$$\sinh(x \pm y) = \sinh(x)\cosh(y) \pm \sinh(y)\cosh(x) \,, \tag{C.15}$$

$$\cosh(x \pm y) = \cosh(x)\cosh(y) \pm \sinh(x)\sinh(y) \,. \tag{C.16}$$

Expressing one by another:

$$\begin{aligned} \tanh(x) &= \frac{1}{2}\sinh(2x)\ \operatorname{sech}^2(x) \\ &= \operatorname{sgn}(x)\ \sqrt{1-\operatorname{sech}^2(x)} \,, \end{aligned} \tag{C.17}$$

$$\tanh(x) = 2\coth(2x) - \coth(x) \,, \tag{C.18}$$

$$\begin{aligned} \coth(x) &= \frac{1}{2}\sinh(2x)\ \operatorname{csch}^2(x) \\ &= \operatorname{sgn}(x)\ \sqrt{1+\operatorname{csch}^2(x)} \,. \end{aligned} \tag{C.19}$$

Half-argument formulas:

$$\sinh\left(\frac{x}{2}\right) = \frac{\sinh(x)}{\sqrt{2\cosh(x)+2}}\,, \tag{C.20}$$

$$\cosh\left(\frac{x}{2}\right) = \sqrt{\frac{\cosh(x)+1}{2}}\,, \tag{C.21}$$

$$\tanh\left(\frac{x}{2}\right) = \frac{\sinh(x)}{\cosh(x)+1} = \frac{\mathrm{e}^x-\mathrm{e}^{-x}}{\mathrm{e}^x+\mathrm{e}^{-x}+2} = \frac{\mathrm{e}^x-1}{\mathrm{e}^x+1}\,, \tag{C.22}$$

$$\coth\left(\frac{x}{2}\right) = \frac{\sinh(x)}{\cosh(x)-1} = \frac{\mathrm{e}^x-\mathrm{e}^{-x}}{\mathrm{e}^x+\mathrm{e}^{-x}-2} = \frac{\mathrm{e}^x+1}{\mathrm{e}^x-1}\,. \tag{C.23}$$

C.1.3 Inverse hyperbolic functions

The inverse hyperbolic functions, often called area functions, are given by

$$\forall x \in \mathbb{R}: \qquad \operatorname{arsinh}(x) \equiv \sinh^{-1}(x) = \ln\left(x+\sqrt{x^2+1}\right)\,, \tag{C.24}$$

$$\forall x \in \mathbb{R}_{\geq 1}: \qquad \operatorname{arcosh}(x) \equiv \cosh^{-1}(x) = \ln\left(x+\sqrt{x^2-1}\right)\,, \tag{C.25}$$

$$\forall x \in (-1,1): \qquad \operatorname{artanh}(x) \equiv \tanh^{-1}(x) = \frac{1}{2}\ln\left(\frac{1+x}{1-x}\right)\,, \tag{C.26}$$

$$\forall x \in \mathbb{R}\setminus[-1,1]: \qquad \operatorname{arcoth}(x) \equiv \coth^{-1}(x) = \frac{1}{2}\ln\left(\frac{x+1}{x-1}\right)\,. \tag{C.27}$$

The hyperbolic secant and cosecant also have inverses but those do not appear as often in physics as the other area functions. We will therefore omit them here. In addition, the following special forms are worth mentioning:

$$\forall x \in (0,1): \qquad 2\operatorname{artanh}(1-2x) = \ln\left(\frac{1}{x}-1\right)\,, \tag{C.28}$$

$$\forall x \in \mathbb{R}\setminus[-1,0]: \qquad 2\operatorname{arcoth}(1+2x) = \ln\left(\frac{1}{x}+1\right)\,. \tag{C.29}$$

Like the hyperbolic functions, the area functions can be expressed in terms of other inverse functions.

$$\operatorname{arsinh}(x) = \operatorname{sgn}(x)\ \operatorname{arcosh}\left(\sqrt{x^2+1}\right) = \operatorname{artanh}\left(\frac{x}{\sqrt{x^2+1}}\right) = \operatorname{sgn}(x)\ \operatorname{arcoth}\left(\sqrt{1+\frac{1}{x^2}}\right)\,, \tag{C.30}$$

$$\operatorname{arcosh}(x) = \operatorname{arsinh}\left(\sqrt{x^2-1}\right) = \operatorname{artanh}\left(\sqrt{1-\frac{1}{x^2}}\right) = \operatorname{arcoth}\left(\frac{x}{\sqrt{x^2-1}}\right)\,, \tag{C.31}$$

$$\operatorname{artanh}(x) = \operatorname{arcoth}\left(\frac{1}{x}\right) = \operatorname{arsinh}\left(\frac{x}{\sqrt{1-x^2}}\right) = \operatorname{sgn}(x)\ \operatorname{arcosh}\left(\frac{1}{\sqrt{1-x^2}}\right), \tag{C.32}$$

$$\operatorname{arcoth}(x) = \operatorname{artanh}\left(\frac{1}{x}\right) = \operatorname{sgn}(x)\ \operatorname{arsinh}\left(\frac{1}{\sqrt{x^2-1}}\right) = \operatorname{sgn}(x)\ \operatorname{arcosh}\left(\frac{|x|}{\sqrt{x^2-1}}\right)\,. \tag{C.33}$$

C.2 Matsubara sums

In the imaginary-time formalism of quantum field theory, the introduction of a finite equilibrium temperature leads to a discretization of momentum space along the time-like direction. As a result, integrals over the continuous momentum variable p^0 at zero temperature turn into an infinite sum over Matsubara frequencies at finite temperature. Such a series can often be performed analytically by means of the Matsubara formalism, see Refs. [266, 273, 286, 316] and also Section 2.4.3 for details. In the following, we would like to provide additional relations in the context of Matsubara summation.

C.2.1 Particle distributions

For a system of identical particles, we define the generalized distribution function

$$\forall a \in \{-1,1\}: \qquad n_a(x) := \frac{1}{\mathrm{e}^x + a}\,, \tag{C.34}$$

which has the following properties:

$$n_a(-x) = a - n_a(x)\,, \tag{C.35}$$

$$\forall m \in \mathbb{Z}: \quad n_{-a}(x) = -n_a(x + \mathrm{i}\pi(1+2m))\,, \tag{C.36}$$

$$\frac{\mathrm{d}}{\mathrm{d}x} n_a(x) = -a\; n_a(x)\; n_a(-x)\,. \tag{C.37}$$

Inserting the previously defined values of a, the distribution function corresponds to either the Fermi-Dirac distribution for fermions or the Bose-Einstein distribution for bosons.

Fermi-Dirac distribution:

$$n_{\mathrm{F}}(x) = n_{a=1}(x) = \frac{1}{2}\left(1 - \tanh\left(\frac{x}{2}\right)\right) = \frac{1}{2} - 2\sum_{n=0}^{\infty} \frac{x}{(2n+1)^2\pi^2 + x^2}\,, \tag{C.38}$$

$$n_{\mathrm{F}}(-x) - n_{\mathrm{F}}(x) = 1 - 2\,n_{\mathrm{F}}(x) = \tanh\left(\frac{x}{2}\right)\,. \tag{C.39}$$

Bose-Einstein distribution:

$$n_{\mathrm{B}}(x) = n_{a=-1}(x) = \frac{1}{2}\left(\coth\left(\frac{x}{2}\right) - 1\right) = \frac{1}{x} - \frac{1}{2} + 2\sum_{n=1}^{\infty} \frac{x}{(2\pi n)^2 + x^2}\,, \tag{C.40}$$

$$n_{\mathrm{B}}(x) - n_{\mathrm{B}}(-x) = 1 + 2\,n_{\mathrm{B}}(x) = \coth\left(\frac{x}{2}\right)\,. \tag{C.41}$$

C.2.2 Exemplary sums

With the generalized Matsubara frequency

$$\forall m \in \mathbb{Z},\; a \in \{-1,1\}: \qquad \varpi_m^{(a)} := \frac{2\pi}{\beta}\left(m + \frac{1+a}{4}\right)\,, \tag{C.42}$$

a simple example of a Matsubara sum is given by

$$\frac{1}{\beta}\sum_{m\in\mathbb{Z}} \frac{1}{\left(\varpi_m^{(a)} + \mathrm{i}\bar{\mu}\right)^2 + \chi^2} = \frac{a}{2|\chi|}\left[n_a(-\beta(|\chi| + \bar{\mu})) - n_a(\beta(|\chi| - \bar{\mu}))\right]\,. \tag{C.43}$$

This identity holds for all $\chi \in \mathbb{R}\setminus\{0\}$ and $\bar{\mu}\in\mathbb{R}$ with the additional constraint of $|\chi|\neq\bar{\mu}$ in the case of $a=-1$. The value of the series at $\chi=0$ can nevertheless be obtained from the right-hand side by taking the limit as χ approaches zero. Here, $\bar{\mu}=|F|\mu$ denotes a chemical potential together with the fermion number F, whereas χ refers to a mass term. Considering more specific cases, we can express the particle distributions in terms of hyperbolic functions for each value of a.

$$\begin{aligned} &n_{\mathrm{F}}(-\beta(|\chi|+\bar{\mu}))-n_{\mathrm{F}}(\beta(|\chi|-\bar{\mu})) \\ &\qquad=\frac{1}{2}\left\{\tanh\left(\frac{\beta}{2}(|\chi|+\bar{\mu})\right)+\tanh\left(\frac{\beta}{2}(|\chi|-\bar{\mu})\right)\right\}=\frac{\sinh(\beta|\chi|)}{\cosh(\beta\chi)+\cosh(\beta\bar{\mu})}\,, \end{aligned} \tag{C.44}$$

$$\begin{aligned} &n_{\mathrm{B}}(\beta(|\chi|-\bar{\mu}))-n_{\mathrm{B}}(-\beta(|\chi|+\bar{\mu})) \\ &\qquad=\frac{1}{2}\left\{\coth\left(\frac{\beta}{2}(|\chi|+\bar{\mu})\right)+\coth\left(\frac{\beta}{2}(|\chi|-\bar{\mu})\right)\right\}=\frac{\sinh(\beta|\chi|)}{\cosh(\beta\chi)-\cosh(\beta\bar{\mu})}\,. \end{aligned} \tag{C.45}$$

With this result at hand, we can generate Matsubara sums for functions of higher powers by differentiation. We demonstrate this idea in the following.

$$\begin{aligned} &\frac{1}{\beta}\sum_{m\in\mathbb{Z}}\frac{1}{\left(\left(\varpi_m^{(a)}+\mathrm{i}\bar{\mu}\right)^2+\chi^2\right)^2}=-\frac{1}{2\chi}\frac{\partial}{\partial\chi}\frac{1}{\beta}\sum_{m\in\mathbb{Z}}\frac{1}{\left(\varpi_m^{(a)}+\mathrm{i}\bar{\mu}\right)^2+\chi^2} \\ &=\frac{a}{4|\chi|^3}\left[n_a(-\beta(|\chi|+\bar{\mu}))-n_a(\beta(|\chi|-\bar{\mu}))\right]+\frac{a\beta}{4\chi^2}\left[n_a'(-\beta(|\chi|+\bar{\mu}))+n_a'(\beta(|\chi|-\bar{\mu}))\right]. \end{aligned} \tag{C.46}$$

As before, we may write the differentiated particle distributions in terms of hyperbolic functions for each value of a.

$$n_{\mathrm{F}}'(-\beta(|\chi|+\bar{\mu}))+n_{\mathrm{F}}'(\beta(|\chi|-\bar{\mu}))=-\frac{1}{4}\left\{\operatorname{sech}^2\left(\frac{\beta}{2}(\chi+\bar{\mu})\right)+\operatorname{sech}^2\left(\frac{\beta}{2}(\chi-\bar{\mu})\right)\right\}\,, \tag{C.47}$$

$$n_{\mathrm{B}}'(-\beta(|\chi|+\bar{\mu}))+n_{\mathrm{B}}'(\beta(|\chi|-\bar{\mu}))=-\frac{1}{4}\left\{\operatorname{csch}^2\left(\frac{\beta}{2}(\chi+\bar{\mu})\right)+\operatorname{csch}^2\left(\frac{\beta}{2}(\chi-\bar{\mu})\right)\right\}\,. \tag{C.48}$$

C.3 Commutation relations

In order to evaluate Matsubara sums in closed form, it is often convenient to follow the strategy of interchanging derivatives with the summation process. That such an interchange is indeed allowed, will be shown in the following. As a preliminary step, we first demonstrate that differentiation can be interchanged with the calculation of a residue.

C.3.1 Relation 1

We consider a generally complex-valued function $f(z,y)$, which is holomorphic in $z\in\mathbb{C}\setminus P$. Here, P denotes a finite set of isolated points, which are poles of the function. In the neighborhood of a pole $z^*=g(y)\in P$, the function can be represented as

$$\forall n\in\mathbb{N}:\quad f(z,y)=\frac{h(z,y)}{(z-g(y))^n}\,, \tag{C.49}$$

where h and g are assumed to be differentiable. We are going to show that the processes of taking the derivative with respect to $y\in\mathbb{R}$ and calculating the residue of $f(\cdot,y)$ at $z=z^*$ do, in fact,

commute. Specifically, we will show that

$$\mathrm{Res}\big(\partial_y f(\cdot,y),g(y)\big)=\frac{\mathrm{d}}{\mathrm{d}y}\,\mathrm{Res}\big(f(\cdot,y),g(y)\big)\ . \tag{C.50}$$

In a context relevant for physics, the real-valued variable y may refer to, e.g., the RG scale, a mass, or an external momentum. We will prove the statement above by starting from the left-hand side.

Using the Leibniz notation (2.165) for partial derivatives, we have

$$\begin{aligned}
&\mathrm{Res}\big(\partial_y f(\cdot,y),g(y)\big)\\
&=\mathrm{Res}\left(\frac{h^{(0,1)}(\cdot,y)}{(\cdot-g(y))^n}+n\left(\frac{\mathrm{d}}{\mathrm{d}y}g(y)\right)\frac{h(\cdot,y)}{(\cdot-g(y))^{n+1}},g(y)\right)\\
&=\frac{1}{n!}\lim_{z\to g(y)}\frac{\partial^n}{\partial z^n}\left[(z-g(y))\,h^{(0,1)}(z,y)+n\left(\frac{\mathrm{d}}{\mathrm{d}y}g(y)\right)h(z,y)\right]\\
&=\frac{1}{n!}\lim_{z\to g(y)}\left[\sum_{j=0}^{n}\binom{n}{j}\left(\frac{\partial^j}{\partial z^j}(z-g(y))\right)\,h^{(n-j,1)}(z,y)+n\left(\frac{\mathrm{d}}{\mathrm{d}y}g(y)\right)h^{(n,0)}(z,y)\right]\\
&=\frac{1}{n!}\lim_{z\to g(y)}\left[(z-g(y))\,h^{(n,1)}(z,y)+n\,h^{(n-1,1)}(z,y)+n\left(\frac{\mathrm{d}}{\mathrm{d}y}g(y)\right)h^{(n,0)}(z,y)\right]\\
&=\frac{1}{(n-1)!}\left[h^{(n-1,1)}(g(y),y)+\left(\frac{\mathrm{d}}{\mathrm{d}y}g(y)\right)h^{(n,0)}(g(y),y)\right]\\
&=\frac{1}{(n-1)!}\,\frac{\mathrm{d}}{\mathrm{d}y}h^{(n-1,0)}(g(y),y)\\
&=\frac{\mathrm{d}}{\mathrm{d}y}\,\frac{1}{(n-1)!}\lim_{z\to g(y)}\frac{\partial^{n-1}}{\partial z^{n-1}}h(z,y)\\
&=\frac{\mathrm{d}}{\mathrm{d}y}\,\frac{1}{(n-1)!}\lim_{z\to g(y)}\frac{\partial^{n-1}}{\partial z^{n-1}}\left[(z-g(y))^n\,f(z,y)\right]\\
&=\frac{\mathrm{d}}{\mathrm{d}y}\,\mathrm{Res}\big(f(\cdot,y),g(y)\big)\ .
\end{aligned}$$

It is worth mentioning that the validity of the commutation relation (C.50) does not rely on the pole being a function of the variable y. In other words, differentiation with respect to y and calculating the residue at $z=g(y)$ can in particular be interchanged for $\frac{\mathrm{d}}{\mathrm{d}y}g(y)=0$.

C.3.2 Relation 2

We consider a generally complex-valued function $f(z,y)$, which is holomorphic in $z\in\mathbb{C}\setminus P$ and differentiable in $y\in\mathbb{R}$. Again, P denotes a finite set of isolated points, which are poles of the function. Suppose that the corresponding Matsubara sum exists for all y, then

$$\frac{1}{\beta}\sum_{m\in\mathbb{Z}}\partial_y f(\varpi_m,y)=\frac{\mathrm{d}}{\mathrm{d}y}\,\frac{1}{\beta}\sum_{m\in\mathbb{Z}}f(\varpi_m,y) \tag{C.51}$$

for all $\beta>0$. In words, the processes of evaluating the Matsubara sum and taking the derivative with respect to a temperature-independent variable can be interchanged. This statement is generally non-trivial since infinite sums do not need to preserve the linearity of the operator applied to them. At the heart of Eq. (C.51) lies the fact that the infinite sum of contributions for different Matsubara frequencies can be turned into a finite sum of residues by means of the Matsubara formalism. Also notice that the statement above holds independently of whether we consider fermionic

or bosonic frequencies. Nevertheless, the intermediate steps linking both sides of Eq. (C.51) are sensitive to the type of frequency. The explicit analytical manipulation proving the commutation relation is presented in the following.

$$\begin{aligned}
\frac{1}{\beta}\sum_{m\in\mathbb{Z}}\partial_y f(\varpi_m^{(a)},y) &= -\mathrm{i}a\sum_{z^*\in P}\mathrm{Res}\left(\partial_y f(\cdot,y)\,n_a(-\mathrm{i}\beta\,\cdot),z^*\right)\\
&= -\mathrm{i}a\sum_{z^*\in P}\mathrm{Res}\left(\partial_y\left[f(\cdot,y)\,n_a(-\mathrm{i}\beta\,\cdot)\right],z^*\right)\\
&\overset{\text{(C.50)}}{=} -\mathrm{i}a\sum_{z^*\in P}\frac{\mathrm{d}}{\mathrm{d}y}\mathrm{Res}\left(f(\cdot,y)\,n_a(-\mathrm{i}\beta\,\cdot),z^*\right)\\
&\overset{|P|<\infty}{=} -\mathrm{i}a\frac{\mathrm{d}}{\mathrm{d}y}\sum_{z^*\in P}\mathrm{Res}\left(f(\cdot,y)\,n_a(-\mathrm{i}\beta\,\cdot),z^*\right)\\
&= \frac{\mathrm{d}}{\mathrm{d}y}\frac{1}{\beta}\sum_{m\in\mathbb{Z}}f(\varpi_m^{(a)},y)\,.
\end{aligned}$$

C.4 Zero-temperature limits

Within this section, we extend our discussion of hyperbolic functions to complex arguments. More specifically, we consider complex numbers from the set $\mathbb{M}=\{z\in\mathbb{C}\mid z\notin\mathrm{i}\mathbb{R}\setminus\{0\}\}$. As a result, we are prepared to give a presentation of commonly encountered zero-temperature limits.

$$\forall z\in\mathbb{M}: \qquad \lim_{T\to0}\tanh\left(\frac{z}{T}\right)=2\theta(\mathfrak{Re}\{z\})-1=\mathrm{sgn}(\mathfrak{Re}\{z\})\,, \tag{C.52}$$

$$\forall z\in\mathbb{M}\setminus\{0\}: \qquad \lim_{T\to0}\coth\left(\frac{z}{T}\right)=2\theta(\mathfrak{Re}\{z\})-1=\mathrm{sgn}(\mathfrak{Re}\{z\})\,, \tag{C.53}$$

$$\forall z\in\mathbb{M}: \qquad \lim_{T\to0}n_{\mathrm{F}}\left(\frac{z}{T}\right)=1-\theta(\mathfrak{Re}\{z\})=\theta(-\mathfrak{Re}\{z\})\,, \tag{C.54}$$

$$\forall z\in\mathbb{M}\setminus\{0\}: \qquad \lim_{T\to0}n_{\mathrm{B}}\left(\frac{z}{T}\right)=\theta(\mathfrak{Re}\{z\})-1=-\theta(-\mathfrak{Re}\{z\})\,, \tag{C.55}$$

$$\forall z\in\mathbb{M}: \qquad \lim_{T\to0}\frac{\mathrm{sech}^2\left(\frac{z}{T}\right)}{T}=\lim_{T\to0}\frac{1-\tanh^2\left(\frac{z}{T}\right)}{T}=2\delta(\mathfrak{Re}\{z\})\,, \tag{C.56}$$

$$\forall z\in\mathbb{M}\setminus\{0\}: \qquad \lim_{T\to0}\frac{\mathrm{csch}^2\left(\frac{z}{T}\right)}{T}=\lim_{T\to0}\frac{\coth^2\left(\frac{z}{T}\right)-1}{T}=0\,. \tag{C.57}$$

It is also worth mentioning that related zero-temperature limits can be obtained by applying derivatives. To give an example, we make use of Eq. (2.185) for $n=1$ and obtain

$$\begin{aligned}
\lim_{T\to0}\frac{1}{T}n_{\mathrm{F}}'\left(\frac{z}{T}\right)&=\lim_{T\to0}\frac{\mathrm{d}}{\mathrm{d}z}n_{\mathrm{F}}\left(\frac{z}{T}\right)=\left[\frac{\mathrm{d}}{\mathrm{d}x}\lim_{T\to0}n_{\mathrm{F}}\left(\frac{x}{T}\right)\right]\Bigg|_{x=\mathfrak{Re}\{z\}}\\
&=\left[\frac{\mathrm{d}}{\mathrm{d}x}(1-\theta(x))\right]\Bigg|_{x=\mathfrak{Re}\{z\}}=-\delta(\mathfrak{Re}\{z\})\,.
\end{aligned} \tag{C.58}$$

D

SYMMETRIZATION OF CS FLOWS

D.1 Preliminaries

The orthogonal group $O(N)$ is a compact Lie group, which is associated with rotations and reflections in $N \in \mathbb{N}$ dimensions. More formally, this group consists of $N \times N$ real-valued orthogonal matrices:

$$O(N) = \left\{ M \in \mathrm{GL}(N,\mathbb{R}) \mid M^{\intercal} M = M M^{\intercal} = \mathbb{1} \right\} , \tag{D.1}$$

where $\mathrm{GL}(N,\mathbb{R})$ denotes the general linear group. With the aid of the determinant condition, we can divide the orthogonal group into two connected subsets. In particular, one subset is the special orthogonal group

$$SO(N) = \left\{ M \in \mathrm{GL}(N,\mathbb{R}) \mid M^{\intercal} M = M M^{\intercal} = \mathbb{1},\ \det(M) = 1 \right\} , \tag{D.2}$$

which is the group of orthogonal matrices with the additional requirement that the determinant evaluates to 1. All elements of $SO(N)$ can be continuously connected to the identity matrix and the group is associated with rotations without reflections. The other subset is the set of orthogonal matrices with $\det(M) = -1$ for $M \in O(N)$. This set is disjoint from $SO(N)$ and does not form a group since it lacks the identity element and also fails to satisfy the group closure property.

A general $N \times N$ matrix has N^2 independent entries,

$$\dim\left(\mathrm{GL}(N,\mathbb{R})\right) = N^2 . \tag{D.3}$$

The orthogonality condition now imposes constraints that reduce the number of independent entries. The determinant condition, however, does not further restrict the number of independent parameters needed to describe any element of the group since the determinant is a discrete operation and cannot trigger continuous deformations. Therefore, the dimensions of the orthogonal group and its special subgroup are identical:

$$\dim\left(O(N)\right) = \dim\left(SO(N)\right) = \frac{N(N-1)}{2} . \tag{D.4}$$

This also means that the two groups share the same generators.

D.2 Derivation of the WTI

We consider a theory S of $N \in \mathbb{N}$ scalar bosons, assembled into the field variable ϕ. These bosons span an N-dimensional space of field degrees of freedom, containing

$$\sum_{i=1}^{N}(N-i) = N^2 - \frac{N(N+1)}{2} = \frac{N(N-1)}{2} \tag{D.5}$$

planes of rotation. General rotations in this boson field space are elements of the group $SO(N)$. It is worth mentioning that elements of a Lie group can be represented with the aid of the exponential function. This exponential map then links the Lie algebra to the corresponding Lie group. To be more concrete, a rotation among the boson fields is given by

$$R(\alpha) = \exp\left(\alpha^j X_j\right) = \mathbb{1} + \alpha^j X_j + \mathcal{O}(\alpha^2)\,, \tag{D.6}$$

where $\alpha^j \in \mathbb{R}$ is the continuous parameter of the rotation, indexed by $j \in \{1,\dots,\frac{N(N-1)}{2}\}$. The object X_j denotes a generator of the rotation within the j-plane of boson field space and is an element of the Lie algebra $\mathfrak{so}(N)$. We would like to highlight that any finite transformation, which is an element of a differentiable group, can be constructed from repeated applications of an infinitesimal transformation. Therefore, it suffices to consider rotations of field degrees of freedom around an infinitesimal angle in the following,

$$\phi \to \phi' = \left(\mathbb{1} + \alpha^j X_j\right)\phi\,. \tag{D.7}$$

It automatically follows that the symmetry properties of a theory are fully encoded in the linear response of the action functional to the symmetry transformation. In particular, if the classical action is invariant under $SO(N)$ transformation of its boson content, it holds that

$$S[\phi] \to S[\phi'] = S\left[\left(\mathbb{1} + \alpha^j X_j\right)\phi\right] = S[\phi] + \alpha^i\,\delta_i S[\phi] = S[\phi]\,. \tag{D.8}$$

This implies that the first variation vanishes:

$$\delta_i S[\phi] = \left(\frac{\partial}{\partial \alpha^i} S\left[\left(\mathbb{1} + \alpha^j X_j\right)\phi\right]\right)\bigg|_{\alpha=0} = \int_q \frac{\delta S[\phi]}{\delta\phi(q)}\, X_i\phi(q) = 0\,. \tag{D.9}$$

Here, q is a generic variable of representation space and may correspond to position or momentum. The generator X_i is a linear operator on the fields and acts independently at each point in representation space. In addition, we emphasize that our considerations here are by no means restricted to the classical action but extend to any other rotation-symmetric functional. We therefore conclude that the condition above should in particular hold pointwise:

$$\frac{\delta S[\phi]}{\delta\phi(q)}\, X_i\phi(q) = 0\,. \tag{D.10}$$

This functional differential equation can be considered a Ward-Takahashi identity (WTI) for rotation symmetry in boson field space. Finally, we would like to remind ourselves that the Lie groups $SO(N)$ and $O(N)$ have the same generators. Thus, the equation above can equally be regarded as an identity for invariance under orthogonal transformations. Every scalar quantity that is $SO(N)$-symmetric is also $O(N)$-symmetric and vice versa. As a result, in a theory with fermions, rotation symmetry in the space of effective bosons can be related to chiral symmetry in the fermionic sector.

Let us now delve into a more concrete example. The quark-meson model as defined in Eq. (3.1) includes four bosons: the sigma meson and three pions. Accordingly, these mesons form a four-dimensional space of field degrees of freedom, within which six planes of rotation can be identified:

$$1.\ \sigma\pi_1\,, \qquad 2.\ \sigma\pi_2\,, \qquad 3.\ \sigma\pi_3\,, \qquad 4.\ \pi_1\pi_2\,, \qquad 5.\ \pi_1\pi_3\,, \qquad 6.\ \pi_2\pi_3\,. \tag{D.11}$$

When the model is subjected to sources of explicit symmetry breaking, the action functional is affected non-uniformly throughout field space by the presence of the symmetry-breaking scale. In our case, the symmetry-breaking mechanisms appear along the σ-direction of field space but leave the pion directions unaffected. Consequently, the action functional violates the WTI for rotations that involve the σ-direction but remains invariant under rotations in the planes $i \in \{4,5,6\}$. Nevertheless, in the absence of physical sources of symmetry breaking, the WTI is expected to hold across the entire field space. In the following, we present the WTI for those rotations in which the σ-direction of field space becomes relevant. For rotations in those planes, the generators are given by

$$X_1 = X_{\sigma\pi_1} = \begin{pmatrix} 0 & -1 & 0 & 0 \\ 1 & 0 & 0 & 0 \\ 0 & 0 & 0 & 0 \\ 0 & 0 & 0 & 0 \end{pmatrix}, \quad X_2 = X_{\sigma\pi_2} = \begin{pmatrix} 0 & 0 & -1 & 0 \\ 0 & 0 & 0 & 0 \\ 1 & 0 & 0 & 0 \\ 0 & 0 & 0 & 0 \end{pmatrix}, \quad X_3 = X_{\sigma\pi_3} = \begin{pmatrix} 0 & 0 & 0 & -1 \\ 0 & 0 & 0 & 0 \\ 0 & 0 & 0 & 0 \\ 1 & 0 & 0 & 0 \end{pmatrix}. \tag{D.12}$$

It then follows from Eq. (D.10) that the WTI for a rotation-symmetric quantity as derived from the quark-meson model can be written as

$$\forall i \in \{1,2,3\}: \qquad \frac{\delta \mathcal{Q}^{(\mathrm{sym})}[\phi]}{\delta \sigma(q)} \pi_i(q) = \frac{\delta \mathcal{Q}^{(\mathrm{sym})}[\phi]}{\delta \pi_i(q)} \sigma(q) \,. \tag{D.13}$$

As an example, this quantity may be given by the effective average action in the absence of physical symmetry breaking,

$$\mathcal{Q}^{(\mathrm{sym})}[\phi] = \lim_{H \to 0} \Gamma_k^{(\mathrm{phys})}[\phi]\big|_{T,\mu} \,. \tag{D.14}$$

Here, we have labeled the effective average action as "physical" to highlight that unphysical sources of symmetry breaking are also possible, which then lead to a violation of the WTI even in the chiral limit. Recall that, in order to calculate the quantum effective action from the Wetterich equation, a regulator function has to be introduced to the classical action. In the case of the Callan-Symanzik regulator, the RG scale represents a mass scale that introduces additional and unphysical symmetry breaking to the fermionic loops. In this scenario, the WTI can be used as a condition for the elimination of artificial symmetry breaking. More concretely, let us consider

$$\mathcal{Q}[\phi] = \lim_{H \to 0} \Gamma_k[\phi]\big|_{T,\mu} \,, \tag{D.15}$$

where the effective average action is generated by the CS flow. Due to the explicit symmetry breaking induced by the regulator, $\mathcal{Q}$ does not satisfy the WTI. In order to obtain the corresponding physical version of the effective average action, it is necessary to establish a symmetrization procedure such that Eq. (D.13) is fulfilled. To construct a symmetric quantity from $\mathcal{Q}$, we make the ansatz

$$\mathcal{Q}^{(\mathrm{sym})}[\phi] = \mathcal{Q}[\phi] + c[\phi] \,. \tag{D.16}$$

In words, we assume that any quantity that remains invariant under rotations of the fields can be suitably decomposed into two asymmetric parts. Notice that our ansatz implies that c can be considered a counterterm for those contributions in $\mathcal{Q}$ that explicitly break the rotation symmetry. The remaining task is then to construct this additional term in accordance with the WTI. We

emphasize that the symmetrization procedure should not alter the dependence of $\mathcal{Q}$ on the pion fields since this subspace is not affected by the CS regulator. It then follows that Eq. (D.13) has to be solved for c with the initial condition

$$c[\sigma = 0, \vec{\pi}] = 0 \,. \tag{D.17}$$

Once a solution has been found, the physical effective average action for our model can be written as

$$\Gamma_k^{(\mathrm{phys})}[\phi]\big|_{T,\mu} = \Gamma_k^{(\mathrm{sym})}[\phi]\big|_{T,\mu} - H \int_{\vec{x}} \int_0^\beta \mathrm{d}x^0 \, \sigma(x) \,. \tag{D.18}$$

It is worth mentioning that the additional term c in Eq. (D.16) generally inherits dependences on the RG scale as well as external parameters from the asymmetric effective average action. Therefore, the addition of c leads to a symmetrization of the entire loop contribution as generated by the Wetterich equation.

D.3 Solution of the WTI

Throughout this work, it is sufficient to consider the symmetrization of functions rather than functionals. In particular, evaluating the field degrees of freedom on a homogeneous background turns the WTI for rotation symmetry into a partial differential equation. This allows us to present a generic solution for c in the following. To this end, we begin by noting that the Callan-Symanzik regulator leaves the $O(3)$ symmetry among the pion fields of our quark-meson model intact. The restoration of the $O(4)$ symmetry in meson field space can therefore be mapped onto the two-dimensional problem of restoring circular symmetry in the plane spanned by $x = \sigma$ and $y = \sqrt{\vec{\pi}^2}$. The WTI (D.13) then turns into

$$\left(y \frac{\partial}{\partial x} - x \frac{\partial}{\partial y} \right) \mathcal{Q}^{(\mathrm{sym})}(x, y) = 0 \,. \tag{D.19}$$

Our prescription for the restoration of symmetry with respect to orthogonal transformations relies on the addition of an auxiliary function c, which serves as a counterterm for symmetry-breaking terms. For some differentiable function $\mathcal{Q}$ of two variables, we hence write

$$\mathcal{Q}^{(\mathrm{sym})}(x, y) = \mathcal{Q}(x, y) + c(x, y) \tag{D.20}$$

in accordance with Eq. (D.16). Since the CS regulator does not affect the pion subspace of our model, the symmetrization procedure should leave this subspace unchanged as well. This constraint fixes the initial condition necessary to uniquely solve the WTI for c. To be more precise, the WTI provides us with the differential equation

$$\left(y \frac{\partial}{\partial x} - x \frac{\partial}{\partial y} \right) c(x, y) = f(x, y) \,, \tag{D.21}$$

where

$$f(x, y) \coloneqq \left(x \frac{\partial}{\partial y} - y \frac{\partial}{\partial x} \right) \mathcal{Q}(x, y) \tag{D.22}$$

and

$$\forall y \in \mathbb{R} : \qquad c(0, y) = 0 \,. \tag{D.23}$$

Making use of, for example, the method of characteristics, a general solution for c is readily found. Taking the fact into account that $\mathcal{Q}$ is a function of y^2 due to intact $O(3)$ symmetry of our theory, we find

$$c(x,y) = F_{\sqrt{x^2+y^2}}\left(\arcsin\left(\frac{x}{\sqrt{x^2+y^2}}\right)\right) - F_{\sqrt{x^2+y^2}}(0)\,, \tag{D.24}$$

where the function F is given by the following indefinite integral:

$$F_\alpha(s) = \int \mathrm{d}s\; f(\alpha\sin(s), \alpha\cos(s))\,. \tag{D.25}$$

In order to gain a better understanding of what exactly our symmetrization procedure does, let us consider the example of

$$\mathcal{Q}(x,y) = g\left(\left(x+\tilde{k}\right)^2 + y^2\right) \tag{D.26}$$

with $\tilde{k} \in \mathbb{R}$. Our goal now is to symmetrize $\mathcal{Q}$ in x and y by the addition of a suitable function c. Following the steps above, we obtain

$$c(x,y) = g\left(\tilde{k}^2 + x^2 + y^2\right) - g\left(\left(x+\tilde{k}\right)^2 + y^2\right) \tag{D.27}$$

such that the symmetrization eventually leads us to

$$\mathcal{Q}^{(\mathrm{sym})}(x,y) = \mathcal{Q}(x,y) + c(x,y) = g\left(\tilde{k}^2 + x^2 + y^2\right)\,. \tag{D.28}$$

We observe that our procedure eliminates the term $2x\tilde{k}$ from the argument of g and hence successfully establishes the circular symmetry for $\mathcal{Q}$. In the limit $\tilde{k} \to 0$, for which $\mathcal{Q}$ is already symmetric, the additional term c vanishes as it should be. We remark that our example can be directly linked to the effective potential as generated from the CS flow of the quark-meson model. Specifically, we may write the loop function as

$$L_k(\Lambda_0, h\phi) = g\left(\left(h\sigma + k'\right)^2 + h^2\vec{\pi}^2\right)\Big|_{k'=\Lambda_0}^{k'=k}\,, \tag{D.29}$$

where we have suppressed a dependence on temperature and chemical potential for simplicity. The corresponding symmetrized version of the loop function then reads

$$L_k^{(\mathrm{sym})}(\Lambda_0, h^2\phi^2) = g\left(k'^2 + h^2\phi^2\right)\Big|_{k'=\Lambda_0}^{k'=k}\,. \tag{D.30}$$

BIBLIOGRAPHY

[1] F. Halzen and A. D. Martin, *QUARKS & LEPTONS* (John Wiley & Sons, 1984).

[2] D. Griffiths, *Introduction to Elementary Particles* (2008).

[3] E. V. Shuryak, "Theory and phenomenology of the QCD vacuum," Phys. Rept. **115**, 151 (1984).

[4] T. Muta, *Foundations of quantum chromodynamics: An Introduction to perturbative methods in gauge theories*, Vol. 5 (1987).

[5] P. Skands, "Introduction to QCD," in *Theoretical Advanced Study Institute in Elementary Particle Physics: Searching for New Physics at Small and Large Scales* (2013) pp. 341–420, arXiv:1207.2389 [hep-ph].

[6] S. R. Coleman and D. J. Gross, "Price of asymptotic freedom," Phys. Rev. Lett. **31**, 851–854 (1973).

[7] K. Rajagopal, "Mapping the QCD phase diagram," Nucl. Phys. A **661**, 150–161 (1999), arXiv:hep-ph/9908360.

[8] M. A. Stephanov, "QCD phase diagram: An Overview," PoS **LAT2006**, 024 (2006), arXiv:hep-lat/0701002.

[9] "The Frontiers of Nuclear Science, A Long Range Plan," (2008), arXiv:0809.3137 [nucl-ex].

[10] K. Fukushima and T. Hatsuda, "The phase diagram of dense QCD," Rept. Prog. Phys. **74**, 014001 (2011), arXiv:1005.4814 [hep-ph].

[11] G. Aarts, F. Attanasio, B. Jäger, E. Seiler, D. Sexty, and I.-O. Stamatescu, "QCD at nonzero chemical potential: recent progress on the lattice," AIP Conf. Proc. **1701**, 020001 (2016), arXiv:1412.0847 [hep-lat].

[12] H.-T. Ding, F. Karsch, and S. Mukherjee, "Thermodynamics of strong-interaction matter from Lattice QCD," Int. J. Mod. Phys. E **24**, 1530007 (2015), arXiv:1504.05274 [hep-lat].

[13] A. L. Watts *et al.*, "Colloquium : Measuring the neutron star equation of state using x-ray timing," Rev. Mod. Phys. **88**, 021001 (2016), arXiv:1602.01081 [astro-ph.HE].

[14] G. Baym, T. Hatsuda, T. Kojo, P. D. Powell, Y. Song, and T. Takatsuka, "From hadrons to quarks in neutron stars: a review," Rept. Prog. Phys. **81**, 056902 (2018), arXiv:1707.04966 [astro-ph.HE].

[15] B. B. Brandt, G. Endrodi, and S. Schmalzbauer, "QCD at nonzero isospin asymmetry," PoS **Confinement2018**, 260 (2018), arXiv:1811.06004 [hep-lat].

[16] C. S. Fischer, "QCD at finite temperature and chemical potential from Dyson–Schwinger equations," Prog. Part. Nucl. Phys. **105**, 1–60 (2019), arXiv:1810.12938 [hep-ph].

[17] J. N. Guenther, "An overview of the QCD phase diagram at finite T and μ," PoS **LATTICE2021**, 013 (2022), arXiv:2201.02072 [hep-lat].

[18] M. Stephanov, "QCD critical point: Recent developments," EPJ Web Conf. **314**, 00042 (2024), arXiv:2410.02861 [nucl-th].

[19] K. Fukushima, "QCD Phase Diagram and Astrophysical Implications," (2025) arXiv:2501.01907 [hep-ph].

[20] J. P. Blaizot, "Theory of the quark gluon plasma," Lect. Notes Phys. **583**, 117–160 (2002), arXiv:hep-ph/0107131.

[21] E. V. Shuryak, "Nonperturbative QCD and Quark-Gluon Plasma," ICTP Lect. Notes Ser. **10**, 55–111 (2002).

[22] S. Sarkar, H. Satz, and B. Sinha, eds., *The Physics of the Quark-Gluon Plasma*, Lecture Notes in Physics, Vol. 785 (Springer Berlin, Heidelberg, 2010).

[23] H. Satz, "The Quark-Gluon Plasma – A Short Introduction," Nucl. Phys. A **862-863**, 4–12 (2011), arXiv:1101.3937 [hep-ph].

[24] K. Fukushima, "Evolution to the quark–gluon plasma," Rept. Prog. Phys. **80**, 022301 (2017), arXiv:1603.02340 [nucl-th].

[25] K. Rajagopal and F. Wilczek, "The Condensed matter physics of QCD," in *At the frontier of particle physics. Handbook of QCD. Vol. 1-3*, edited by M. Shifman and B. Ioffe (2000) pp. 2061–2151, arXiv:hep-ph/0011333.

[26] D. H. Rischke, "The quark-gluon plasma in equilibrium," Prog. Part. Nucl. Phys. **52**, 197–296 (2004), arXiv:nucl-th/0305030.

[27] I. A. Shovkovy, "Two Lectures on Color Superconductivity," Found. Phys. **35**, 1309–1358 (2005), arXiv:nucl-th/0410091.

[28] M. Buballa, "NJL-model analysis of dense quark matter," Physics Reports **407**, 205–376 (2005), arXiv:hep-ph/0402234.

[29] M. G. Alford, A. Schmitt, K. Rajagopal, and T. Schäfer, "Color superconductivity in dense quark matter," Rev. Mod. Phys. **80**, 1455–1515 (2008), arXiv:0709.4635 [hep-ph].

[30] J. Braun and B. Schallmo, "From quarks and gluons to color superconductivity at supranuclear densities," Phys. Rev. D **105**, 036003 (2022), arXiv:2106.04198 [hep-ph].

[31] I. Bombaci and D. Logoteta, "Equation of state of dense nuclear matter and neutron star structure from nuclear chiral interactions," Astron. Astrophys. **609**, A128 (2018), arXiv:1805.11846 [astro-ph.HE].

[32] N. Antoniou *et al.* (NA49-future), "Study of hadron production in hadron nucleus and nucleus nucleus collisions at the CERN SPS," (2006).

[33] F. Wilczek, "Prelude to Compressed Baryonic Matter," Lect. Notes Phys. **814**, 1–10 (2011), arXiv:1001.2729 [hep-ph].

[34] T. Galatyuk (HADES), "HADES overview," Nucl. Phys. A **931**, 41–51 (2014).

[35] H. Sako *et al.*, "Towards the heavy-ion program at J-PARC," Nucl. Phys. A **931**, 1158–1162 (2014).

[36] V. D. Kekelidze, R. Lednicky, V. A. Matveev, I. N. Meshkov, A. S. Sorin, and G. V. Trubnikov, "Three stages of the NICA accelerator complex," Eur. Phys. J. A **52**, 211 (2016).

[37] J. Chen *et al.*, "Properties of the QCD matter: review of selected results from the relativistic heavy ion collider beam energy scan (RHIC BES) program," Nucl. Sci. Tech. **35**, 214 (2024), arXiv:2407.02935 [nucl-ex].

[38] M. M. Aggarwal *et al.* (STAR), "An Experimental Exploration of the QCD Phase Diagram: The Search for the Critical Point and the Onset of De-confinement," (2010), arXiv:1007.2613 [nucl-ex].

[39] B. I. Abelev *et al.* (STAR Collaboration), "Identified particle production, azimuthal anisotropy, and interferometry measurements in Au + Au collisions at $\sqrt{s_{NN}} = 9.2$ gev," Phys. Rev. C **81**, 024911 (2010).

[40] L. Adamczyk *et al.* (STAR Collaboration), "Energy dependence of moments of net-proton multiplicity distributions at rhic," Phys. Rev. Lett. **112**, 032302 (2014).

[41] A. Aduszkiewicz *et al.* (NA61/SHINE), "Multiplicity and transverse momentum fluctuations in inelastic proton–proton interactions at the CERN Super Proton Synchrotron," Eur. Phys. J. C **76**, 635 (2016), arXiv:1510.00163 [hep-ex].

[42] W.-j. Fu, J. M. Pawlowski, and F. Rennecke, "QCD phase structure at finite temperature and density," Phys. Rev. D **101**, 054032 (2020), arXiv:1909.02991 [hep-ph].

[43] F. Gao and J. M. Pawlowski, "Chiral phase structure and critical end point in QCD," Phys. Lett. B **820**, 136584 (2021), arXiv:2010.13705 [hep-ph].

[44] P. J. Gunkel and C. S. Fischer, "Locating the critical endpoint of QCD: Mesonic backcoupling effects," Phys. Rev. D **104**, 054022 (2021), arXiv:2106.08356 [hep-ph].

[45] J. Bernhardt, C. S. Fischer, and P. Isserstedt, "Critical Endpoint of QCD and Baryon Number Fluctuations in a Finite Volume," PoS **FAIRness2022**, 066 (2023), arXiv:2301.10990 [hep-ph].

[46] W.-j. Fu, X. Luo, J. M. Pawlowski, F. Rennecke, and S. Yin, "Ripples of the QCD Critical Point," (2023), arXiv:2308.15508 [hep-ph].

[47] D. A. Clarke, P. Dimopoulos, F. Di Renzo, J. Goswami, C. Schmidt, S. Singh, and K. Zambello, "Searching for the QCD critical endpoint using multi-point Padé approximations," (2024), arXiv:2405.10196 [hep-lat].

[48] G. Ecker, "Chiral perturbation theory," Prog. Part. Nucl. Phys. **35**, 1–80 (1995), arXiv:hep-ph/9501357.

[49] S. Scherer, "Introduction to chiral perturbation theory," Adv. Nucl. Phys. **27**, 277 (2003), arXiv:hep-ph/0210398.

[50] V. Bernard, "Chiral Perturbation Theory and Baryon Properties," Prog. Part. Nucl. Phys. **60**, 82–160 (2008), arXiv:0706.0312 [hep-ph].

[51] H. A. Bethe, "Nuclear Many-Body Problem," Phys. Rev. **103**, 1353–1390 (1956).

[52] M. Baldo, "The Many-Body Theory of the Nuclear Equation of State," Int. Rev. Nucl. Phys. **8**, 1–120 (1999).

[53] C. Simenel, "Nuclear Quantum Many-Body Dynamics: From Collective Vibrations to Heavy-Ion Collisions," Eur. Phys. J. A **48**, 152 (2012), arXiv:1209.3375 [nucl-th].

[54] A. H. Mueller, "Perturbative QCD at High-Energies," Phys. Rept. **73**, 237 (1981).

[55] G. Altarelli, "Experimental Tests of Perturbative QCD," Ann. Rev. Nucl. Part. Sci. **39**, 357–406 (1989).

[56] R. S. Thorne and W. K. Tung, "PQCD Formulations with Heavy Quark Masses and Global Analysis," in *HERA and the LHC: 4th Workshop on the Implications of HERA for LHC Physics* (2008) pp. 332–351, arXiv:0809.0714 [hep-ph].

[57] J. Ghiglieri, A. Kurkela, M. Strickland, and A. Vuorinen, "Perturbative Thermal QCD: Formalism and Applications," Phys. Rept. **880**, 1–73 (2020), arXiv:2002.10188 [hep-ph].

[58] R. Stock, "The QCD Phase Diagram: Expectations and Challenges," PoS **CPOD2009**, 001 (2009), arXiv:0909.0601 [nucl-ex].

[59] N. Brambilla *et al.*, "QCD and Strongly Coupled Gauge Theories: Challenges and Perspectives," Eur. Phys. J. C **74**, 2981 (2014), arXiv:1404.3723 [hep-ph].

[60] U. Heinz *et al.*, "Exploring the properties of the phases of QCD matter - research opportunities and priorities for the next decade," (2015), arXiv:1501.06477 [nucl-th].

[61] M. Peardon, "Monte carlo simulations of lattice qcd," in *QCD and Numerical Analysis III*, edited by A. Bori~i, A. Frommer, B. Joó, A. Kennedy, and B. Pendleton (Springer Berlin Heidelberg, Berlin, Heidelberg, 2005) pp. 41–54.

[62] J. M. Katzy, "QCD Monte-Carlo model tunes for the LHC," Prog. Part. Nucl. Phys. **73**, 141–187 (2013).

[63] J. Giedt, "Lattice gauge theory and physics beyond the standard model," PoS **LATTICE2012**, 006 (2012).

[64] J. N. Guenther, "Overview of the QCD phase diagram: Recent progress from the lattice," Eur. Phys. J. A **57**, 136 (2021), arXiv:2010.15503 [hep-lat].

[65] A. Pásztor, "Lattice QCD Overview," EPJ Web Conf. **296**, 01009 (2024).

[66] P. de Forcrand, "Simulating QCD at finite density," PoS **LAT2009**, 010 (2009), arXiv:1005.0539 [hep-lat].

[67] V. A. Goy, V. Bornyakov, D. Boyda, A. Molochkov, A. Nakamura, A. Nikolaev, and V. Zakharov, "Sign problem in finite density lattice QCD," PTEP **2017**, 031D01 (2017), arXiv:1611.08093 [hep-lat].

[68] C. E. Berger, L. Rammelmüller, A. C. Loheac, F. Ehmann, J. Braun, and J. E. Drut, "Complex Langevin and other approaches to the sign problem in quantum many-body physics," Phys. Rept. **892**, 1–54 (2021), arXiv:1907.10183 [cond-mat.quant-gas].

[69] J. M. Maldacena, "The Large N limit of superconformal field theories and supergravity," Adv. Theor. Math. Phys. **2**, 231–252 (1998), arXiv:hep-th/9711200.

[70] E. Witten, "Anti-de Sitter space and holography," Adv. Theor. Math. Phys. **2**, 253–291 (1998), arXiv:hep-th/9802150.

[71] V. E. Hubeny, "The AdS/CFT Correspondence," Class. Quant. Grav. **32**, 124010 (2015), arXiv:1501.00007 [gr-qc].

[72] F. J. Dyson, "The S matrix in quantum electrodynamics," Phys. Rev. **75**, 1736–1755 (1949).

[73] J. S. Schwinger, "On the Green's functions of quantized fields. 1." Proc. Nat. Acad. Sci. **37**, 452–455 (1951).

[74] Y. Nambu and G. Jona-Lasinio, "Dynamical Model of Elementary Particles Based on an Analogy with Superconductivity. I." Phys. Rev. **122**, 345–358 (1961).

[75] Y. Nambu and G. Jona-Lasinio, "Dynamical model of elementary particles based on an analogy with superconductivity. II." Phys. Rev. **124**, 246–254 (1961).

[76] S. P. Klevansky, "The Nambu-Jona-Lasinio model of quantum chromodynamics," Rev. Mod. Phys. **64**, 649–708 (1992).

[77] T. Hatsuda and T. Kunihiro, "QCD phenomenology based on a chiral effective Lagrangian," Phys. Rept. **247**, 221–367 (1994), arXiv:hep-ph/9401310.

[78] W.-j. Fu, "QCD at finite temperature and density within the fRG approach: an overview," Commun. Theor. Phys. **74**, 097304 (2022), arXiv:2205.00468 [hep-ph].

[79] F. Ihssen, J. M. Pawlowski, F. R. Sattler, and N. Wink, "Towards quantitative precision for QCD at large densities," (2023), arXiv:2309.07335 [hep-th].

[80] W.-j. Fu, J. M. Pawlowski, R. D. Pisarski, F. Rennecke, R. Wen, and S. Yin, "The QCD moat regime and its real-time properties," (2024), arXiv:2412.15949 [hep-ph].

[81] J. Braun, T. Dörnfeld, B. Schallmo, and S. Töpfel, "Renormalization group studies of dense relativistic systems," Phys. Rev. D **104**, 096002 (2021), arXiv:2008.05978 [hep-ph].

[82] J. Braun *et al.*, "Renormalised spectral flows," SciPost Phys. Core **6**, 061 (2023), arXiv:2206.10232 [hep-th].

[83] S. Töpfel, A. Geißel, and J. Braun, "Subtleties in the calculation of correlation functions for hot and dense systems," Phys. Rev. D **111**, 016023 (2025), arXiv:2410.06674 [nucl-th].

[84] S. Töpfel, J. M. Pawlowski, and J. Braun, "Phase structure of quark matter and in-medium properties of mesons from Callan-Symanzik flows," (2024), arXiv:2412.16059 [hep-ph].

[85] K. G. Wilson, "Renormalization group and critical phenomena. 1. Renormalization group and the Kadanoff scaling picture," Phys. Rev. B **4**, 3174–3183 (1971).

[86] K. G. Wilson, "Renormalization group and critical phenomena. 2. Phase space cell analysis of critical behavior," Phys. Rev. B **4**, 3184–3205 (1971).

[87] C. Wetterich, "Exact evolution equation for the effective potential," Phys. Lett. B **301**, 90–94 (1993), arXiv:1710.05815 [hep-th].

[88] J. Braun, M. Leonhardt, and J. M. Pawlowski, "Renormalization group consistency and low-energy effective theories," SciPost Phys. **6**, 056 (2019), arXiv:1806.04432 [hep-ph].

[89] M. Kontsevich, "Deformation Quantization of Poisson Manifolds," Letters in Mathematical Physics **66**, 157–216 (2003).

[90] N. Moshayedi, *Kontsevich's Deformation Quantization and Quantum Field Theory*, Vol. 2311 (2022).

[91] S. Bates and A. Weinstein, *Lectures on the Geometry of Quantization*, Vol. 8 (American Mathematical Society, 1997) Manuscript in electronic form available at https://math.berkeley.edu/~alanw/GofQ.pdf.

[92] E. Lerman, "Geometric quantization; a crash course," (2012), arXiv:1206.2334 [math.SG].

[93] P. A. M. Dirac, "The Lagrangian in quantum mechanics," Phys. Z. Sowjetunion **3**, 64–72 (1933).

[94] R. P. Feynman, "Space-Time Approach to Non-Relativistic Quantum Mechanics," Rev. Mod. Phys. **20**, 367–387 (1948).

[95] R. P. Feynman and A. R. Hibbs, *Quantum mechanics and path integrals*, International series in pure and applied physics (McGraw-Hill, New York, NY, 1965).

[96] N. Wiener, "Differential-Space," J. Math. Phys. **2**, 131–174 (1923).

[97] N. Wiener, "The Average value of a Functional," Proc. London Math. Soc. **22**, 454–467 (1924).

[98] N. Wiener, "Generalized harmonic analysis," Acta Math. **55**, 117–258 (1930).

[99] M. Kac, "Wiener and integration in function spaces," Bulletin of the American Mathematical Society **72**, 52 – 68 (1966).

[100] B. Simon, *Functional Integration and Quantum Physics*, 2nd ed., Pure and Applied Mathematics. A Series of monographs and textbooks (American Mathematical Soc., 2005).

[101] J. Glimm and A. Jaffe, *Quantum Physics: A Functional Integral Point of View* (Springer-Verlag New York, 1987).

[102] C. Dewitt-Morette, P. Cartier, and A. Folacci, eds., *Functional Integration*, NATO Science Series B: 361 (Springer New York, 1997).

[103] B. C. Hall, *Quantum Theory for Mathematicians*, Graduate Texts in Mathematics No. 267 (Springer New York, 2013).

[104] H. Kleinert, *Path Integrals in Quantum Mechanics, Statistics, Polymer Physics, and Financial Markets*, 5th ed., EBL-Schweitzer (World Scientific, 2009).

[105] J. Zinn-Justin, *Path Integrals in Quantum Mechanics* (Oxford University Press, 2004).

[106] J. Bagger, N. Lambert, S. Mukhi, and C. Papageorgakis, "Multiple Membranes in M-theory," Phys. Rept. **527**, 1–100 (2013), arXiv:1203.3546 [hep-th].

[107] A. Gadde, S. S. Razamat, and B. Willett, "'Lagrangian' for a Non-Lagrangian Field Theory with $\mathcal{N} = 2$ Supersymmetry," Phys. Rev. Lett. **115**, 171604 (2015), arXiv:1505.05834 [hep-th].

[108] C. Wetterich, "Spinors in euclidean field theory, complex structures and discrete symmetries," Nucl. Phys. B **852**, 174–234 (2011), arXiv:1002.3556 [hep-th].

[109] F. A. Berezin, *The Method of Second Quantization* (Academic Press Inc., 1966).

[110] W. Greiner and J. Reinhardt, *Field Quantization* (Springer Berlin, Heidelberg, 1996).

[111] J. Feldman, H. Knorrer, and E. Trubowitz, *Fermionic Functional Integrals and the Renormalization Group* (American Mathematical Soc., 2002).

[112] L. D. Faddeev and V. N. Popov, "Feynman Diagrams for the Yang-Mills Field," Phys. Lett. B **25**, 29–30 (1967).

[113] T. Kugo, *Eichtheorie* (Springer Berlin, Heidelberg, 1997).

[114] B. DeWitt, *Supermanifolds*, 2nd ed., Cambridge Monographs on Mathematical Physics (Cambridge University Press, 1992).

[115] G. Soff and H. Kalka, *Supersymmetrie*, Teubner Studienbücher Physik (Vieweg+Teubner Verlag, Wiebaden, 1997).

[116] S. Sawin, "Path integration in two-dimensional topological quantum field theory," J. Math. Phys. **36**, 6130–6136 (1995), arXiv:gr-qc/9505040.

[117] R. F. Streater and A. S. Wightman, *PCT, Spin and Statistics, and All That* (Princeton University Press, 1989).

[118] M. E. Peskin and D. V. Schroeder, *An Introduction to Quantum Field Theory* (Addison-Wesley, Reading, USA, 1995).

[119] A. Zee, *Quantum Field Theory in a Nutshell*, 2nd ed. (Princeton University Press, 2010).

[120] L. F. Abbott, "Introduction to the Background Field Method," Acta Phys. Polon. B **13**, 33 (1982).

[121] J. Zinn-Justin, *Quantum Field Theory and Critical Phenomena*, 5th ed., International Series of Monographs on Physics (Oxford University Press, 2021).

[122] X.-G. Wen, *Quantum Field Theory of Many-Body Systems* (Oxford University Press, Oxford, 2007).

[123] R. K. P. Zia, E. F. Redish, and S. R. McKay, "Making sense of the Legendre transform," American Journal of Physics **77**, 614–622 (2009), arXiv:0806.1147.

[124] G. Jona-Lasinio, "Relativistic field theories with symmetry breaking solutions," Nuovo Cim. **34**, 1790–1795 (1964).

[125] S. R. Coleman and E. J. Weinberg, "Radiative Corrections as the Origin of Spontaneous Symmetry Breaking," Phys. Rev. D **7**, 1888–1910 (1973).

[126] H. Gies, "Introduction to the functional RG and applications to gauge theories," Lect. Notes Phys. **852**, 287–348 (2012), arXiv:hep-ph/0611146.

[127] R. Jackiw, "Functional evaluation of the effective potential," Phys. Rev. D **9**, 1686 (1974).

[128] J. Iliopoulos, C. Itzykson, and A. Martin, "Functional Methods and Perturbation Theory," Rev. Mod. Phys. **47**, 165 (1975).

[129] H. Kleinert, *Particles and Quantum Fields* (World Scientific Publishing, 2016).

[130] P. C. West, "Supersymmetry and Finiteness," Conf. Proc. C **8306011**, 127 (1983).

[131] S. Teufel and R. Tumulka, "Hamiltonians without ultraviolet divergence for quantum field theories," Quantum Stud.: Math. Found. **8**, 17–35 (2021), arXiv:1505.04847 [quant-ph].

[132] K. G. Wilson and J. B. Kogut, "The Renormalization group and the epsilon expansion," Phys. Rept. **12**, 75–199 (1974).

[133] T. R. Morris, "Momentum scale expansion of sharp cutoff flow equations," Nucl. Phys. B **458**, 477–503 (1996), arXiv:hep-th/9508017.

[134] K. G. Wison, "Renormalization of a scalar field theory in strong coupling," Phys. Rev. D **6**, 419–429 (1972).

[135] M. E. Peskin, "Ken Wilson: Solving the Strong Interactions," J. Statist. Phys. **157**, 651–665 (2014), arXiv:1405.7086 [physics.hist-ph].

[136] M. Flory, R. C. Helling, and C. Sluka, "How I Learned to Stop Worrying and Love QFT," (2012), arXiv:1201.2714 [math-ph].

[137] C. M. Bender and C. Heissenberg, "Convergent and Divergent Series in Physics," in *22nd Saalburg Summer School on Foundations and New Methods in Theoretical Physics* (2017) arXiv:1703.05164 [math-ph].

[138] C. P. Burgess, "Quantum gravity in everyday life: General relativity as an effective field theory," Living Rev. Rel. **7**, 5–56 (2004), arXiv:gr-qc/0311082.

[139] H. W. Hammer, S. König, and U. van Kolck, "Nuclear effective field theory: status and perspectives," Rev. Mod. Phys. **92**, 025004 (2020), arXiv:1906.12122 [nucl-th].

[140] C. P. Burgess, *Introduction to Effective Field Theory* (Cambridge University Press, 2020).

[141] W. D. Goldberger, "Effective field theories of gravity and compact binary dynamics: A Snowmass 2021 whitepaper," in *Snowmass 2021* (2022) arXiv:2206.14249 [hep-th].

[142] V. P. Nair, *Quantum field theory: A modern perspective* (Springer-Verlag New York, 2005).

[143] L. P. Kadanoff, "Scaling laws for Ising models near T_c," Physics Physique Fizika **2**, 263–272 (1966).

[144] A. Matusis, L. Susskind, and N. Toumbas, "The IR / UV connection in the noncommutative gauge theories," JHEP **12**, 002 (2000), arXiv:hep-th/0002075.

[145] R. D. Ball and R. S. Thorne, "Renormalizability of effective scalar field theory," Annals Phys. **236**, 117–204 (1994), arXiv:hep-th/9310042.

[146] J. I. Latorre and T. R. Morris, "Exact scheme independence," JHEP **11**, 004 (2000), arXiv:hep-th/0008123.

[147] S. Arnone, A. Gatti, T. R. Morris, and O. J. Rosten, "Exact scheme independence at two loops," Phys. Rev. D **69**, 065009 (2004), arXiv:hep-th/0309242.

[148] J. a. F. Melo, "Introduction to Renormalisation," (2019), arXiv:1909.11099 [hep-th].

[149] N. Goldenfeld, *Lectures On Phase Transitions And The Renormalization Group* (Westview Press, 1992).

[150] P. M. Stevenson, "Optimized Perturbation Theory," Phys. Rev. D **23**, 2916 (1981).

[151] N. N. Bogoljubov and D. V. Širkov, "Charge renormalization group in quantum field theory," Nuovo Cim. **3**, 845–863 (1956).

[152] E. C. G. Stueckelberg and A. Petermann, "The normalization group in quantum theory," Helv. Phys. Acta **24**, 317–319 (1951).

[153] E. C. G. Stueckelberg de Breidenbach and A. Petermann, "Normalization of constants in the quanta theory," Helv. Phys. Acta **26**, 499–520 (1953).

[154] M. Gell-Mann and F. E. Low, "Quantum electrodynamics at small distances," Phys. Rev. **95**, 1300–1312 (1954).

[155] R. Brunetti, M. Dütsch, and K. Fredenhagen, "Perturbative algebraic quantum field theory and the renormalization groups," Adv. Theor. Math. Phys. **13**, 1541–1599 (2009), arXiv:0901.2038 [math-ph].

[156] M. Dütsch, "Connection between the renormalization groups of Stückelberg-Petermann and Wilson," Confluentes Mathematici **4**, 1240001 (2012), arXiv:1012.5604 [hep-th].

[157] F. J. Wegner and A. Houghton, "Renormalization group equation for critical phenomena," Phys. Rev. A **8**, 401–412 (1973).

[158] F. J. Wegner, "Critical Phenomena and the Renormalization Group," Lect. Notes Phys. **37**, 171–196 (1975).

[159] J. Polchinski, "Renormalization and Effective Lagrangians," Nucl. Phys. B **231**, 269–295 (1984).

[160] C. Wetterich, "Average action and the renormalization group equations," Nuclear Physics B **352**, 529–584 (1991).

[161] C. Wetterich, "Exact renormalization group equations for the average action and systematic expansions," Int. J. Mod. Phys. A **9**, 3571–3602 (1994).

[162] S. Szpigel and R. J. Perry, "The Similarity renormalization group," in *Quantum Field Theory: A 20th Century Profile*, edited by A. N. Mitra (2000) pp. 59–81, arXiv:hep-ph/0009071.

[163] S. Kehrein, *The Flow Equation Approach to Many-Particle Systems* (Springer Berlin, Heidelberg, 2006).

[164] G. Catarina and B. Murta, "Density-matrix renormalization group: a pedagogical introduction," Eur. Phys. J. B **96**, 111 (2023), arXiv:2304.13395 [cond-mat.str-el].

[165] R. Bauerschmidt, D. C. Brydges, and G. Slade, *Introduction to a renormalisation group method*, Vol. 2242 (Springer, 2019) arXiv:1907.05474 [math-ph].

[166] R. J. Creswick, H. A. Farach, and C. P. Poole, *Introduction to Renormalization Group Methods in Physics*, 2nd ed. (Dover Publications, 2016).

[167] P. Kopietz, L. Bartosch, and F. Schütz, *Introduction to the functional renormalization group*, Vol. 798 (Springer Berlin, Heidelberg, 2010).

[168] M. Salmhofer, *Renormalization: An introduction* (Springer Berlin, Heidelberg, 1999).

[169] K. Costello, *Renormalization and Effective Field Theory* (American Mathematical Society, 2011).

[170] M. E. Fisher, "Renormalization group theory: Its basis and formulation in statistical physics," Rev. Mod. Phys. **70**, 653–681 (1998).

[171] T. R. Morris, "Elements of the continuous renormalization group," Prog. Theor. Phys. Suppl. **131**, 395–414 (1998), arXiv:hep-th/9802039.

[172] C. Bagnuls and C. Bervillier, "Exact renormalization group equations and the field theoretical approach to critical phenomena," Int. J. Mod. Phys. A **16**, 1825 (2001), arXiv:hep-th/0101110.

[173] J. Polonyi, "Lectures on the functional renormalization group method," Central Eur. J. Phys. **1**, 1–71 (2003), arXiv:hep-th/0110026.

[174] H. Sonoda, "The Exact Renormalization Group: Renormalization theory revisited," (2007) arXiv:0710.1662 [hep-th].

[175] D. F. Litim, "Wilsonian flow equation and thermal field theory," in *Summer School on Introduction to Thermal Field Theory (TFT 98)* (1998) arXiv:hep-ph/9811272.

[176] J. Berges, N. Tetradis, and C. Wetterich, "Non-perturbative renormalization flow in quantum field theory and statistical physics," Phys. Rept. **363**, 223–386 (2002), arXiv:hep-ph/0005122.

[177] J. M. Pawlowski, "Aspects of the functional renormalisation group," Annals Phys. **322**, 2831–2915 (2007), arXiv:hep-th/0512261.

[178] B.-J. Schaefer and J. Wambach, "Renormalization group approach towards the QCD phase diagram," Phys. Part. Nucl. **39**, 1025–1032 (2008), arXiv:hep-ph/0611191.

[179] B. Delamotte, "An Introduction to the nonperturbative renormalization group," Lect. Notes Phys. **852**, 49–132 (2012), arXiv:cond-mat/0702365.

[180] N. Dupuis, L. Canet, A. Eichhorn, W. Metzner, J. M. Pawlowski, M. Tissier, and N. Wschebor, "The nonperturbative functional renormalization group and its applications," Phys. Rept. **910**, 1–114 (2021), arXiv:2006.04853 [cond-mat.stat-mech].

[181] D. F. Litim and J. M. Pawlowski, "Completeness and consistency of renormalisation group flows," Phys. Rev. D **66**, 025030 (2002), arXiv:hep-th/0202188.

[182] N. Tetradis and C. Wetterich, "Critical exponents from effective average action," Nucl. Phys. B **422**, 541–592 (1994), arXiv:hep-ph/9308214.

[183] M. Reuter and C. Wetterich, "Effective average action for gauge theories and exact evolution equations," Nucl. Phys. B **417**, 181–214 (1994).

[184] U. Ellwanger and C. Wetterich, "Evolution equations for the quark-meson transition," Nucl. Phys. B **423**, 137–170 (1994), arXiv:hep-ph/9402221.

[185] J. Braun, "Fermion Interactions and Universal Behavior in Strongly Interacting Theories," J. Phys. G **39**, 033001 (2012), arXiv:1108.4449 [hep-ph].

[186] A. Baldazzi, R. B. A. Zinati, and K. Falls, "Essential renormalisation group," SciPost Phys. **13**, 085 (2022), arXiv:2105.11482 [hep-th].

[187] F. Ihssen and J. M. Pawlowski, "Flowing fields and optimal RG-flows," (2023), arXiv:2305.00816 [hep-th].

[188] H. Gies and C. Wetterich, "Renormalization flow of bound states," Phys. Rev. D **65**, 065001 (2002), arXiv:hep-th/0107221.

[189] J. Braun, L. Fister, J. M. Pawlowski, and F. Rennecke, "From Quarks and Gluons to Hadrons: Chiral Symmetry Breaking in Dynamical QCD," Phys. Rev. D **94**, 034016 (2016), arXiv:1412.1045 [hep-ph].

[190] J. París-López, R. Alkofer, A. Maas, W. Mian, M. Mitter, J. Pawlowski, and H. Sanchis-Alepuz, "Calculating hadron properties from dynamical hadronization in the Functional Renormalisation Group," J. Phys. Conf. Ser. **1024**, 012009 (2018).

[191] L. Batini, E. Grossi, and N. Wink, "Dissipation dynamics of a scalar field," Phys. Rev. D **108**, 125021 (2023), arXiv:2309.06586 [hep-th].

[192] L. P. Kadanoff, "Critical Behavior. Universality and Scaling," in *From Order to Chaos* (World Scientific, 1971) pp. 222–239.

[193] L. P. Kadanoff, "Scaling, Universality and Operator Algebra," in *12th School of Modern Physics on Phase Transitions and Critical Phenomena* (1976).

[194] H. E. Stanley, "Scaling, universality, and renormalization: Three pillars of modern critical phenomena," Rev. Mod. Phys. **71**, S358–S366 (1999).

[195] H. Kleinert and V. Schulte-Frohlinde, *Critical properties of ϕ^4-theories* (World Scientific, 2001).

[196] A. Franklin, "On the renormalization group explanation of universality," Philosophy of Science **85**, 225–248 (2018).

[197] R. Percacci, "A Short introduction to asymptotic safety," in *Time and Matter* (2011) pp. 123–142, arXiv:1110.6389 [hep-th].

[198] J. Braun, H. Gies, and D. D. Scherer, "Asymptotic safety: a simple example," Phys. Rev. D **83**, 085012 (2011), arXiv:1011.1456 [hep-th].

[199] D. F. Litim and M. J. Trott, "Asymptotic safety of scalar field theories," Phys. Rev. D **98**, 125006 (2018), arXiv:1810.01678 [hep-th].

[200] A. Eichhorn, "Asymptotically safe gravity," in *57th International School of Subnuclear Physics: In Search for the Unexpected* (2020) arXiv:2003.00044 [gr-qc].

[201] A. Pastor-Gutiérrez, J. M. Pawlowski, and M. Reichert, "The Asymptotically Safe Standard Model: From quantum gravity to dynamical chiral symmetry breaking," SciPost Phys. **15**, 105 (2023), arXiv:2207.09817 [hep-th].

[202] D. F. Litim, "Scheme independence at first order phase transitions and the renormalization group," Phys. Lett. B **393**, 103–109 (1997), arXiv:hep-th/9609040.

[203] S. Pokorski, *Gauge Field Theories*, 2nd ed. (Cambridge University Press, 2000).

[204] C. Wetterich, "Quadratic Renormalization of the Average Potential and the Naturalness of Quadratic Mass Relations for the Top Quark," Z. Phys. C **48**, 693–705 (1990).

[205] S. Bornholdt and C. Wetterich, "Average action for models with fermions," Z. Phys. C **58**, 585–594 (1993).

[206] J. Braun and H. Gies, "Chiral phase boundary of QCD at finite temperature," JHEP **06**, 024 (2006), arXiv:hep-ph/0602226.

[207] J. Braun, H. Gies, and J. M. Pawlowski, "Quark Confinement from Color Confinement," Phys. Lett. B **684**, 262–267 (2010), arXiv:0708.2413 [hep-th].

[208] J. M. Pawlowski and N. Strodthoff, "Real time correlation functions and the functional renormalization group," Phys. Rev. D **92**, 094009 (2015), arXiv:1508.01160 [hep-ph].

[209] D. U. Jungnickel and C. Wetterich, "Effective action for the chiral quark-meson model," Phys. Rev. D **53**, 5142–5175 (1996), arXiv:hep-ph/9505267.

[210] D. F. Litim, "Optimized renormalization group flows," Phys. Rev. D **64**, 105007 (2001), arXiv:hep-th/0103195.

[211] D. F. Litim, "Optimization of the exact renormalization group," Phys. Lett. B **486**, 92–99 (2000), arXiv:hep-th/0005245.

[212] D. F. Litim, "Mind the gap," Int. J. Mod. Phys. A **16**, 2081–2088 (2001), arXiv:hep-th/0104221.

[213] D. F. Litim and J. M. Pawlowski, "Non-perturbative thermal flows and resummations," JHEP **11**, 026 (2006), arXiv:hep-th/0609122.

[214] T. R. Morris, "A manifestly gauge invariant exact renormalization group," in *Workshop on the Exact Renormalization Group* (1998) pp. 1–40, arXiv:hep-th/9810104.

[215] T. R. Morris, "A gauge invariant exact renormalization group I," Nucl. Phys. B **573**, 97–126 (2000), arXiv:hep-th/9910058.

[216] T. R. Morris, "A gauge invariant exact renormalization group II," JHEP **12**, 012 (2000), arXiv:hep-th/0006064.

[217] S. Arnone, T. R. Morris, and O. J. Rosten, "Manifestly Gauge Invariant Exact Renormalization Group," Fields Inst. Commun. **50**, 1 (2007), arXiv:hep-th/0606181.

[218] O. J. Rosten, "Aspects of Manifest Gauge Invariance," PoS **FACESQCD**, 035 (2010), arXiv:1102.3091 [hep-th].

[219] O. J. Rosten, "Fundamentals of the Exact Renormalization Group," Phys. Rept. **511**, 177–272 (2012), arXiv:1003.1366 [hep-th].

[220] U. Ellwanger, "Flow equations and BRS invariance for Yang-Mills theories," Phys. Lett. B **335**, 364–370 (1994), arXiv:hep-th/9402077.

[221] U. Ellwanger, M. Hirsch, and A. Weber, "Flow equations for the relevant part of the pure Yang-Mills action," Z. Phys. C **69**, 687–698 (1996), arXiv:hep-th/9506019.

[222] U. Ellwanger, M. Hirsch, and A. Weber, "The Heavy quark potential from Wilson's exact renormalization group," Eur. Phys. J. C **1**, 563–578 (1998), arXiv:hep-ph/9606468.

[223] M. Reuter, "Effective average actions and nonperturbative evolution equations," in *5th Hellenic School and Workshops on Elementary Particle Physics* (1996) arXiv:hep-th/9602012.

[224] M. Bonini, M. D'Attanasio, and G. Marchesini, "BRS symmetry for Yang-Mills theory with exact renormalization group," Nucl. Phys. B **437**, 163–186 (1995), arXiv:hep-th/9410138.

[225] M. Reuter and C. Wetterich, "Gluon condensation in nonperturbative flow equations," Phys. Rev. D **56**, 7893–7916 (1997), arXiv:hep-th/9708051.

[226] F. Freire, D. F. Litim, and J. M. Pawlowski, "Gauge invariance and background field formalism in the exact renormalization group," Phys. Lett. B **495**, 256–262 (2000), arXiv:hep-th/0009110.

[227] L. F. Abbott, "The Background Field Method Beyond One Loop," Nucl. Phys. B **185**, 189–203 (1981).

[228] S. Floerchinger, "Analytic Continuation of Functional Renormalization Group Equations," JHEP **05**, 021 (2012), arXiv:1112.4374 [hep-th].

[229] R.-A. Tripolt, L. von Smekal, and J. Wambach, "Flow equations for spectral functions at finite external momenta," Phys. Rev. D **90**, 074031 (2014), arXiv:1408.3512 [hep-ph].

[230] J. M. Pawlowski, N. Strodthoff, and N. Wink, "Finite temperature spectral functions in the O(N)-model," Phys. Rev. D **98**, 074008 (2018), arXiv:1711.07444 [hep-th].

[231] J. Braun, K. Schwenzer, and H.-J. Pirner, "Linking the quark meson model with QCD at high temperature," Phys. Rev. D **70**, 085016 (2004), arXiv:hep-ph/0312277.

[232] B.-J. Schaefer and J. Wambach, "The phase diagram of the quark-meson model," Nucl. Phys. A **757**, 479–492 (2005), arXiv:nucl-th/0403039.

[233] D. F. Litim and J. M. Pawlowski, "Non-perturbative thermal flows and resummations," JHEP **11**, 026 (2006), arXiv:hep-th/0609122.

[234] J.-P. Blaizot, A. Ipp, R. Mendez-Galain, and N. Wschebor, "Perturbation theory and non-perturbative renormalization flow in scalar field theory at finite temperature," Nucl. Phys. A **784**, 376–406 (2007), arXiv:hep-ph/0610004.

[235] A. J. Helmboldt, J. M. Pawlowski, and N. Strodthoff, "Towards quantitative precision in the chiral crossover: masses and fluctuation scales," Phys. Rev. D **91**, 054010 (2015), arXiv:1409.8414 [hep-ph].

[236] J. Braun, "Thermodynamics of QCD low-energy models and the derivative expansion of the effective action," Phys. Rev. D **81**, 016008 (2010), arXiv:0908.1543 [hep-ph].

[237] L. Canet, B. Delamotte, D. Mouhanna, and J. Vidal, "Optimization of the derivative expansion in the nonperturbative renormalization group," Phys. Rev. D **67**, 065004 (2003), arXiv:hep-th/0211055.

[238] D. F. Litim, "Critical exponents from optimized renormalization group flows," Nucl. Phys. B **631**, 128–158 (2002), arXiv:hep-th/0203006.

[239] D. F. Litim and D. Zappala, "Ising exponents from the functional renormalisation group," Phys. Rev. D **83**, 085009 (2011), arXiv:1009.1948 [hep-th].

[240] C. Bervillier, A. Juttner, and D. F. Litim, "High-accuracy scaling exponents in the local potential approximation," Nucl. Phys. B **783**, 213–226 (2007), arXiv:hep-th/0701172.

[241] F. Benitez, J. P. Blaizot, H. Chate, B. Delamotte, R. Mendez-Galain, and N. Wschebor, "Solutions of renormalization group flow equations with full momentum dependence," Phys. Rev. E **80**, 030103 (2009), arXiv:0901.0128 [cond-mat.stat-mech].

[242] L. Canet, B. Delamotte, D. Mouhanna, and J. Vidal, "Nonperturbative renormalization group approach to the Ising model: A derivative expansion at order ∂^4," Phys. Rev. B **68**, 064421 (2003), arXiv:hep-th/0302227.

[243] D. Roscher, J. Braun, and J. E. Drut, "Phase structure of mass- and spin-imbalanced unitary Fermi gases," Phys. Rev. A **91**, 053611 (2015), arXiv:1501.05544 [cond-mat.quant-gas].

[244] N. J. Higham, *Functions of Matrices* (Society for Industrial and Applied Mathematics, 2008).

[245] B. C. Hall, *Lie Groups, Lie Algebras, and Representations*, 2nd ed., Graduate Texts in Mathematics (Springer Cham, 2015).

[246] K. G. Wilson, "Problems in physics with many scales of length," Sci. Am. **241**, 140–157 (1979).

[247] A. Koenigstein, M. J. Steil, N. Wink, E. Grossi, J. Braun, M. Buballa, and D. H. Rischke, "Numerical fluid dynamics for FRG flow equations: Zero-dimensional QFTs as numerical test cases. I. The O(N) model," Phys. Rev. D **106**, 065012 (2022), arXiv:2108.02504 [cond-mat.stat-mech].

[248] A. Koenigstein, M. J. Steil, N. Wink, E. Grossi, and J. Braun, "Numerical fluid dynamics for FRG flow equations: Zero-dimensional QFTs as numerical test cases. II. Entropy production and irreversibility of RG flows," Phys. Rev. D **106**, 065013 (2022), arXiv:2108.10085 [cond-mat.stat-mech].

[249] M. J. Steil and A. Koenigstein, "Numerical fluid dynamics for FRG flow equations: Zero-dimensional QFTs as numerical test cases. III. Shock and rarefaction waves in RG flows reveal limitations of the $N\to\infty$ limit in O(N)-type models," Phys. Rev. D **106**, 065014 (2022), arXiv:2108.04037 [cond-mat.stat-mech].

[250] L. Salasnich, N. Manini, and A. Parola, "Condensate fraction of a Fermi gas in the BCS-BEC crossover," Phys. Rev. A **72**, 023621 (2005), arXiv:cond-mat/0506074 [cond-mat.stat-mech].

[251] M. J. H. Ku, A. T. Sommer, L. W. Cheuk, and M. W. Zwierlein, "Revealing the superfluid lambda transition in the universal thermodynamics of a unitary fermi gas," Science **335**, 563–567 (2012), arXiv:1110.3309 [cond-mat.quant-gas].

[252] V. A. Rubakov and M. E. Shaposhnikov, "Electroweak baryon number nonconservation in the early universe and in high-energy collisions," Usp. Fiz. Nauk **166**, 493–537 (1996), arXiv:hep-ph/9603208.

[253] D. J. Schwarz, "The first second of the universe," Annalen Phys. **12**, 220–270 (2003), arXiv:astro-ph/0303574.

[254] N. K. Glendenning, *Compact stars* (Springer New York, 1997).

[255] M. Leonhardt, M. Pospiech, B. Schallmo, J. Braun, C. Drischler, K. Hebeler, and A. Schwenk, "Symmetric nuclear matter from the strong interaction," Phys. Rev. Lett. **125**, 142502 (2020), arXiv:1907.05814 [nucl-th].

[256] S. Huth, C. Wellenhofer, and A. Schwenk, "New equations of state constrained by nuclear physics, observations, and QCD calculations of high-density nuclear matter," Phys. Rev. C **103**, 025803 (2021), arXiv:2009.08885 [nucl-th].

[257] C. Y. Wong, *Introduction to High-Energy Heavy-Ion Collisions* (World Scientific, Singapore, 1995).

[258] M. H. Thoma, "Applications of high temperature field theory to heavy ion collisions," in *Quark-Gluon Plasma 2*, edited by R. C. Hwa (1995) pp. 51–134, arXiv:hep-ph/9503400.

[259] B. Friman, C. Hohne, J. Knoll, S. Leupold, J. Randrup, R. Rapp, and P. Senger, eds., *The CBM Physics Book*, Vol. 814 (Springer Berlin, Heidelberg, 2011).

[260] A. D. Linde, "Phase Transitions in Gauge Theories and Cosmology," Rept. Prog. Phys. **42**, 389 (1979).

[261] M. Buballa, "Phase diagram of quark matter under compact star conditions," AIP Conf. Proc. **892**, 476–478 (2007).

[262] P. Braun-Munzinger and J. Wambach, "The Phase Diagram of Strongly-Interacting Matter," Rev. Mod. Phys. **81**, 1031–1050 (2009), arXiv:0801.4256 [hep-ph].

[263] L. M. Haas, J. Braun, and J. M. Pawlowski, "On the QCD phase diagram at finite chemical potential," AIP Conf. Proc. **1343**, 459–461 (2011), arXiv:1012.4735 [hep-ph].

[264] J. Braun, M. Leonhardt, and M. Pospiech, "Fierz-complete NJL model study. III. Emergence from quark-gluon dynamics," Phys. Rev. D **101**, 036004 (2020), arXiv:1909.06298 [hep-ph].

[265] J.-L. Kneur, M. B. Pinto, and T. E. Restrepo, "Renormalization group improved QCD thermodynamics," PoS **XVHadronPhysics**, 040 (2022).

[266] T. Matsubara, "A New approach to quantum statistical mechanics," Prog. Theor. Phys. **14**, 351–378 (1955).

[267] J. S. Schwinger, "Brownian motion of a quantum oscillator," J. Math. Phys. **2**, 407–432 (1961).

[268] L. V. Keldysh, "Diagram technique for nonequilibrium processes," Zh. Eksp. Teor. Fiz. **47**, 1515–1527 (1964).

[269] H. Umezawa, H. Matsumoto, and M. Tachiki, *Thermo Field Dynamics and Condensed States* (North Holland, Amsterdam, 1982).

[270] Y. Takahashi and H. Umezawa, "Thermo field dynamics," Int. J. Mod. Phys. B **10**, 1755–1805 (1996).

[271] N. Landsman and C. van Weert, "Real- and imaginary-time field theory at finite temperature and density," Physics Reports **145**, 141–249 (1987).

[272] M. Le Bellac, *Quantum and Statistical Field Theory* (Clarendon Press, Oxford, 1991).

[273] A. K. Das, *Finite Temperature Field Theory* (World Scientific, New York, 1997).

[274] J. I. Kapusta and C. Gale, *Finite-Temperature Field Theory*, 2nd ed., Cambridge Monographs on Mathematical Physics (Cambridge University Press, Cambridge, 2006).

[275] A. K. Das, "Topics in finite temperature field theory," in *Quantum field theory: A 20th century profile*, edited by A. N. Mitra (2000) pp. 383–411, arXiv:hep-ph/0004125.

[276] M. G. Mustafa, "An introduction to thermal field theory and some of its application," Eur. Phys. J. ST **232**, 1369–1457 (2023), arXiv:2207.00534 [hep-ph].

[277] J. Goldstone, "Field Theories with Superconductor Solutions," Nuovo Cim. **19**, 154–164 (1961).

[278] J. Goldstone, A. Salam, and S. Weinberg, "Broken Symmetries," Phys. Rev. **127**, 965–970 (1962).

[279] H. Yamakawa, *Modern Theory of Polymer Solutions* (Harper & Row, New York, 1971).

[280] S. Baeurle and E. Nogovitsin, "Challenging scaling laws of flexible polyelectrolyte solutions with effective renormalization concepts," Polymer **48**, 4883–4899 (2007).

[281] S. G. Brush, "Functional integrals and statistical physics," Rev. Mod. Phys. **33**, 79–92 (1961).

[282] F. Guerra, L. Rosen, and B. Simon, "The $P(\phi)_2$ Euclidean quantum field theory as classical statistical mechanics," Annals of Mathematics **101**, 191–259 (1975).

[283] S. Albeverio and R. Høegh-Krohn, "Uniqueness and the Global Markov Property for Euclidean Fields. The Case of Trigonometric Interactions," Commun. Math. Phys. **68**, 95–128 (1979).

[284] C. Itzykson and J. M. Drouffe, *Statistical Field Theory. Vol. 1: From Brownian Motion to Renormalization and Lattice Gauge Theory*, Cambridge Monographs on Mathematical Physics (CUP, 1989).

[285] B. M. McCoy, "The Connection between statistical mechanics and quantum field theory," in *7th Physics Summer School on Statistical Mechanics and Field Theory* (1994) pp. 26–128, arXiv:hep-th/9403084.

[286] A. Altland and B. Simons, *Condensed Matter Field Theory* (Cambridge University Press, 2023).

[287] A. Wipf, *Statistical Approach to Quantum Field Theory*, Lecture Notes in Physics, Vol. 992 (2021).

[288] G. Baym and N. D. Mermin, "Determination of Thermodynamic Green's Functions," J. Math. Phys. **2**, 232–234 (1961).

[289] J. Berges, "Introduction to nonequilibrium quantum field theory," AIP Conf. Proc. **739**, 3–62 (2004), arXiv:hep-ph/0409233.

[290] E. A. Calzetta and B.-L. B. Hu, *Nonequilibrium Quantum Field Theory* (Cambridge University Press, 2008).

[291] J. Berges and D. Mesterhazy, "Introduction to the nonequilibrium functional renormalization group," Nucl. Phys. B Proc. Suppl. **228**, 37–60 (2012), arXiv:1204.1489 [hep-ph].

[292] B. J. P. Jones, "The Physics of Neutrinoless Double Beta Decay: A Primer," in *Theoretical Advanced Study Institute in Elementary Particle Physics: The Obscure Universe: Neutrinos and Other Dark Matters* (2021) arXiv:2108.09364 [nucl-ex].

[293] K. Kamikado, N. Strodthoff, L. von Smekal, and J. Wambach, "Fluctuations in the quark-meson model for QCD with isospin chemical potential," Phys. Lett. B **718**, 1044–1053 (2013), arXiv:1207.0400 [hep-ph].

[294] W.-j. Fu, J. M. Pawlowski, and F. Rennecke, "Strangeness Neutrality and QCD Thermodynamics," SciPost Phys. Core **2**, 002 (2020), arXiv:1808.00410 [hep-ph].

[295] J. Braun and B. Schallmo, "Zero-temperature thermodynamics of dense asymmetric strong-interaction matter," Phys. Rev. D **106**, 076010 (2022), arXiv:2204.00358 [nucl-th].

[296] R. Kubo, "Statistical mechanical theory of irreversible processes. 1. General theory and simple applications in magnetic and conduction problems," J. Phys. Soc. Jap. **12**, 570–586 (1957).

[297] P. C. Martin and J. S. Schwinger, "Theory of many particle systems. 1." Phys. Rev. **115**, 1342–1373 (1959).

[298] R. Haag, N. M. Hugenholtz, and M. Winnink, "On the Equilibrium states in quantum statistical mechanics," Commun. Math. Phys. **5**, 215–236 (1967).

[299] F. M. Haehl, R. Loganayagam, P. Narayan, A. A. Nizami, and M. Rangamani, "Thermal out-of-time-order correlators, KMS relations, and spectral functions," JHEP **12**, 154 (2017), arXiv:1706.08956 [hep-th].

[300] M. Przanowski and J. Tosiek, "Notes on thermodynamics in special relativity," Physica Scripta **84**, 055008 (2011).

[301] C. Farías, V. A. Pinto, and P. S. Moya, "What is the temperature of a moving body?" Scientific Reports **7**, 17657 (2017).

[302] A. S. Parvan, "Lorentz transformations of the thermodynamic quantities," Annals Phys. **401**, 130–138 (2019).

[303] X. Hao, S. Liu, and L. Zhao, "Relativistic transformation of thermodynamic parameters and refined Saha equation," (2021), arXiv:2105.07313 [gr-qc].

[304] T. D. Cohen, "Functional integrals for QCD at nonzero chemical potential and zero density," Phys. Rev. Lett. **91**, 222001 (2003), arXiv:hep-ph/0307089.

[305] N. Khan, J. M. Pawlowski, F. Rennecke, and M. M. Scherer, "The Phase Diagram of QC_2D from Functional Methods," (2015), arXiv:1512.03673 [hep-ph].

[306] W.-j. Fu, J. M. Pawlowski, F. Rennecke, and B.-J. Schaefer, "Baryon number fluctuations at finite temperature and density," Phys. Rev. D **94**, 116020 (2016), arXiv:1608.04302 [hep-ph].

[307] J. Braun, M. Leonhardt, and M. Pospiech, "Fierz-complete NJL model study: Fixed points and phase structure at finite temperature and density," Phys. Rev. D **96**, 076003 (2017), arXiv:1705.00074 [hep-ph].

[308] G. Aarts, "Can stochastic quantization evade the sign problem? The relativistic Bose gas at finite chemical potential," Phys. Rev. Lett. **102**, 131601 (2009), arXiv:0810.2089 [hep-lat].

[309] D. J. Weir, "Studying a relativistic field theory at finite chemical potential with the density matrix renormalization group," Phys. Rev. D **82**, 025003 (2010), arXiv:1003.0698 [hep-lat].

[310] C. Gattringer and T. Kloiber, "Lattice study of the Silver Blaze phenomenon for a charged scalar ϕ^4 field," Nucl. Phys. B **869**, 56–73 (2013), arXiv:1206.2954 [hep-lat].

[311] G. Markó, U. Reinosa, and Z. Szép, "Bose-Einstein condensation and Silver Blaze property from the two-loop Φ-derivable approximation," Phys. Rev. D **90**, 125021 (2014), arXiv:1410.6998 [hep-ph].

[312] N. Strodthoff, B.-J. Schaefer, and L. von Smekal, "Quark-meson-diquark model for two-color QCD," Phys. Rev. D **85**, 074007 (2012), arXiv:1112.5401 [hep-ph].

[313] R. Schmidt and T. Enss, "Excitation spectra and rf-response near the polaron-to-molecule transition from the functional renormalization group," Phys. Rev. A **83**, 063620 (2011), arXiv:1104.1379 [cond-mat.quant-gas].

[314] J. Braun, H. Gies, L. Janssen, and D. Roscher, "Phase structure of many-flavor QED_3," Phys. Rev. D **90**, 036002 (2014), arXiv:1404.1362 [hep-ph].

[315] T. Cohen and W. J. Knight, "Convergence and divergence of $\sum_{n=1}^{\infty} \frac{1}{n^p}$," Mathematics Magazine **52**, 178–178 (1979).

[316] D. J. Gross, R. D. Pisarski, and L. G. Yaffe, "QCD and Instantons at Finite Temperature," Rev. Mod. Phys. **53**, 43 (1981).

[317] E. L. Dodd, *On iterated limits of multiple sequences*, Vol. 61 (Mathematische Annalen, 1905).

[318] P. R. Beesack, "Iterated and double limits," Annales Polonici Mathematici **47**, 51–64 (1986).

[319] Z. Kadelburg and M. M. Marjanović, "Interchanging two limits," The Teaching of Mathematics **8**, 15–29 (2005).

[320] H. A. Weldon, "Simple Rules for Discontinuities in Finite Temperature Field Theory," Phys. Rev. D **28**, 2007 (1983).

[321] T. Gorda, J. Österman, and S. Säppi, "Augmenting the residue theorem with boundary terms in finite-density calculations," Phys. Rev. D **106**, 105026 (2022), arXiv:2208.14479 [hep-th].

[322] D. Nickel, "Inhomogeneous phases in the Nambu-Jona-Lasino and quark-meson model," Phys. Rev. D **80**, 074025 (2009), arXiv:0906.5295 [hep-ph].

[323] M. Buballa and S. Carignano, "Inhomogeneous chiral condensates," Prog. Part. Nucl. Phys. **81**, 39–96 (2015), arXiv:1406.1367 [hep-ph].

[324] M. Buballa, S. Carignano, and L. Kurth, "Inhomogeneous phases in the quark-meson model with explicit chiral-symmetry breaking," Eur. Phys. J. ST **229**, 3371–3385 (2020), arXiv:2006.02133 [hep-ph].

[325] J. Lenz, L. Pannullo, M. Wagner, B. Wellegehausen, and A. Wipf, "Inhomogeneous phases in the Gross-Neveu model in 1+1 dimensions at finite number of flavors," Phys. Rev. D **101**, 094512 (2020), arXiv:2004.00295 [hep-lat].

[326] J. Berges, D.-U. Jungnickel, and C. Wetterich, "Two flavor chiral phase transition from nonperturbative flow equations," Phys. Rev. D **59**, 034010 (1999), arXiv:hep-ph/9705474.

[327] C. G. Callan, Jr., "Broken scale invariance in scalar field theory," Phys. Rev. D **2**, 1541–1547 (1970).

[328] K. Symanzik, "Small distance behavior in field theory and power counting," Commun. Math. Phys. **18**, 227–246 (1970).

[329] J. Bardeen, L. N. Cooper, and J. R. Schrieffer, "Microscopic theory of superconductivity," Phys. Rev. **106**, 162 (1957).

[330] J. Bardeen, L. N. Cooper, and J. R. Schrieffer, "Theory of superconductivity," Phys. Rev. **108**, 1175–1204 (1957).

[331] L. S. Celenza and C. M. Shakin, "Description of the Gluon Condensate," Phys. Rev. D **34**, 1591–1600 (1986).

[332] E. V. Gorbar and A. A. Natale, "Relating the quark and gluon condensates through the QCD vacuum energy," Phys. Rev. D **61**, 054012 (2000), arXiv:hep-ph/9906299.

[333] K. I. Kondo, "Vacuum condensates, effective gluon mass and color confinement," in *International Conference on Color Confinement and Hadrons in Quantum Chromodynamics* (2004) pp. 140–151, arXiv:hep-th/0311033.

[334] J. Horak, F. Ihssen, J. Papavassiliou, J. M. Pawlowski, A. Weber, and C. Wetterich, "Gluon condensates and effective gluon mass," SciPost Phys. **13**, 042 (2022), arXiv:2201.09747 [hep-ph].

[335] M. A. Shifman, A. I. Vainshtein, and V. I. Zakharov, "Instantons in non-perturbative QCD vacuum," Nucl. Phys. B **165**, 45 (1980).

[336] T. Schäfer and E. V. Shuryak, "Instantons in QCD," Rev. Mod. Phys. **70**, 323–426 (1998), arXiv:hep-ph/9610451.

[337] S. Vandoren and P. van Nieuwenhuizen, "Lectures on instantons," (2008), arXiv:0802.1862 [hep-th].

[338] J. R. Pelaez, "From controversy to precision on the sigma meson: a review on the status of the non-ordinary $f_0(500)$ resonance," Phys. Rept. **658**, 1 (2016), arXiv:1510.00653 [hep-ph].

[339] S. Navas *et al.* (Particle Data Group), "Review of particle physics," Phys. Rev. D **110**, 030001 (2024).

[340] H.-T. Ding, P. Hegde, O. Kaczmarek, F. Karsch, A. Lahiri, S.-T. Li, S. Mukherjee, H. Ohno, P. Petreczky, C. Schmidt, and P. Steinbrecher, "Chiral Phase Transition Temperature in $(2+1)$-Flavor QCD," Phys. Rev. Lett. **123**, 062002 (2019), arXiv:1903.04801 [hep-lat].

[341] K. Rajagopal, "The Chiral phase transition in QCD: Critical phenomena and long wavelength pion oscillations," in *Quark-Gluon Plasma* 2, edited by R. C. Hwa (1995) pp. 484–554, arXiv:hep-ph/9504310.

[342] V. V. Braguta, "Phase Diagram of Dense Two-Color QCD at Low Temperatures," Symmetry **15**, 1466 (2023).

[343] J. Berges and K. Rajagopal, "Color superconductivity and chiral symmetry restoration at nonzero baryon density and temperature," Nucl. Phys. B **538**, 215–232 (1999), arXiv:hep-ph/9804233.

[344] F. Xu and M. Huang, "The chiral and deconfinement phase transitions," Central Eur. J. Phys. **10**, 1357–1360 (2012), arXiv:1202.5942 [hep-ph].

[345] F. Sun, K. Xu, and M. Huang, "Splitting of chiral and deconfinement phase transitions induced by rotation," Phys. Rev. D **108**, 096007 (2023), arXiv:2307.14402 [hep-ph].

[346] B.-J. Schaefer and J. Wambach, "Susceptibilities near the QCD (tri)critical point," Phys. Rev. D **75**, 085015 (2007), arXiv:hep-ph/0603256.

[347] J. M. Pawlowski and F. Rennecke, "Higher order quark-mesonic scattering processes and the phase structure of QCD," Phys. Rev. D **90**, 076002 (2014), arXiv:1403.1179 [hep-ph].

[348] T. Yokota, T. Kunihiro, and K. Morita, "Functional renormalization group analysis of the soft mode at the QCD critical point," PTEP **2016**, 073D01 (2016), arXiv:1603.02147 [hep-ph].

[349] R.-A. Tripolt, B.-J. Schaefer, L. von Smekal, and J. Wambach, "Low-temperature behavior of the quark-meson model," Phys. Rev. D **97**, 034022 (2018), arXiv:1709.05991 [hep-ph].

[350] S. Resch, F. Rennecke, and B.-J. Schaefer, "Mass sensitivity of the three-flavor chiral phase transition," Phys. Rev. D **99**, 076005 (2019), arXiv:1712.07961 [hep-ph].

[351] J. Eser, F. Divotgey, and M. Mitter, "Low-energy limit of the $O(4)$ quark-meson model," PoS **CD2018**, 060 (2019), arXiv:1902.04804 [hep-ph].

[352] B.-J. Schaefer, J. M. Pawlowski, and J. Wambach, "The Phase Structure of the Polyakov–Quark-Meson Model," Phys. Rev. D **76**, 074023 (2007), arXiv:0704.3234 [hep-ph].

[353] V. Skokov, B. Stokic, B. Friman, and K. Redlich, "Meson fluctuations and thermodynamics of the Polyakov loop extended quark-meson model," Phys. Rev. C **82**, 015206 (2010), arXiv:1004.2665 [hep-ph].

[354] V. Skokov, B. Friman, and K. Redlich, "Quark number fluctuations in the Polyakov loop-extended quark-meson model at finite baryon density," Phys. Rev. C **83**, 054904 (2011), arXiv:1008.4570 [hep-ph].

[355] R. Stiele, L. M. Haas, J. Braun, J. M. Pawlowski, and J. Schaffner-Bielich, "QCD thermodynamics of effective models with an improved Polyakov-loop potential," PoS **ConfinementX**, 215 (2012), arXiv:1303.3742 [hep-ph].

[356] T. K. Herbst, M. Mitter, J. M. Pawlowski, B.-J. Schaefer, and R. Stiele, "Exploring the Phase Structure and Thermodynamics of QCD," PoS **QCD-TNT-III**, 030 (2013), arXiv:1401.1735 [hep-ph].

[357] S. K. Rai and V. K. Tiwari, "Thermodynamics and phase diagrams of the Polyakov quark-meson model with on-shell versus curvature mass parameter fixing," Phys. Rev. D **108**, 074014 (2023), arXiv:2305.16180 [hep-ph].

[358] J. Eser, M. Grahl, and D. H. Rischke, "Functional Renormalization Group Study of the Chiral Phase Transition Including Vector and Axial-vector Mesons," Phys. Rev. D **92**, 096008 (2015), arXiv:1508.06928 [hep-ph].

[359] F. Rennecke and B.-J. Schaefer, "Fluctuation-induced modifications of the phase structure in (2+1)-flavor QCD," Phys. Rev. D **96**, 016009 (2017), arXiv:1610.08748 [hep-ph].

[360] C. Jung, F. Rennecke, R.-A. Tripolt, L. von Smekal, and J. Wambach, "In-Medium Spectral Functions of Vector- and Axial-Vector Mesons from the Functional Renormalization Group," Phys. Rev. D **95**, 036020 (2017), arXiv:1610.08754 [hep-ph].

[361] H. Zhang, D. Hou, T. Kojo, and B. Qin, "Functional renormalization group study of the quark-meson model with ω meson," Phys. Rev. D **96**, 114029 (2017), arXiv:1709.05654 [hep-ph].

[362] M. Osman, D. Hou, W. Wang, and H. Zhang, "Functional renormalization group study of the quark-meson model with ω and ρ vector mesons," (2024), arXiv:2402.15474 [hep-ph].

[363] J. O. Andersen and M. P. Nødtvedt, "Color superconductivity in the two-flavor quark-meson diquark model," (2024), arXiv:2408.12361 [hep-ph].

[364] H.-L. Chen, Z.-B. Zhu, and X.-G. Huang, "Quark-meson model under rotation: A functional renormalization group study," Phys. Rev. D **108**, 054006 (2023), arXiv:2306.08362 [hep-ph].

[365] V. Koch, "Aspects of chiral symmetry," Int. J. Mod. Phys. E **6**, 203–250 (1997), arXiv:nucl-th/9706075.

[366] H. Sazdjian, "Introduction to chiral symmetry in QCD," EPJ Web Conf. **137**, 02001 (2017), arXiv:1612.04078 [hep-ph].

[367] J. W. Holt, M. Rho, and W. Weise, "Chiral symmetry and effective field theories for hadronic, nuclear and stellar matter," Phys. Rept. **621**, 2–75 (2016), arXiv:1411.6681 [nucl-th].

[368] H. F. Baker, "Alternants and Continuous Groups," Proceedings of the London Mathematical Society **s2-3**, 24–47 (1905).

[369] J. E. Campbell, "On a Law of Combination of Operators bearing on the Theory of Continuous Transformation Groups," Proceedings of the London Mathematical Society **s1-28**, 381–390 (1896).

[370] J. E. Campbell, "On a Law of Combination of Operators (Second Paper)," Proceedings of the London Mathematical Society **s1-29**, 14–32 (1897).

[371] F. Hausdorff, "Die symbolische Exponentialformel in der Gruppentheorie," Ber. Verh. Sächs. Ges. Wiss. Leipzig. Mathe-phys. Kl. **58**, 19–48 (1906).

[372] S. Blanes and F. Casas, "On the convergence and optimization of the Baker–Campbell–Hausdorff formula," Linear Algebra and its Applications **378**, 135–158 (2004).

[373] A. Bonfiglioli and R. Fulci, *Topics in Noncommutative Algebra*, Lecture Notes in Mathematics (Springer Berlin, Heidelberg, 2012).

[374] K. Fujikawa, "Path Integral Measure for Gauge Invariant Fermion Theories," Phys. Rev. Lett. **42**, 1195–1198 (1979).

[375] K. Fujikawa, "Path Integral for Gauge Theories with Fermions," Phys. Rev. D **21**, 2848 (1980), [Erratum: Phys.Rev.D 22, 1499 (1980)].

[376] T. Kunihiro, "Chiral Symmetry and Axial Anomaly in Hadron and Nuclear Physics: a review," AIP Conf. Proc. **1235**, 23 (2010), arXiv:1006.0852 [nucl-th].

[377] J. Braun, M. Leonhardt, J. M. Pawlowski, and D. Rosenblüh (QCD), "Chiral and effective $U(1)_A$ symmetry restoration in QCD," (2020), arXiv:2012.06231 [hep-ph].

[378] G. Källén, "On the definition of the Renormalization Constants in Quantum Electrodynamics," Helv. Phys. Acta **25**, 417 (1952).

[379] H. Lehmann, "Über Eigenschaften von Ausbreitungsfunktionen und Renormierungskonstanten quantisierter Felder," Nuovo Cim. **11**, 342–357 (1954).

[380] S. Weinberg, *The Quantum Theory of Fields. Vol. 1: Foundations* (Cambridge University Press, 1995).

[381] N. D. Hari Dass, *Strings to Strings*, Lecture Notes in Physics (Springer Cham, 2023).

[382] R.-A. Tripolt, N. Strodthoff, L. von Smekal, and J. Wambach, "Spectral Functions for the Quark-Meson Model Phase Diagram from the Functional Renormalization Group," Phys. Rev. D **89**, 034010 (2014), arXiv:1311.0630 [hep-ph].

[383] R.-A. Tripolt, J. Weyrich, L. von Smekal, and J. Wambach, "Fermionic spectral functions with the Functional Renormalization Group," Phys. Rev. D **98**, 094002 (2018), arXiv:1807.11708 [hep-ph].

[384] M. L. Goldberger and S. B. Treiman, "Decay of the pi meson," Phys. Rev. **110**, 1178–1184 (1958).

[385] T.-P. Cheng and L.-F. Li, *Gauge Theory of Elementary Particle Physics* (Oxford University Press, Oxford, 1984).

[386] J. Braun, M. Leonhardt, and M. Pospiech, "Fierz-complete NJL model study. II. Toward the fixed-point and phase structure of hot and dense two-flavor QCD," Phys. Rev. D **97**, 076010 (2018), arXiv:1801.08338 [hep-ph].

[387] W. Florkowski and B. L. Friman, "Screening of the meson fields in the Nambu-Jona-Lasinio model," Acta Phys. Polon. B **25**, 49–71 (1994).

[388] N. Strodthoff and L. von Smekal, "Polyakov-Quark-Meson-Diquark Model for two-color QCD," Phys. Lett. B **731**, 350–357 (2014), arXiv:1306.2897 [hep-ph].

[389] J. Braun, B. Klein, H. J. Pirner, and A. H. Rezaeian, "Volume and quark mass dependence of the chiral phase transition," Phys. Rev. D **73**, 074010 (2006), arXiv:hep-ph/0512274.

[390] J. Braun, B. Klein, and P. Piasecki, "On the scaling behavior of the chiral phase transition in QCD in finite and infinite volume," Eur. Phys. J. C **71**, 1576 (2011), arXiv:1008.2155 [hep-ph].

[391] M. Leonhardt, M. Pospiech, B. Schallmo, J. Braun, C. Drischler, K. Hebeler, and A. Schwenk, "Symmetric nuclear matter from the strong interaction," Phys. Rev. Lett. **125**, 142502 (2020), arXiv:1907.05814 [nucl-th].

[392] J. M. Pawlowski, "The QCD phase diagram: Results and challenges," AIP Conf. Proc. **1343**, 75–80 (2011), arXiv:1012.5075 [hep-ph].

[393] B. Klein, "Modeling Finite-Volume Effects and Chiral Symmetry Breaking in Two-Flavor QCD Thermodynamics," Phys. Rept. **707-708**, 1–51 (2017), arXiv:1710.05357 [hep-ph].

[394] Z. Fang, Y.-L. Wu, and L. Zhang, "Chiral phase transition and QCD phase diagram from AdS/QCD," Phys. Rev. D **99**, 034028 (2019), arXiv:1810.12525 [hep-ph].

[395] H. T. Ding, O. Kaczmarek, F. Karsch, P. Petreczky, M. Sarkar, C. Schmidt, and S. Sharma, "Curvature of the chiral phase transition line from the magnetic equation of state of (2+1)-flavor QCD," Phys. Rev. D **109**, 114516 (2024), arXiv:2403.09390 [hep-lat].

[396] N. Tetradis, "The Quark meson model and the phase diagram of two flavor QCD," Nucl. Phys. A **726**, 93–119 (2003), arXiv:hep-th/0303244.

[397] M. Ishii, H. Kouno, and M. Yahiro, "Model prediction for temperature dependence of meson pole masses from lattice QCD results on meson screening masses," Phys. Rev. D **95**, 114022 (2017), arXiv:1609.04575 [hep-ph].

[398] F. Gao and M. Ding, "Thermal properties of π and ρ meson," Eur. Phys. J. C **80**, 1171 (2020), arXiv:2006.05909 [hep-ph].

[399] J. Horak, J. Papavassiliou, J. M. Pawlowski, and N. Wink, "Ghost spectral function from the spectral Dyson-Schwinger equation," Phys. Rev. D **104** (2021), 10.1103/PhysRevD.104.074017, arXiv:2103.16175 [hep-th].

[400] J. Horak, J. M. Pawlowski, J. Rodríguez-Quintero, J. Turnwald, J. M. Urban, N. Wink, and S. Zafeiropoulos, "Reconstructing QCD spectral functions with Gaussian processes," Phys. Rev. D **105**, 036014 (2022), arXiv:2107.13464 [hep-ph].

[401] J. Horak, J. M. Pawlowski, and N. Wink, "On the quark spectral function in QCD," SciPost Phys. **15**, 149 (2023), arXiv:2210.07597 [hep-ph].

[402] L. D. Landau and E. M. Lifshitz, *Fluid Mechanics*, 2nd ed. (Pergamon Press, 1987).

[403] M. S. Green, "Markoff Random Processes and the Statistical Mechanics of Time-Dependent Phenomena," J. Chem. Phys. **20**, 1281–1295 (1952).

[404] M. S. Green, "Markoff Random Processes and the Statistical Mechanics of Time-Dependent Phenomena. II. Irreversible Processes in Fluids," J. Chem. Phys. **22**, 398–414 (1954).

[405] H. Mori, "A quantum-statistical theory of transport processes," Journal of the Physical Society of Japan **11**, 1029–1044 (1956).

[406] A. Hosoya, M.-a. Sakagami, and M. Takao, "Nonequilibrium Thermodynamics in Field Theory: Transport Coefficients," Annals Phys. **154**, 229 (1984).

[407] S. Jeon and L. G. Yaffe, "From quantum field theory to hydrodynamics: Transport coefficients and effective kinetic theory," Phys. Rev. D **53**, 5799–5809 (1996).

[408] G. Aarts and J. M. Martinez Resco, "Transport coefficients and quantum fields," in *5th Internationa Conference on Strong and Electroweak Matter* (2003) pp. 96–110, arXiv:hep-ph/0212268.

[409] R. B. Bird, W. E. Steward, and E. N. Lightfoot, *Transport Phenomena*, 2nd ed. (John Wiley & Sons, 2002).

[410] A. Hosoya and K. Kajantie, "Transport Coefficients of QCD Matter," Nucl. Phys. B **250**, 666–688 (1985).

[411] N. Masuda, A. Nakamura, S. Sakai, F. Shoji, and J. Urakawa, "Transport coefficients from lattice QCD thermodynamics," Nucl. Phys. B Proc. Suppl. **42**, 526–528 (1995).

[412] P. B. Arnold, G. D. Moore, and L. G. Yaffe, "Transport coefficients in high temperature gauge theories. 1. Leading log results," JHEP **11**, 001 (2000), arXiv:hep-ph/0010177.

[413] P. B. Arnold, G. D. Moore, and L. G. Yaffe, "Transport coefficients in high temperature gauge theories. 2. Beyond leading log," JHEP **05**, 051 (2003), arXiv:hep-ph/0302165.

[414] E. V. Shuryak, "What RHIC experiments and theory tell us about properties of quark-gluon plasma?" Nucl. Phys. A **750**, 64–83 (2005), arXiv:hep-ph/0405066.

[415] A. Beraudo *et al.*, "Extraction of Heavy-Flavor Transport Coefficients in QCD Matter," Nucl. Phys. A **979**, 21–86 (2018), arXiv:1803.03824 [nucl-th].

[416] A. Jaiswal *et al.*, "Dynamics of QCD matter — current status," Int. J. Mod. Phys. E **30**, 2130001 (2021), arXiv:2007.14959 [hep-ph].

[417] G. Aarts and J. M. Martinez Resco, "Shear viscosity in the $O(N)$ model," JHEP **02**, 061 (2004), arXiv:hep-ph/0402192.

[418] M. Iwasaki, H. Ohnishi, and T. Fukutome, "Shear viscosity and spectral function of the quark matter," (2006), arXiv:hep-ph/0606192.

[419] M. Haas, L. Fister, and J. M. Pawlowski, "Gluon spectral functions and transport coefficients in Yang–Mills theory," Phys. Rev. D **90**, 091501 (2014), arXiv:1308.4960 [hep-ph].

[420] N. Christiansen, M. Haas, J. M. Pawlowski, and N. Strodthoff, "Transport Coefficients in Yang–Mills Theory and QCD," Phys. Rev. Lett. **115**, 112002 (2015), arXiv:1411.7986 [hep-ph].

[421] P. Lowdon, R.-A. Tripolt, J. M. Pawlowski, and D. H. Rischke, "Spectral representation of the shear viscosity for local scalar QFTs at finite temperature," Phys. Rev. D **104**, 065010 (2021), arXiv:2104.13413 [hep-th].

[422] R.-A. Tripolt, L. von Smekal, and J. Wambach, "Spectral functions and in-medium properties of hadrons," Int. J. Mod. Phys. E **26**, 1740028 (2017), arXiv:1605.00771 [hep-ph].

[423] J. Fehre, D. F. Litim, J. M. Pawlowski, and M. Reichert, "Lorentzian Quantum Gravity and the Graviton Spectral Function," Phys. Rev. Lett. **130**, 081501 (2023), arXiv:2111.13232 [hep-th].

[424] J. Horak, F. Ihssen, J. M. Pawlowski, J. Wessely, and N. Wink, "Scalar spectral functions from the spectral functional renormalization group," Phys. Rev. D **110**, 056009 (2024), arXiv:2303.16719 [hep-th].

[425] K. Otto, C. Busch, and B.-J. Schaefer, "Regulator scheme dependence of the chiral phase transition at high densities," Phys. Rev. D **106**, 094018 (2022), arXiv:2206.13067 [hep-ph].

[426] T. Toimela, "Perturbative QED and QCD at Finite Temperatures and Densities," Int. J. Theor. Phys. **24**, 901 (1985), [Erratum: Int.J.Theor.Phys. 26, 1021 (1987)].

[427] J. Friedel, "Xiv. the distribution of electrons round impurities in monovalent metals," The London, Edinburgh, and Dublin Philosophical Magazine and Journal of Science **43**, 153–189 (1952).

[428] J. Friedel, "Electronic structure of primary solid solutions in metals," Advances in Physics **3**, 446–507 (1954).

[429] J. Friedel, "Metallic alloys," Nuovo Cimento **7**, 287–311 (1958).

[430] A. L. Fetter and J. D. Walecka, *Quantum Theory of Many-Particle Systems* (McGraw-Hill, 1971).

[431] J. I. Kapusta and T. Toimela, "Friedel Oscillations in Relativistic QED and QCD," Phys. Rev. D **37**, 3731 (1988).

[432] J. Diaz Alonso, A. Perez Canyellas, and H. Sivak, "Linear Response and Friedel Oscillations of the Pion Field in Relativistic Nuclear Matter," Nucl. Phys. A **505**, 695–716 (1989).

[433] H. Liu, D.-f. Hou, and J.-r. Li, "Oscillatory behavior of the in-medium interparticle potential in hot gauge system with scalar bound states," Commun. Theor. Phys. **51**, 1107–1112 (2009), arXiv:hep-ph/0703305.

[434] C. Mu and P. Zhuang, "Quark Potential in a Quark-Meson Plasma," Eur. Phys. J. C **58**, 271–279 (2008), arXiv:0803.0581 [nucl-th].

[435] A. Koenigstein, L. Pannullo, S. Rechenberger, M. J. Steil, and M. Winstel, "Detecting inhomogeneous chiral condensation from the bosonic two-point function in the (1 + 1)-dimensional Gross–Neveu model in the mean-field approximation*," J. Phys. A **55**, 375402 (2022), arXiv:2112.07024 [hep-ph].

[436] A. Koenigstein and L. Pannullo, "Inhomogeneous condensation in the Gross-Neveu model in noninteger spatial dimensions 1≤d<3. II. Nonzero temperature and chemical potential," Phys. Rev. D **109**, 056015 (2024), arXiv:2312.04904 [hep-ph].

[437] A. Koenigstein and M. Winstel, "Revisiting the spatially inhomogeneous condensates in the (1 + 1)-dimensional chiral Gross–Neveu model via the bosonic two-point function in the infinite-N limit," J. Phys. A **57**, 335401 (2024), arXiv:2405.03459 [hep-th].

[438] B.-J. Schaefer and M. Wagner, "The Three-flavor chiral phase structure in hot and dense QCD matter," Phys. Rev. **D79**, 014018 (2009), arXiv:0808.1491 [hep-ph].

[439] G. 't Hooft, "A Planar Diagram Theory for Strong Interactions," Nucl. Phys. B **72**, 461 (1974).

[440] A. A. Migdal, "Loop Equations and 1/N Expansion," Phys. Rept. **102**, 199–290 (1983).

[441] R. F. Lebed, "Phenomenology of Large N_c QCD," Czech. J. Phys. **49**, 1273–1306 (1999), arXiv:nucl-th/9810080.

[442] M. Moshe and J. Zinn-Justin, "Quantum field theory in the large N limit: A Review," Phys. Rept. **385**, 69–228 (2003), arXiv:hep-th/0306133.

[443] J. Braun, S. Finkbeiner, F. Karbstein, and D. Roscher, "Search for inhomogeneous phases in fermionic models," Phys. Rev. D **91**, 116006 (2015), arXiv:1410.8181 [hep-ph].

[444] J. Braun, F. Karbstein, S. Rechenberger, and D. Roscher, "Crystalline ground states in Polyakov-loop extended Nambu–Jona-Lasinio models," Phys. Rev. D **93**, 014032 (2016), arXiv:1510.04012 [hep-ph].

[445] T. F. Motta, J. Bernhardt, M. Buballa, and C. S. Fischer, "Toward a stability analysis of inhomogeneous phases in QCD," Phys. Rev. D **108**, 114019 (2023), arXiv:2306.09749 [hep-ph].

[446] R. D. Pisarski and F. Rennecke, "Signatures of Moat Regimes in Heavy-Ion Collisions," Phys. Rev. Lett. **127**, 152302 (2021), arXiv:2103.06890 [hep-ph].

[447] F. Rennecke and R. D. Pisarski, "Moat Regimes in QCD and their Signatures in Heavy-Ion Collisions," PoS **CPOD2021**, 016 (2022), arXiv:2110.02625 [hep-ph].

[448] F. Rennecke, R. D. Pisarski, and D. H. Rischke, "Particle interferometry in a moat regime," Phys. Rev. D **107**, 116011 (2023), arXiv:2301.11484 [hep-ph].

[449] M. Haensch, F. Rennecke, and L. von Smekal, "Medium induced mixing, spatial modulations, and critical modes in QCD," Phys. Rev. D **110**, 036018 (2024), arXiv:2308.16244 [hep-ph].

[450] L. Pannullo, M. Wagner, and M. Winstel, "Regularization effects in the Nambu–Jona-Lasinio model: Strong scheme dependence of inhomogeneous phases and persistence of the moat regime," Phys. Rev. D **110**, 076006 (2024), arXiv:2406.11312 [hep-ph].

[451] J. Schwinger, "On the Euclidean Structure of Relativistic Field Theory," Proc. Nat. Acad. Sci. **44**, 956–965 (1958).

[452] J. Schwinger, "Four-dimensional euclidean formulation of quantum field theory," in *8th International Annual Conference on High Energy Physics* (1958) pp. 134–140.

[453] J. Schwinger, "Euclidean Quantum Electrodynamics," Phys. Rev. **115**, 721–731 (1959).

[454] T. Nakano, "Quantum Field Theory in Terms of Euclidean Parameters," Progress of Theoretical Physics **21**, 241–259 (1959).

[455] K. Symanzik, "A Modified Model of Euclidean Quantum Field Theory," Courant Institute of Mathematical Sciences Report (1964).

[456] K. Symanzik, "Euclidean Quantum Field Theory. I. Equations for a Scalar Model," Journal of Mathematical Physics **7**, 510–525 (1966).

[457] K. Symanzik, "Euclidean quantum field theory," Conf. Proc. C **680812**, 152–226 (1968).

[458] E. Nelson, "Quantum fields and markoff fields," in *Proceedings of Symposia in Pure Mathematics* (American Mathematical Society, 1973) pp. 413–420.

[459] E. Nelson, "The free Markoff field," Journal of Functional Analysis **12**, 211–227 (1973).

[460] A. M. Jaffee, "High-Energy Behavior in Quantum Field Theory. I. Strictly Localizable Fields," Phys. Rev. **158**, 1454–1461 (1967).

[461] F. Constantinescu and W. Thalheimer, "Ultradistributions and quantum fields: Fourier-Laplace transforms and boundary values of analytic functions," Rept. Math. Phys. **16**, 167–180 (1979).

[462] S. Nagamachi and N. Mugibayashi, "Theory of fourier hyperfunctions and its applications to quantum field theory," Lett. Math. Phys. **1**, 259–264 (1976).

[463] S. Nagamachi and N. Mugibayashi, "Hyperfunction Quantum Field Theory," Commun. Math. Phys. **46**, 119–134 (1976).

[464] S. Nagamachi and N. Mugibayashi, "Quantum Field Theory in Terms of Fourier Hyperfunctions," Publ. Res. Inst. Math. Sci. Kyoto **12**, 309–341 (1977).

[465] S. Nagamachi and N. Mugibayashi, "The Haag-Ruelle formulation of scattering in hyperfunction quantum field theory," Rept. Math. Phys. **16**, 181–201 (1979).

[466] R. O. W. Jr., "Hyperfunction solutions of the zero-rest-mass field equations," Communications in Mathematical Physics **78**, 567 – 600 (1980).

[467] S. Nagamachi and N. Mugibayashi, "Hyperfunctions and renormalization," J. Math. Phys. **27**, 832–839 (1986).

[468] S. Nagamachi and E. Brüning, "Hyperfunction quantum field theory: Analytic structure, modular aspects, and local observable algebras," J. Math. Phys. **42**, 99–129 (2001).

[469] S. Nagamachi and E. Brüning, "Hyperfunction Quantum Field Theory: Localized Fields Without Localized Test Functions," Lett. Math. Phys. **63**, 141–155 (2003).

[470] M. A. Solovev, "An Extension of Distribution Theory and of the Paley-Wiener-Schwartz Theorem Related to Quantum Gauge Theory," Commun. Math. Phys. **184**, 579–596 (1997), arXiv:hep-th/9601005.

[471] M. A. Solovev, "Wick-Ordered Entire Functions of the Indefinite Metric Free Field," Lett. Math. Phys. **41**, 265–277 (1997).

[472] M. A. Soloviev, "Lorentz-Covariant Ultradistributions, Hyperfunctions, and Analytic Functionals," Theor. Math. Phys. **128**, 1252–1270 (2001), arXiv:math-ph/0112052.

[473] J. R. Klauder, *A Modern Approach to Functional Integration* (Birkhäuser, New York, 2011).

[474] K. Osterwalder and R. Schrader, "Axioms for Euclidean Green's Functions," Commun. Math. Phys. **31**, 83–112 (1973).

[475] K. Osterwalder and R. Schrader, "Axioms for Euclidean Green's Functions II," Commun. Math. Phys. **42**, 281 (1975).

[476] F. Constantinescu and W. Thalheimer, "Euclidean Green's Functions for Jaffe Fields," Commun. Math. Phys. **38**, 299–316 (1974).

[477] S. Nagamachi and N. Mugibayashi, "Hyperfunction quantum field theory II. Euclidean Green's Functions," Commun. Math. Phys. **49**, 257–275 (1976).

[478] F. Strocchi, *Selected Topics on the General Properties of Quantum Field Theory*, Vol. 51 (World Scientific, 1993).

[479] D. Schlingemann, "From Euclidean field theory to quantum field theory," Rev. Math. Phys. **11**, 1151–1178 (1999), arXiv:hep-th/9802035.

[480] D. Schlingemann, "Euclidean field theory on a sphere," (1999), arXiv:hep-th/9912235.

[481] P. Kravchuk, J. Qiao, and S. Rychkov, "Distributions in CFT. Part II. Minkowski space," Journal of High Energy Physics **2021**, 94 (2021), arXiv:2104.02090.

[482] M. C. Lee and J. Glimm, "Axioms for Quantum Gauge Fields," (2023), arXiv:2112.08575 [math-ph].

[483] E. Nelson, "Construction of quantum fields from Markoff fields," Journal of Functional Analysis **12**, 97–112 (1973).

[484] E. Nelson, "Probability theory and euclidean field theory," in *Constructive Quantum Field Theory*, edited by G. Velo and A. Wightman (Springer Berlin, Heidelberg, 1973) pp. 94–124.

[485] E. Seiler and B. Simon, "Nelson's Symmetry and All That in the Yukawa$_2$ and $(\phi^4)_3$ Field Theories," Annals of Physics **97**, 470–518 (1976).

[486] A. S. Wightman, "Quantum Field Theory in Terms of Vacuum Expectation Values," Phys. Rev. **101**, 860–866 (1956).

[487] H. Lehmann, K. Symanzik, and W. Zimmermann, "Zur Formulierung quantisierter Feldtheorien," Nuovo Cim. **1**, 205–225 (1955).

[488] H. Lehmann, K. Symanzik, and W. Zimmermann, "On the Formulation of Quantized Field Theories – II," Nuovo Cim. **6**, 319–333 (1957).

[489] D. Ruelle, "On the Asymptotic Condition in Quantum Field Theory," Helv. Phys. Acta **35**, 147–163 (1962).

[490] R. Haag and D. Kastler, "An Algebraic Approach to Quantum Field Theory," J. Math. Phys. **5**, 848–861 (1964).

[491] R. Haag, *Local Quantum Physics*, 2nd ed. (Springer-Verlag Berlin, Heidelberg, New York, 1996).

[492] M. Atiyah, "Topological quantum field theories," Inst. Hautes Etudes Sci. Publ. Math. **68**, 175–186 (1989).

[493] D. Buchholz, "Current trends in axiomatic quantum field theory," Lect. Notes Phys. **558**, 43–64 (2000), arXiv:hep-th/9811233 [hep-th].

[494] E. Frenkel, "Lectures on the Langlands Program and Conformal Field Theory," in *Les Houches School of Physics: Frontiers in Number Theory, Physics and Geometry* (2007) pp. 387–533, arXiv:hep-th/0512172.

[495] H. Halvorson and M. Muger, "Algebraic Quantum Field Theory," in *Philosophy of physics*, edited by J. Butterfield and J. Earman (2007) pp. 731–864, arXiv:math-ph/0602036.

[496] M. Dedushenko, "Snowmass white paper: The quest to define QFT," International Journal of Modern Physics A **38**, 2330002 (2023), arXiv:2203.08053 [hep-th].

[497] R. Luo, Q.-R. Wang, and Y.-N. Wang, "Lecture notes on generalized symmetries and applications," Phys. Rept. **1065**, 1–43 (2024), arXiv:2307.09215 [hep-th].

[498] G. C. Wick, "Properties of Bethe-Salpeter Wave Functions," Phys. Rev. **96**, 1124–1134 (1954).

[499] J. Samuel, "Wick rotation in the tangent space," Class. Quant. Grav. **33**, 015006 (2016), arXiv:1510.07365 [gr-qc].

[500] F. D'Andrea, M. A. Kurkov, and F. Lizzi, "Wick rotation and fermion doubling in noncommutative geometry," Phys. Rev. D **94**, 025030 (2016), arXiv:1605.03231 [hep-th].

[501] K. Osterwalder and R. Schrader, "Euclidean Fermi Fields and a Feynman-Kac Formula for Boson-Fermion Models," Helv. Phys. Acta **46**, 277–302 (1973).

[502] J. Fröhlich and K. Osterwalder, "Is There a Euclidean Field Theory for Fermions?" Helv. Phys. Acta **47**, 781 (1975).

[503] M. R. Mehta, "Euclidean continuation of the Dirac fermion," Phys. Rev. Lett. **65**, 1983–1986 (1990), [Erratum: Phys.Rev.Lett. 66, 522 (1991)].

[504] P. van Nieuwenhuizen and A. Waldron, "On Euclidean spinors and Wick rotations," Phys. Lett. B **389**, 29–36 (1996), arXiv:hep-th/9608174.

[505] C. D. Roberts and R. T. Cahill, "A Bosonization of QCD and Realizations of Chiral Symmetry," Austral. J. Phys. **40**, 499 (1987).

[506] D. Ebert, "Bosonization in particle physics," Lect. Notes Phys. **508**, 103–114 (1998), arXiv:hep-ph/9710511.

[507] D. Senechal, "An Introduction to bosonization," in *CRM Workshop on Theoretical Methods for Strongly Correlated Fermions* (1999) arXiv:cond-mat/9908262.

[508] S. Rao and D. Sen, "An Introduction to bosonization and some of its applications," (2000), arXiv:cond-mat/0005492.

[509] J. Jaeckel and C. Wetterich, "Flow equations without mean field ambiguity," Phys. Rev. D **68**, 025020 (2003), arXiv:hep-ph/0207094.

[510] J. Jaeckel, "Understanding the Fierz ambiguity of partially bosonized theories," in *37th Rencontres de Moriond on QCD and Hadronic Interactions* (2002) pp. 215–218, arXiv:hep-ph/0205154.

[511] P. Kopietz, "Bosonization of interacting fermions in arbitrary dimensions," (2006), arXiv:cond-mat/0605402 [cond-mat.str-el].

[512] J. Hubbard, "Calculation of partition functions," Phys. Rev. Lett. **3**, 77–80 (1959).

[513] R. L. Stratonovich, "On a Method of Calculating Quantum Distribution Functions," Soviet Physics Doklady **2**, 416 (1957).

[514] F. Rennecke, "Vacuum structure of vector mesons in QCD," Phys. Rev. D **92**, 076012 (2015), arXiv:1504.03585 [hep-ph].

Wissenschaftlicher Werdegang

seit 02/2020	**Promotion** Technische Universität Darmstadt
04/2017–12/2019	**Master of Science** Technische Universität Darmstadt Masterthesis: „Skalierungsverhalten in dichter Materie“
10/2012–12/2016	**Bachelor of Science** Technische Universität Darmstadt Bachelorthesis: „Vergleich des Rabi- und Jaynes-Cummings-Modells“
07/2012	**Allgemeine Hochschulreife** Gymnasium Lohne

Erklärungen laut Promotionsordnung

§8 Abs. 1 lit. c PromO

Ich versichere hiermit, dass die elektronische Version meiner Dissertation mit der schriftlichen Version übereinstimmt.

§8 Abs. 1 lit. d PromO

Ich versichere hiermit, dass zu einem vorherigen Zeitpunkt noch keine Promotion versucht wurde. In diesem Fall sind nähere Angaben über Zeitpunkt, Hochschule, Dissertationsthema und Ergebnis dieses Versuchs mitzuteilen.

§9 Abs. 1 PromO

Ich versichere hiermit, dass die vorliegende Dissertation selbstständig und nur unter Verwendung der angegebenen Quellen verfasst wurde.

§9 Abs. 2 PromO

Die Arbeit hat bisher noch nicht zu Prüfungszwecken gedient.

Darmstadt, den 21.01.2025

_____

(Sebastian Töpfel)